

2016-17 Entry Cohort

Photochemical Functionalisation of Arenes and Hetereoarenes.

A thesis submitted in partial fulfillment of the requirements for the degree of Doctor of Philosophy in Organic Chemistry

prepared by:

Thomas H. Sheridan
New College, University of Oxford

Project Supervisor: Prof. Jonathan W. Burton
Date: Sunday 11th April, 2021

Contents

Acknowledgements **vii**

Declaration **xi**

Abbreviations **xiii**

Abstract **xvii**

Notes on Convention **xix**

1 Introduction **1**

1.1 Organophotocatalysis 1

1.2 DDQ as an Organophotocatalyst 10

1.2.1 Fukuzumi method for photoexcited DDQ catalysed arene oxidation 12

1.2.2 König method of DDQ-photocatalysed arene oxidation . . . 15

1.3 Arene Radical Cations as Reactive Intermediates 19

1.3.1 Structure and bonding 19

1.3.2 Reactivity 21

1.4 C–F Bond Activation 23

1.4.1 Classical S_NAr 24

1.4.2 Solvent effects 27

1.5 Project Aims 28

2 Photochemical DDQ-Mediated Oxidations of Simple Arenes 31

2.1 Chapter Introduction 31

2.2 Photochemical C – H Bond Hydroxylation of Arenes 32

2.2.1 Effect of light source and photochemical setup 33

2.2.2 Reaction additives - oxidants & acids 37

2.2.3 Catalyst loading 40

2.2.4 Results following optimisation 42

2.3 Photochemical Dual Hydroxylation-Nitration of Arenes 45

2.3.1 Application of flow chemistry 47

2.3.2 Catalyst optimisation and the use of computational methods 49

2.4 Chapter Summary 55

3 Radical Cation Accelerated Substitutions 57

3.1 Chapter Introduction 57

3.2 Photochemical DDQ-mediated defluorinative S_NAr 58

3.2.1 Modifications to light source and photochemical setup . . 58

3.2.2 Optimisation of defluorination chemistry 59

3.2.3 Initial Mechanistic Proposal 69

3.2.4 Arene scope of defluorination chemistry 76

3.2.5 Reoptimisation of S_NAr conditions for pyridine substrates . 81

3.2.6 Arene scope analytics 88

3.2.7 Nucleophile scope of S_NAr chemistry 97

3.2.8 Lambert method for electrophotochemical S_NAr 103
3.3 Radical Cation Accelerated Deprotection of Tosylates 106
3.4 Chapter Summary 108

4 Conclusion and Future Work 111

4.1 Oxidative Functionalisation and Dual-Functionalisation of Arenes . . 111
4.2 Radical Cation Accelerated S_NAr 112
4.3 Other Chemistry with Aryl Radical Cations 113
4.4 Final Considerations 116

5 Experimental Details 119

5.1 General Experimental Details 119
5.2 Photochemical Procedures 121
5.3 Computational Methods 124
5.3.1 Natural Population Analysis 124
5.3.2 Computational Redox Potentials, E 134
5.3.3 Computational Electrophilicity Index, ω 137
5.3.4 The S_NAr parameter and linear parameter 139
5.4 Full Optimisation Details 143
5.4.1 Optimisation of Anisole Formation 143
5.4.2 Optimisation for Fluoropyridines and Related Arenes . . . 145
5.4.3 Optimisation for the Use of Azole Nucleophiles 148
5.5 Summary of Control Experiments 149
5.6 General Experimental Procedures 151
5.7 Compound Synthesis and Characterisation 153

1D NMR Spectra **191**

GCMS Traces **233**

References **275**

Acknowledgements

That's a fool's experiment. But I love fools' experiments. I am always making them.

Charles Robert Darwin[1]

Firstly I must thank Prof. Jonathan Burton; thank you Jon not only for the opportunity to work in your group also for the constant support you have ~~afforded~~ given me. I have thoroughly enjoyed my 3+ years in the group, and being fortunate enough to have you as a supervisor was a big part of that. I appreciate all you have done for me, from helping me present in Bangkok to bringing in pastries during a pandemic.

I would also like to thank my industrial supervisors: Dr. Hatice Yayla (Pfizer), Dr. Yajing Lian (Pfizer), Dr. Julien Genovino (Pfizer), and Dr. Nat Monck (UCB). Their help was highly relevant to the work within this thesis. Although I did not get to meet all of you in person, I always found our meetings helpful in focusing our research efforts. Special thanks to Dr. Nat Monck, and Dr. Hatice Yayla for managing to make it over for some meetings.

Additionally, thanks must go to the SBM CDT – along with the EPSRC and all industrial sponsors – and the Clarendon Fund for providing my funding over the past 4+ years. I am truly grateful for this opportunity and so I thank all those involved in the running of the SBM:

Prof. Darren Dixon, Prof. Martin Smith, Dr. Lara Laurenço Venda, Dr. Maitaine Fernandez Chento, and Laura Thomas. I would also like to thank all the CRL staff, who not only ensured the running of the building and the running of samples, but who managed to do so during a global pandemic.

I also owe a great debt of gratitude to my proofreaders, without whom this thesis would not have be possible – certainly at least not with out 4× the number of, commas, arranged, almost at, random. Thank you, Prof. Jonathan Burton, Nada Kurdi, Jack Sutro, Dan Brown, and Pol Hernández Lladó. Jack Sutro has earned himself a second honorable mention here, for working on revisions over the festive period! I certainly owe you all a drink (at the very least), when it is legal for us all to meet in a pub to do so!

The Burton group has felt like family over these past few years, and so I want to thank everyone who has been a part of it over these last few years. Sam Chan, Sean Guggiari, Kilian Garrec, Joe Mason, Manjeet Kumar, Nada Kurdi, Jack Sutro, Dan Brown, Owen Smith, Pol Hernández Lladó, Stuart Astle, Nicoleta Lazar, and Harry Hicks. Although I'm not calling you all out by name, I would also like to express my gratitude to all the Part II and SBM rotation students we have had in the group during my time here. Everyone has done so much to make it a welcoming and highly pleasant working environment with lots of advice, many happy times, and many top quality memes.

Thanks also to my SBM and CRL friends, who have heard me complain of being tired over many lunch times, and... well... just heard me, from many corridors away. I like to imagine my loud guffaws brightened everyones days! For everyone who strongly disagrees with this assessment, I sincerely apologise!

Thanks to my family for their constant support. 2020 has been especially odd for not seeing them as much. I am definitely looking forward to more normality in the future (hopefully

this jinxes nothing).

Finally, thanks goes to my wonderful fiancée Naomi. Her constant support has made not only this thesis possible but the last 5+ years of my life possible. Her unwavering patience with me seems all the more incredible, given I have largely been glued to a keyboard during the course of a pandemic. Thank you.

Declaration

The work described in this thesis is entirely the work of the author except where specifically indicated and does not include any collaborative work. This thesis has not been previously submitted for a degree, diploma or any other qualification at the University of Oxford or elsewhere.

Thomas H. Sheridan

April, 2021

Abbreviations

Ac	Acyl
Acr	Acridinium
APCI	Atmospheric Pressure Chemical Ionisation
aq.	Aqueous
Ar	Aryl
BET	Back Electron Transfer
Boc	*tert*-Butyloxycarbonyl
BPMP	Bypyridyl Metal Photocatalyst
nBu	Butyl
cat.	Catalyst *or* catalytic
χ	Electronegativity
CI	Chemical Ionisation
conc.	Concentration
COSY	Correlation Spectroscopy
Cy	Cyclohexyl
DCE	1,2-Dichloroethane
DCM	Dichloromethane
DDQ	2,3-Dichloro-5,6-dicyano-1,4-benzoquinone
decomp.	Decomposition
°C	Degrees Celsius
DFT	Density Functional Theory
DIPC	Diisopropylcarbinol
DMAP	4-(Dimethylamino)pyridine
DMSO	Dimethylsulfoxide
$E_{X/Y}$	Redox potential for the X ⟶ Y transformation
EDG	Electron Donating Group
EI	Electron Impact
EnT	Energy Transfer
ϵ	Dielectric Constant
equiv.	Equivalents
ESI	Electrospray Ionisation
Et	Ethyl
ET	Electron Transfer
η	Hardness
eV	Electron-Volts
EWG	Electron Withdrawing Group
GCMS	Gas Chromatography - Mass Spectrometry
HAT	Hydrogen Atom Transfer
HBD	Hydrogen Bond Donor
HFIP	1,1,1,3,3,3-Hexafluoro-2-propanol
HMBC	Heteronuclear Multiple Bond Correlation

	Spectroscopy
$h\nu$	Light Energy
HOMO	Highest Occupied Molecular Orbital
HRMS	High Resolution Mass Spectrometry
HSQC	Heteronuclear Single Quantum Coherence Spectroscopy
i	*ipso*
iPr	*iso*-Propyl
IR	Infrared
ISC	Intersystem Crossing
IUPAC	International Union of Pure and Applied Chemistry
J	Coupling Constant
KIE	Kinetic Isotope Effect
LED	Light-Emitting Diode
lit.	Literature
LRMS	Low Resolution Mass Spectrometry
LUMO	Lowest Unoccupied Molecular Orbital
m	*meta*
mCPBA	meta-Chloroperoxybenzoic acid
Me	Methyl
Mes	Mesityl
m.p.	Melting Point
Ms	Mesyl (Methanesulfonyl)
μ	Electronic Chemical Potential (or micro, depending on context)
m/z	Mass/Charge Ratio
NBO	Natural Bond Orbital
nHex	Hexyl
NMR	Nuclear Magnetic Resonance
NO	Natural Orbital
NPA	Natural Population Analysis (also known as 'Natural Bond Orbital (NBO) Analysis')
Ns	Nosyl
Nu	Nucleophile
o	*ortho*
ω	Electrophilicity Index
p	*para*
PG	Protecting Group
Ph	Phenyl
ppm	Parts Per Million
Pr	Propyl
Q	Electric charge in 'elementary charge'
quant.	Quantitative
R	Generic group/substituent
$\mathbf{R}_f$	Retardation Factor
rt	Room Temperature
sat.	Saturated
sBu	*sec*-Butyl
SCE	Saturated Calomel Electrode
SHE	Standard Hydrogen Electrode
SOMO	Singly Occupied Molecular Orbital
τ	Lifetime
TBHP	*tert*-Butyl hydroperoxide
TBN	*tert*-Butyl nitrite
tBu	*tert*-Butyl

temp.	Temperature	**TPT**	2,4,6-Triphenylpyrylium Tetrafluoroborate
Tf	Trifluoromethanesulfonyl	**TS**‡	Transition State
TFA	Trifluoroacetic acid	**Ts**	Tosyl (*para*-Toluenesulfonyl)
TFE	2,2,2-Trifluoroethanol	**UV**	Ultraviolet
THF	Tetrahydrofuran	**vs**	verses
TLC	Thin Layer Chromatography	**X**	(pseudo)Halide (unless stated otherwise)
TON	Turn-Over Number		

Abstract

This thesis describes work focused on the application of potently oxidising organophotocatalysts to synthetic methodologies. The main motivation for this work is to enable chemical transformation of otherwise unreactive species. There are many organophotocatalysts described in the literature, and they often exhibit from high reduction potentials. However, most of the work herein is centred around the common reagent 2,3-dichloro-5,6-dicyano-1,4-benzoquinone (DDQ), **1**.

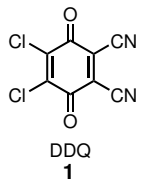

DDQ
1

Figure 1. *The organophotocatalyst DDQ, the main focus of photochemical arene functionalisation research.*

An overview of the relative benefits of organophotochemistry and a discussion of DDQ photochemistry is given in **Chapter 1**. Also included in this chapter is an analysis of the chemistry of aryl radical cations – a key intermediate in the work that follows. **Chapter 2** covers our investigations into net oxidative organophotochemistry. **Chapter 3** covers the work undertaken on net redox neutral transformations. This latter class was more productive on the whole, and led to a new defluorinative organophotochemical S_NAr process. The conclusions of

this thesis, and an outline for future work, is then provided in **Chapter 4**. Finally, all pertinent experimental details are provided from **Chapter 5** onwards.

Notes on Convention

The work presented in this thesis will make significant use of redox potentials, E. Redox potentials in this thesis will always be written in the form $E_{X/Y}$ to represent the half-cell potential for the transformation of X into Y. For cases where the transformation of X into Y represents a reduction (e.g. for DDQ acting as a single electron oxidising agent: $E_{DDQ/DDQ^{\bullet-}}$), this may be referred to as a reduction potential (or the term redox potential may still be used). Conversely, for cases where the transformation of X into Y represents an oxidation (e.g. for an arene undergoing a single electron oxidation: $E^{o}_{Ar/Ar^{\bullet+}}$), this may be referred to as an oxidation potential (or the term redox potential may still be used). Note: E^{o} is sometimes used in this thesis to emphasise the use of standard temperature and pressure. This is most commonly done on computational results (see **Subsection 5.3.2**).

All redox potentials given in this thesis are relative to either the Saturated Calomel Electrode (SCE) or to the Standard Hydrogen Electrode (SHE). Unless explicitly stated otherwise, the redox potential will be given relative to the SCE. For all redox potentials given relative to the SCE the solvent in which the measurement was conducted is MeCN (this is also true for all computational redox values, where solvation will have been modelled *implicitly*, see **Subsection 5.3.2**). For any potential given relative to the SHE the solvent in which the measurement was conducted is water.

Chapter 1

Introduction

1.1 Organophotocatalysis

A vast number of photocatalysts exist.[2–5] Most common, amongst the various types, are transition metal photocatalysts – often ruthenium or iridium with bipyridine (or related) ligands (BPMPs – bypyridyl metal photocatalysts,[6] top left **Figure 1.1**). Indeed, there is an extensive body of work detailing the use of these photocatalysts in organic transformations.[2,3,6] In addition to such catalysts (and related analogs), there has been recent renewed interest in utilising high turn-over number (TON) metal-porphyrin based photocatalysts (top right **Figure 1.1**),[7] and the 'highly-oxidising' decatungstate catalysts – such as tetrabutylammonium decatungstate (TBADT), $E_{\text{TBADT}^*/\text{TBADT}^{\bullet-}} = +2.44$ V vs SCE (bottom **Figure 1.1**) – for organic synthesis.[8–10] However, these metal-based photocatalysts, of which much is known, will largely be out of the scope of this thesis except where relevant for comparison.

By contrast organophotocatalysts (**Figure 1.2**), especially relative to BPMPs and related photocatalysts, are much less developed as a class for use as photocatalysts in synthetic organic chemistry. However, that is certainly beginning to change.[4,11] The work by Fukuzumi, Nicewicz, and others (particularly on the development of acridinium based catalysts) demon-

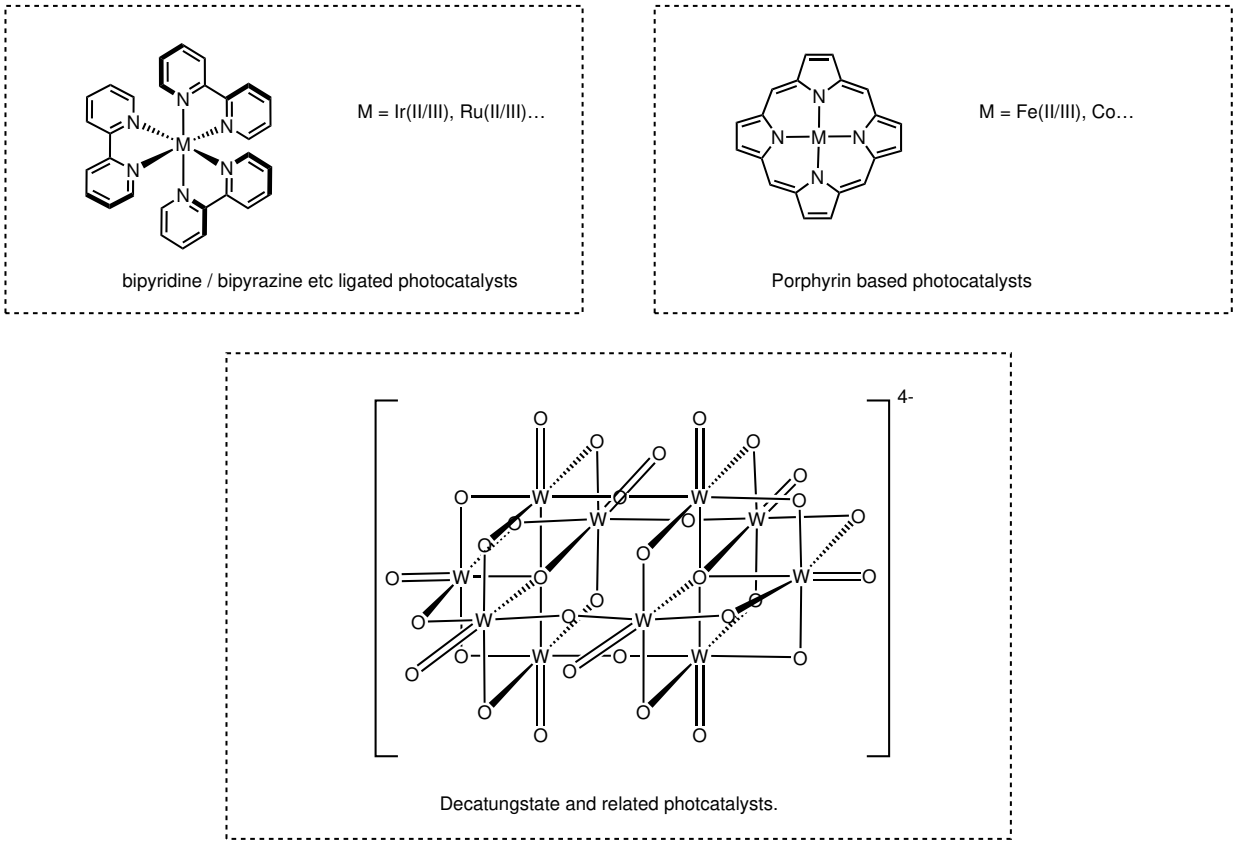

Figure 1.1. *Common classes of photocatalyst.*

strates the ability for organophotocatalysts to be as tunable as bipyridine and related ligands typically used in metallophotocatalysis.[12–28] Indeed, recent papers are beginning to detail 'guides' on rational optimisation of organophotocatalysts to better achieve the desired reaction outcome.[29–32]

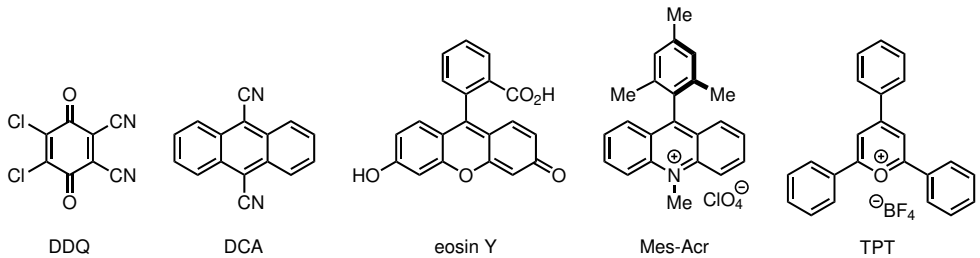

Figure 1.2. *A small selection of some common organophotocatalysts.*

Currently (low earth abundance) transition metal photocatalysts, such as those discussed above, are still the default choice of photocatalyst for many synthetic groups. One of the

reasons for this is the low catalyst loadings required for such catalysts, which can often be orders of magnitude below those needed for their organic counterparts.[4] Additionally, and in part due to this lower loading, they tend to be involved in fewer unwanted side reactions.[4]

While the utility of such catalysts is not in question, many mistakenly assume that the only advantage from switching from these catalysts to organophotocatalysts would be the ability to perform 'metal-free' reactions. It is true that many photocatalytic procedures performed by metal photocatalyst can be achieved with organophotocatalysts. Examples are the works of Nicewicz *et al.* and König *et al.* on catalytic enantioselective α-alkylation, shown below (**Scheme 1.1**).[33,34] Here, the structurally very different photocatalysts work in an almost identical way, with electron transfer to the bromomalonate causing C – Br bond cleavage, resulting in a bromide ion and a malonate radical. The resultant radical is then able to add into the enamine formed from the aldehyde reagent and the organocatalyst. However, the diversity of moieties that can be present in organic chromophores also allow for unique photochemical transformations to occur.[35–40] There are already many examples of this, and as the sub-field receives further study, this body of work will continue to grow significantly.[4,25,35–37,41–55] It is outside of the scope of this thesis to give a detailed review of all of the various, unique, chemistries enabled by organophotocatalysts. Nevertheless, some examples will now be discussed due to the relevance of certain features to the chemistry that follows.

Figure 1.2 shows only five organophotocatalysts, however, each of these five can be viewed as a member of a class of structurally related photocatalysts. Indeed, there are many more structural classes of organophotocatalysts than the five represented. However, these five classes, which can be described as: quinone, cyanoarene, xanthene, acridinium, and pyrylium respectively (left to right **Figure 1.2**), warrant further discussion due to their relative widespread use and/or interesting properties. The quinone class, represented by DDQ, will be discussed

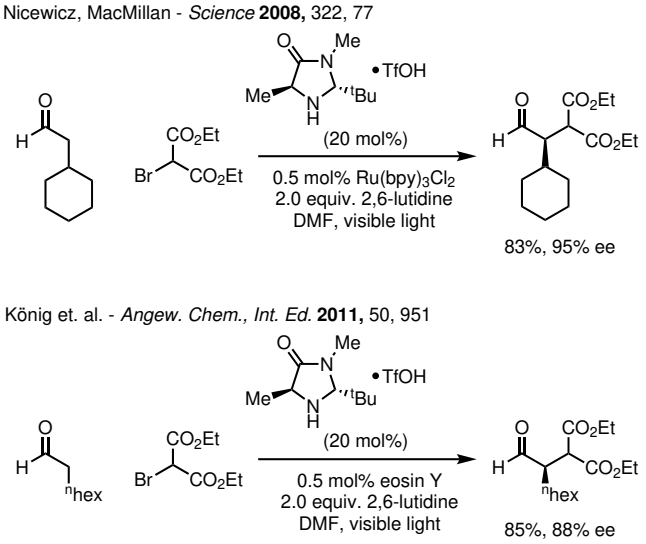

Scheme 1.1. *Reaction with metal photocatalyst, and similar transformation with organophotocatalyst (eosin y).* [33,34]

in the following section (**Section 1.2**) as the photochemistry of DDQ is central to this thesis. For now, it suffices to state that the photochemistry of the quinone class is dominated by photooxidations as the key mechanistic step. [41,42]

The chemistry of the cyanoarene class of organophotocatalysts, of which 9,10-dicyanoanthracene (DCA) is a prominent member, is also largely dominated by photooxidation steps. [35,43–47] Cyanoarenes were used as photocatalysts more commonly in earlier work and show photochemistry from their excited singlet state, which does suffer from shorter lifetime than equivalent triplets (fluorescence being spin allowed, while phosphorescence is not). [48] Cyanoarene photocatalysts also tend to readily undergo back-electron transfer, further reducing their efficiency (effectively lowering their quantum yield, Φ). [35] This possible limitation, however, can be utilised to aid the closing of an electron transfer (ET) catalytic cycle (**Scheme 1.2**), as shown by Arnold *et al.*. [35] This work by Arnold and coworkers shows the oxidation of biphenyl by photoexcited DCB. The resultant biphenyl radical cation can remove an electron from the styrene substrate. The styrene radical cation formed is acidic enough to be deprotonated under the reaction conditions, and the resultant neutral radical can be reduced by the radical anion of

DCB. Finally, reprotonation of this propenyl anion can occur on either 'end' of the system. The elegance of this system is that the desired, less stable, product is unconjugated and cannot be oxidised by the byphenyl radical cation – driving the reaction forward. Of the classes presented here, the cyanoarenes are the least used in the recent photochemistry literature. The following xanthene class, however, receives much attention.

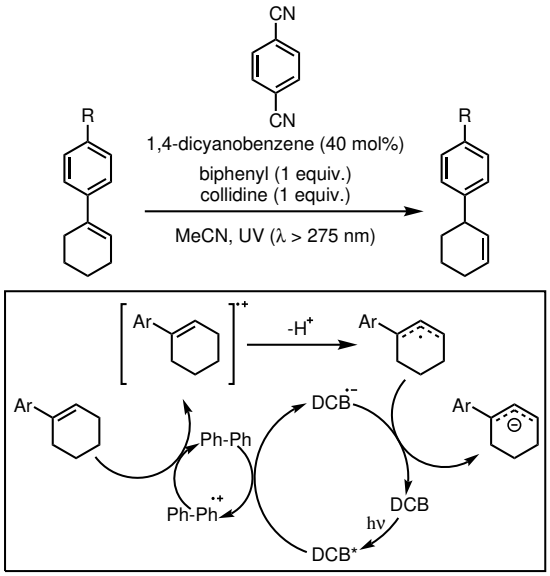

Scheme 1.2. *1,4-Dicyanobenzene (DCB) induced photochemical isomerisation*[35]

Xanthenes, which include eosin Y, fluorescein, rose Bengal and the rhodamines, are a particularly versatile class of organophotocatalysts.[36,49–54] Being strong chromophores, amenable to a number of electron transfer processes, as well as being inexpensive, they have been applied to a wide range of photochemistry and are often excellent 'first choice' catalysts.[4] It is beyond the scope of this introduction to give a comprehensive discussion, detailing the numerous examples, of the applications of the photocatalysts of this class. One example, which does help to illustrate the simplicity and efficiency of these photocatalyst, is the work of Zhang and coworkers (**Scheme 1.3**).[36] As can be seen, this work presents a one-pot synthesis of tetrahydroquinolines, from N,N-dimethylanilines and maleimides, in air. Here eosin Y (EY in the catalytic cycle) can be seen to be catalysing a Povarov reaction *via* an initial single

electron oxidation.[56] The main disadvantage with the xanthene class are the more modest redox potentials they tend to exhibit, with photoexcited reduction potentials often less then $+1$ V vs SCE.[57]

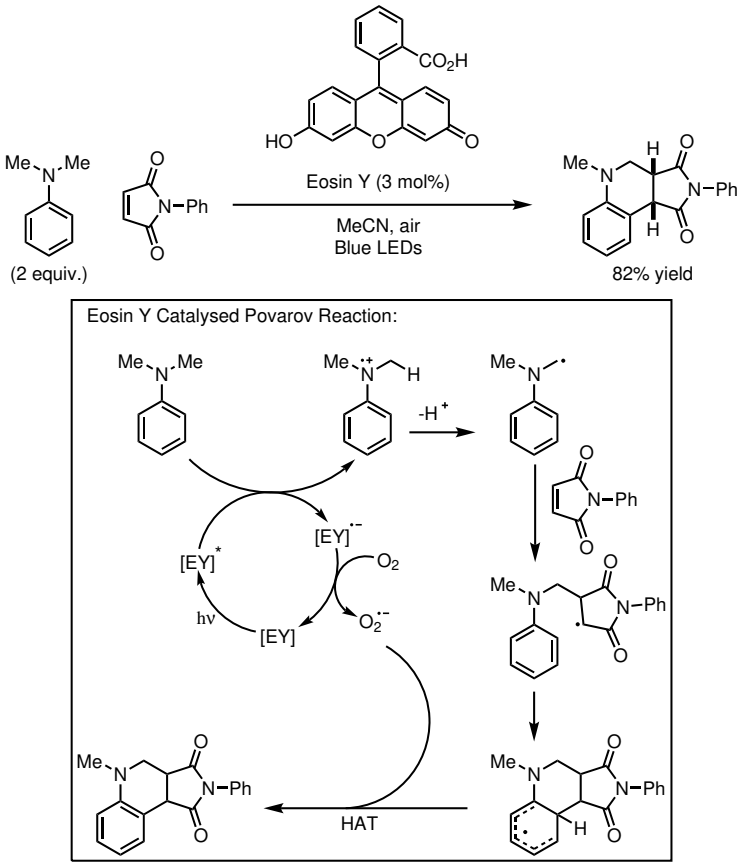

Scheme 1.3. *Zhang and coworkers method for the synthesis of tetrahydroquinolines from N,N-dimethylanilines and maleimides using Eosin Y as a photocatalyst, with visible light and under aerobic conditions.*[36]

This limitation is particularly noticeable when compared to the acridinium class, of which many variants exist and can be prepared.[29] However, relative to xanthenes, the commercially available acridiunium catalysts are more expensive. Additionally, the inherent positive charge of the acridinium catalyst limits its photoredox chemistry to photooxidation (with few exceptions),[25] while the xanthenes can participate in either photooxidation[36,50,52,53] or photoreduction,[49,51,54] depending on substrate and conditions. The beneficial side to this cationic nature is of course that reduction potentials of the acridinium catalysts are much greater than those

of xanthenes – and, as such, they can oxidise a greater range of species. A relevant example of acridinium photochemistry is discussed at length in **Subsection 1.3.2** (**Scheme 1.11**).[23]

Finally, the pyryliums (and thiapyryliums), such as TPT, are a class of relatively modular (can be made with a range of arene groups), cationic, oxidising photocatalysts.[37,55,58,59] Like many photocatalysts, they are active in the longer-lived triplet excited state. Triplet excited species are, in general, longer-lived than singlets due to the spin-forbidden nature of phosphorescence back to the ground state. However, in many practical applications, triplet states are in fact readily quenched by $^3O_2$.[60–62] This typically means extra measures are needed to ensure rigorous oxygen removal from the reaction mixture (such as freeze-pump-thaw degassing). Pyryliums offer a significant advantage here – they are triplet state photocatalysts but they are virtually free of triplet quenching by molecular oxygen under most conditions.[4,63,64] This is simply due to the fact that pyryliums can perform photooxidation many orders of magnitude faster than the rate of quenching.[4,63,64] The neutral radical formed after such an electron transfer is also unable to reduce molecular oxygen to superoxide ($O_2^{\bullet -}$). The net result of this is that the pyrylium class is very tolerant to aerobic conditions, which is clearly attractive for many practical reasons. This is demonstrated efficiently by the work of Nicewicz *et al.* on forming endoperoxides (**Scheme 1.4**), where molecular oxygen is trapped *via* clean reaction with the oxidised substrate, without being perturbed by the pyrylium photocatalyst.[37] Their main flaw is that they can be readily deactivated, and removed from the catalytic cycle, by direct reaction with nucleophiles and/or dimerisation of the neutral radical formed post electron-transfer.[65]

Although not exemplified in the discussion above, it should be understood that many of the photocatalysts discussed here are also efficient catalysts for energy transfer (EnT) processes as well as for photoredox processes. However, for the purposes of this thesis, only

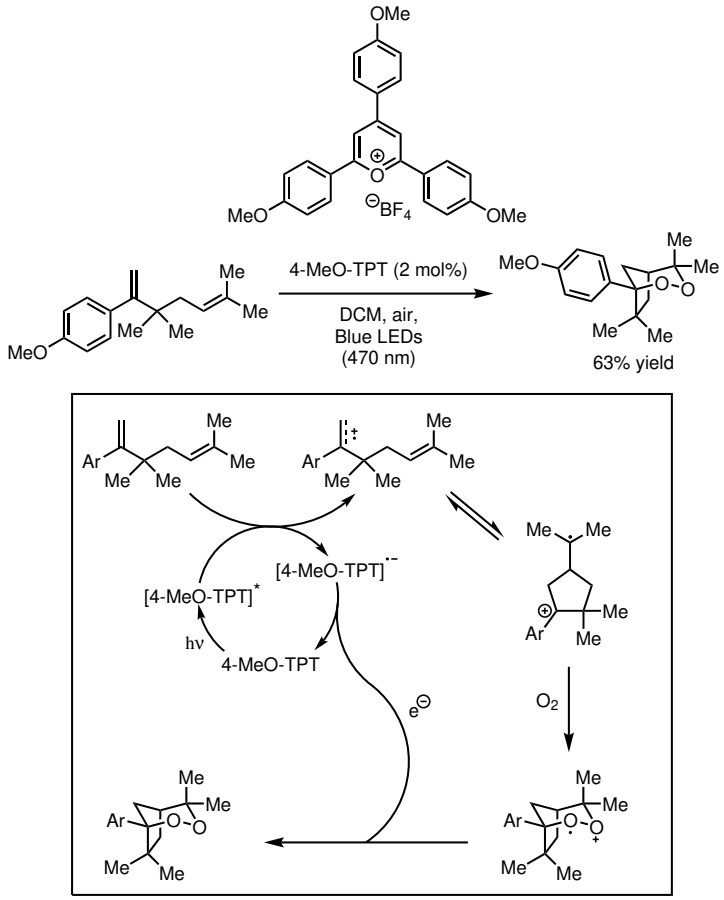

Scheme 1.4. *Cyclisation with molecular oxygen to form endoperoxides, catalysed by a pyrylium photocatalyst.*[37]

photoredox chemistries will be discussed. For an excellent review on EnT photochemistry, see the work of Glorius and coworkers.[66]

Much of the chemistry, outlined above, involves the single electron photooxidation of a range of molecules by organophotocatalysts. Indeed, one of the most noticeable potential benefits to photoredox chemistry that organophotocatalysts can provide is the great range and vast tunability of the redox potentials of these catalysts (**Figure 1.3**). Organophotocatalysts typically access more highly oxidising excited states than their metal based counterparts. This is particularly true relative to the more commonly used Ru/Ir based catalyst with bipyridine and related ligands (BPMPs). This ability of organophotocatalysts to access significantly oxidising but 'stable' (in this context 'stable' is used to imply that the lifetime of the pho-

toexcited state is long enough to allow chemical transformations to occur) is exemplified by the very large value of $E_{DDQ^{T_1}/DDQ^{\bullet-}} = +3.18$ V vs SCE for the T_1 excited state of DDQ.[41] No homogeneous metal based photocatalyst, yet detailed in the literature, is known to have a reduction potential that surpasses or matches this value. TBADT is the homogeneous metal photocatalyst that comes closest to this value, with $E_{TBADT^*/TBADT^{\bullet-}} = +2.44$ V vs SCE.[8,10] This still falls significantly short of the potential for photoexcited DDQ, and TBADT is not yet one of the commonly used metal photocatalysts. For this reason, and its relevance to the work that follows, use of DDQ as an organophotocatalysts will now be discussed.

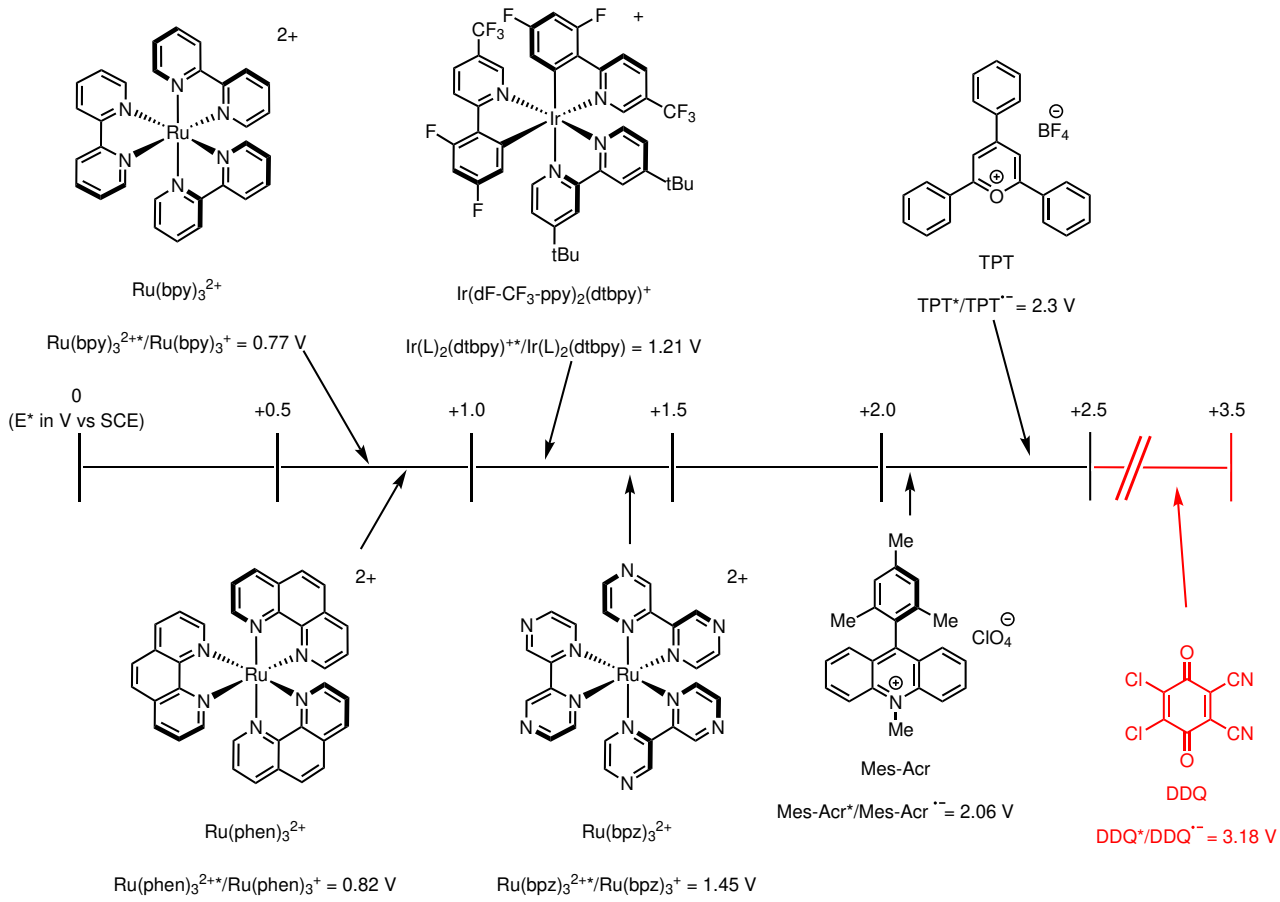

Figure 1.3. *Reduction potentials for a range of oxidising (relative to SCE) photocatalysts.*[4,23,41,63,67–70]

1.2 DDQ as an Organophotocatalyst

2,3-Dichloro-5,6-dicyano-1,4-benzoquinone (DDQ) is, as outlined above, a potent quinone based photoxidant showing activity from the first excited triplet state ($E_{\mathrm{DDQ}^{\mathrm{T}_1}/\mathrm{DDQ}^{\bullet-}} = +3.18$ V vs SCE).[41] It shows maximum light absorption ($\lambda_{\mathrm{max}}^{\mathrm{abs}}$) at around 400 nm (in MeCN),[41] making blue light LEDs ideal for photoexcitation. Excitation of DDQ manifests as an $n - \pi^*$ transition, followed by rapid intersystem crossing (ISC) to give the long lived ($\tau = 2.4\ \mu s$ in MeCN) first excited triplet state.[41] Below are shown the LUMO and HOMO in ground state DDQ and the corresponding SOMO orbitals in the T_1 state of DDQ (**Figure 1.4**, calculated by the author at the B3LYP/6-311G level of theory). Here, the disappearance of the coefficients on the oxygen atoms going from the ground state HOMO (**Figure 1.4b**) to the corresponding SOMO (**Figure 1.4d**), and the concomitant increase in the coefficient on the ring and cyano groups, is clearly visualised. This is indicative of the $n - \pi^*$ transition.

As well as its lesser known and utilised photooxidations, DDQ is also a moderately strong (and much used) oxidising agent in the ground state ($E_{\mathrm{DDQ/DDQ}^{\bullet-}} = +0.49$ V vs SCE).[71] To use DDQ effectively as a photooxidant, therefore, it must be ensured that oxidation reactions will not occur from the ground state and complicate the reactivity. Indeed, the inherent stability of the radical anion of DDQ ($\mathrm{DDQ}^{\bullet-}$) can be problematic as it retards the oxidation of $\mathrm{DDQ}^{\bullet-}$ needed to return DDQ to the catalytic cycle. Solutions to this potential issue will be discussed in the context of the situations under which it arises (see below). As may be expected the charge density in $\mathrm{DDQ}^{\bullet-}$ is spread over many electronegative atoms, with charge build-up occurring mainly on the oxygen atoms, and to a lesser extent on nitrogen. A natural population analysis (often referred to as a natural bond order, NBO, analysis) is a common computational method for visualising the charge distribution within a molecule. Below is shown the summary

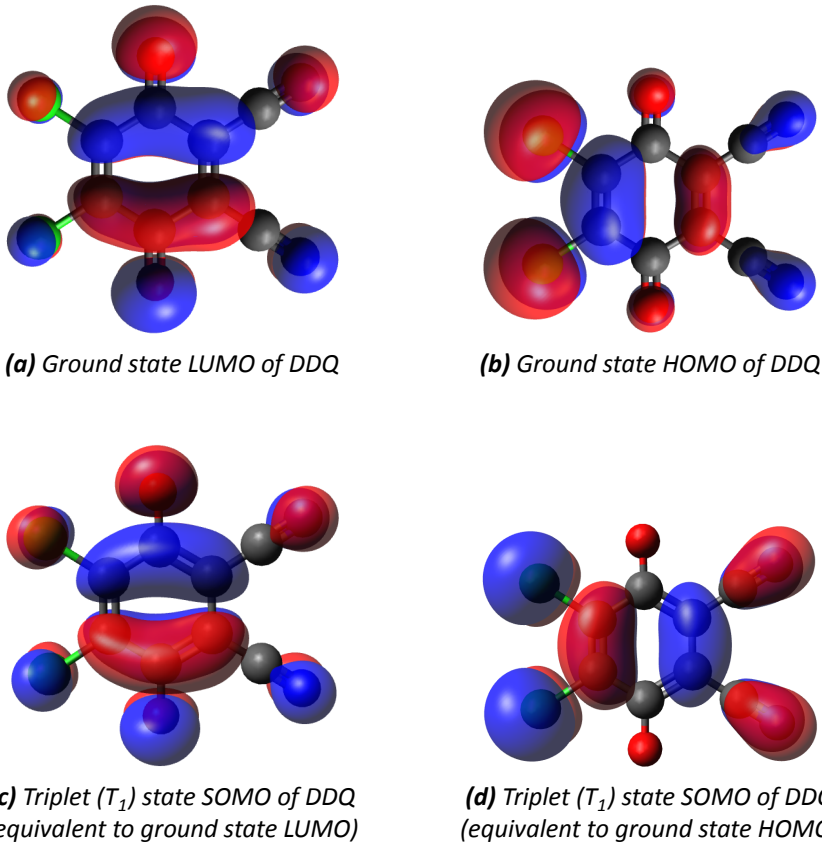

(a) *Ground state LUMO of DDQ*

(b) *Ground state HOMO of DDQ*

(c) *Triplet (T_1) state SOMO of DDQ (equivalent to ground state LUMO)*

(d) *Triplet (T_1) state SOMO of DDQ (equivalent to ground state HOMO)*

Figure 1.4. *Molecular orbitals, calculated by the author at the B3LYP/6-311G level of theory, of ground state and first excited triplet state (T_1) of DDQ.*

of the findings of our NBO analysis for $DDQ^{\bullet -}$ (**Figure 1.5**), the full details of which can be found in **Subsection 5.3.1**. The largest (most negative) charge build up is localised on the oxygen atoms, with the second most being on nitrogen. While this is unsurprising, it is nonetheless informative to see how relatively low these magnitudes are, demonstrating just how stable the DDQ radical anion is.

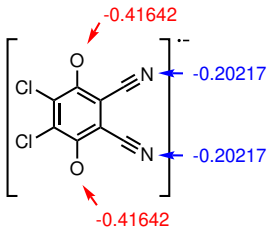

Figure 1.5. *Largest charge build ups found in the NBO analysis of $DDQ^{\bullet -}$, conducted by the author at the B3LYP/6-31G(d,p) level of theory.*

The other important caveat to the use of DDQ as a photocatalyst, is the simple fact that it

is an efficient Michael acceptor.[42] Hence, reagents and conditions must be chosen with care in order to prevent unwanted side reactions and catalyst deactivation.

What now follows is a discussion of the reported literature in which DDQ is utilised as a photocatalyst, at the start of our work. As would be expected, this chemistry was dominated by photooxidations, and highlights well the advantages and disadvantages in using DDQ for this purpose.

1.2.1 Fukuzumi method for photoexcited DDQ catalysed arene oxidation

Fukuzumi and coworkers reported, in 2013, a method for the direct oxidation of benzene to phenol.[41] This method utilised DDQ as the photocatalyst, O_2 as terminal oxidant, *tert*-butyl nitrite (TBN) as a catalytic reoxidant, and H_2O as nucleophile (**Scheme 1.5**).

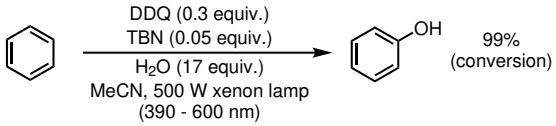

Scheme 1.5. *Fukuzumi method for photochemical conversion of benzene into phenol.*[41]

The mechanistic proposal for this chemistry (**Scheme 1.6**) invokes the single electron oxidation of benzene by photoexcited DDQ*, in the T_1 state, to form the radical cation of benzene ($PhH^{\bullet+}$) and the radical anion of DDQ ($DDQ^{\bullet-}$). The characteristics of such radical cations, along with synthetically relevant examples, will be presented in a later section of this discussion (**Section 1.3**). Once the radical cation has been formed it can accept an electron back from $DDQ^{\bullet-}$ to reform benzene and ground state DDQ. Alternatively, the radical cation can undergo nucleophilic attack by water which, following deprotonation and hydrogen atom abstraction, results in the phenol product.

The cycle is completed by oxidation of the reduced DDQ ($DDQH_2$) by O_2 as the terminal oxidant. It should be acknowledged that this reoxidation of $DDQH_2$ to DDQ by O_2 is not

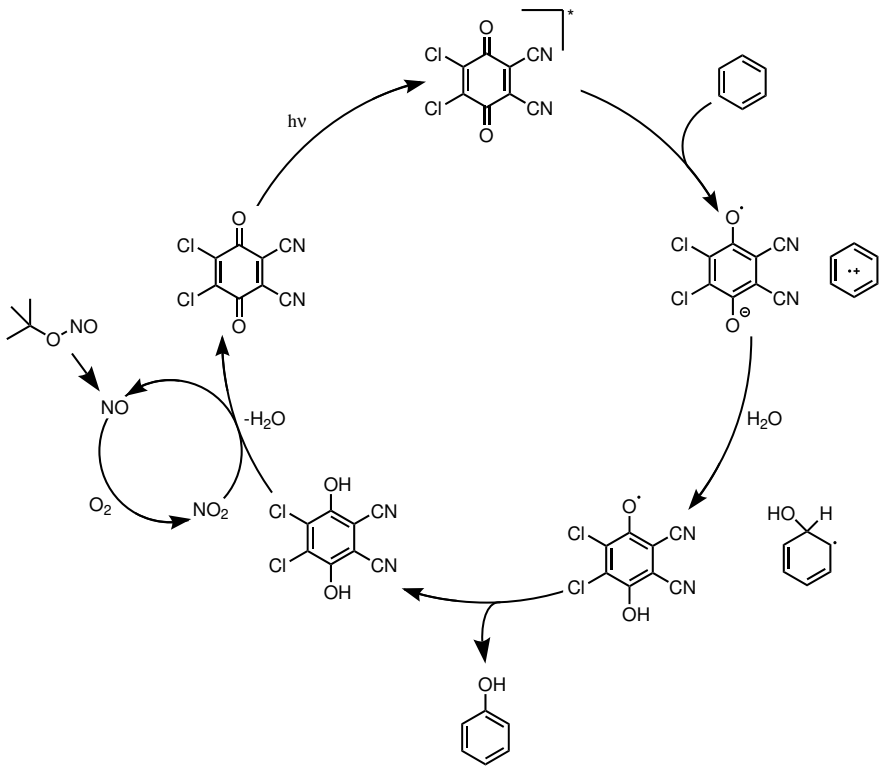

Scheme 1.6. *Mechanism proposed by Fukuzumi and coworkers, for the photochemical oxidation of benzene into phenol.*[41]

thermodynamically favourable without the NO/NO_2 redox couple – and hence without the addition of tert-butyl nitrite (TBN) to the reaction. The reduction potential of O_2, $E_{O_2/H_2O_2} = +0.67$ V vs SHE, is not sufficiently large enough to overcome that of DDQ (in the $DDQ/DDQH_2$ redox couple), $E_{DDQ/DDQH_2} = +0.75$ V vs SHE.[72,73] However, the NO/NO_2 redox couple obviates this problem as NO reduces O_2 *via* a four-electron process (without forming H_2O_2). Once formed, NO_2 is able to reoxidise $DDQH_2$ (although literature data is unclear with respect to the value of reduction potential the NO/NO_2 redox couple).[72,73]

The lack of further oxidation of the phenol product is initially surprising, given that phenol is much easier to oxidise than benzene ($E_{PhOH^{\bullet+}/PhOH} = +1.60$ V vs SCE, $E_{PhH^{\bullet+}/PhH} = +2.48$ V vs SCE).[74,75] However, it can be understood by examining the rates of two competing processes. Simply, there is competition between rate of nucleophilic attack of water on the radical cation formed and the back electron transfer from $DDQ^{\bullet-}$. It is intuitive that the rate of

nucleophilic attack on the more 'electron rich' $PhOH^{\bullet+}$ is less efficient than nucleophilic attack on $PhH^{\bullet+}$. However, this is not the full explanation of why *no* 'over-oxidation' is observed. It is also reasoned by Fukuzumi and coworkers that the driving force for the back electron transfer to $PhH^{\bullet+}$ (1.97 eV) is so great compared with that to $PhOH^{\bullet+}$ (1.09 eV) that the back electron transfer to $PhH^{\bullet+}$ may actually occur in the Marcus inverted region - significantly retarding the electron transfer, while that to $PhOH^{\bullet+}$ occurs rapidly in the Marcus top region (**Figure 1.6**).[76] This hypothesis was supported by relevant absorption spectra. Combined, these factors result in back electron transfer being the only observed outcome.

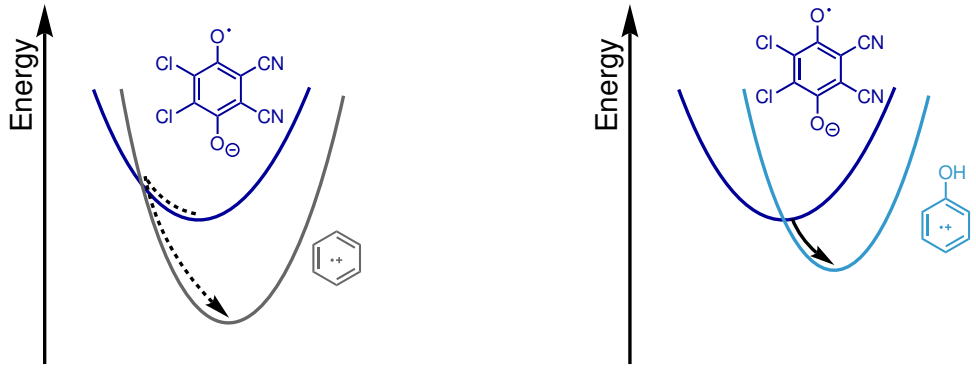

(a) *Back electron transfer (ET) in inverted region. ET slow.*

(b) *Back electron transfer (ET) in 'Top' region. ET very fast.*

Figure 1.6. *A simple qualitative Marcus analysis of the back ET reactions of* $DDQ^{\bullet-}$ *with the radical cation of starting material* ***(a)*** *and product* ***(b)****.*[4,41]

Despite the quantitative yield obtained with benzene, the reaction proved to be highly sensitive to the arene substrate. Even monosubstituted halobenzenes gave greatly reduced yields (**Table 1.1**). This observation was of interest: the potential difference between photoexcited catalyst and substrate was still significant in these cases, and the range of wavelengths used in Fukuzumi's study seemed likely to be wide enough to irradiate potential π-complexes that may have formed (which could have been a factor).[42] While the cause of this significant reduction in yield on moving from benzene to halobenzenes was not immediately obvious,

regaining reaction performance for these substrates became one of the initial problems we sort to solve *via* further optimisation.

Table 1.1. *Fukuzumi's results with halobenzenes.*[41]

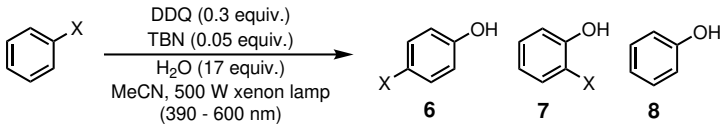

Entry	Halide (X)	GC Yield **6**(%) : **7**(%) : **8**(%)
1	X = Br	11 : 3 : 0
2	X = Cl	28 : 6 : 0
3	X = F	24 : 6 : 14

Another interesting observation (**Table 1.1**) was the formation of phenol (**8**) in 14% from fluorobenzene, as well as the usual oxidation products. This was explained in terms of charge build up, which was highlighted in the NBO analysis conducted by Fukuzumi (**Figure 1.7**), in the radical cation making *ipso* attack feasible for **11**. Optimisation of this defluorination process is another area explored during the course of our work.

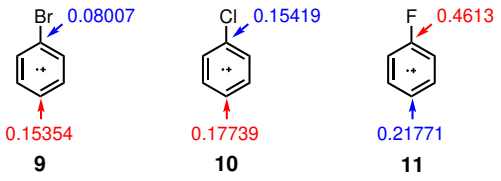

Figure 1.7. *Fukuzumi's NBO analysis results for the radical cations of monosubstituted halobenzenes.*[41]

1.2.2 König method of DDQ-photocatalysed arene oxidation

König is another pioneer of DDQ-mediated arene photooxidation chemistry. König and coworkers studied C – N bond formation for a range of nitrogen nucleophiles and arenes / heteroarenes

(**Scheme 1.7**).[42] Here König, like Fukuzumi, utilised sub-stoichiometric TBN under aerobic conditions to enable turnover (reoxidation) of DDQ. Unlike Fukuzumi, however, König was able to apply this chemistry to a range of substrates.[41] It can be seen that this comes with an increase in TBN loading (from 0.05 equiv. in Fukuzumis work, to 0.20 equiv. here), however, this is not prohibitive modification of conditions, and allows for a slight reduction in DDQ loading from 30 mol% to 20 mol%.

The far greater scope in (hetero)arene (**Scheme 1.7**) in this work relative to that by Fukuzumi can be explained, in some cases, by the greater nucleophilicity (compared to water) of some of the nucleophiles used by König. For example, pyrazole was used as the nucleophile for products **30**–**37**, which would more effectively intercept even short-lived radical cations. However, that certainly cannot be the case for all of the nucleophiles used in this work, especially for the carbamate and related nucleophiles (**12**–**26**). As such König proposed two potential mechanisms (**Scheme 1.8**). The first is clearly analogous to that proposed by Fukuzumi, with an aryl radical cation as the key intermediate.[41] The second involves the single electron oxidation of the nitrogen lone-pair of the nucleophile, by photoexcited DDQ (in the T_1 excited state). It is suggested that this arises from a charge-transfer complex between ground state DDQ and nucleophile. The addition of the deprotonated radical of the nucleophile to the arene gives rise to the same species as the nucleophilic addition of the neutral nucleophile to the aryl radical cation.

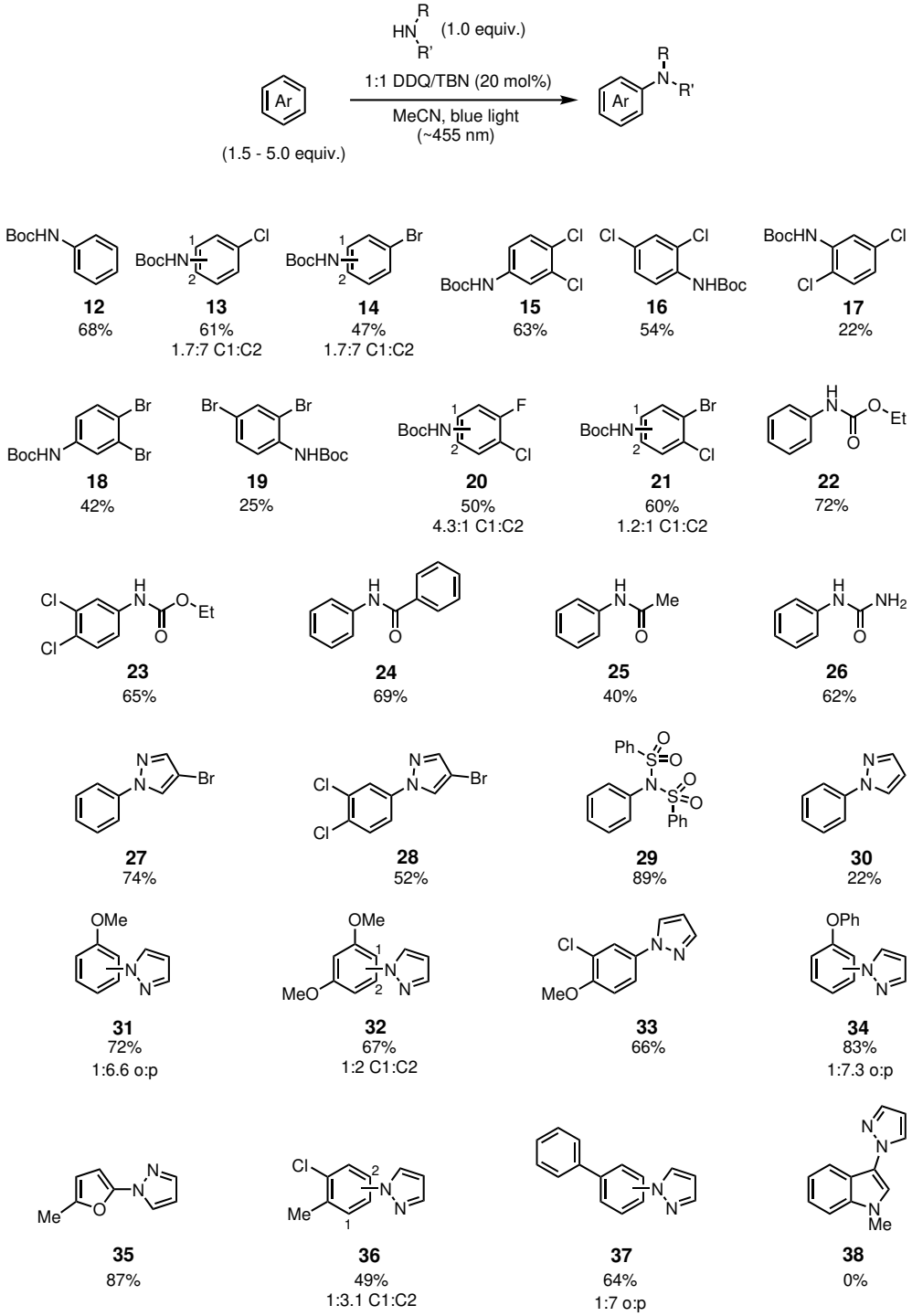

Scheme 1.7. *König and co-workers' method for photochemical C–H bond functionalisation of a range of arenes / heteroarenes and selected scope*[42]

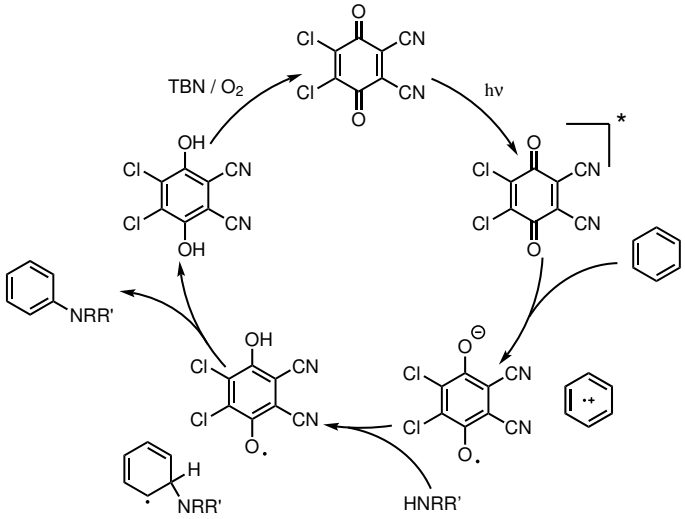

(a) *Arene oxidation mechanism*

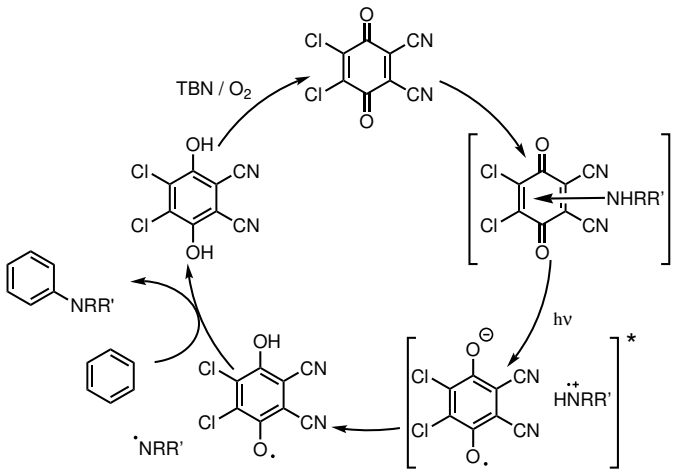

(b) *Nucleophile oxidation mechanism*

Scheme 1.8. *The two mechanisms proposed by König for this arene photooxidation methodology.*[42]

This work by König also highlights one of the fundamental limitations of using DDQ as a catalyst (photo- or otherwise): its high electrophilicity can result in non-reversible reaction with reasonably nucleophilic substrates. König *et al.* were able to isolate one such addition product (**39**) when they attempted to use *N*-methyl indole (**40**) in their chemistry (**Scheme 1.9**). This addition product was the only product of the reaction, hence the 0% yield for **38** (**Scheme 1.7**). As will be demonstrated later, it can be common to run into such difficulties in DDQ catalysis.

In order to help obviate this problem, reaction between the nucleophile and the aryl radical cation generated, *via* photooxidation, must be clean and rapid - ensuring that the nucleophile is consumed before it can engage in catalyst deactivating pathways. The lifetime (τ) of the aryl radical cation must be sufficient to allow this desired reactivity to take place. It can be seen that aryl radical cation intermediates are central to the work described and hence they merit further discussion.

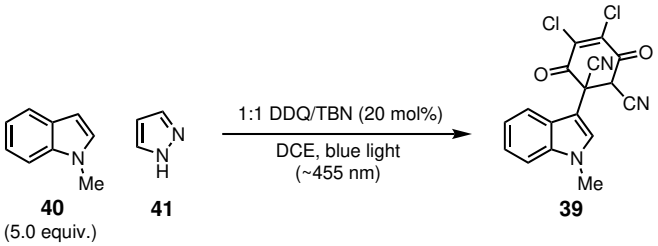

Scheme 1.9. *Addition of N-methyl indole to DDQ under reaction conditions*[42]

1.3 Arene Radical Cations as Reactive Intermediates

Aryl radical cations have been implicated as reactive intermediates in much of the above discussion. Indeed, they play a crucial role in the work that follows. It is worth considering the nature and reactivity of such species. Fortunately, there is much in the literature on these fascinating species. A summary of the pertinent details now follows.

1.3.1 Structure and bonding

The simplest aryl radical cation, that of benzene (**Figure 1.8**), possesses unusual bonding.[77,78] The crude approximation of the molecular orbitals of benzene given by its 'Frost Cycle' correctly predicts its degenerate HOMO.[79] Hence, if the structure of the radical cation was unchanged upon oxidation, this would result in one unpaired electron delocalised between two degenerate orbitals. As such, the structure of the radical cation is in fact Jahn-Teller distorted.[77,78,80]

This distortion can take one of two forms: 'compression' or 'elongation'. Both of these

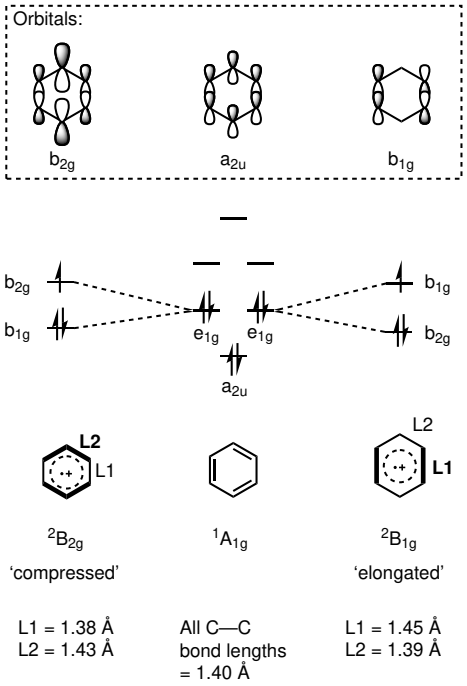

Figure 1.8. *Distortion upon one-electron oxidation of benzene calculated at the B3LYP/6-311G level of theory.[77,78] Adapted from reference [77].*

states show D_{2h} symmetry (neutral, undistorted, benzene of course shows D_{6h} symmetry), but differ in electronic state. The elongated form is the $^2B_{1g}$ state and the compressed form, $^2B_{2g}$. The compressed form is thought to be the lower energy state in the gas phase, but computationally this energy difference came to 0.1 kcal mol^{-1} meaning solvent effects likely play a key role in the structure adopted.[77,78]

Aryl radical cations, as is true of most reactive intermediates, are short lived. Many groups have studied ways of increasing their effective lifetime (τ). One of the most successful methods of doing so, has been to employ fluorinated alcoholic solvents, most noticeably 1,1,1,3,3,3--hexafluoro-2-propanol (HFIP) and 2,2,2-trifluoroethanol (TFE). It is believed that these solvents stabilise the aryl radical cations without (meaningfully) reacting with them, due to their high dielectric constants ($\epsilon = 15.7$ for HFIP), and low nucleophilicities.[81–83]

1.3.2 Reactivity

Aryl radical cations are often seen in hole catalysis mechanisms.[82,84] The two exemplar classes of this 'hole catalysis' chemistry include: Diels-Alder reactions and non-classical S_NAr reactions.[2,23,84] The hole catalysis Diels-Alder chemistry is particularly well developed and a typical example of the process, from Yoon and coworkers, is shown below (**Scheme 1.10**).[85] This chemistry is not overall dearomative but instead involves the aryl radical cation of a styryl species acting as a powerful transient electron withdrawing group (EWG) to enable reactivity with the dienophile. Thus the aryl radical cation intermediate extends 'normal-electron-demand' Diels-Alder chemistry to otherwise 'electron-rich' dienophiles.

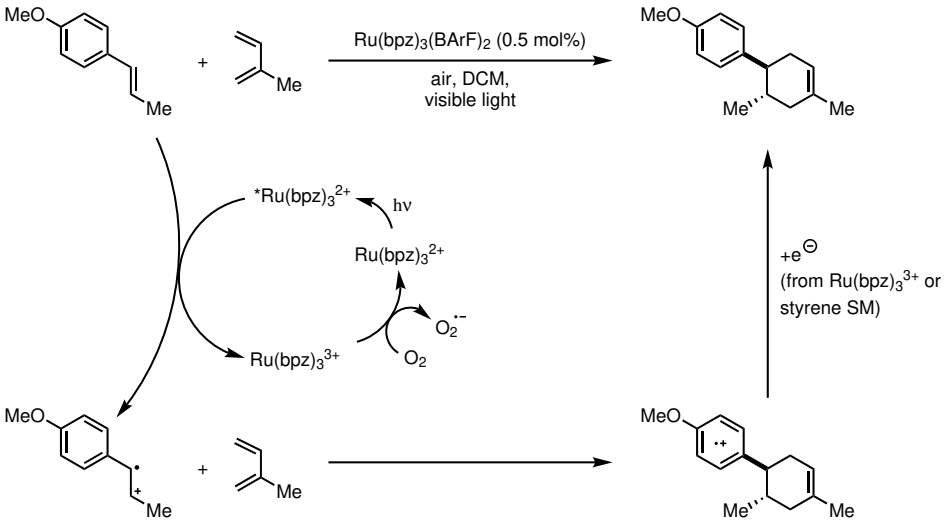

Scheme 1.10. *Diels-Alder chemistry of aryl radical cations, exemplified by the work of Yoon and coworkers.*[85]

The S_NAr chemistry of aryl radical cations is of particular relevance to this thesis. Classical S_NAr is dominated mainly by defluorinations of 'electron-poor' (hetero)arenes.[86,87] As such, a discussion of classical S_NAr can be found within the following section on C–F bond activation (**Section 1.4**). However, whilst the majority of the work contained within this thesis was being conducted there were *no* literature methods for non-classical defluorinative S_NAr proceeding

via aryl radical cations (save for reports of trace side products[23,41]). As will be detailed later, the reason for this was likely the difficulty in oxidising fluoroarenes into their corresponding aryl radical cations (due to the relatively high oxidation potentials of these species).

In fact, it was not until 2017, after we had initially begun the work contained in this thesis, that any non-classical S_NAr, where reactivity was unambiguously ascribed to an aryl radical cation intermediate, was published by Nicewicz and coworkers (**Scheme 1.11**).[23] As can be seen, this is a demethoxylative S_NAr of aryl radical cations, generated *via* photoexcited acridinium catalysts. The anisole starting materials have much more tractable oxidation potentials, relative to the equivalent fluoroarenes, and as such can be oxidised cleanly by the acridinium catalysts used in this work. It can also be seen that the use of TFE as co-solvent, here, is employed in order to stabilise the transient aryl radical cations of the anisoles under study (see **Subsection 1.3.1**).

A selection from the scope of this work is also given below (**Scheme 1.11**). It should be noted that some of the substrates used by Nicewicz did also contain $C_{Ar}-F$ bonds (e.g. **45** & **46**), and in some cases there was evidence of some formation of defluorination products in these cases. This is in line with the observation of defluorination and resultant phenol formation by Fukuzumi (**Subsection 1.2.1**).[41] Both phenomena are most feasibly explained by S_NAr at the $C_{Ar}-F$ centre. It is this defluorinative non-classical S_NAr chemistry we sought to optimise and develop into a practical synthetic method, as part of our work on organophotocatalysis and (hetero)arene functionalisation. However, in order to properly begin the discussion on our work towards such a method, it is first necessary to discuss $C-F$ bond activation as a topic, including classical S_NAr.

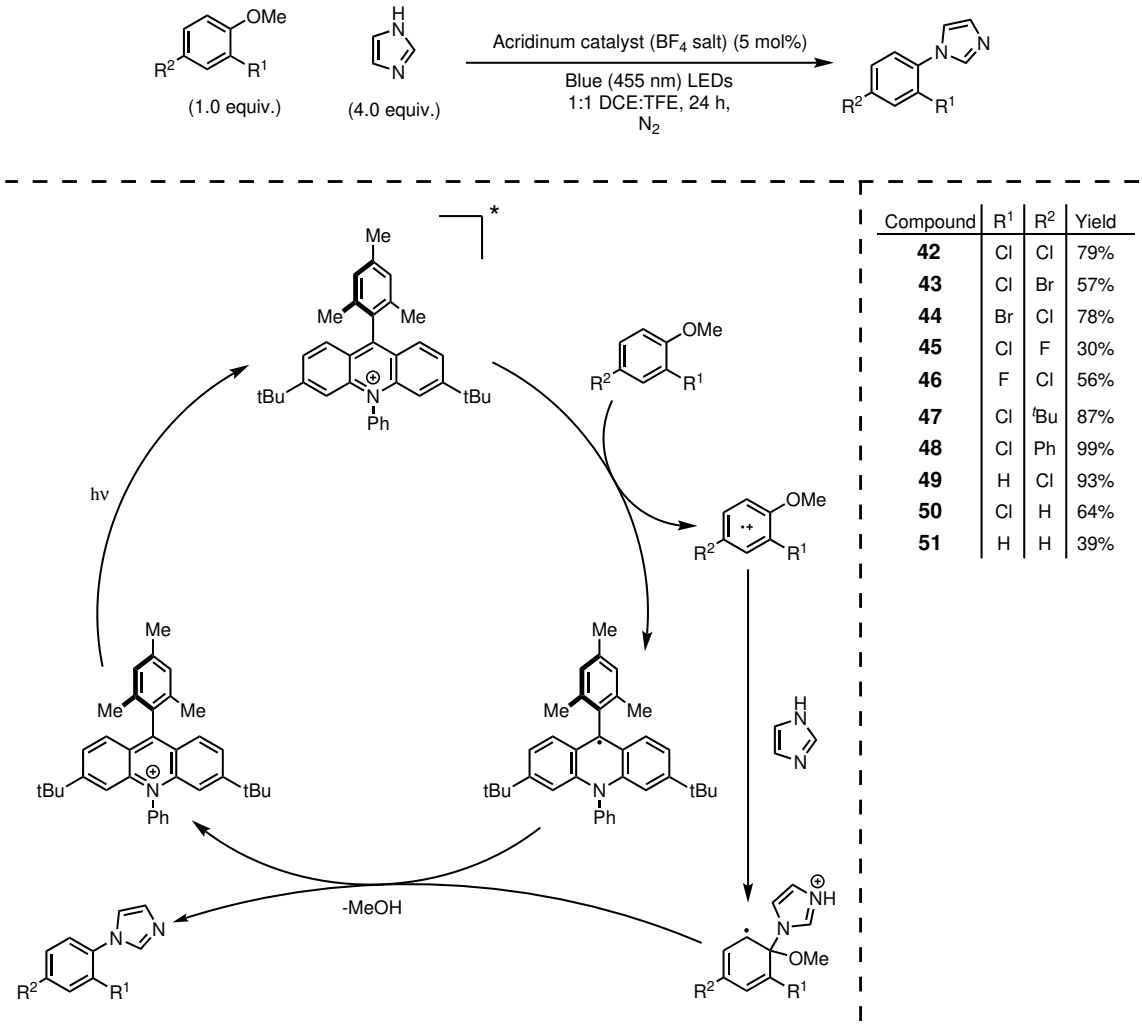

Compound	R^1	R^2	Yield
42	Cl	Cl	79%
43	Cl	Br	57%
44	Br	Cl	78%
45	Cl	F	30%
46	F	Cl	56%
47	Cl	^{t}Bu	87%
48	Cl	Ph	99%
49	H	Cl	93%
50	Cl	H	64%
51	H	H	39%

Scheme 1.11. *Demethoxylative S_NAr of aryl radical cations developed by Nicewicz.* [23]

1.4 C–F Bond Activation

The C–F bond in fluorobenzene is known to have a BDE of around 150 kcal mol^{-1} (154 kcal mol^{-1} in C_6F_6), making it one of the the strongest carbon – heteroatom bonds.[88,89] Hence, C–F bond activation is not an easy task. However, it is often attractive due to the high degree of polarisation in the C–F bond, and due to the orthogonality of many C–F bond functionalisation methods to other substitution conditions. Interest in efficient C–F activation processes has existed for some time now, and further studies continue to appear in the literature.[88,90–95] Indeed, the importance of C–F bond functionalisation is best exemplified by the prevalence

of its most common class: in 2014 of *J. Med. Chem.* manuscripts, S_NAr was found to be the second most commonly mentioned reaction, behind only amide formation.[96] This prevalence is particularly impressive given that it is a reaction that has been under active study since at least the 1930s.[86,87,97,98] Some considerations of classical S_NAr will now be discussed.

1.4.1 Classical S_NAr

The synthetic importance of S_NAr chemistry, particularly to medicinal chemistry, is a point worth emphasizing. In addition to being the second most commonly mentioned reaction (in a study of 2014 *J. Med. Chem.* manuscripts), it was also found to be the third most commonly used final step reaction in the same study;[96] with first and second place going to amide formation and Suzuki-Miyaura coupling respectively. This maybe surprising at first sight, considering how many efficient metal-catalysed process could be used to perform the same net transformation with a range of (pseudo)halides. However, the use of S_NAr chemistry can allow for orthogonality to other halides, and as Moody *et al.* points out, many reactions in the more general organic chemistry literature are performed under palladium (or copper) catalysed conditions with complex ligands, when a simple S_NAr would suffice and give equally high yields.[99] Many researchers assume complications surrounding the fluoride ion (in particular concern around forming HF) to be prohibitive. However, sequestration of fluoride is easily and efficiently achieved with inexpensive and readily available salts. Most notably, calcium propionate ($Ca(EtCO_2)_2$) which, when included in S_NAr reactions (as 1 equivalent), was able to reduce fluoride levels in the aqueous wash to ≈9ppm (down from >1300ppm in the control).[100] As such, the issue is easily obviated and S_NAr processes are operationally straightforward.

The traditional view of S_NAr is that of a simple two-step (addition-elimination) process, proceeding *via* a Meisenheimer complex (e.g. **52a**).[86,87] However, the degree of concerted-

ness in S_NAr is a subject which has been under scrutiny for decades, as work by Williams and others demonstrates.[101,102] Recent work by Jacobsen *et al.*, following on from these earlier studies, details very clearly how this idealised view from undergraduate studies only truly holds under highly specific reaction conditions.[103] In the most archetypal of cases (first scheme, **Scheme 1.12**); where the leaving group is fluoride (and hence bond breaking is slow, allowing for powerful inductive stabilisation of the resultant Meisenheimer complex) *and* where powerful electron withdrawing groups (EWGs) are attached (allowing for significant mesomeric stabilisation of the resultant Meisenheimer complex **52a**), the Meisenheimer complex is a 'true' intermediate and the two-step mechanism holds. However, when a better leaving group is being substituted on a ring system with lower capacity to stabilise the charge build up, the Meisenheimer 'complex' (**53a**) was found to be the transition state of a concerted reaction (second scheme, **Scheme 1.12**). Finally, Jacobsen and co-workers demonstrated a so-called 'borderline' example (third scheme, **Scheme 1.12**), where a moderate leaving group (chloride) is used and there is a high degree of mesomeric stabilisation of charge build up. Here the Meisenheimer complex (**54a**) is neither truly an intermediate, nor truly a transition state. This unusual borderline line case is best understood from a qualitative Marcus theory analysis (**Figure 1.9c**).[103]

Jacobsen verified these findings by use of natural abundance ^{13}C KIE experiments (utilising $^{13}C-{}^{19}F$ satellite peaks in the ^{19}F NMR spectrum), and computational work. It should be noted that in the concerted case (second scheme, **Scheme 1.12**), there is significant donation of electron density from the incoming nucleophile into the $C=N\,\pi^*$ antibonding orbital, and donation of of the nitrogen lone pair (n_N) into the $C-Br\,\sigma^*$ antibonding orbital.

This work highlights the importance of concerted S_NAr reactions. Indeed, interest in 'concerted S_NAr' (sometimes referred to as 'cS_NAr') has grown in the literature.[104,105] Although

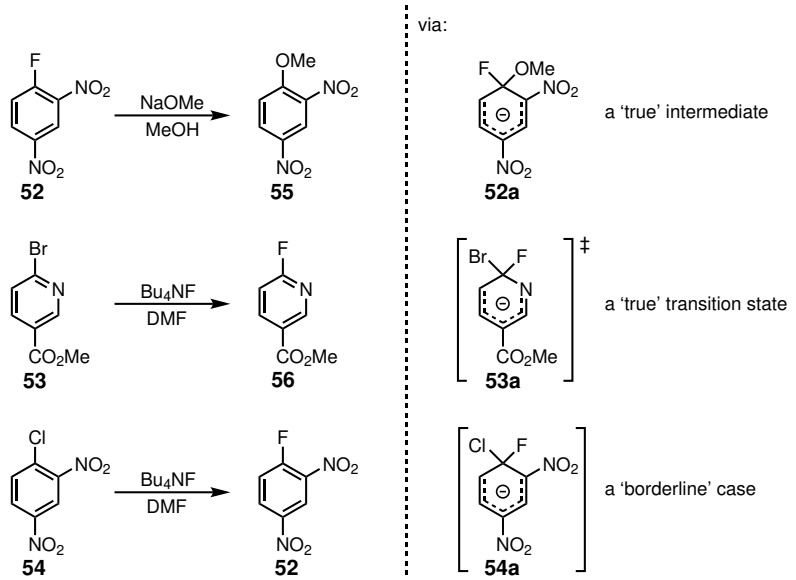

Scheme 1.12. *Jacobsen examples of S_NAr reactions where the so-called 'Meisenheimer complex' can be seen as: a 'true' intermediate (first scheme), a 'true' TS‡ (second scheme), or as a borderline case (third scheme).*[103]

traditional stereochemical dogma will, rightly, have us discount simple nucleophilic attack on the C–X σ* orbital of an aryl halide, we must be cognizant that this only holds when the transition state is 'starting material - like'.[103] The computational work here suggest that the transition state in these concerted S_NAr reactions more closely resembles the charge distribution in the Meisenheimer complex, a 'Meisenheimer transition state'.

As can be interpreted from this work, the ease at which the leaving group can be expelled plays an import role in determining the nature of the reaction pathway for the transformation. This being a consideration which may otherwise have been overlooked, especially given the tendency to focus on the addition (usually rate-limiting) step of classical S_NAr reaction.[86,87] This means it is worth understanding solvent effects (and the effects of other additives) on loss of fluoride as this may be enough to shift the reaction pathway from a two-step mechanism to a more borderline case (or even from a borderline situation to a truly concerted mechanism). As such, these effects will now be discussed.

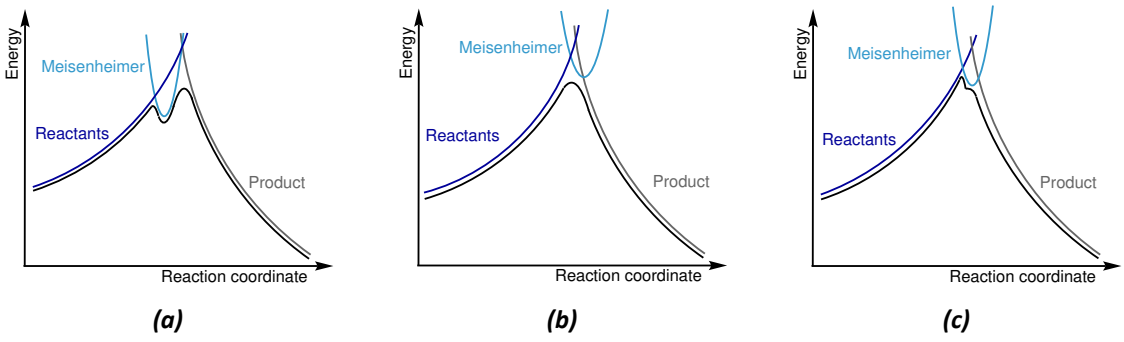

Figure 1.9. *Qualitative Marcus analysis for the cases of S_NAr discussed.* ***(a)*** *Shows the case where Meisenheimer complex is stable and long lived enough to become an intermediate on the reaction pathway.* ***(b)*** *Shows the case for an poorly stabilised Meisenheimer 'complex', where it can be treated as the transition state for the reaction.* ***(c)*** *Shows the borderline case, here the Meisenheimer complex is not a maxima ($TS^{\ddagger}$), but neither is it a true minima (intermediate).*[103] *Adapted from refrence [103].*

1.4.2 Solvent effects

The role of solvent in C–F bond activation is an important one. Organofluorine species have been shown to have significant hydrogen bonding ability.[106] Indeed, hydrogen bonding has been used to great effect in activating C–F bonds to different reactions involving loss of fluoride.[95] A number of these examples come from the Paquin group and include the use of water/isopropanol,[91] and triols,[90,93] as the hydrogen bond donor (HBD). Paquin and coworkers use of 1:1 water/isopropanol (**Scheme 1.13**) demonstrates the utilisation of even moderate HBD to great effect in C–F activation.[91] Here Paquin showed, *via* DFT calculation, that a triple arrangement of water molecules formed around the departing F^-, increasing its leaving group ability. This arrangement of water molecules lead to their work on triol-based activation. Given the strong preference of fluorinated alcoholic solvents to form strong hydrogen bonding interactions, it is little surprise that solvents such as HFIP have been used to great effect in C–F bond activation reactions.[92,94] It is worth considering that these fluorinated alcoholic solvents are efficient both at activating the leaving fluoride group *via* hydrogen bonding interactions

and, as outlined in the discussion on radical cation stabilisation (**Subsection 1.3.1**), stabilising cations (mainly due to there high dielectric constants and low reactivity to cations). This is especially relevant given that radical cations may be key intermediates in these C–F bond functionalisation processes.[81–83]

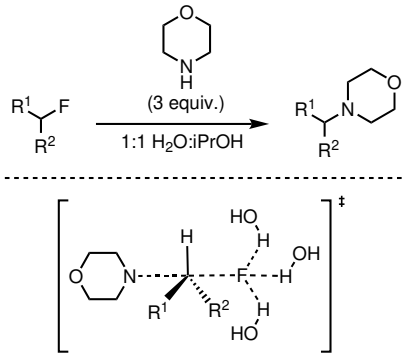

Scheme 1.13. *Scheme showing the 1:1 water:IPA assisted S_N2 of an alkyl fluoride by Paquin et al.*[91]

1.5 Project Aims

With consideration of the large body of work outlined above, we sought to develop operationally simple photochemical transformations utilising organophotocatalysis. In particular, we recognized a disconnect between the proficiency with which DDQ can perform photooxidations ($E_{DDQ^T1/DDQ^{\bullet-}} = +3.18$ V vs SCE),[41] and low number of literature examples which exploit this efficient process. As such, the work which follows focuses on the use of DDQ as a photocatalyst (with a few exceptions where relevant). In doing so, we investigate single electron oxidations of substrates (e.g. fluoroarenes) whose oxidation potential are beyond the operationally useful range of most bipyridyl metal photocatalyst (BPMP) and many of the other organophotocatalysts also. In this way we sought to generate highly destabilised radical cations, which could then readily combine with nucleophiles. This work can broadly be split into net oxidative processes, and net redox neutral processes (e.g. photochemical S_NAr).

Of the relevant literature presented in the preceding sections, there is one notable omis-

sion. In 2020 Lambert *et al.* published on photoelectrochemical defluorinative S_NAr – with a DDQ photocatalyst,[107] not long before we published on a similar but purely photochemical process.[108] The work of Lambert and coworkers is instead presented, and discussed fully, within the Results and Discussions section of this thesis (**Subsection 3.2.8**), immediately following discussion of our method. This allows for a more comparative analysis of these similar works.

Of the chemistry that follows, the results of the net oxidative processes can be seen as more mixed than those of the net redox neutral chemistries. This can, in part, be rationalised in terms of the inherent difficulties of utilising terminal oxidants in photochemical reactions (due to the issues surrounding both solubility and importantly triplet quenching). Indeed, Yoon and others often emphasize the heuristic that electrochemical processes are more efficient at net redox reactions while photochemistry is generally superior in terms of net redox neutral reactions.[109,110] This general observation is often explained in terms of the homogeneity of the electron sink and source (the photocatalyst) throughout the reaction medium - in contrast to the case in electrochemistry where diffusion to the electrodes is required for a 'back-electron transfer' process to occur.[110] Despite this, it was study of these net oxidative processes that resulted in our net redox neutral processes, and as such it is useful to detail these chemistries first.

Chapter 2

Photochemical DDQ-Mediated Oxidations of Simple Arenes

2.1 Chapter Introduction

Discussions in this chapter will focus on efforts to utilise DDQ as a photocatalyst (see **Section 1.2**) for arene C–H functionalisation (oxidation). The literature precedents for this chemistry, the work of Fukuzumi and König,[41,42] were known when we sought to add to this field of study and have been discussed previously (**Subsection 1.2.1** and **Subsection 1.2.2** respectively). However, it should be mentioned that König's results were published slightly after initial investigations had begun. The scope of this chapter will, therefore, include: investigations into the expansion of the Fukuzumi method to other arenes (**Section 2.2**), and the development of a dual C–H functionalisation (**Section 2.3**). Additionally, discussion will also consider the suitability of the chosen photocatalyst using computational methods as an aid to reaction reaction design (**Subsection 2.3.2**).

2.2 Photochemical C–H Bond Hydroxylation of Arenes

We initially began our attempt to develop a photochemical C–F bond functionalisation starting from conditions based on the Fukuzumi procedure, with slight but important modifications (**Scheme 2.1**).[41] Firstly, a higher (tripled) loading of *tert*-butyl nitrite (TBN) was used compared with Fukuzumi's conditions, in the hope of achieving greater conversion. Secondly and significantly, a truly visible light, light source was utilised in this work (as opposed to the xenon lamp of Fukuzumi's work, this is discussed more below). Additionally, fewer equivalents of H_2O were used as we found no benefit to increasing nucleophile loading beyond 1.5 equivalents.

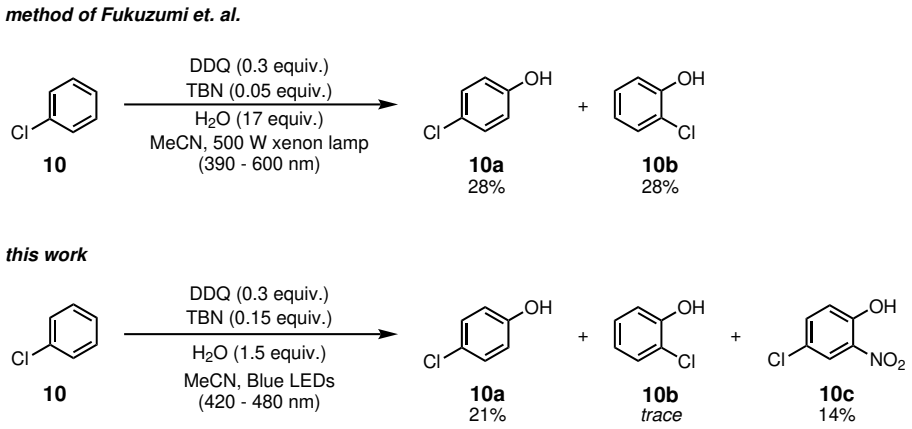

Scheme 2.1. *Comparison of Fukuzumi's method, and the modified method presented here, with chlorobenzene (**10**) as a substrate.*[41]

The difference in product distribution (**Scheme 2.1**), in particular the formation of the nitrated product **10c**, is unmistakable. Indeed, the recorded yield of this product (14%) is highly indicative of the cause (it being approximately identical to the loading of TBN used). However, before fully discussing the implications of this, it is worth understanding the differences in the light source used in this work compared to that utilised by Fukuzumi.

There is extensive work in the photochemistry literature detailing the difference in reaction outcome when difference light sources are employed.[111] Therefore, it is worth considering if this effect does play a part in the differential product distribution between the methods.

The effect of ultraviolet wavelengths in the method of Fukuzumi could potentially be suppressing the formation of the nitrated product (**10c**). The attempt to move away from the UV emitting xenon lamp of Fukuzumi and coworkers, in favour of blue LEDs, was done to improve the energy efficiency, the safety and the scope of the chemistry (as well as for reasons of operational simplicity).[2,112] Any improvement in scope was hoped to be enabled by eliminating (or reducing) the excitation of molecules present in the reaction other than DDQ, which UV wavelengths would be more apt to do, and thus prevent (or minimise) side reactions.[2,112] The details and differences between these light source will now be more fully discussed.

2.2.1 Effect of light source and photochemical setup

In their literature procedure, Fukuzumi *et al.* utilised a 500 W xenon lamp with a colour glass filter, giving irradiation between 390–600 nm.[41] In contrast, we used 3 W LEDs giving irradiation between 420–480 nm (**Subsection 5.2**). This may initially seem like an inefficient choice, given that DDQ has a maximum light absorption (λ_{max}^{abs}) at around 400 nm (in MeCN).[41] However, DDQ shows a broad absorption band, and we were prepared to screen a range of solvents in this work which would likely perturb the λ_{max}^{abs}. Additionally, and on this theme, DDQ is known to form charge transfer complexes with substrates and nucleophiles.[42] This would again result in a new λ_{max}^{abs}, the λ_{max}^{abs} of the charge transfer complex. Empirical literature data suggested that the blue wavelengths of light were effective in eliciting excitation in many of these DDQ-X transfer complexes; as such we were keen to try and develop this chemistry as a truly visible light processes.[42,113] This would engender greater practicality in the method as discussed. Indeed, this hope seems to have been borne out by the first result (**Scheme 2.1**) – showing that these lights were able to promote the reaction in comparable yields to the xenon lamp of Fukuzumi (albeit with a slight change in conditions).

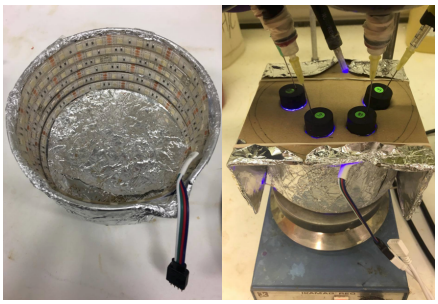

(a) *Initial photosetup used.*

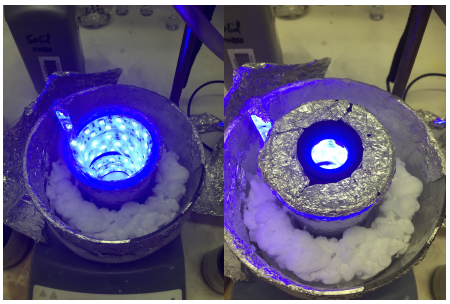

(b) *second generation photosetup used.*

Figure 2.1. *The photosetups (or 'photoreactors') used for the C–H activation chemistry under discussion. Both are based on same 3 W blue LEDs. However,* ***(a)*** *showed a lower light intensity than* ***(b)*** *but could run more samples simultaneously.*[4,41]

For this early work, two photoreactors were made in order to house the LEDs and reaction vessels. Both of these light setups (the terms light setups, photosetups, and photoreactors will be used interchangeably in this thesis) are based on the same 3 W blue LEDs strips. In the initially constructed photoreactor (**Figure 2.1a**), a strip of LEDs was placed around the inside of a crystallisation beaker, and a cardboard 'rack' placed on top so that up to four vials could be held inside the reactor at a distance of 2 cm from the LEDs. The setup was cooled with a nitrogen line and was measured to have an operating temperature of approximately 30 ^{o}C. The second generation photoreactor (**Figure 2.1b**) had the same continual strip of 3 W blue LEDs placed around the inside of a 100 mL beaker, and a rubber Büchner ring placed on top so that a vial could be held inside the reactor. This meant a much greater light intensity for each reaction, but allowed for only one sample to run at a time. This setup also generated much more heat and so the reactor itself was then placed in the center of a crystallisation dish filled with dry ice pellets. This was found to be the most efficient way to maintain a constant internal temperature, with only occasional 'top ups' of dry ice during the course of a reaction. This method was found to cool the internal temperature to approximately -35 ^{o}C and maintain this temperature for extended periods.

Even with the significantly lower internal temperature of second generation photoreactor (about 65 ^{o}C cooler than the initial photoreactor), it was able to greatly outperform the lower light intensity initial photoreactor in terms of reaction time. This is to be entirely expected of a truly photochemical process, and the magnitude of this effect is highlighted in the difference between the time course study with the initial photoreactor (**Table 2.1**) and that with the second generation setup (**Table 2.2**).

Table 2.1. *Time course study using initial photoreactor*

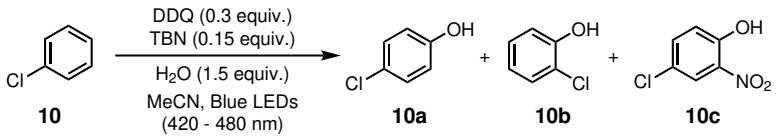

Entry	Time (h)	GC Yield				
		10a(%)	:	**10b**(%)	:	**10c**(%)
1	1	*trace*	:	*trace*	:	16
2	7	*trace*	:	*trace*	:	15
3	24	15	:	*trace*	:	17
4	48	17	:	*trace*	:	16
5	72	21	:	*trace*	:	14

Examining the time course data for this reaction (**Table 2.1** and **Table 2.2**) provides another mechanistic insight. What is likely happening is the rapid nitration of all of the initially formed phenol **10a** to give **10c**. Once this nitration has consumed the NO/NO_2, generated from the TBN, only slow formation of phenol product (**10a**) is seen – with one turn over of DDQ. Alternatively, as **10c** is itself a blue light absorbing compound (being bright yellow on isolation), it could be inhibiting further formation of **10a** by reducing effective light intensity

Table 2.2. *Time course study using second generation photoreactor*

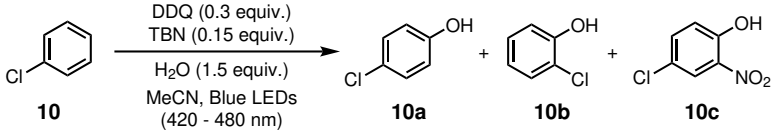

Entry	Time (h)	GC Yield				
		10a(%)	:	**10b**(%)	:	**10c**(%)
1	1	21	:	*trace*	:	17
2	4	22	:	*trace*	:	17
3	7	21	:	*trace*	:	16
4	7^a	14	:	*trace*	:	13

^{a}Reaction run without dry ice cooling.

for DDQ. Conversely, it is also possible that the additional slow formation of **10a** (seen after 24 h in **Table 2.1**) is due to **10c** acting as a photocatalyst with $DDQH_2$ no longer being oxidised into active catalyst at a sufficient rate. Presently, data is unavailable to further examine either hypotheses, but this could form the basis of future work – with controls including resubjecting **10c** and/or **10a** to the standard reaction conditions and noting product distribution, and also investigating the use of **10** as a catalyst for this transformation.

No difference in result was obtained when using a balloon of air compared to having the vial headspace, and any air absorbed by the solvent, as the only supply of air for the reaction. This would imply that the headspace volume of air was sufficient for these reaction. The stoichiometry for this proposal is consistent with complete consumption of the added TBN (0.15 equiv.) if we allow the 13–17% range of **10c** yield (**Table 2.1** and **Table 2.2**) to approximate to 15% (reasonable given the accuracy of GC trace area measurement and any μL syringe measurement error). This reinforces the initial speculation that product **10c** arises from nitration

of phenol product **10a**. Further experiments were conducted to confirm this hypotheses and to try to suppress the formation of **10c** whilst increasing conversion to the desired **10a**. This work is presented below.

2.2.2 Reaction additives - oxidants & acids

Attempts were made to better understand the formation of nitrophenol **10c** and thereby afford a way to suppress it. Control experiments were performed to ensure that once the nitrophenol product (**10c**) had formed in the reaction, it was chemically stable (**Scheme 2.2**). We also discovered that the hydroxylation reaction did not occur in the absence of irradiation but the phenols formed could be nitrated with TBN in the dark. These results were later confirmed by the work of Heinrich *et al.* who demonstrated a similar process.[114] It is of interest to note that, that Heinrich's work also demonstrated lower yields for nitration under UV irradiation (as compared to visible light irradiation) but not complete inhibition.[114]

As described previously (**Subsection 1.2.1**), TBN is present in the reaction mixture in order to catalyse the reoxidation of $DDQH_2$ back to DDQ by molecular oxygen. It follows then, that the simple solution to eliminate this nitration byproduct (**10c**) would be to change the oxidant. A range of alternative oxidants to TBN were screened, and these results are shown below (**Table 2.3**). However, it proved difficult to find a suitable replacement to TBN, even when using species such as iron(II) phthalocyanine (**57**) which has previously been shown to be efficient at similar molecular–oxygen utilising oxidations.[115,116] Indeed, iron(II) phthalocyanine (**57**) has been used in the literature to perform the same function as TBN in other DDQ oxidations – albeit non-photochemical oxidations – by Shen and coworkers (**Scheme 2.3**).[116]

For cases where the inorganic oxidant was not soluble in the reaction medium (**Table 2.3** Entry 3, 4, 7, and 8), the reaction was also attempted in 1:1 MeCN:H_2O. However, despite

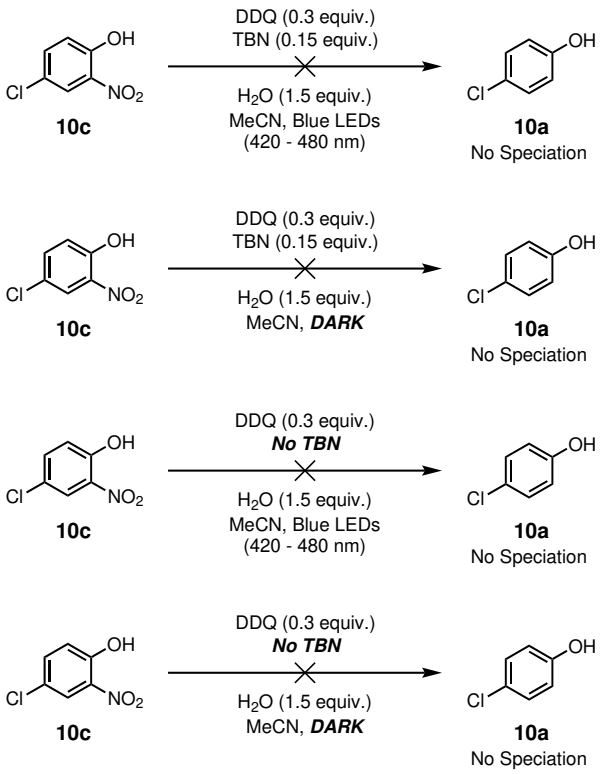

Scheme 2.2. *Control reactions probing the speciation, or lack there of, of the reaction byproduct* ***10c****.*

significantly improved homogeneity, these reactions also exclusively returned only starting material. This is likely due to the instability of the catalyst (DDQ) in water.[117] This irksome limitation of the catalyst is simply due to a Michael reaction between the catalyst and water when excess of water is present. This issue has been touched upon previously (**Section 1.2**).

Mineral acids such as H_2SO_4 (**Table 2.3**, Entry 5 and 6) are inherently oxidising, and for that reason are included here. The data presented does suggest that H_2SO_4 is having an effect on reaction outcome. However, it is possible that this effect is due to H_2SO_4 enabling the proton transfers necessary for the formation of product. Indeed, the work of Fukuzumi and the subsequent theoretical study by Thiel and coworkers, suggest the importance of pH in the mechanism.[41,76] The suggestion being that acid could promote the proton-coupled electron transfer (PCET) step of the mechanism (**Scheme 2.4**) – the conversion of the semiquinone of DDQ ($DDQH^{\bullet}$) and the nucleophile intercepted radical of the arene (**58a**) to reduced DDQ

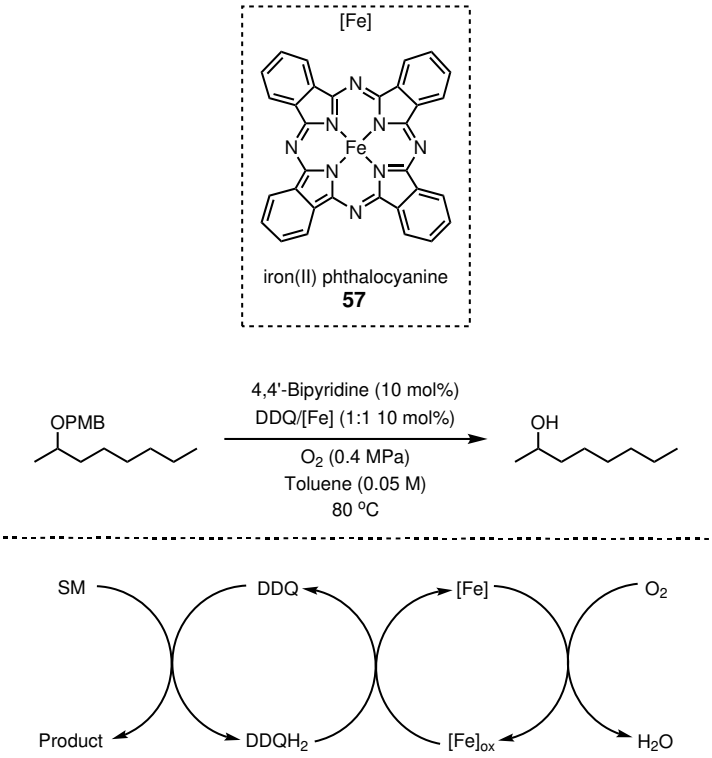

Scheme 2.3. *Use of iron(II) phthalocyanine (**57**) as a reoxidant for DDQ (with O_2 being the terminal oxidant), as demonstrated by Shen and coworkers.* [116]

($DDQH_2$) and phenol (**58**). A more thorough discussion of this mechanism can be found in the Introduction of this thesis (**Subsection 1.2.1**).

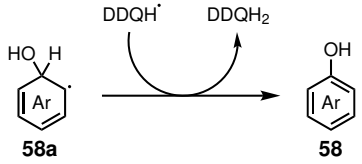

Scheme 2.4. *The proton coupled electron transfer (PCET) step proposed by Fukuzumi in his suggest mechanism for his DDQ photocatalysed C–H activation chemistry; and subsequently highlighted for its acid sensitivity by the theoretical studies of Thiel and coworkers.* [41,76]

Interestingly, when H_2SO_4 (or other acids) were added to the reaction when TBN was present, no noticeable improvement in yield was observed (**Table 2.4**). This would imply a lower reaction pH was not necessarily a factor. However, it should be noted that at the other extreme - when the reaction is repeated with KOH (0.3 equiv.) - the reaction mixture darkens significantly and only starting material is recovered. This is likely attributed to poor catalyst

Table 2.3. *Preliminary oxidant screen*

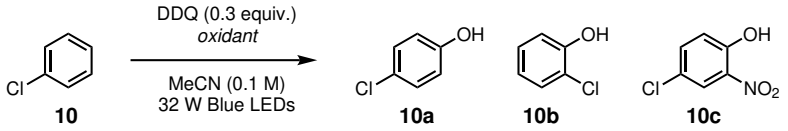

Entry	Oxidant (equiv.)	Observations
1	TBN (0.15)	Bright yellow reaction mixture gradually turning brown. **10a** formed in 21% yield, **10c** formed in 14% yield, and only trace **10b** detected.
2	TBHP (0.3)	Dull yellow reaction mixture gradually darkening. Mostly yielding only starting material but with 8% **10a** by GC-MS.
3	MnO_2 (1.0)	Very dark reaction mixture formed. Oxidant not well solubilised. Only SM recovered.
4	$Mn(OAc)_3 \cdot 2\,H_2O$ (1.0)	Same as Entry 3.
5	H_2SO_4 (0.3)	Bright yellow reaction mixture gradually turning brown. **10a** formed in 16% yield and only trace **10b** detected.
6	H_2SO_4 (1.0)	Bright yellow reaction mixture gradually turning brown. **10a** formed in 18% yield and only trace **10b** detected.[a]
7	Iron(II) phthalocyanine (0.3)	Same as Entry 3.
8	$NaNO_2$ (0.3)	Same as Entry 3.

stability at high pH.[117]

Given that the oxidant is only needed to regenerate DDQ from $DDQH_2$, then it could be imagined that using stoichiometric DDQ without an oxidant would work as well if not more efficiently. However, unexpected results were obtained when DDQ loading was investigated (see below).

2.2.3 Catalyst loading

Although it can be seen as a 'brute-force' approach, it could be envisaged that the simplest method to obviate the encountered catalyst turn over problem would be to increase catalyst

Table 2.4. *Acid screen, with TBN as oxidant.*

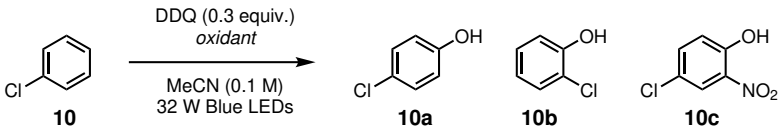

10 **10a** **10b** **10c**

Entry	Acid (0.3 equiv.)	GC Yield					Acid pK_a (in water)	Acid pK_a (in MeCN)[118]
		10a(%)	:	**10b**(%)	:	**10c**(%)		
1	H_2SO_4	22	:	*trace*	:	15	−3	6.72
2	HCl	20	:	*trace*	:	13	−7	9.39
3	H_3PO_4	21	:	*trace*	:	12	2.1	-
4	AcOH	16	:	*trace*	:	13	4.76	27.01
5	TFA	20	:	*trace*	:	13	−0.3	14.16
6	TfOH	12	:	*trace*	:	11	−14	1.52

loading. Interestingly, this approach failed to give improved results (**Table 2.5**). This would imply additional complications beyond simple catalyst turn-over issues.

It could be that there was slow degradation of the catalyst by the water in the reaction. The fact that this was not seen in Fukuzumi's reaction with benzene, could be explained by the initial electron transfer event being more efficient than in the case with chlorobenzene.[41] This would mean a slower reaction for chlorobenzene than benzene and hence, more time for this competing degradation to affect the catalyst. However, if this were the case, we would have expected a better yield from the second generation photoreactor. This would be due to the reaction times being much shorter, a result of the higher light intensity. This higher light intensity would increase the efficiency of DDQ photoexcitation – and hence improve the rate of the desired transformation. The supposed Michael addition by water, however, is a

Table 2.5. *Effect of DDQ loading on reaction progress after 48 H.*

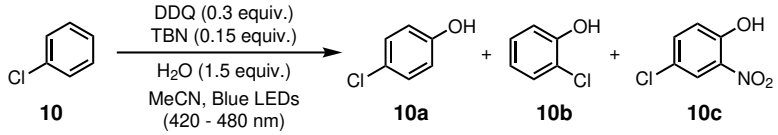

10 **10a** **10b** **10c**

Entry	DDQ Loading	GC Yield				
		10a(%)	:	**10b**(%)	:	**10c**(%)
1	0.3 equiv.	17	:	*trace*	:	16
2	0.5 equiv.	17	:	*trace*	:	12
3	0.7 equiv.	17	:	*trace*	:	12
4	1.0 equiv.	18	:	*trace*	:	13

ground state phenomena and as such it rate should not be affected. As such, this degradation hypothesis cannot be seen to accurately explain the observed results. Further work will need to be undertaken to understand and finally solve this issue.

2.2.4 Results following optimisation

Given the conditions that the optimisation process had found, even if significant changes were not feasible, we wished to determine the scope of this chemistry in its current iteration (**Scheme 2.5**). As would be expected, results for simple alcohols (products **10e–10j**) were similar, although trace reactivity was seen with *t*BuOH as a nucleophile (products **10k–10m**). This may be suggestive of nucleophilic attack being rate determining in this case. As Fukuzumi and Thiels work highlights the reversibility of the electron transfer process, if nucleophilic attack is sluggish the majority of the ion pair complexes (i.e. $DDQ^{\bullet -} - Arene^{\bullet +}$ complexes) would be allowed to relax back to ground state *via* back-electron transfer without progressing through to product.

It can also be seen that the aryl ethers did not nitrate as readily as the phenols. Surprisingly, as **59a** shows, we were unable to get reactivity with internally tethered alcohols. Furthermore, despite the high reactivity of the aryl radical cation intermediates, we were unable to successfully implement weaker nucleophiles – such as acetic acid (see **10d**) – in the reaction. The difference between chloro and bromoarenes (**10** & **9**) was similar to shown by Fukuzumi and of those sampled, reactivity was not seen with the heteroarenes tested (**60**–**63**). These results were somewhat expected as we had failed to overcome the issue of catalyst turnover.

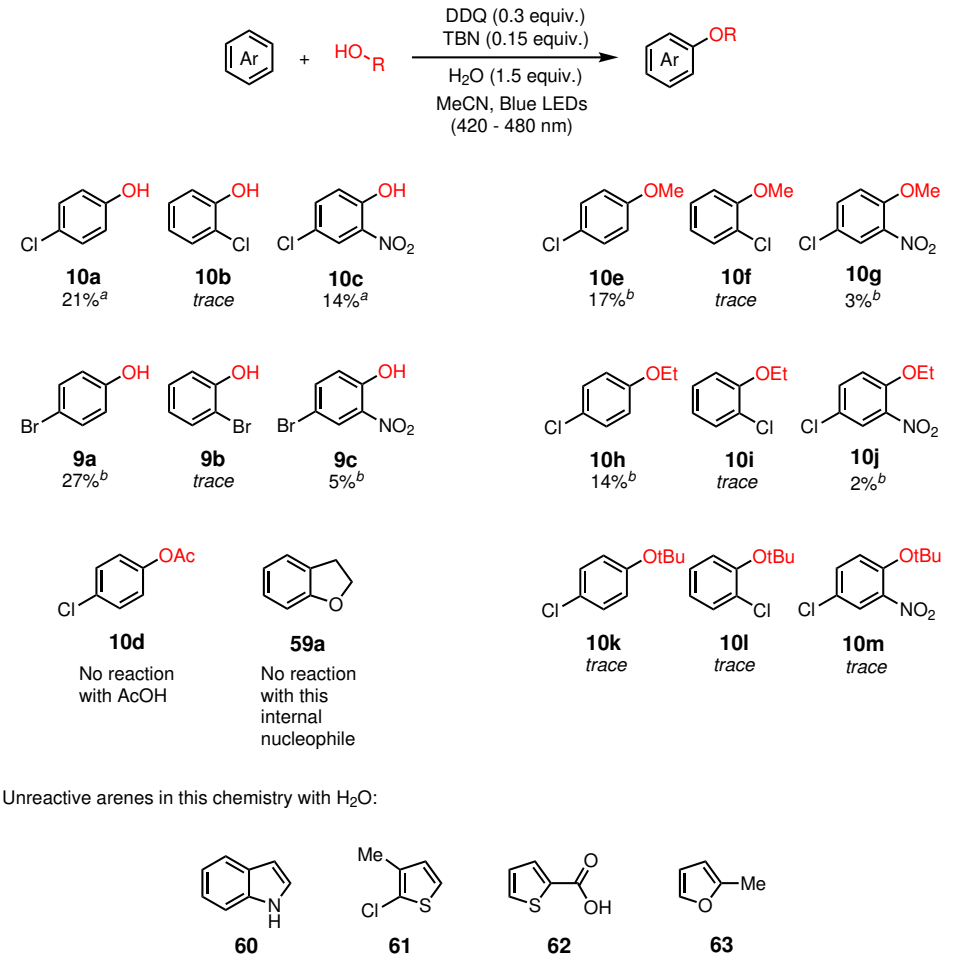

Scheme 2.5. *Scope of this initial photochemical arene oxidation methodology.* [a]*GC yields (see appendix* ***GCMS Traces****).* [b]*NMR yields using 1,3,5-trimethoxybenzene as internal standard.*

It should be noted that reaction solvent was screened in the group by researcher Lucy Harwood and acetonitrile was found to be the optimum choice for the reaction. The reaction

was found to be completely inhibited when the solvent was MeOH, DMSO, or DMF. THF and DCM were found to only give trace amount of product.

The results above (**Scheme 2.5**) did not favour the likelihood of generalising the above method to a wide range of arenes as we had initially hoped. However, the results of the alcohols were suggestive of the possibility that modifications could allow good yields for a range of alcohols with a simple arene. As such, work was done to test this hypothesis using benzene as the simple arene.

Given that similar conversion to that obtained with water was unsurprisingly obtained with the simple alcohols tested, and also that the work of Fukuzumi indicated that benzene was more amenable to these processes,[41] efforts were made towards a method for the convenient photochemical phenylation of alcohols (**Scheme 2.6**). This involved attempts to protect alcohols using DDQ in benzene:TFE solvent mixture. This solvent choice being made to provide excess benzene for the oxidation step, and TFE to help stabilise the reactive intermediates of the reaction pathway (**Subsection 1.3.1**). By this stage success with similar conditions had already been achieved in our work on a different photochemical process (see **Subsection 3.2.2**). Indeed the more powerful light setup used here (which is described in **Subsection 3.2.1**) also had be initial applied to other work and will be discussed more in the following chapter (**Chapter 3**). However, this briefly investigated process is described here as it is more closely related to the other work in this chapter, being that it too is a photooxidation. Despite initial hopes for this process, it failed to give meaningful results with alcohols of greater structural interest than those mentioned previously, e.g. **64** and **65**. This is possibly further indication that these processes are limited by rate of nucleophile attack. While use of benzene co-solvent would have shifted the maximum absorbance band for DDQ, the overall reaction colour was still a clear orange solution indicating that our light source would be effective for

excitation.

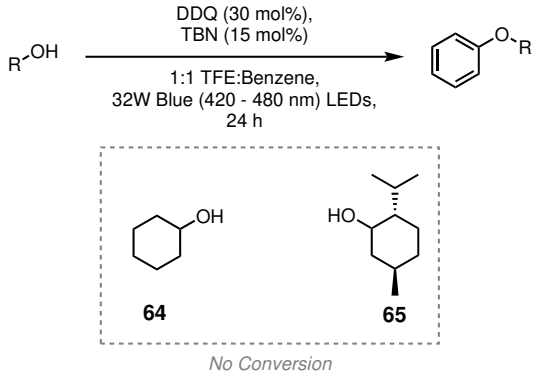

Scheme 2.6. *Photochemical phenylation method.*

Instead of further attempts to investigate this process, the decision was made to return focus to the hydroxylation chemistry described above, but with emphasis now placed on deliberately optimising for the nitration product. It can be seen that this would involve utilising super-stoichiometric TBN loadings. This modification, it was reasoned, should also help alleviate the issues still surrounding catalyst turnover.

2.3 Photochemical Dual Hydroxylation-Nitration of Arenes

In the previously described arene hydroxylation reaction, we observed formation of ∼15% nitrophenol (**10c**). The yield of this product was in line with the amount of TBN used in the reaction (0.15 equiv.). As was by this point expected, when TBN loading was increased above this level, the yield of this product increased concomitantly. At super-stoichiometric TBN loadings (1.2 equiv.), **10c** became the only observed product and was isolated in 74% yield (**Scheme 2.7**).

The results from this short scope (**Scheme 2.7**) show generally more robust results than the equivalent hydroxylation chemistry previously studied. However, the method still cannot reasonably be labeled as generally applicable. As can be seen, much lower conversion was observed for bromobenzene (**9**) than chlorobenzene **10**. Attempting to react iodobenzene (**66**) under these conditions had the somewhat predictable result of causing oxidation of the iodine

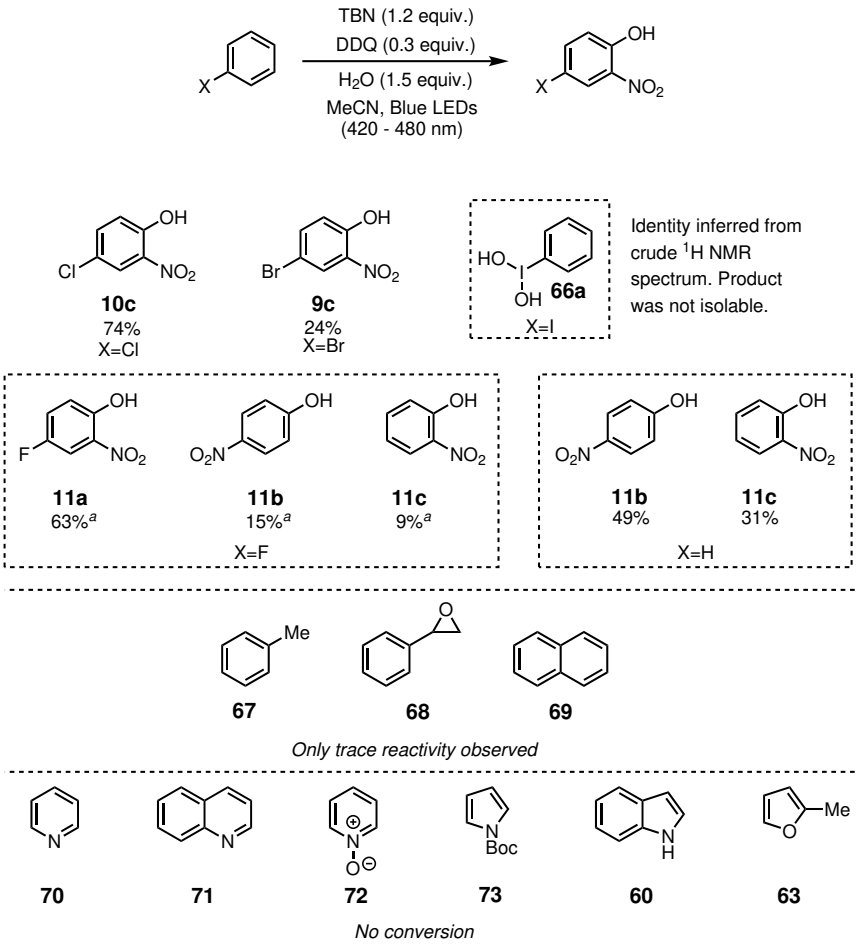

Scheme 2.7. *Scope of dual functionalisation (hydroxylation-nitration) method.*[a] *Conversion by GC.*

atom, as opposed to oxidising the ring (giving **66a**). Benzene shows the expected result of mixed *ortho* and *para* nitrophenol formation (**11b** & **11c**). It can also been seen that almost no headway was made with ring systems other than benzene (**60**, **63**, and **69**–**73**), with even the carbocycle naphthalene (**69**) giving no measurable conversion. Perhaps the most interesting outcome from this scope, however, was that of fluorobenzene (**11**). As well as showing the expected product (**11a**), fluorobenzene also appeared to yield two defluorinated nitrophenols (**11b** & **11c** – the same products seen from using benzene as a substrate). Indeed, this result would go on to spur interest in a different body of work which is presented later in this thesis (**Chapter 3**). For now, no further discussion of these defluorinated products will be given in order to prevent repetition later.

All the results in **Scheme 2.7** were gathered over 7 hr in the second generation photoreactor. In order to try and improve these results, an attempt was made to reduce the reaction time still further *via* construction and investigation of a simple flow reactor. This would also enable scale up of the chemistry. Most of the applications of this setup were in the investigation of the defluoroination result of fluorobenzene (**11**) which is the subject of **Chapter 3**, however, this setup is introduced now as its first implementation was in the scale up of the chlorobenzene (**10**) hydroxylation-nitration reaction.

2.3.1 Application of flow chemistry

Much can be found in the literature on the benefits of flow chemistry, especially pertaining to photochemical reactions.[119,120] Many of the positive attributes of typically associated with flow chemistry complement the needs of photochemistry. Photochemistry, for example, operates most efficiently with the smallest pathlength possible (i.e. the greatest penetration of light into the reaction mixture). Flow chemistry allows significantly shorter pathlengths than conventional setups, being as small as the diameter of the tubing used. Hence, this discrepancy between flow and batch photochemistry becomes more pronounced on larger scales. In such cases, batch processes would require more lights and elongated reaction vessels to maintain the pathlength of a smaller scale experiment. Where as, a flow setup would require no modification, it would merely have to be run longer (or at a faster flow rate if the chemistry permitted).

It was hoped that application of flow chemistry to the photochemical hydroxylation-nitration chemistry detailed above would enable faster reaction times and in doing so possibly giving a yield increase, as well as, allow larger scale processes. Fortunately, a plethora of research papers can be found offering advice on the assembly of such apparatus out of easily available

laboratory equipment.[121–124] With this information available, a simple flow reactor was put together with the aim of using it in our photochemical processes (**Figure 2.2**).

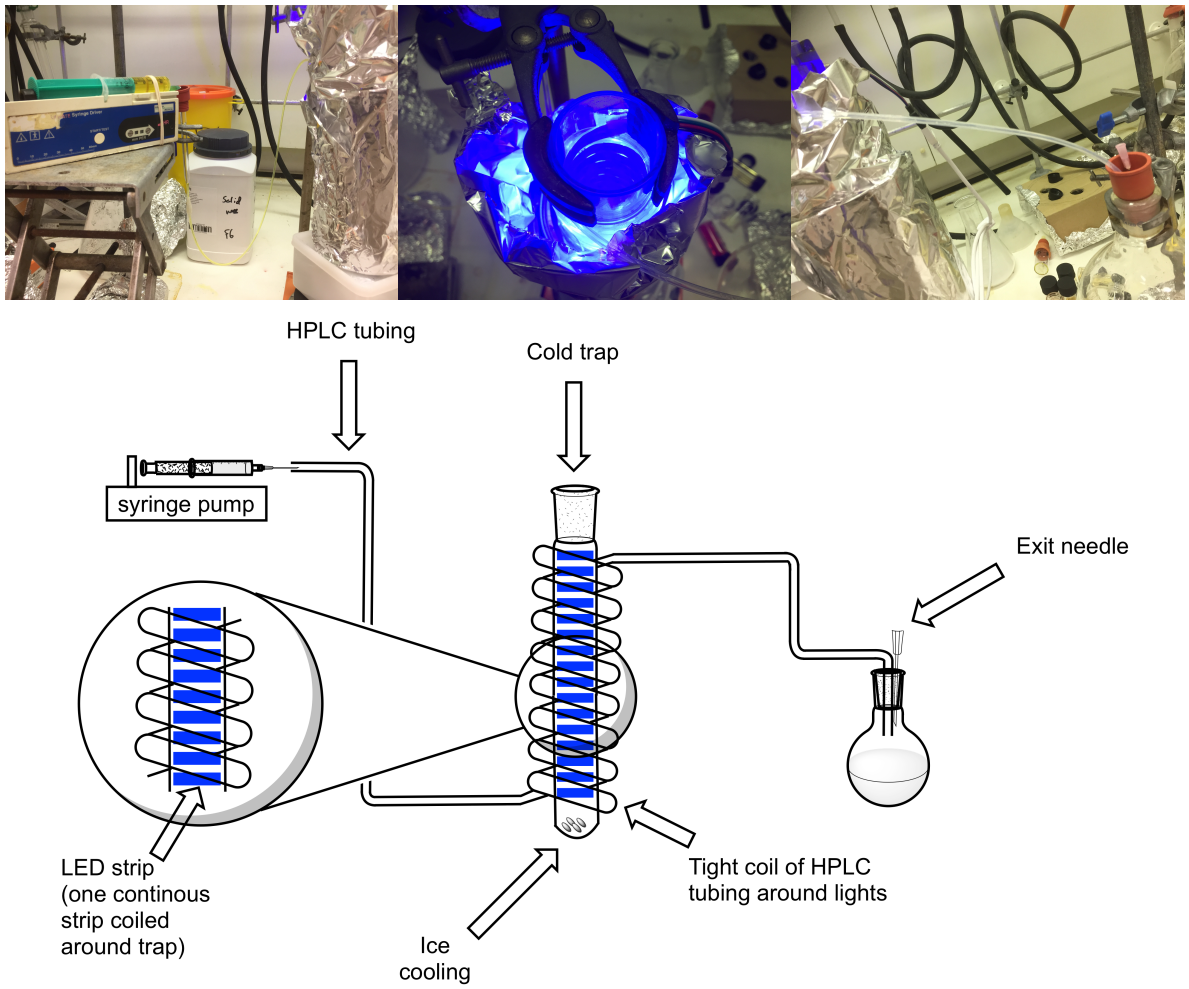

Figure 2.2. *The 'Flow' photoreactor set-up used in this project, including schematic of design (bottom).*

For this flow reactor, the same 3 W blue LEDs described previously were placed around the outside of a cold finger trap, with HPLC tubing coiled around them. The cold trap itself was filed with ice and water for cooling. As can be seen, this simple reactor has no mixing chamber and the reaction mixture preformed in a vial before being taken up in a single syringe. While mixing chambers tend to be more common, it was not deemed necessary in our case. This is because the reaction does not occur until photoexcitation happens (until the irradiated, coiled, section of tubing is reached). The advantages of forgoing a mixing chamber include:

reducing the likelihood of leaks, improved maintenance of pressure, and key for our simple setup the ability to drive the flow setup effectively with a single syringe pump.[122,123]

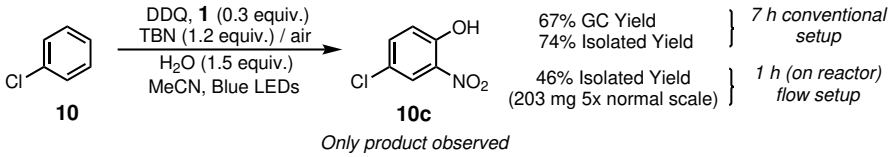

Scheme 2.8. *Application of flow chemistry to the hydroxylation-nitration of chlorobenzene.*

The result of applying this setup to the hydroxylation-nitration of chlorobenzene can be seen above (**Scheme 2.8**). As expected a much larger scale reaction was enabled by this flow process in a more useful time scale (1 h on flow reactor – 4.5 h total time of operation vs 7 h total time on batch). This setup was then used mainly as a way of studying the unusual defluorination result observed when fluorobenzene (**11**) was used as a substrate in this reaction. All further discussion of that work will be left to the following chapter (**Chapter 3**).

By this stage, with the development work that had already been carried out, a picture of the limits of the chemistry discussed had come into focus. Useful insights into the efficiency of these oxidations had been gained, and interesting side reactions, the development of which will be important to this thesis, had been noted. Before summarising these points and progressing to the work they eventually inspired, it would be beneficial to demonstrate some of the thoughts and concerns that were developing surrounding both the use of DDQ as photocatalyst and the practicality of moving to a catalyst with equivalent oxidising efficiency. To do this some computational work, that was undertaken, will be highlighted.

2.3.2 Catalyst optimisation and the use of computational methods

As demonstrated, DDQ (**1**) is a widely available, inexpensive, organophotocatalyst. One of main limitations, however, is its reactivity to nucleophiles (and stronger nucleophiles would be necessary in the case of more election-rich arenes). It seemed necessary, therefore, to

carry out investigations (both experimental and computational) into potential alternatives that retained the high oxidation potential but with lower ground state reactivity. For these investigations, focus was initially kept on the quinone core. This choice was made to allow the suggestion of structural changes based on analogy to DDQ. Indeed, this type of strategy in photocatalyst design has been much adulated in more recent literature.[29–32] However, this approach does pose challenges pertaining to the practicality of the synthesis and the stability of compounds arising from the suggested modifications. To begin this process, and gain a better understanding of the proficiency of different quinones to act as photocatalysts in the hydroxylation-nitration reaction, a range of quinone based dyes were screened for activity.

The results of the initial experimentally screened photocatalysts is shown in **Scheme 2.9**. It was hoped they would show some improvement over DDQ, or show some useful feature for future development. However, all of the tested quinones apart from **1** and **78** showed no conversion to product, and **78** gave only 5% yield. Given that the screening of catalysts experimentally on an ad hoc basis was shown to be an inefficient process, our efforts moved to determining potential candidates computationally based upon their redox potentials.

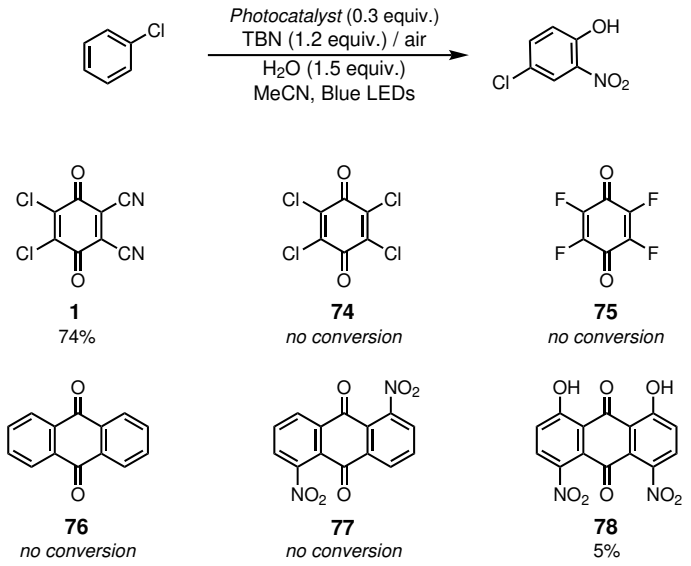

Scheme 2.9. *Experimentally tested quinone based photocatalysts.*

In accordance with **Experimental Details 5.3**, the ground state $E^{o}_{\mathrm{PC/PC^{\bullet-}}}$ values for a range of known quinone based molecules were calculated and compared to their experimental literature values. This was done in order to test the reliability of the chosen computational method. The reason for calculating the ground potential (as opposed to that of the photoexcited triplet state) is threefold: ground states are less computationally demanding to calculate, more literature values for ground state potentials exist (allowing us to initially verify our method by comparing our results to known values), and finally because this is a method we needed to develop for a latter study (this can be seen in **Subsection 3.2.6** of **Chapter 3**). The use of ground state potentials to give us an indication of how oxidising an excited state will be *within* a class such as the quinones is largely reasonable. The assumption that the more oxidising the ground state, the more oxidising the excited state can be seen to be true for the quinones for which such data is available (e.g. DDQ is more oxidising in the ground and triplet state, $E^{o}_{\mathrm{DDQ/DDQ^{\bullet-}}} = +\,0.49$ V and $E^{o}_{\mathrm{DDQ^{T1}/DDQ^{\bullet-}}} = +\,3.18$ V vs SCE respectively, than *p*-chloranil (**74**), $E^{o}_{\mathbf{74}/\mathbf{74}^{\bullet-}} = +\,0.00$ V and $E^{o}_{\mathbf{74}^{\mathrm{T1}}/\mathbf{74}^{\bullet-}} = +\,2.46$ V vs SCE respectively, which in turn is more oxidising than anthraquinone (**76**), $E^{o}_{\mathbf{76}/\mathbf{76}^{\bullet-}} = -\,0.96$ V and $E^{o}_{\mathbf{76}^{\mathrm{T1}}/\mathbf{76}^{\bullet-}} = +\,1.77$ V vs SCE respectively).[71,125]

The results of these calculations can be seen in **Table 2.6** and are plotted in **Figure 2.3**. From these results, it can be seen that there is overall an excellent correlation of experimental and calculated $E^{o}_{\mathrm{PC/PC^{\bullet-}}}$, with the only outlier being *p*-chloranil, which bears four heavy atoms. In addition, while the outlier is 0.268 V different from its experimental value (a noticeable difference in energy) for our purposes - the identification of possible photocatalysts - it is an acceptable difference. This is due to the fact that the calculated values would only be used to aid selection of candidates prior to the synthesis of those of interest.

Table 2.6. *Computation of known E^o values, relative to SCE.*

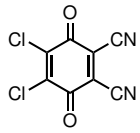
1

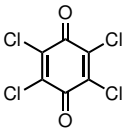
74

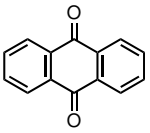
76

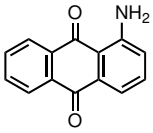
79

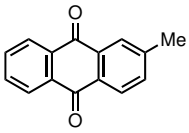
80

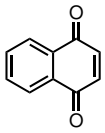
81

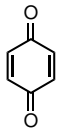
82

Catalyst	Solvent	Calculated E^o_{cal} / V	Literature E^o_{exp} / V	$\lvert E^o_{cal} - E^o_{exp} \rvert$
DDQ (**1**)	MeCN	0.488	0.49[71]	0.002
p-chloranil (**74**)	DMSO	0.298	0.03[125]	0.268
anthraquinone (**76**)	MeCN	−0.968	−0.96[71]	0.008
1-amino-anthraquinone (**79**)	DMSO	−1.102	−1.04[125]	0.062
2-methylantraquinone (**80**)	DMSO	−1.009	−0.98[125]	0.029
naphthoquinone (**81**)	MeCN	−0.708	−0.72[71]	0.012
quinone (**82**)	MeCN	−0.504	−0.54[71]	0.036

It can also be seen (**Table 2.6** and **Figure 2.3**) how pre-eminent DDQ is, in terms of oxidation, even in the ground state compared to other members of the quinone class. This is possible evidence, that it maybe difficult to find (or design) a suitable alternative catalyst from within the same class. However, this approach still came across as the most reasonable starting point. Additionally, and of particular import to the work discussed in **Subsection 3.2.6**, this approach has provided a practicable way of calculating redox potentials for species of interest. Such computational redox potentials will be useful in assessing the viability of electron transfer processes in species for which experimental data is not availible.

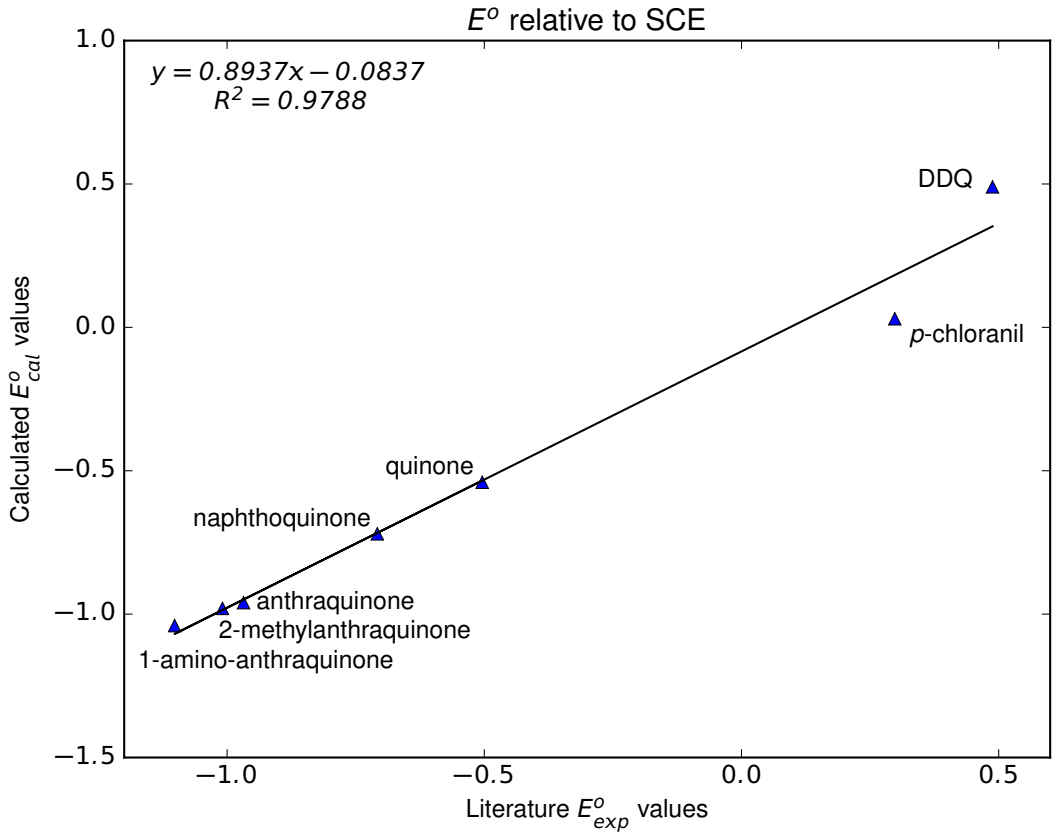

Figure 2.3. *Computational line of fit.*

With confidence in the accuracy of the computational method established, the ground state E^o potentials for a range of other quinone based compounds, with unknown values was performed. This yielded the E^o_{cal} values for **83**-**97** as shown in **Figure 2.4**. These results raised

a number of potential hits for future work. However, many of the more promising motifs in terms of potential, e.g. **91**, were neither straightforward modifications, nor would they be predicted to offer a significant improvement in chemical stability (i.e. resistance to Michael reaction). Therefore, this was ultimately seen as a useful method for possibly aiding future catalyst selection, but not as something we sought to explore further with the current chemistry and parameters.

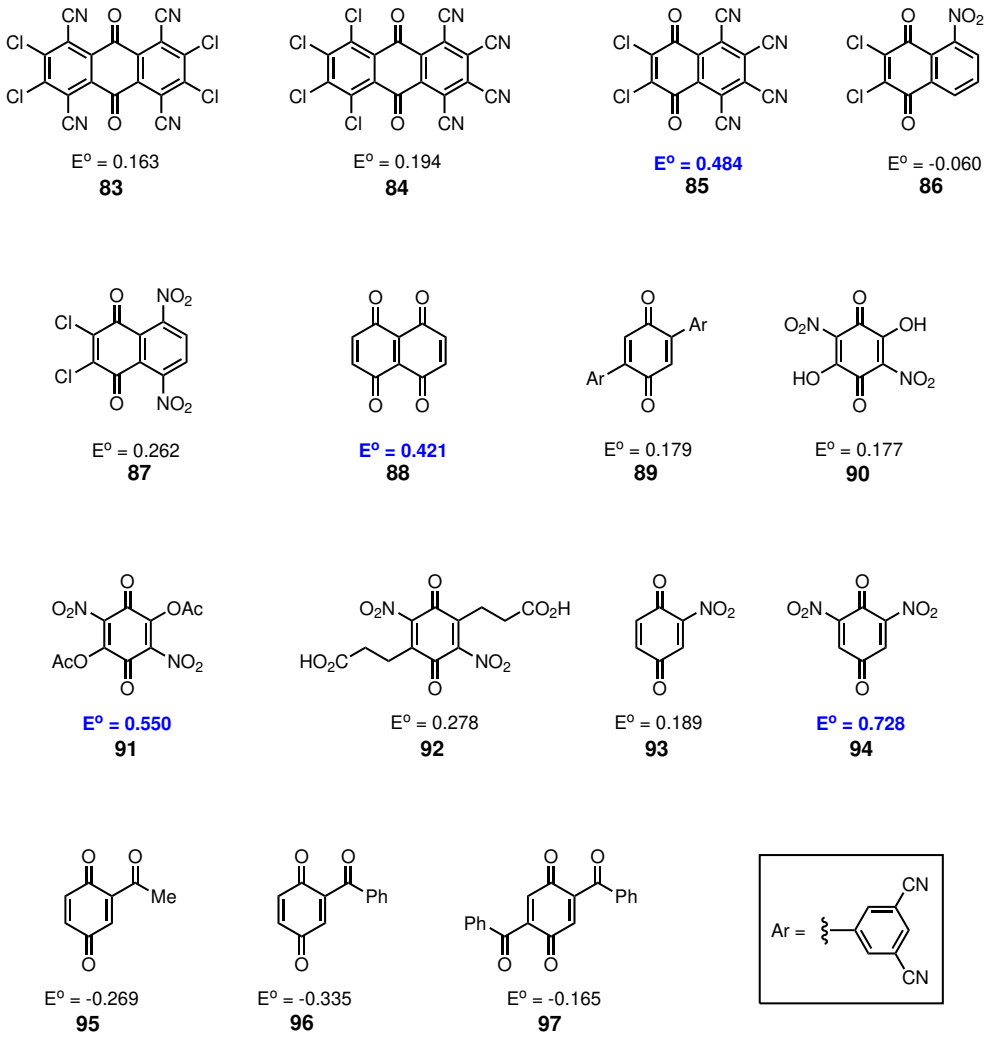

Figure 2.4. *Computational potential values of unknowns.*

2.4 Chapter Summary

In this chapter, attempts have been described to develop a method, based on the earlier work of Fukuzumi and coworkers, for a more general oxidation of arenes to phenols and additionally for a simple benzylation of alcohols. With these methods coming up against some fundamental limitations, we moved towards a dual hydroxylation-nitration chemistry; which showed improved if not particularly broad applicability. We also demonstrated significant development of the practical aspects of photochemistry and discussed some ideas on the nature of the catalyst.

It can be seen that the work shown in this chapter represents the starting point of our photochemical investigations that will be further elaborated upon later in this thesis. It highlights our interest in DDQ a photocatalyst, our interest in photooxidations, and the utilisation of aryl radical cations as reactive intermediates. Whilst it could not be claimed that the methods shown within to be synthetically relevant they did allow for a better understanding of these processes. Indeed, the surprising efficiency of the unoptimised defluorination of fluorobenzene under the hydroxylation-nitration conditions did lead to the development of a practical S_NAr method. It is that S_NAr method to which attention is now directed, and full details are provided in the following chapter (**Chapter 3**).

CHAPTER

3

RADICAL CATION ACCELERATED SUBSTITUTIONS

3.1 Chapter Introduction

The previous chapter described net-oxidative transformations. Here work on net redox-neutral substitutions is presented. The work in this chapter also utilises DDQ as a photocatalyst, and involves the generation of aryl radical cations as the key reactive intermediate. The main example of this chemistry, on which this chapter is focused, is the defluorinative photochemical S_NAr of fluoroarenes (**Section 3.2**). Discussion of related non-classical S_NAr methodology can be found in the introduction of this thesis (**Section 1.4**). Here the development of this process from the side reaction seen previously (**Section 2.3**) to a straightforward practical method for the C–F functionalisation of mildly electron-poor fluoroarenes is delineated.

In this discussion, the nature of the light source used is evaluated (**Subsection 3.2.1**), the optimisation is presented in detail (**Subsection 3.2.2**), and the initial mechanistic assumptions are examined (**Subsection 3.2.3**). Following this the scope of the chemistry is explored, with re-optimisations as necessary, starting with arenes (**Subsection 3.2.4**) and then different classes of nucleophile (**Subsection 3.2.7**). During this part of the discussion computational methods

are described which enable a data analytic study of the existing arene scope compared to selected substrate properties. This allows for a rapid predictive tool for rapidly assessing the potential viability of potential arene substrates. Of course, this approach comes with caveats attached and these too are discussed. The recent similar method of Lambert *et al.* is also discussed in this chapter (**Subsection 3.2.8**). Finally a different radical cation accelerated substitution is summarised, the photochemical deprotection of tosylates, which was found as a side reaction in this chemistry (**Section 3.3**).

3.2 Photochemical DDQ-mediated defluorinative S_NAr

Before discussion of the development of this photochemical S_NAr process, it is worth introducing the light source used in this work. While some initial development utilised photosetups introduced previously (these are indicated when they occur), the majority of the photochemistry in this chapter is driven by a new 32 W light source detailed below.

3.2.1 Modifications to light source and photochemical setup

Previous work described the application of 3 W LEDs in one of three setups. Herein, a 32 W light source of the popular Kessil brand was used. The 3 W LEDs used previously gave irradiation between 420–480 nm (**Subsection 5.2**), while the 32 W LED Kessil lamp gave irradiation between 420–520 nm (**Subsection 5.2**).[126,127] This broader band should allow for more efficient excitation, which would would already have been improved by the increase in light intensity of the 32 W lamp relative to the 3 W strips. The setup used to deploy this LED lamp in our chemistry is shown below (**Figure 3.1**). It should also be noted, in the interest of completeness, that a 3 W blue laser was also tested (with irradiation though the open top of the vial), as work by others had indicated the benefits of less powerful but much more penetrative lasers relative to more dispersive standard LED light sources.[128–131] However, this work

will not be covered as it showed no benefits in our cases – implying we had sufficient light penetration, and that light intensity (luminous intensity) was a more important factor.

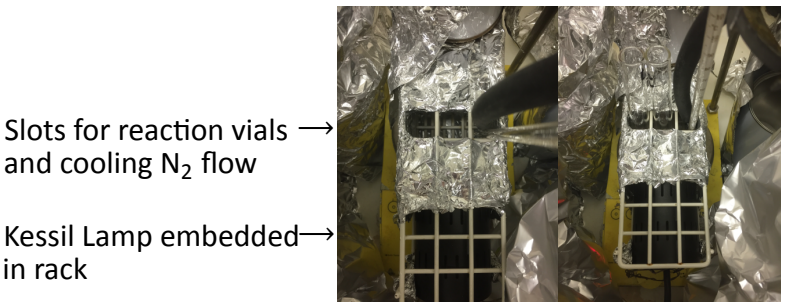

Figure 3.1. *The 32 W photoreactor set-up used in this project.*

For this setup, a 32 W LED lamp was mounted inside a test tube rack with a cooling flow of nitrogen gas. This approach enabled reaction vials to be placed the same distance from the lamp (1 cm) by simply using the same row on the rack (ensuring a consistent pathlength). With the cooling as described, the reactor was found to hold a constant temperature of between 36–43 ^{o}C during the course of photochemical experiment. As with previous setups, this new setup was placed on top of a stirrer plate to allow for reaction homogeneity.

This simple but much more powerfully light intense system was expected to give improved performance, and greater reproducibility, given that Kessil brand lamps are now a ubiquitous standard for photochemistry and are used by many groups.[126,127] The use of a rack to help maintain a consistent pathlength also aids in this endeavor. With this practical consideration now accounted for, the optimisation of the chemistry under study can now be fully discussed.

3.2.2 Optimisation of defluorination chemistry

The methods used to defluorinate aromatics (or in alternative parlance 'to perform an sp^2 C – F bond activation'), in contrast to other halogens, is limited to one of two discreet categories. These are: S_NAr or transition-metal-catalysed oxidative addition; the latter however is non-trivial to achieve.[132] The reason for both this lack of diversity of methods, and the complexities

in fully utilising the methods that do exist, can largely be explained by the high $C_{Ar}-F$ mean bond enthalpy (~520 kJ mol^{-1}).[89]

While there have been several recent advancements in the 'transition-metal-catalysed oxidative addition' category, many of these approaches are still hampered by the requirement for esoteric ligands whose syntheses are nontrivial and/or require harsh conditions.[132] In the case of defluorinative S_NAr all examples were thermal, required high temperatures, and only performed well on highly electron deficient substrates – until the work of Lambert and coworkers (published after the majority of the following sections were carried out).[107]

In **Section 2.3**, the reaction of fluorobenzene under the 'hydroxylation-nitration' conditions is shown. This result is shown again below (**Scheme 3.1**). Along with the expected fluoronitrophenol (**11a**), *para*- and *ortho*-nitrophenol (**11b** and **11c**) were also formed in the reaction.

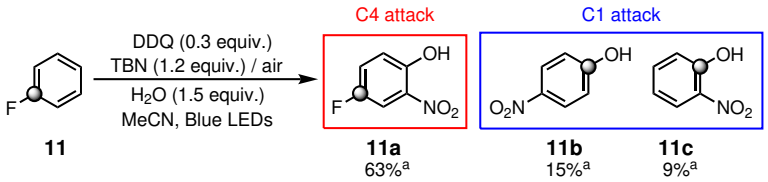

Scheme 3.1. *Initial defluorination observation.* [a]*Conversion by GC.*

The first hypothesis for the formation of products **11b** and **11c** was the idea that, under the reaction conditions, nitration of the fluorobenzene to form *p/o*-nitrofluorobenzene **98** / **99**, which would then undergo an S_NAr reaction (**Scheme 3.2**), was occurring.

However, it also seemed feasible that instead of a classical S_NAr on nitrated fluorobenzene, the reaction products could be formed *via* a photochemical S_NAr on the radical cation of fluorobenzene. To test both hypotheses, a set of control experiments were conducted (**Table 3.1**). Firstly, as can be seen in **Table 3.1**, products are *only* observed when the reaction both contains DDQ and is irradiated. In all other cases, only starting material is obtained. For the purposes of

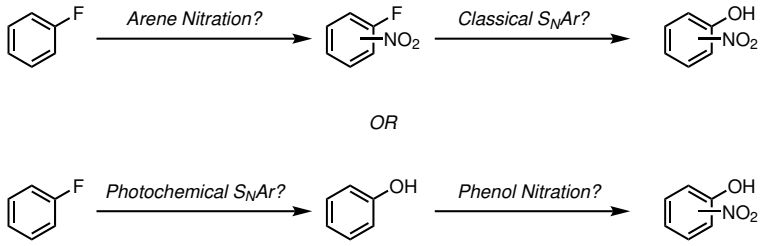

Scheme 3.2. *Two possible sets of reactions that explain the observed product distribution of the hydroxylation-nitration chemistry of fluorobenzene. The* ***Top*** *route was our initial hypothesis and supposes a direct nitration of the arene followed by a classical S_NAr substitution. While the* ***Bottom*** *route shows a photochemical S_NAr of the fluoride by water, followed by phenol nitration.*

the control reactions 'in the dark', the reaction vessels were coated with aluminium foil such that no light could penetrate and placed in the photochemical setup (**Subsection 3.2.1**) with the light and cooling on to replicate the ambient temperature experienced in the irradiated examples (which can reach 40 ^{o}C).

The inference from such data is that the reaction is indeed both photochemical in nature *and* mediated by DDQ (i.e. does not proceed *via* direct substrate excitation). This was therefore considered to be a potentially interesting method of photochemical C – F activation (as opposed to a nitration followed by a classical S_NAr) of an only mildly electron deficient substrate relative to those commonly observed in similar thermal substitutions.[87,104] As such, work began on the optimisation of the transformation.

Some metal acetates were screened in the hope that forming a fluoride salt with a reasonable lattice enthalpy would help drive the reaction to the defluorination products **11b** and **11c** in preference to the C – H activation product **11a** (**Table 3.2**). Unfortunately, we faced the issue of DDQ stability when the solvent was changed to allow dissolution of the metal acetates into the reaction medium. DDQ has a low water stability,[117] and DDQ degradation seems the most likely explanation of the results contained within **Table 3.2** where the solvent was changed to a 2:1 mixture of water:acetonitrile. Optimisation efforts were refocused elsewhere.

Table 3.1. *Control reactions to determine if thermal S_NAr occurs under the given reaction conditions and starting from the substrate shown.*

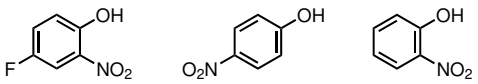

11a **11b** **11c**

Entry	Conditions	Substrate	GC Conversion (%) (**11a**:**11b**:**11c**)
1	Standard conditions[a]	fluorobenzene	63:15:9
		p-nitrofluorobenzene	No Reaction
		o-nitrofluorobenzene	No Reaction
2	Standard conditions without DDQ	fluorobenzene	No Reaction
		p-nitrofluorobenzene	No Reaction
		o-nitrofluorobenzene	No Reaction
3	Standard conditions in the dark	fluorobenzene	No Reaction
		p-nitrofluorobenzene	No Reaction
		o-nitrofluorobenzene	No Reaction
4	Standard conditions without DDQ in the dark	fluorobenzene	No Reaction
		p-nitrofluorobenzene	No Reaction
		o-nitrofluorobenzene	No Reaction

[a]Standard conditions = DDQ (0.3 equiv.), TBN (1.2 equiv), H_2O (1.5 equiv.), MeCN, 32 W blue LEDs

Table 3.2. *Screen of metal acetate additives.*

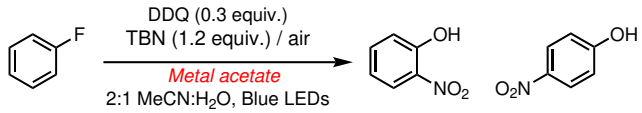

Entry	Metal acetate	Equivalents	Result
1	No Additive	-	No Reaction
2	CsOAc	0.3	No Reaction
3	CsOAc	1.2	No Reaction
4	LiOAc	0.3	No Reaction
5	LiOAc	1.2	No Reaction
6	NaOAc	0.3	No Reaction
7	NaOAc	1.2	No Reaction

Given the difference in mean bond enthalpy between $C_{Ar}-H$ and $C_{Ar}-F$ (~440 kJ mol^{-1} vs ~520 kJ mol^{-1}),[89] we postulated that the C–H activation process (i.e. *para* substitution) could be favoured over the C–F activation process (i.e. *ipso* substitution) at lower temperatures. **Figure 3.2** shows the relative integration of the C3 proton of 2-nitrophenol (**11c**) and 4-fluoro-2-nitrophenol (**11a**) in the crude reaction mixture of the hydroxylation-nitration of fluorobenzene (**11**) after 1 h, run at r.t. and −41 °C. The ^{1}H NMR signals of 4-nitrophenol (**11b**) were obscured in the crude proton spectrum and thus have been omitted from the following discussion. The results of this experiment seem to bear out the hypothesis that *para* attack products could be selectively formed *via* a reduction in reaction temperature. However, this would not give access to the desired defluorination product. It was at this point we realised the need to perform a rational redesign of the reaction conditions if we wished substantial

improvements to the yield of the defluorination product.

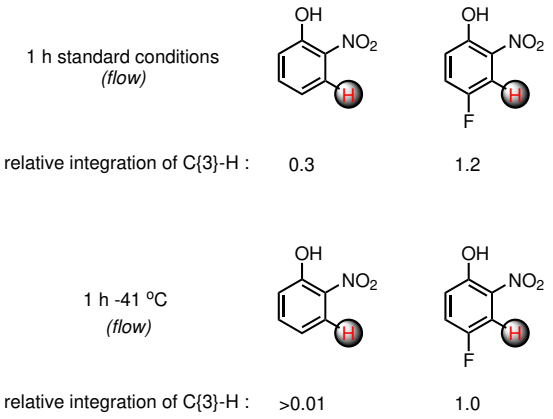

Figure 3.2. *The effect of temperature on product distribution in the hydroxylation-nitration reaction of fluorobenzene*

The first aspect of this redesign was to investigate the solvent and nucleophile. Here, methanol was the initial candidate for the solvent screen (**Scheme 3.3**), as it could also act as the nucleophile for the reaction but did not cause the same issues with DDQ stability that water did. Another aspect was, given that the nitration of the phenol reaction product complicated the product distribution, TBN was removed from the reaction, for these experiments, to simplify the product distribution (by eliminating the possibility of nitration). It should also be noted that, for the photochemical S_NAr reaction, the overall transformation is net redox neutral – hence a reoxidant such as TBN is no longer fundamentally needed in the reaction. With these newly rationalised conditions in hand, we needed to select a test substrate for this method. While fluorobenzene (**11**) would have been a reasonable substrate choice, we sought a model with an *ipso* carbon more strongly activated to the desired S_NAr chemistry as the use of a slightly biased substrate should allow for a faster start to the optimisation. For this model, we selected 2,4–dichlorofluorobenzene (**100**).

The benefits of using polyfluorinated alcoholic solvents in reactions involving both aryl radical cation intermediates (**Subsection 1.3.1**) and C – F activation (**Subsection 1.4.2**) have been

discussed previously. Given these known rate enhancement effects, it was considered pertinent to test such solvents in this chemistry. This was deemed especially necessary, as at this time both radical cation intermediates and C – F activation were considered to be important to the presumed mechanism of this chemistry (see **Subsection 3.2.3** shortly). 1,1,1,3,3,3-Hexafluoro-2-propanol (HFIP), when used as solvent with 10 equiv. of methanol as nucleophile gave markedly higher yielding result, 92% isolated yield of **100a** after 24 h (**Scheme 3.3**). 2,2,2-Trifluoroethanol (TFE), and a 1:1 mixture of TFE to 1,2-dichloroethane (DCE) performed similarly well and it was found that both the reaction time and the nucleophile loading could be reduced. The DCE co-solvent approach was selected as it reduced costs relative to the TFE only conditions, DCE was selected over DCM to minimise solvent loss by evaporation. Control reactions for these conditions (**Scheme 3.4**) indicated the absence of any noticeable background reaction. The full optimisation data can be seen in **Table 3.3**.

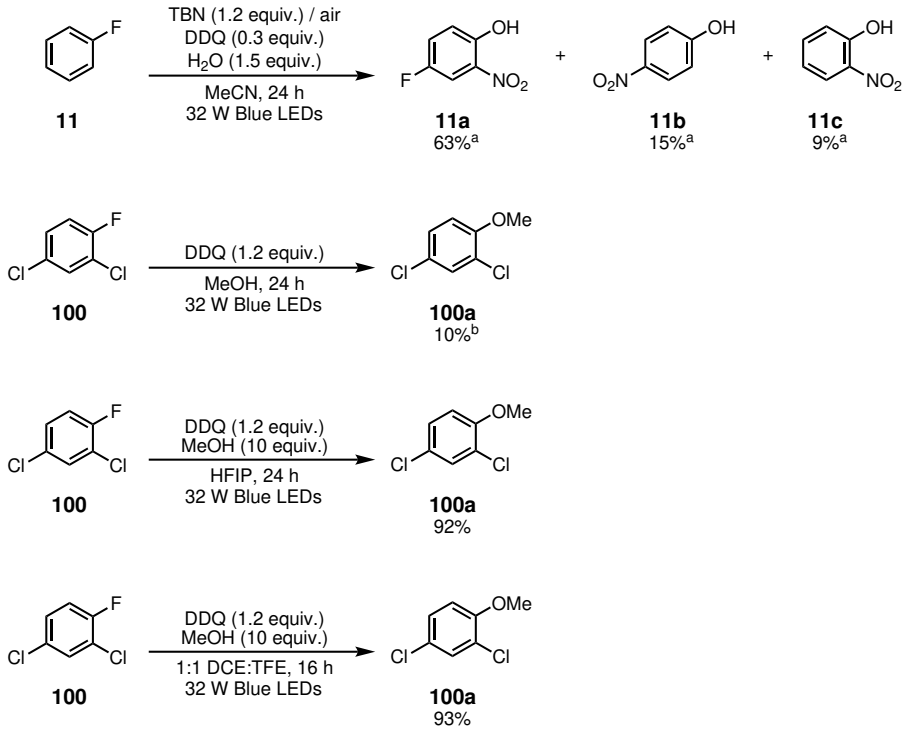

Scheme 3.3. *A sample of results from the initial optimisation work*

The reaction maintained its high yield at double the substrate (**100**) concentration (1.0 M)

but started to show a drop at 1.5 M (**Table 3.3**, entries 1–3), not unexpectedly for a photochemical process (where light penetration is a key factor). Methanol was a poor solvent for the reaction, and spiking it with low levels of HFIP gave no improvement – clearly implying the need for excess polyfluorinated alcohol (**Table 3.3**, entries 5–7). The reaction proceeded faster in TFE than HFIP (**Scheme 3.3**), possibly as a result of a viscosity effect (with HFIP giving a thicker solution than TFE and thus slowing down diffusion rates). Substituting TFE for 1:1 DCE:TFE showed no drop in rate or yield (**Table 3.3**, entries 8 & 9) and was chosen in preference to neat TFE as it was more cost effective. DCE was used for this role and not DCM to allow for the reaction temperature inside the photoreactor. The need for a polyfluorinated co-solvent was made clear by the use of DCE on its own, where only low yields of product were obtained – although some improvement was seen by application of quantities of TFA (**Table 3.3**, entries 10–12). When MeCN was tested as potential co-solvent with TFE, it performed well but the overall yield was lower than that of neat TFE (**Table 3.3**, entry 14). Interestingly, the use of MeCN as the sole solvent gave the only example of chloride substitution for substrate **100** (12% substitution of the *para*-Cl in addition to 44% F substitution. **Table 3.3**, entry 13).

Nucleophile loading was then investigated, with results showing a high dependency of reaction yield on nucleophile loading in HFIP (**Table 3.3**, entries 15-17). Fortunately, the importance of nucleophile loading seemed lessened in 1:1 DCE:TFE (**Table 3.3**, entries 21 & 26), again possibly due to the lower viscosity of this medium. Pleasingly, catalyst loading could be reduced to below stoichiometric levels, down to 0.3 equivalents. However, this could only be achieved with rigorous freeze-pump-thaw degassing, and simply sparging the reaction mixture proved completely ineffective (**Table 3.3**, entries 18-27). This sensitivity to molecular oxygen is not totally surprising given its high propensity for triplet quenching.[60–62] Unfortunately, however, whether or not a sub-stoichiometric loading could be used was later shown to be

highly substrate specific. This is likely owing to the large changes in reactivity of the aryl radical cations that can be brought about by subtle changes in structure. However, before discussing the scope of this chemistry and the changes which may or may not be needed for certain substrates, it is worth considering the implications of that data gathered with respect to mechanistic aspects of this chemistry.

Table 3.3. *S_NAr optimisation table for the reaction of **100** with methanol, to form **100a**, under 32 W blue light.*

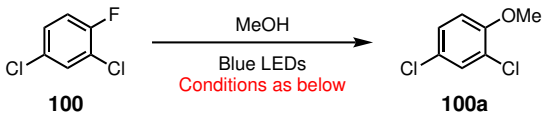

100 **100a**

Entry	Scale / mmol	[**100**] / M	Solvent	Additive (equiv.)	DDQ equiv.	MeOH equiv.	Atmosphere	Isolated Yield
1	0.5	0.1	HFIP	-	1.2	10	Air	92%
2	1.0	0.2	HFIP	-	1.2	10	Air	90%
3	1.5	0.3	HFIP	-	1.2	10	Air	72%
4	0.5	0.1	MeOH	-	1.2	*solvent*	Air	10%
5	0.5	0.1	MeOH	HFIP (1)	1.2	*solvent*	Air	>10%[a]
6	0.5	0.1	MeOH	HFIP (2)	1.2	*solvent*	Air	>10%[a]
7	0.5	0.1	MeOH	HFIP (10)	1.2	*solvent*	Air	5%
8	0.5	0.1	TFE	-	1.2	10	Air	93%
9	0.5	0.1	1:1 DCE:TFE	-	1.2	10	Air	94%

Continued overleaf...

Entry	Scale / mmol	[**100**] / M	Solvent	Addi-tive (equiv.)	DDQ equiv.	MeOH equiv.	Atmo-sphere	Isolated Yield
10	0.5	0.1	DCE	-	1.2	10	Air	18%
11	0.5	0.1	DCE	TFA (2)	1.2	10	Air	37%
12	0.5	0.1	DCE	TFA (5)	1.2	10	Air	52%
13	0.5	0.1	MeCN	-	1.2	10	Air	44%[b]
14	0.5	0.1	1:1 MeCN:TFE	-	1.2	10	Air	85%
15	0.5	0.1	HFIP	-	1.2	5	Air	53%
16	0.5	0.1	HFIP	-	1.2	2	Air	18%
17	0.5	0.1	HFIP	-	1.2	1.2	Air	11%
18	0.5	0.1	HFIP	-	0.6	10	Air	81%
19	0.5	0.1	HFIP	-	0.3	10	Air	24%
20	0.5	0.1	HFIP	-	0.2	10	Air	23%
21	1.0	0.2	1:1 DCE:TFE	-	1.2	10	Air	95%
22	1.0	0.2	1:1 DCE:TFE	-	0.6	10	Air	82%
23	1.0	0.2	1:1 DCE:TFE	-	0.3	10	Air	81%
24	0.5	0.1	1:1 DCE:TFE	-	1.2	10	N_2[c]	88%

Continued overleaf...

Entry	Scale / mmol	[**100**] / M	Solvent	Additive (equiv.)	DDQ equiv.	MeOH equiv.	Atmosphere	Isolated Yield
25	0.5	0.1	1:1 DCE:TFE	-	0.3	10	N_2 [c]	74%
26	0.5	0.1	1:1 DCE:TFE	-	1.2	2	Air	93%
27	0.5	0.1	1:1 DCE:TFE	-	0.3	10	N_2 [d]	91%

[a]from analysis of the crude ^{1}H NMR spectrum. [b]12% of the *para*-Cl substitution product. [c]solution sparged with N_2. [d]O_2 removed *via* Freeze-Pump-Thaw under N_2.

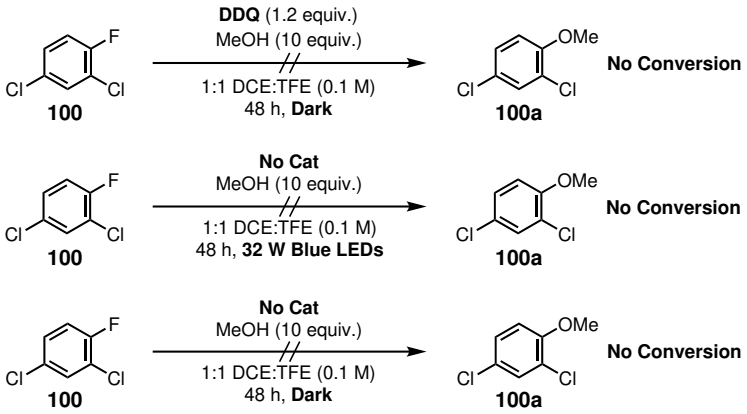

Scheme 3.4. *Control reactions for the photochemical S_NAr of dichlorofluorobenzene,* ***100****.*

3.2.3 Initial Mechanistic Proposal

The data gathered during the optimisation of the reaction lends weight to the role of DDQ as (an albeit stoichiometric) photocatalyst in this reaction (**Subsection 3.2.2**). With this known, along with the previous work of Fukuzumi,[41] the catalytic cycle below was proposed for this reaction (**Scheme 3.5**).

This proposed mechanism is relatively straightforward involving the oxidation of the substrate (in this case **100**) by photoexcited DDQ ($E_{DDQ^{T1}/DDQ^{\bullet-}} = +3.18$ V vs SCE) and then sub-

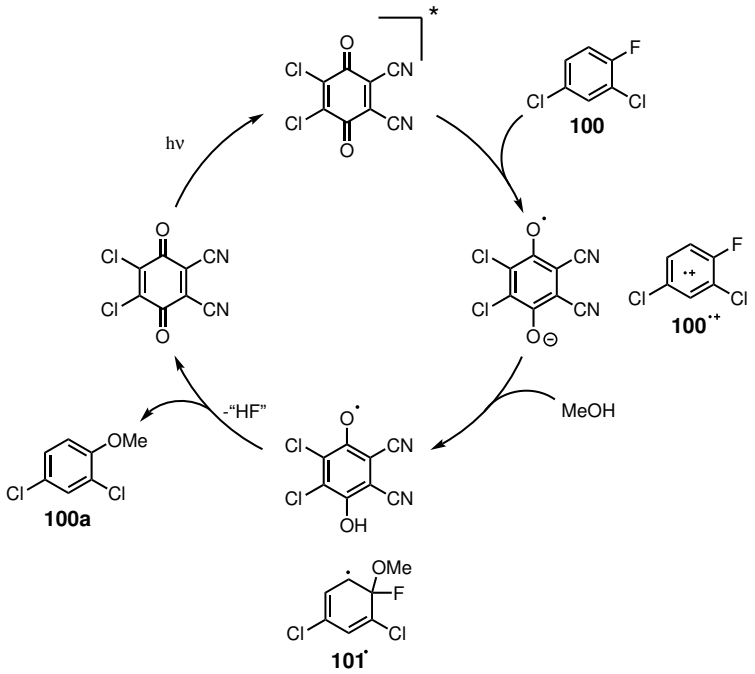

Scheme 3.5. *Initial Mechanistic Proposal*

sequent S_NAr on the activated species **100**$^{\bullet+}$; followed by back-electron transfer to give the product and ground state DDQ.

However, there are many aspects of this initial proposal worthy of further discussion. The electron transfer (ET) event from starting arene (**100**) to triplet excited state DDQ is central to this process and some of the subtleties of the electron transfer event should be understood. For the electron transfer event molecular orbital overlap between the photocatalyst and the substrate is of course required, based on other studies with DDQ and arenes it is likely to be a face-on arrangement of catalyst and substrate (**Scheme 3.6**). However, this could occur by collision between photoexcited triplet DDQ and ground state substrate, or alternatively a charge-transfer complex could form prior to photoexcitation (**Scheme 3.6**). Once election transfer has occurred the DDQ$^{\bullet-}$ – Substrate$^{\bullet+}$ now exist as an ion pair which can be described as a triplet contact radical ion pair (TCRIP) (**Scheme 3.6**). The next unknown is the extent of dissociation of this ion pair into free ions before nucleophilic attack. TCRIPs are known to

generally dissociate (or undergo 'cage escape') more rapidly than the rate of back-electron transfer (BET), the reason being the disallowed nature of the spin-flip transition required for back-electron transfer to take place (**Scheme 3.7**).[4] The opposite is true for singlet contact radical ion pairs (SCRIPs), which arise from singlet state photocatalysts.[4] However, we can infer nothing yet about the rate of nucleophilic attack nor how this compares to the rate of cage escape. This results in a need to give careful consideration to the role our counter ion, $DDQ^{\bullet -}$, is playing in the rest of the mechanism.

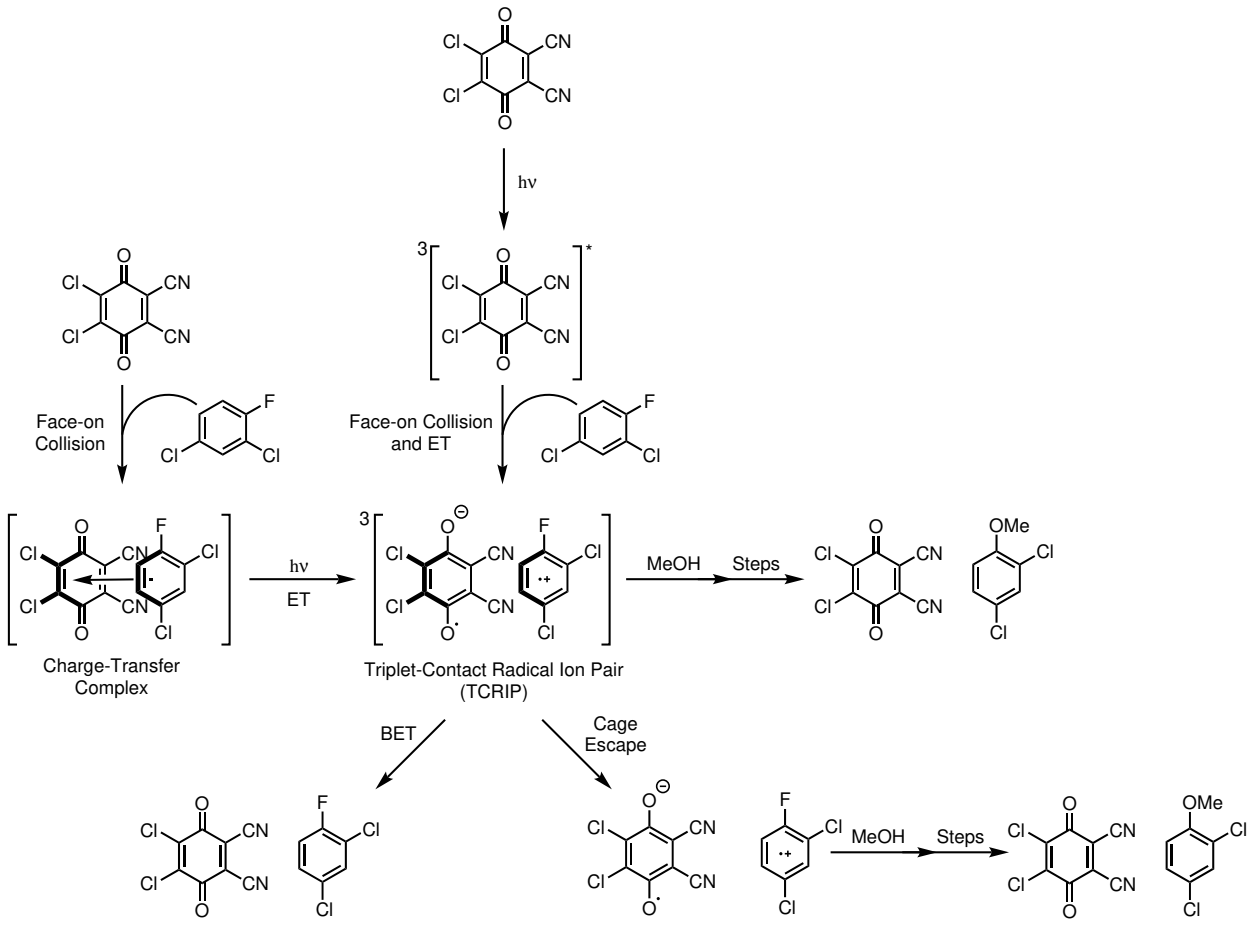

Scheme 3.6. *Examination of the initial electron transfer process, and resultant ion pairs.*

The next issue that may stand out here is the question of the products tolerance to the reaction condtions, more than that is the product of the reaction actually more reactive in the reaction than the substrate? This would initially seem very plausible given the much lower ox-

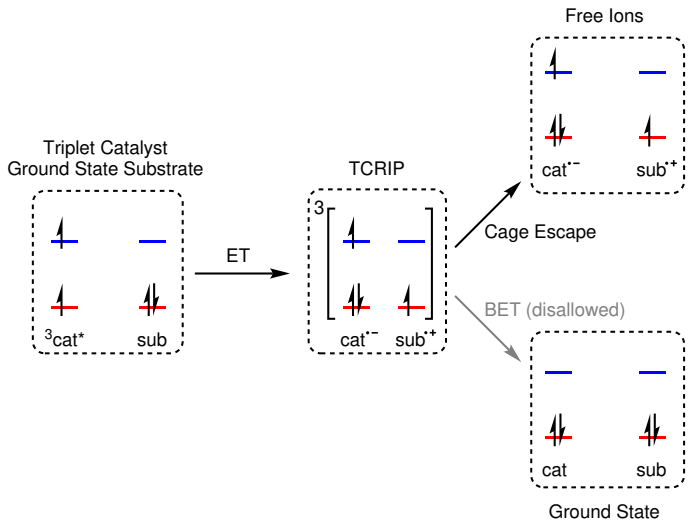

Scheme 3.7. *Outline of BET and cage escape processes from TCRIPs, highlighting the inherent need for a spin-flip transition for BET. Red energy levels indicate HOMO/SOMO, blue energy levels indicate LUMO/SOMO.*

idation potential of anisole **100a** (calculated by author as: $E_{Ar/Ar^{\bullet+}} = 1.59$ V vs SCE) vs that of fluoroarene **100** (calculated by author as: $E_{Ar/Ar^{\bullet+}} = 2.32$ V vs SCE). Despite this, resubjection of **100a** to the same reaction conditions with ethanol as the nucleophile gave only recovered starting material (**Scheme 3.8**). A similar observation is seen in the arene oxidation chemistry of Fukuzumi.[41] In this case, benzene is oxidised to phenol by photoexcited DDQ but no further oxidation of the product phenol is observed. As demonstrated by the work of Thiel, the explanation in that case proved to be the rapid rate of the back-electron transfer from the radical anion of DDQ to the radical cation of phenol (**Subsection 1.2.1**).[76] We believe a similar effect is in operation here.



Scheme 3.8. *Resubjection experiment of isolated **100a** to the reaction conditions, with ethanol as a nucleophile*

The other key question raised by this proposed catalytic cycle is the nature of the path-

way (or 'reaction coordinate') between the substitution 'intermediate' (cyclohexadienyl radical **101•** and related species) and product (**100a**). Indeed, the precise nature of **101•** and whether or not it is a true intermediate or true transition state (or a borderline case) as raised earlier (**Subsection 1.4.1**) can itself called into question. However, given the nature of the leaving group (fluoride), the mild stabilisation given by the chloride substituents, and what is know regarding the stability of cyclohexadienyl radicals,[133] it seems reasonable to propose **101•** as an intermediate in this chemistry. Some possible pathways, from this intermediate to product, are given overleaf (**Scheme 3.9**).

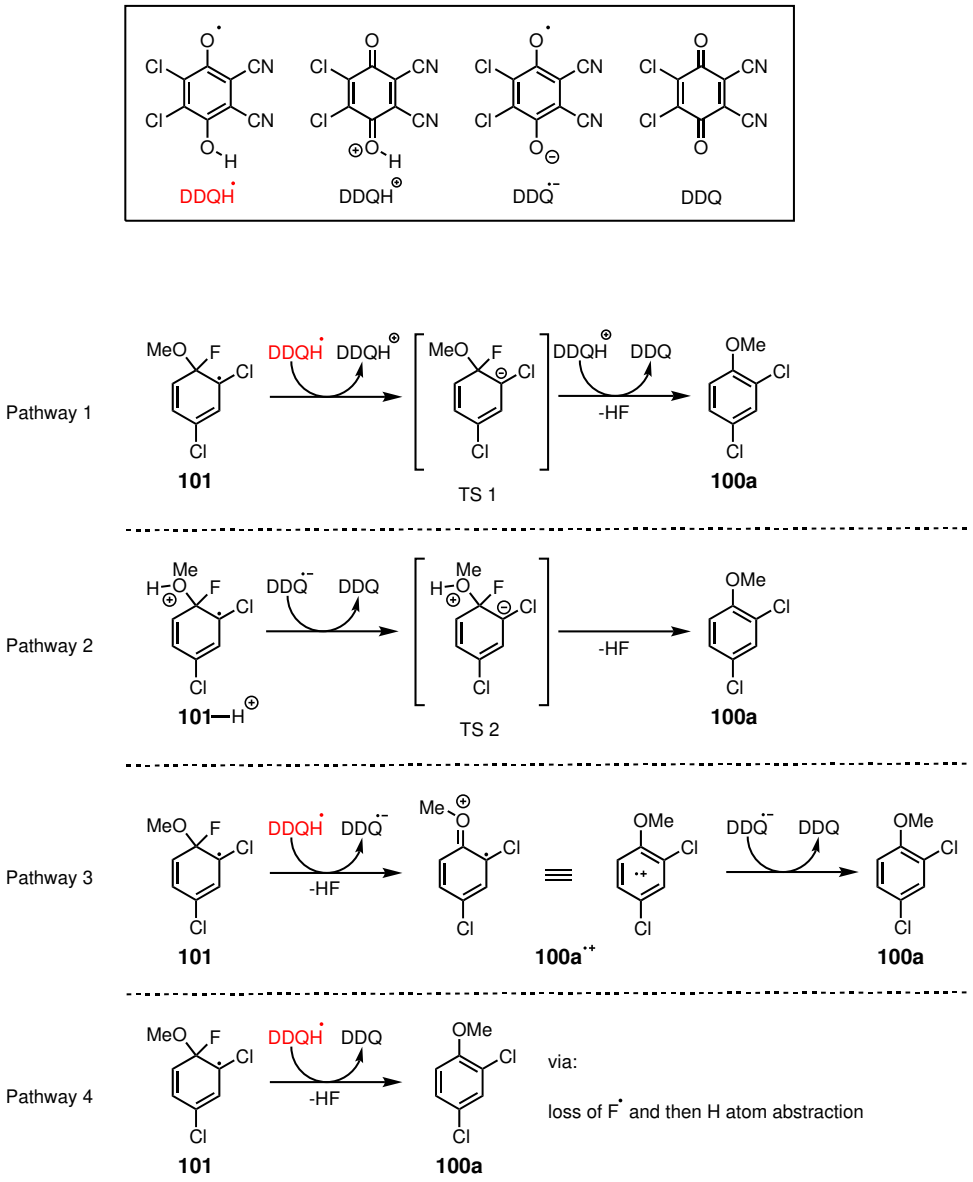

Scheme 3.9. *Possible pathways between cyclohexadieneyl radical (**101**•) and product (**100a**)*

Pathways 1 and 2 (**Scheme 3.9**) are essentially identical, differing only in protonation states. The merits of these two pathways is that they invoke the difficult and slow C – F bond breaking step only as the final act of the pathway. However, they do depend upon fairly high energy Meisenheimer-like transition states. Pathway 3 relies upon ejection of F^- as the first step, with concomitant proton scavenging from semiquinone $DDQH^{\bullet}$ and this process would be aided by the lone pair of the ipso methoxy group. This results in the highly plausible radical cation intermediate $\mathbf{100a}^{\bullet+}$, an exact analogy to the radical cation of the starting material. Pathway

4 suggest the homolytic cleavage of C–F bond, resulting directly in product. In this case, $F^{\bullet}$ could scavenge $H^{\bullet}$ from the semiquinone. This is the simplest pathway in terms of curly arrow mechanisms, but the likelihood of a homolytic C–F bond cleavage is low, given the high C–F bond enthalpy. A thorough DFT study would likely be needed to give confidence in assigning one of these pathways (or other alternatives) to this chemistry, but it seems reasonable to tentatively favour pathway 3 given the underlying chemistry. The implications of this pathway are further discussed in **Subsection 3.2.4**, along with discussions on the nature of the rate determining step.

An additional feature of the catalytic cycle, common to all of the pathways given above, worth further comment is the formal loss of HF. As discussed in the Introduction (**Section 1.4**), HF production in S_NAr reactions can be easily dealt with by the addition of $Ca(EtCO_2)_2$ (or other salt) either in the reaction or in the work up. Both of these methods were tested in a number of the examples that follow without any real effect on the reaction outcome (in the work that follows, results are given for $Ca(EtCO_2)_2$–free experiments, unless otherwise stated). While fluoride count was not measured, on the scale at which we operated, no issues were encountered. Flash column chromatography was also performed by pre-adsorption of the reaction mixture on to silica to aid fluoride sequestration. An interesting practical observation is that despite many reactions reusing the same vials (as reaction vessels), no etching was observed under our conditions (with or without $Ca(EtCO_2)_2$).

To continue developing a further understanding of this chemistry, exploration of the scope of the current method, starting with the arene scope, was seen as the logical next step. Based on the mechanistic proposal we were proposing, and experience with related chemistries, the sensitivity of the reaction to a change in arene is an aspect we were anxious to explore.

3.2.4 Arene scope of defluorination chemistry

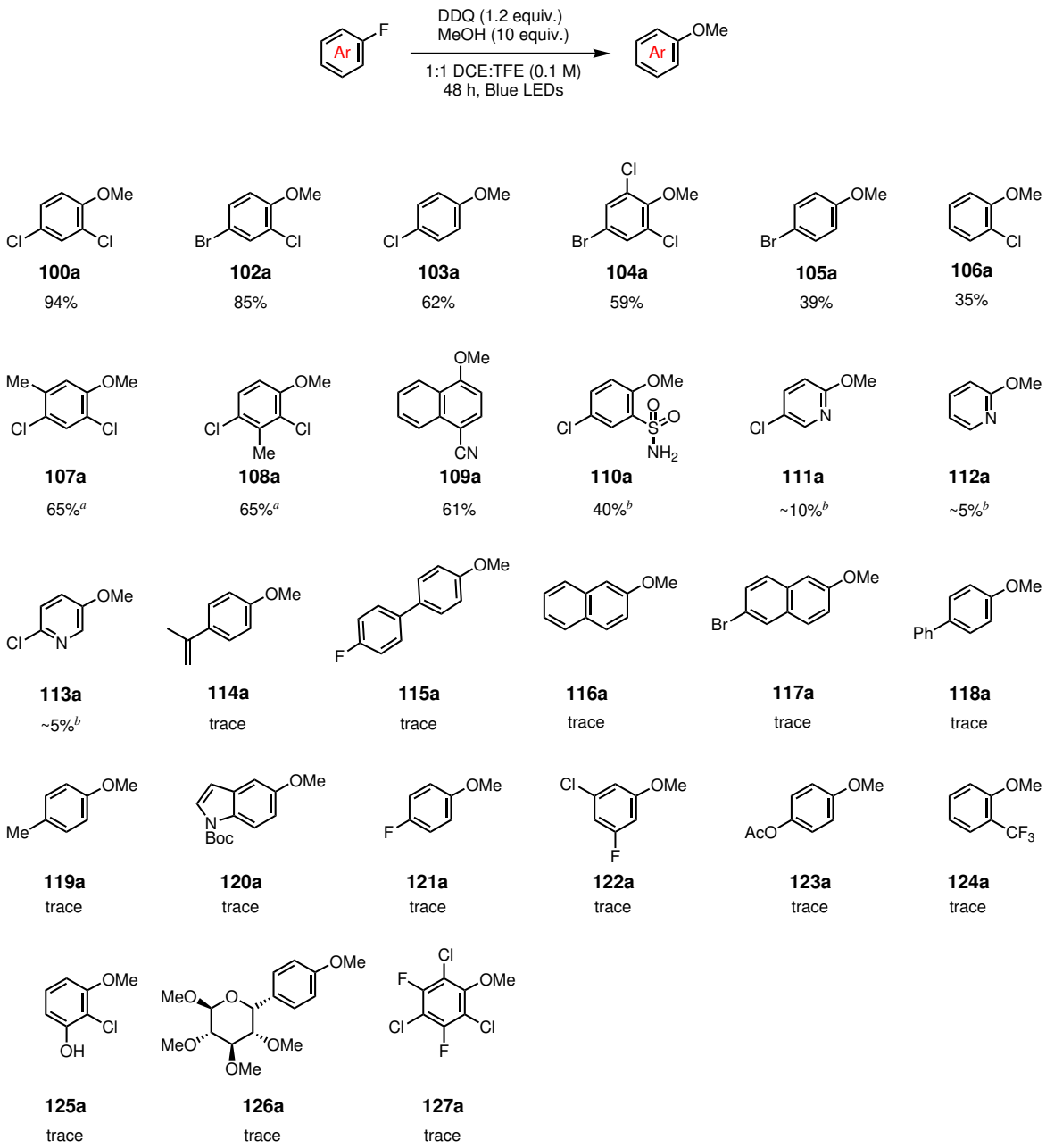

Scheme 3.10. *Initial arene scope of the methodology with isolated yields (unless otherwise stated).* [a] *Starting arene used from commercial supplier as a 1:1 mix of regioisomers.* [b] *Conversion by GC.*

The initial arene scope of the of the reaction can be seen above (**Scheme 3.10**). Here we utilise the super-stoichiometric DDQ variant of the chemistry, this is simply due to the fact that it proved to be a much more general method. Compound **100** gave yields in the low-mid

90% range for both the FPT (freeze-pump-thaw) degassed, 0.3 equiv. DDQ, and the super-stoichiometric method (including multiple repeats); **103** for example, gave only 11-14% for the FPT method, almost a sixth of its yield with super-stoichiometric DDQ. Given the inexpensive nature of DDQ, this is not prohibitive, and as such the super-stoichiometric method was taken forward as the more general version of the method. Of course, as is true of all methods, this could be optimised for a specific substrate of choice, and given the high variability in product yields, it is very possible that a certain desired substrate could be high yielding given a very low DDQ loading with the FPT method. This issue is re-examined when the nucleophile scope is considered **Subsection 3.2.7**.

Despite a number of substrates yielding only a *trace* of the desired product (**114–127**), the overall aspect of the scope was positive, maintaining usable yields for a range of mildly electron poor fluoroarenes, substrates which pose a challenge to classical S_NAr. Oxygenation on the ring was generally not tolerated by this method, e.g. **123** and **125**. This is likely due to the same back-electron transfer phenomenon that prevents further substitution of the anisole products. Fortunately however, the reaction does seem tolerant of having benzylic positions present in the arene without observed side reaction (products **107a**/**108a**), and also of other interesting functional groups such as sulfonamides (product **110**).

This transformation seems to occupy a rather unusual chemical space. When the fluoroarene is easily oxidised and the resultant radical cation is therefore not highly electrophilic, e.g. **114**, then the product yield is low. If the fluoroarene is itself electrophilic and its radical cation very highly reactive but difficult to form, e.g. **124**, then issues still persist. It is interesting to see that the substrates of the former case are those most applicable to transition-metal-catalysed oxidative addition, and the latter those most applicable to classical S_NAr. Here, however, the 'Goldilocks zone' is found for mildly electron poor fluoroarenes, such as **103**, where

both the single-electron oxidation of the arene and the S_NAr on the resultant radical cation are rapid. Furthermore, this 'Goldilocks requirement' of the electron deficiency being 'just right' does not limit the application of this photochemistry to halogenofluorobenzenes. Indeed, this work indicated that good yields were maintained when a strongly electron withdrawing group was mitigated by an alternative electron donating group or electron donating ring system. For example, cyanonaphthalene **109** was a perfectly viable substrate for this process, with the extra electron density of the naphthalene ring system offsetting the powerful cycano group sufficiently for this chemistry. This feature of the reactivity, the balance needed between ease of oxidation and S_NAr reactivity of resultant cation, is well exemplified by the series of results **100a**, **102a**–**105a**. Here we see a steady decrease in yield on going from **100a** to **102a** to **103a** to **105a**, i.e. as the reactivity of the radical cation intermediate decreases. However, we also see a decrease on going from **100a** to **104a** – possible indicating the point at which oxidation potential of the arene substrate seems to become the more important factor. The reason for lower yield for **106a** compared to **103a** is not clear from this simple analysis (although no *para* substitution – i.e. C–H activation – was observed for **106a**, it is possible that a low level occurs and this uses up enough of the catalyst to reduce the yield of the desired product, as no reoxidant is present).

The question immediately raised by these observed, empirical, trends in yield is what do they imply about the nature of the reaction pathway? The mechanism put forward in **Subsection 3.2.3** allows for approximate reaction coordinates to be proposed, such as **Figure 3.3**. This reaction coordinate is drawn with the S_NAr step rate determining and not the initial oxidation of the substrate. This would seem at first to fit with the observations outlined above. While reaction yield is not directly correlated to the rate of the rate determining step, in most cases (a fact demonstrated computationally in **Subsection 5.3.2**) the large reduction potential of

photoexcited DDQ ($E_{DDQ^{T_1}/DDQ^{\bullet-}} = +3.18$ V vs SCE) is greater than the oxidation potentials of the arene substrates under investigation. It would be plausible, therefore, to infer from Marcus theory that for most cases formation of the radical cation of the starting material (electron transfer, ET), while reversible (back electron transfer, BET), is rapid and not rate determining.

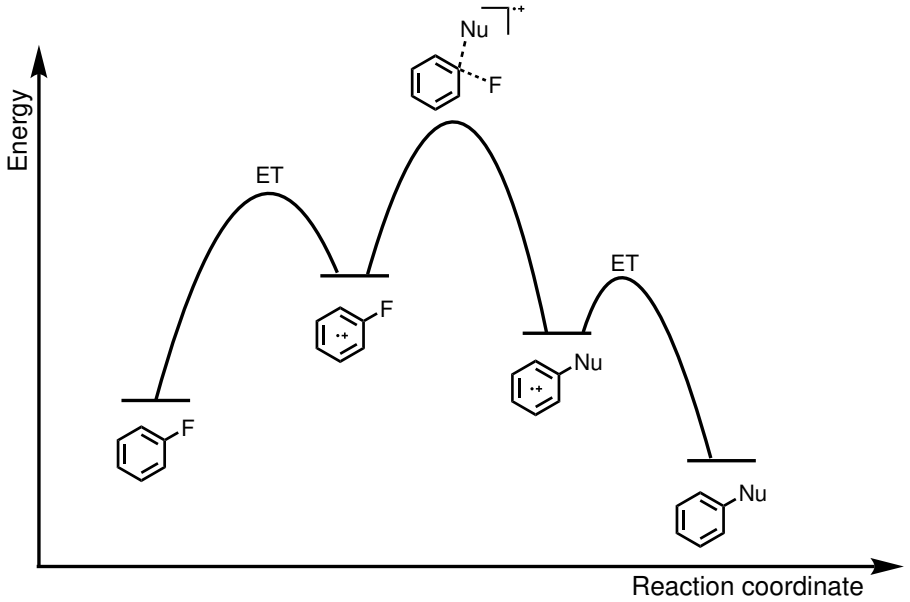

Figure 3.3. *Simple reaction pathway (not to scale), to allow for discussion of reaction mechanism.*

The simple explanation for the empirical 'Goldilocks zone' would, therefore, be as long as the above condition (i.e. ET is rapid and BET is slower than S_NAr) held true, that the most electrophilic arenes would have the lowest energy pathway to product (most rapid nucleophilic attack step). However, the factors are linked, increasing the electrophilicity of the arene would also tend to increase its oxidation potential. As such, the reaction pathway (**Figure 3.3**) cannot be viewed accurately as two independent halves - as nucleophilic attack becomes faster, electron transfer becomes slower. Eventually, a point is reached where electron transfer becomes rate determining and yields appear to drop off rapidly at further increases in redox potential / electrophilicity from this point.

However, this too can be seen as an over-simplification, it certainly may seem counter in-

tuitive to suggest nucleophilic attack on a radical cation as a rate determining step in many of the cases. This is because the actual likely rate determining step is loss of fluoride. The pathway in **Figure 3.3** is shown concerted (a Meisenheimer transition state) contrary to the suggested formation of a cyclohexadienyl radical intermediate proposed in the discussion in **Subsection 3.2.3**. Hence, we can present a further modified reaction pathway, **Figure 3.4**. Given the large C–F bond activation energy, we could propose an early transition state between the cyclohexadienyl radical intermediate and the radical cation of the product. Invocation of Hammond's postulate would therefore lead us to suspect stabilisation of the cyclohexadienyl radical intermediate (a proxy for the energy of the C–F bond breaking transition state) as the likely underlying cause for the observed trend with arene electrophilicity, as literature data suggests a similar correlation with stabilities of cyclohexadienyl radicals.[133]

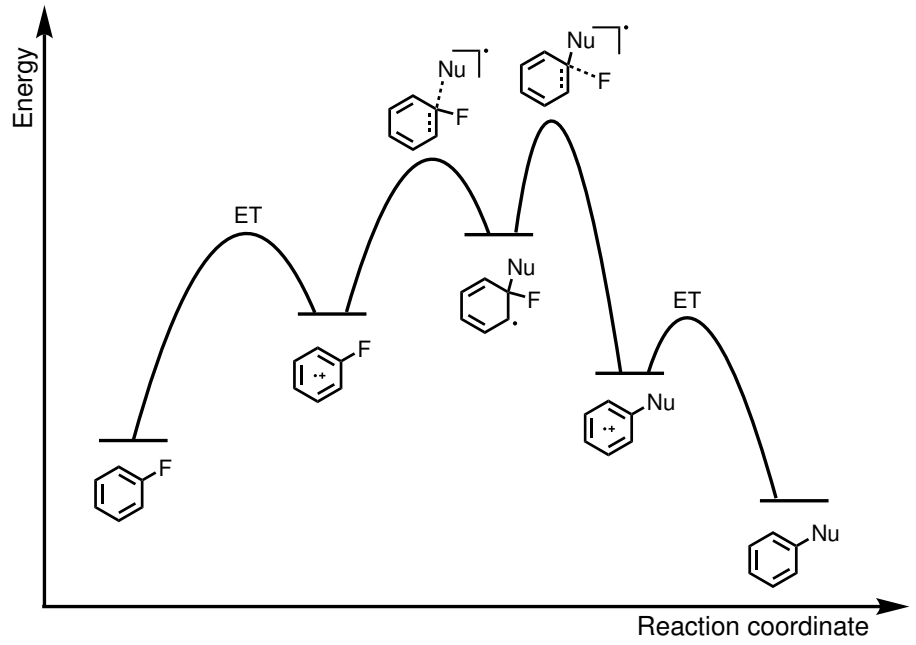

Figure 3.4. *Modified reaction pathway (not to scale), to allow for discussion of reaction mechanism.*

With the reason for the observed trends in yield now better understood, the results of the pyridine heterocycles used in this scope, **111a**, **112a** and **113a**, still at first inspection appear outré. Given that the oxidation potential of 2-fluoro-5-chloropyridine ($E^{o}_{\mathrm{Ar/Ar}^{\bullet+}} = 2.6$ V)

is only 0.3 V in excess of that of 2,4-dichlorofluorobenzene ($E^{o}_{\mathrm{Ar/Ar}^{\bullet+}} = 2.3$ V), a yield of higher than 5-10% should therefore be expected (although this will be considered in greater depth in **Subsection 3.2.6**). However, the reaction solvent, TFE, is likely to strongly hydrogen bond with these pyridine substrates making them more pyridinium-like. Some doubts may justifiably be raised as to whether this conversion is due to the photochemistry at all or whether it is in fact merely due to a background thermal reaction in this case. To alleviate this concern, control reactions were put in place to ensure there was no background reaction. Given the the reactor's operating temperature of only slightly above room temperature and the relatively low nucleophilicity of methanol, it should come as no surprise that these diagnostic control reactions confirmed that there was no background conversion in these cases. These results are shown below (**Table 3.4**), and are discussed in more detail (along with attempts to improve the yield of the desired product) in the following section.

3.2.5 Reoptimisation of S_NAr conditions for pyridine substrates

The initial results gathered when applying this chemistry to fluoropyridines, while only exhibiting low product yield, seemed promising as a starting point for further optimisation. Indeed, of particular interest was the unusual substitution of a C5 fluoride in preference to a C2 chloride (for substrate **113**). As such, a range of modifications were attempted to improve this performance and these are shown below (**Table 3.4**).

Given the number of attempts made to reoptimise this methodology for pyridine substrates, it is worth discussing **Table 3.4** quite fully. The use of TMS protected nucleophiles (entries 7-9, 11, and 25) was initially hoped to aid the C–F bond breaking step, the idea being that the formation of the stronger Si–F bond (129 kcal/mol)[134] would provide an additional driving force for the reaction. However, the results certainly show that this silylated nucle-

ophile offered no benefit with respect to increased product yield.

Although the oxidation potentials of fluoropyridines are similar to the equivalent chlorofluorobenzenes (i.e. the potential of 2-fluoropyridine is slightly larger than that of 4-chloro-1-fluorobenzene, and 2-fluoro-5-chloropyridine has a potential slightly larger than 2,4-dichloro-1-fluorobenzene – see discussion in next subsection, **Subsection 3.2.6**), it is possible that the potential difference for the single electron transfer to the catalyst is no longer feasible. This becomes more likely, when the effect of hydrogen bonding between the pyridine and the TFE solvent is considered (with a H–bonded 'pyridinium-like' species being much harder to oxidise). As such, the use of leaving groups other than fluoride was considered. In particular, O-based leaving groups were thought to be suitable alternatives, given the significant polarisation of the *ipso* carbon, but with more tractable oxidation potentials. Substrates **112a**, **128** and **129** were tested and the results are shown in entries 12-14. No improvements were seen with respect to formation of the desired S_NAr product. However, interestingly tosylpyridine (**128**) was found to detosylate cleanly giving pyridone (**130**). This too was found to be a photochemical process, with substitution occurring on the tosyl ring as opposed to the pyridyl ring. This process was subject to some exploration, as is described later in this chapter (**Section 3.3**).

Other attempts to solve the perceived oxidation potential problem were then made. Quinolines such as **131** were tested in the hope the potential would be in the effective range for this chemistry (entry 15) as was *N*-oxide **113b** (entry 16). This was not particularly successful, neither were attempts to improve yield by addition of bases to increase the pH and reduce the H-bonding effects.

Altering the solvent had some effect. Having either nucleophile or fluoropyridine as the reaction solvent (entry 18 and 20) did give useful conversion, but this approach clearly has

practicality issues, as well as a likely thermal component to the yield when the loadings are that high (see also entry 23). The use of DCE without TFE to eliminate H-bonding effects was unsuccessful (entry 19). This was also the case when ethyl acetate was used as solvent (entry 21). When no solvent was used (entry 22) and the reaction components were dry stirred under blue light irradiation, then the yields once again became usable. Interesting this seems to be a truly photochemical effect (entry 24). Use of nitrobenzene, 1-octanol, or diisopropylcarbinol (DIPC) as solvents (entries 27-29) also proved ineffectual in increasing product yield. Use of phenol as reaction solvent (at 45 ^{o}C to ensure melting point was exceeded) lead to some substitution with phenol but again this was likely to be a thermal process. Using pyridine as the solvent even in combinations with TFE resulted in the solution visibly darkening and no product was formed (entries 37 and 38). Attempts to use 2,2-difluoroethanol (DFE) as a less acidic (less strongly H-bond donating) alternative to TFE did not prove useful (entry 41).

The use of Lewis acidic additives was considered as a possible solution to the conversion issues. Here, $Ti(OMe)_4$ (entries 32–36) and $FeCl_3$ (entries 39–43) were investigated. While $Ti(OMe)_4$ had no effect on the reaction outcome, $FeCl_3$ showed some promise. There was initial concern that this could be a thermal S_NAr but the result of the control appears to rule this out (entry 42). The issue with this method is the low conversion with this very simple pyridine, and the fact when tested with our more interesting C_5-F substituted substrate (**113**) only trace conversion was observed (entry 43).

The use of a proton scavenger was hoped to help in case of partial protonation of pyridines was indeed occurring, without degrading DDQ as bases were so apt to do. β-Pinene was thus tested to investigate whether or not this effect could be achieved.[135–137] Unfortunately this too was unsuccessful (entry 44).

Table 3.4. *Optimisation for Fluoropyridine and Related Arenes*

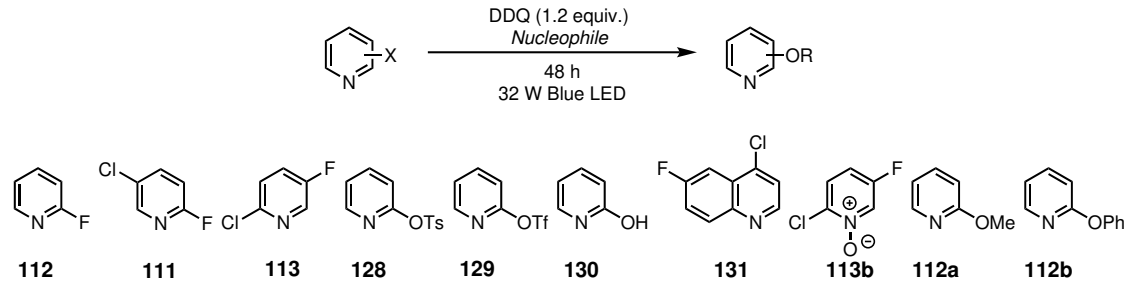

Entry	SM	Nuc (10 eq.)	Solvent[a]	Additive (eq.)	Other	Result
1	**112**	MeOH	1:1 TFE:DCE			~5% conversion
2	**111**	MeOH	1:1 TFE:DCE			~10% conversion
3	**113**	MeOH	1:1 TFE:DCE			~5% conversion
4	**112**	MeOH	1:1 TFE:DCE		No Light	No conversion
5	**111**	MeOH	1:1 TFE:DCE		No Light	No conversion
6	**113**	MeOH	1:1 TFE:DCE		No Light	No conversion
7	**112**	TMSOEt	1:1 TFE:DCE			No conversion
8	**112**	TMSOEt	1:1 TFE:DCE			No conversion
9	**112**	TMSOEt	1:1 TFE:DCE			No conversion
10	**112**	MeOH	MeCN			No conversion
11	**112**	TMSOEt	MeCN			No conversion
12	**112a**	EtOH	1:1 TFE:DCE			No conversion

Continued overleaf...

Entry	SM	Nuc (10 eq.)	Solvent[a]	Additive (eq.)	Other	Result
13	**128**	EtOH	1:1 TFE:DCE			Detosylation to give **130**
14	**129**	EtOH	1:1 TFE:DCE			No conversion
15	**131**	MeOH	1:1 TFE:DCE			Trace
16	**113b**	MeOH	1:1 TFE:DCE			No conversion
17	**112**	MeOH	1:1 TFE:DCE	DMAP (1.0 eq.)		No conversion
18	**112**	MeOH[b]	MeOH			~50% conversion
19	**112**	MeOH	DCE			Trace
20	**112**	MeOH[f]	**112** (5 mL)			Significant conversion to **112a**[c]
21	**112**	MeOH	Ethyl acetate			No conversion
22	**112**	MeOH	Solvent free			~50% conversion[c]
23	**112**	MeOH[b]	MeOH		No Light	~40% conversion
24	**112**	MeOH	Solvent free		No Light	~5% conversion
25	**112**	TMSOEt	Solvent free			No conversion
26	**113**	MeOH[b]	MeOH			No conversion
27	**112**	MeOH	$PhNO_2$			No conversion

Continued overleaf...

Entry	SM	Nuc (10 eq.)	Solvent[a]	Additive (eq.)	Other	Result
28	**112**	MeOH	1-Octanol			No conversion
29	**112**	MeOH	DIPC[e]			No conversion
30	**112**	MeOH	Phenol		45 °C	~30% conversion to **112b**
31	**112**	MeOH	Phenol	$Ti(OMe)_4$ (1.0 eq.)	45 °C	~55% conversion to **112b** and ~5% of **112a**[c]
32	**112**	MeOH	1:1 TFE:DCE	$Ti(OMe)_4$ (1.0 eq.)		No conversion
33	**112**	MeOH	DCE	$Ti(OMe)_4$ (1.0 eq.)		No conversion
34	**112**	MeOH	DCE	$Ti(OMe)_4$ (1.0 eq.)		No conversion
35	**112**	MeOH	1:4 TFE:DCE			No conversion
36	**112**	MeOH	1:4 TFE:DCE	$Ti(OMe)_4$ (1.0 eq.)		No conversion
37	**112**	MeOH	Pyridine			No conversion
38	**112**	MeOH	1:1 Pyridine:TFE			No conversion
39	**112**	MeOH	DCE	$FeCl_3$ (2.0 eq.)		>40% conversion
40	**112**	MeOH	1:1 TFE:DCE	$FeCl_3$ (2.0 eq.)		No conversion
41	**112**	MeOH	1:1 DFE:DCE			No conversion

Continued overleaf...

Entry	SM	Nuc (10 eq.)	Solvent[a]	Additive (eq.)	Other	Result
42	**112**	MeOH	DCE	$FeCl_3$ (2.0 eq.)	No Light	No conversion
43	**113**	MeOH	DCE	$FeCl_3$ (2.0 eq.)		trace
44	**112**	MeOH	1:1 TFE:DCE	β-Pinene (2.0 eq.)		No conversion[d]
45	**112**	MeOH	Solvent free		No DDQ	No conversion
46	**113**	MeOH	Solvent free			trace
47	**112**	MeOH	DCE			~40% conversion
48	**112**	MeOH	1:1 TFE:DCE			~30% conversion

[a]Concentration, with respect to arene, is kept at 0.1 M unless otherwise stated. [b]MeOH as solvent, not 10 eq. [c]Formation of byproduct with $M^{+\bullet}$ = 181 m/z was also observed. [d]Many isomers of pinene observed as well as OMe incorporation into the pinene structure. [e]Diisopropylcarbinol. [f]MeOH as limiting reagent (1 eq.), not 10 eq.

The difficulty encountered with the pyridine substrates appeared to be due to the fundamental requirements of this photochemistry. In particular, as was found in the initial optimisation (**Table 3.3**, **Subsection 3.2.2**), a fluorinated alcoholic solvent such as TFE is important to the chemistry. This effect is likely due to the dual stabilisation such a solvent can provide, i.e. stabilisation of both the radical cation of the substrate and, through H–bonding, the radical anion of the photocatalyst. Such stabilisation is likely to be what allows the process to be feasible – as poor results with other solvent classes would attest to. However, while this effect offers no real downside for the carbocyclic arenes, in the case of the pyridines the implica-

tions of a strongly H–bond donating solvent is clear. Indeed, as discussed, it is very likely this effect that raised the oxidation potential of these substrates beyond the effective range of the photocatalyst.

The above explanation for the poor yields of desired product when fluoropyridines are used as substrates, while reasonable, was somewhat speculative at this stage. Furthermore, it raised the question of just how important the redox potentials of the substrates were to the chemistry. As seen previously, the initial arene substrate scope (**Scheme 3.10**, **Subsection 3.2.4**) seemed to have rough correlation, by inspection, to the electron richness of the arene. More interestingly, though, it was not a simple positive or simple negative correlation. There is clearly an inflection point occurring around the electron density held by arenes similar to 2,4-dichlorofluorobenzene (**100**). This is the so-called 'Goldilocks effect' mentioned above. This qualitative observation was explained in terms of the stability of the cyclohexadienyl radical intermediate (proxied by the electrophilicity of the substrate) relative to the easy of oxidation of the substrate by photoexcited DDQ. However, we had the means to quantify these effects, and had already demonstrated the calculation of redox potentials (**Subsection 2.3.2**) and numerous scales exist for the measurement and now calculation of electrophilicity. As such, the work towards a quantitative understanding of the performance of a substrate in this chemistry is given below.

3.2.6 Arene scope analytics

Analytics can be seen as the study of trends to aid prediction of future outcomes. The empirical, qualitative, trends recognised between reaction yield and both substrate oxidation potential and substrate electrophilicity (proxy for cyclohexadienyl radical stability) seen in the above work led to efforts to quantify these seemingly important factors, and investigate to what ex-

tent – if any – prediction of the reaction yield of other substrates would be possible from these values. For a given nucleophile (for our analysis we shall continue to utilise methanol) these factors can be represented by the oxidation potential of the arene ($E^{o}_{Ar/Ar^{\bullet+}}$) and its 'electrophilicity index' (ω) - essentially a measure of how electrophilic a species is.[138–142]

$E^{o}_{Ar/Ar^{\bullet+}}$ has been discussed in **Subsection 2.3.2** and further detail is given in **Experimental Details 5.3**, so an additional presentation of its calculation will not be rendered here. The calculation of ω however can be seen below (**Equations 1.1-1.3**). Here μ is the electronic chemical potential, η is what is known as 'hardness', and E_H / E_L are the HOMO and LUMO energies respectively.[138–142] As can be seen, this index is essentially just a value derived from the HOMO – LUMO gap of the species. This is a simple but surprisingly effective measure of electrophilicity. Many, increasingly complex, variants of this index exist.[138–142] However, many papers show that the increasingly complex indices are not necessarily the most accurate. For our purposes the electrophilicity index as presented was deemed to be sufficient.

$$\omega = \frac{\mu^2}{2 \times \eta} \quad \text{(Eqn 1.1)}$$

$$\mu = \frac{E_H + E_L}{2} \quad \text{(Eqn 1.2)}$$

$$\eta = E_L - E_H \quad \text{(Eqn 1.3)}$$

Given the data gathered in the initial arene scope (**Scheme 3.10**), we were able to calculate the value of $E^{o}_{Ar/Ar^{\bullet+}}$ and ω for each substrate (that gave a measurable yield). It should be noted, that we are calculating ω for the starting material, not the radical cation nor cyclohexadienyl radical directly. This is reasonable as we only seek to indirectly infer the stability of

the cyclohexadienyl radical and this reduces computational difficulty. Indeed, the reason we use electrophilicity as a measure at all is that it is a convenient proxy for the stability of the cyclohexadienyl radical intermediate.

These calculated values are collected in a table in the experimental details of this thesis (**Subsection 5.3.2**–**Subsection 5.3.4**) and plotted against isolated yield in **3.5a** and **3.5b**. Strikingly, there are already noticeable trends in these, unrefined, data. Indeed, the electrophilicity index, ω, up to 1.7 eV is extremely well correlated with isolated yield and even at higher values there is a noticeable but opposite trend (**3.5a**). There were also discernible trends within the redox potential - isolated yield data. However, it can be seen that adherence to these trends is much lower in this case, with more outliers.

It was clear, therefore, that the correlation of isolated yield was stronger with electrophilicity index than it was with oxidation potential; a surprising result as we would have initially predicted the exact opposite situation. This, however, ties in well with reaction pathway put forward in **Figure 3.4**. There were still some outliers within the electrophilicity index data, these seemed to correspond to substrates which were readily oxidisable whilst retaining a large electrophilicity index (e.g. 1-fluoro-4-cyanonapthalene (**109**), ω = 2.31 eV).

As such a range of parameters were generated though trial and error combinations of $E^{o}_{\mathrm{Ar/Ar^{\bullet+}}}$ and ω, with higher weighting given to ω. Of these parameters one was seen to show the closest correlation. This parameter had the value: $\omega + \left(\frac{\omega + E^{o}_{\mathrm{Ox}}}{2}\right)$ and was named the 'S_NAr parameter'. As can be seen the S_NAr parameter contains both electrophilicity index terms and a oxidation potential term but is weighted in favour of the electrophilicity index. It gives a very good positive correlation for 'low' values of S_NAr parameter and an acceptable negative correlation for 'high' values, although more data points in this high value range would be beneficial (**Figure 3.5 (c)**). This plot is then linearised in **Figure 3.5 (d)** by determining the S_NAr

parameter value below the turning point of all points above the turning point, by simultaneous equations (for full details please see **Subsection 5.3.4**).

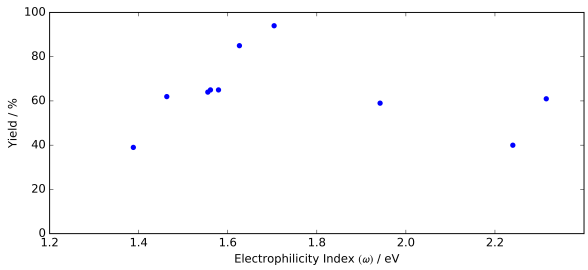

(a) *Plot of reaction yield and electrophilicity index*

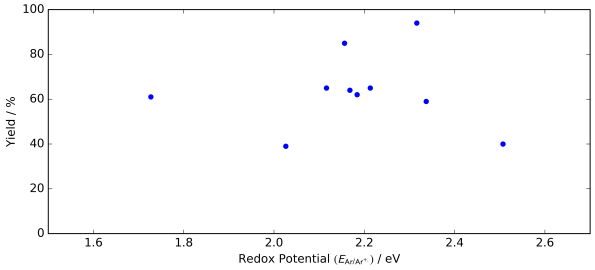

(b) *Plot of reaction yield and oxidation potential*

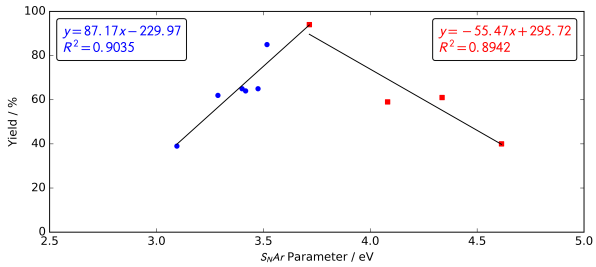

(c) *Correlation between reaction yield and developed 'S_NAr' parameter*

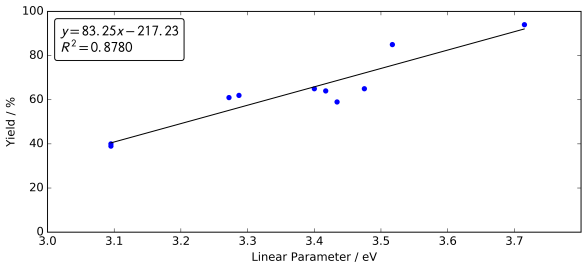

(d) *Figure a linearised plot of* ***(c)*** *(achieved by using the equations of the lines)*

Figure 3.5. *Correlations of various parameters of starting arene with reaction yield for the reaction with methanol under standard conditions*

The advantage of this linear parameter is that it allows for simple conversion of the calculated parameter into a predicted yield. Whilst we initially did not expect this would be used to predict reaction yields *a priori*, the application of this data to reaction planning did seem achievable. For example, below is gathered yield ranges and the linear parameter values that accompany them (**Table 3.5**). Thus when trying to determine if a given fluoroarene is amenable to this process then a quick calculation of redox potential (which is possibly already know from literature data) and electrophilicity index would allow prediction of the approximate yield expected. It is hoped that this will be a useful predictive tool for substrate selection, and will continue to be improved upon. Of course, this is limited in the sense that it is predicting the yield of the reaction with methanol as a nucleophile, although if a substrate is

predicted to be high yielding with methanol then it would be expected to do well with other alcohols, allowing for additional complexities such as steric effects as they arise. The obvious question to ask of this data is how accurate are the predictions of this simple model. As stated, this model was not originally created with the idea of accurately predicting reaction yields, but rather to help discern between fluoroarene substrate that would be expected to work and those that would not in this chemistry. However, with this data available it seemed sensible to see how applicable this could be to the actual prediction of the chemical outcome.

Table 3.5. *A rough guide to yield for a given linear parameter value*

Entry	Parameter range	Yield range
1	<2.72	<10%
2	2.72-2.85	10-20%
3	2.85-2.97	20-30%
4	2.97-3.09	30-40%
5	3.09-3.21	40-50%
6	3.21-3.33	50-60%
7	3.33-3.45	60-70%
8	3.45-3.57	70-80%
9	3.57-3.69	80-90%
10	>3.69	>90%

As such a range of fluoroarenes were selected and their parameters calculated. The photochemistry was performed to obtain isolated yields and the linear parameters were converted into predicted yields (**Table 3.6**). The first caveat of this roughly predictive tool can be seen clearly for this table. The predicted parameter value translates into the yield that can be expected, when the S_NAr chemistry is all that occurs. For the indanones (**137** and **138**), it is believed we observed only reversible addition into the carbonyl by methanol. Determination of the reaction outcome in the case of the boronic acids (**135** and **136**) was more challeng-

ing with starting material being recovered along with a variety of trace products in each case. Regardless, these boronic acids do not undergo the S_NAr chemistry. However, if the S_NAr is the predominant reactivity, then some reasonable predictions can be achieved. From these results, we can see a mean discrepancy of 10% between the predicted yield and the isolated yield. We were pleased with this in its own right, as that is perfectly reasonable for allowing a quick and rough prediction of how viable a given substrate is (as long as the S_NAr predominates reactivity). However, closer examination gives further insight here. It can be seen that two of these substrates are highly aligned with predicted results (**132** and **139**, entries 1 and 8), while two others are notably more different (**133** and **134**, entries 2 and 3). The discrepancy seen for **133** could simply be due to the overestimation of the effect of *meta* substituents as the meta chloride likely offers much less enhancement to the stability of the cyclohexadienyl radical intermediate than the equivalent *ortho* chloride. This effect was likely less significant in **132** as bromides have a weaker directing effect. The difference with **134** is probably due to it falling on the right hand of the two intersecting lines, i.e. the trend like with fewer data points and thus inherently more error.

Another use for this data is re-examination of certain phenomena. Firstly the pyridine substrates are worth discussing in light of this semi-predictive tool. Below is shown data related to the fluoropyridines discussed previously (**Table 3.7**). The first three entries of this table gives the predicted yields of these substrates based purely on the computational method adumbrated above. As can be plainly seen, this model vastly over-predicts the expected yields of these species. The reason that this model is likely to be breaking down here has been mentioned previously - the H-bonding interaction between the pyridine and the TFE solvent. Entry 4 shows the worst case scenario, a fully protonated 2-fluoropyridinum (**112c**). This situation is unlikely here but it does represent the extreme limit of H-bonding. As can be seen, and com-

Table 3.6. *attempted prediction of yield based on given linear parameter value*

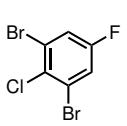
132

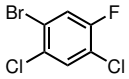
134

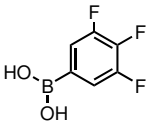
136

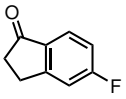
138

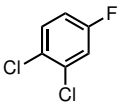
133

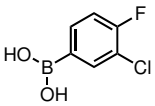
135

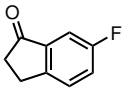
137

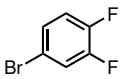
139

Entry	Arene	Linear Parameter	Predicted Yield	Isolated Yield	|Predicted Yield − Isolated Yield|
1	**132**	3.00	33%	33%	0%
2	**133**	3.69	90%	74%	16%
3	**134**	3.61	83%	61%	22%
4	**135**	3.37	63%	-	-
5	**136**	3.38	64%	-	-
6	**137**	2.72	9%	-	-
7	**138**	3.44	69%	-	-
8	**139**	3.42	67%	64%	3%

pletely expected, the oxidation potential is almost 1 V above that the reduction potential of the photoexcited DDQ catalyst (+3.18 V). This would completely rule out the transformation, not just for this extreme case but likely also for any case of strong H-bonding, which is almost certainly present in these examples with these conditions.

Table 3.7. *Pyridines and their linear parameter value*


112

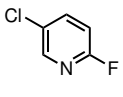
111

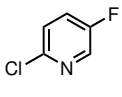
128

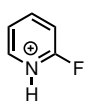
112c

Entry	Pyridine	$E^{o}_{Ar/Ar^{\bullet+}}$ / V	ω / V	Linear Parameter	Predicted Yield
1	**112**	+2.73	1.64	3.71	91%
2	**111**	+2.59	1.98	3.26	54%
3	**113**	+2.61	1.99	3.23	52%
4	**112c**	+4.12	9.44	−4.30	0%

The final caveat worth discussing, is the leaving group dependency of this method. The linear parameter allows this rough yield prediction, only because it could be correlated with yield data (**3.5d**). That data was gathered for the substitution of fluoride by methanol and as such prediction can in principal only be made for such systems. In practice, the next subsection (**Subsection 3.2.7**) will show that simple alcohols, e.g. ethanol and IPA, unsurprisingly give very similar yields to methanol and as such could be crudely predicted in this way. However more structurally complex alcohols present other subtleties, rendering their prediction with these values unreliable. No such 'wiggle room' exists with the identity of the leaving group, however. Even for **139** in which the yield of the product predicted was within 3% of the isolated value (Entry 8, **Table 3.6**), the method described above gave no indication as to which fluoride would be substituted or even if a mixture of product should be expected. Based on previous results it was hoped that the most 'activated' C–F bond - that is of the fluoride *para* to the bromide (and *ortho* to the other fluoride) as opposed to that which is *meta* to the bromide (and *ortho* to the first fluoride) - would be the major site of substitution. Indeed substitution of the aforementioned fluoride was the only substitution observed, with the fluoride *meta* to the bromide being untouched. As such, the prediction can be seen to be specific for the activated fluoride in the system and not simple any fluoride which may be present. Additionally, it is worth considering other potential leaving groups, and the most interesting to consider in the light of the products we are making, the previous work by Nicewicz,[23] and the resubjection experiment discussed previously, is of course methoxide as a leaving group.

As can be seen (**Table 3.8**), if the parameter value were to hold for other leaving groups (not that we would expect that behaviour to be accurate), then **100a** and **116a** would potentially be viable substrates for this chemistry. While substitution of an anisole by methanol could be studied with deuterated methanol, ethanol as will be shown below gives yields within

Table 3.8. *Linear parameter values for selected anisoles*

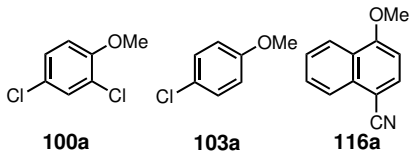

100a **103a** **116a**

Entry	Anisole	Linear Parameter	Predicted Yield
1	**100a**	2.82	18%
2	**103a**	2.41	0%
3	**116a**	3.40	66%

3% of methanol yields with fluoroarenes and, as such, can be used here for simplicity instead. Indeed, the result of reaction between **100a** and ethanol under standard conditions has been presented already when we sought to determine if the product reacted further in the reaction (**Scheme 3.8**). In that experiment, no substitution was observed. However, this could be due to the fact that the predicted yield here is only 18% and in **Table 3.6** there were discrepancies between predicted and actual vales which were greater than 18%. Although, it should be said, in all of those cases the parameter value was much higher (on this scale) than 2.82 implying that it is the higher values which it is less accurate for, which coincides with there being less data points at those values to allow prediction in the first place. However, it can be seen that **116a** is somewhat different; not only is its predicted yield much higher and far beyond the errors we have seen so far (when other factors were not in play) but also seems more intuitive that the cyano group could allow the molecule to overcome the back electron transfer problem with the catalyst (discussed previously) when the arene is functionalised with oxygen substituents.

The outcome of this resubjection experiment is shown below (**Scheme 3.11**) and is identical to that with **100a** i.e. no conversion was observed. This result is reasonably definitive that this parameter will only give insight into fluoride substitution, which seems perfectly reason-

able given the nature of the data used to generate yields from it. However, if these values were replotted against isolated yield values from other substitutions it could potentially be useful for rough prediction in those cases, or it may require tweaks such as to the weighting of $E^{o}_{\mathrm{Ar/Ar}^{\bullet+}}$ to ω but such modifications, even with other parameters would be quite doable. With these reaction analytics now completed for arene substrates it was next time to consider the nucleophile scope of this chemistry.



Scheme 3.11. *Resubjection experiment of isolated* ***116a*** *to the reaction conditions, with ethanol as a nucleophile*

3.2.7 Nucleophile scope of S_NAr chemistry

The initial nucleophiles scoped for this chemistry were alternative alcohols (**Scheme 3.12**). Of the very simple alcohols: methanol (product **100a**), ethanol (product **100b**), isopropanol (product **100c**) and *tert*-butanol, only *tert*-butanol failed to give product (with only 3% of the TFE solvent adduct, **100d**, being recovered instead); the others gave excellent yields. Other alcohol nucleophiles also gave good to excellent yields such as cyclopropylmethanol (product **100g**) and (*R*)–1,3–butanediol (products: **100i** and **100j**). It is worth noting the 3:1 ratio of product **100i** to product **100j**, which demonstrates a reasonable preference for attack by a primary alcohol over that from a secondary alcohol. However, many other examples of alcohol nucleophiles seemed to give lower than would be expected yields (for example: products **100e**, **100f**, **100h** and **100z**). In examples such as products **100k–100m**, functional group tolerance is likely a key factor in the poor yields obtained, with other sites of oxidation being a key part of that issue. A similar statement could be made for the low to no yields obtained

from phenol nucleophiles (products: **100x** and **100y**), where oxidation of the aromatic ring of the nucleophile would occur in preference to that of the arene substrate.

Alcohols containing cyclic ethers seemed to perform noticeably poorly (products **100n–100r**). A possible factor, in this poor performance, was illuminated in a later examination of the reaction with methanol in 1:1 TFE:THF solvent mixture. In those experiments the major reaction product was a methoxylated-THF species, implying the arene is not the site of oxidation in those cases. Nitrogen based nucleophiles also performed poorly here giving trace product (products: **100t–100w**). Part of the reason only trace amounts of product were detected is like due to the fact that trace formation of König like products (i.e. the C–H activation products) were also detected (see **Subsection 1.2.2**), but even if all that material had been desired product, the yields would have still been reasonably poor.

Another feature of **Scheme 3.12** worth mentioning is the fact that the super-stoichiometric DDQ conditions are once again used. As with the arene scope some alcohols performed well with 0.3 equiv. DDQ loading and FPT degassing. For example, isopropanol under these conditions gave 76% yield of **100c**, while the yield of **100f** reduce to 20% when this method was used. Once again optimisation for specific cases maybe possible, but for this scope the most general procedure was used.

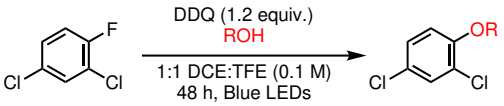

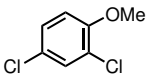

100a
MeOH (10 equiv.) 94%
MeOH (2 equiv.) 93%

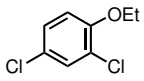

100b
EtOH (10 equiv.)
87%

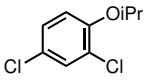

100c
iPrOH (10 equiv.)
89%

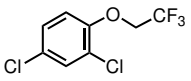

100d
*t*BuOH (10 equiv.)
3%

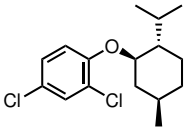

100e
(-)-menthol (5 equiv.)
21%

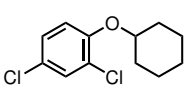

100f
cyclohexanol (10 equiv.)
64%

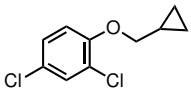

100g
cyclopropylmethanol (10 equiv.)
87%

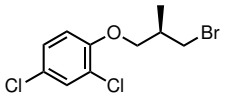

100h
(*R*)-$BrCH_2(Me)CHCH_2OH$
(2 equiv.) 36%

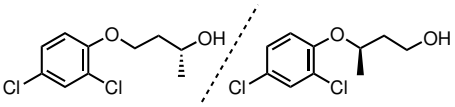

100i / **100j**
(*R*)-1,3-butanediol (2 equiv.)
80% 3:1 (mixture)

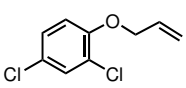

100k
allyl alcohol (10 equiv.)
16%

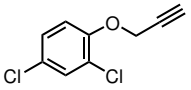

100l
propargyl alcohol (10 equiv.)
trace

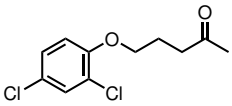

100m
5-hydroxyl-2-pentanone (10 equiv.)
0%

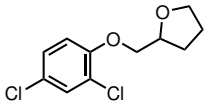

100n
furfuryl alcohol (10 equiv.)
0%

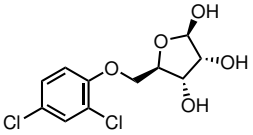

100o
D-(-)-ribose (10 equiv.)
0%

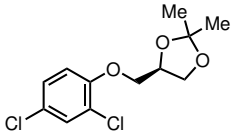

100p
(*R*)-(-)-2,2-dimethyl-1,3-dioxolane-4-methanol (10 equiv.)
0%

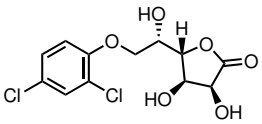

100q
L-gulonic acid γ-lactone (10 equiv.)
0%

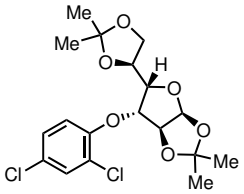

100r
diacetone-D-glucose (10 equiv.)
0%

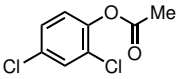

100s
acetic acid (10 equiv.) 0%
acetic anhydride (10 equiv.) 0%

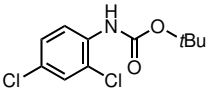

100t
tert-butyl carbamate (10 equiv.)
trace

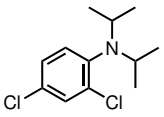

100u
DIPA (10 equiv.)
trace

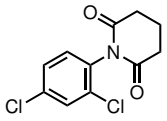

100v
glutarimide (10 equiv.)
trace

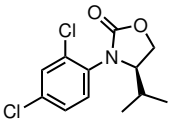

100w
(4*R*)-(+)-4-isopropyl-2-oxazolidinone (10 equiv.)
trace

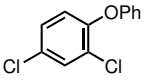

100x
phenol (10 equiv.)
trace

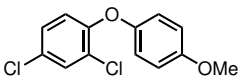

100y
p-methoxyphenol (10 equiv.)
0%

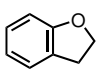

100z
0%

Scheme 3.12. *Initial nucleophile scope of the methodology.*

It was initially hoped that more nucleophilic heterocycles such as imidazoles and pyrazoles would solve some of these problems as they should react more efficiently with the aryl radical cations. However some reoptimisation was first needed to achieve this. This was due to the fact that the increased nucleophilicity proved problematic for the DDQ catalyst when all were added to the reaction vessel at the same instance. As such, optimisation focused on the slow addition of the nucleophilic component and/or reduction in DDQ loading.

This lead to reoptimisation for azoles (**Table 3.9**). As can be seen, lower nucleophile loading could be used here than for alcohols (**Table 3.9**, entries 1–4). Not only is pyrazole a stronger nucleophile than the alcohols screened, but also a large excess of pyrazole could react with the catalyst. We also see that, in the case of pyrazole with 4-chlorofluorobenzene, rigorous freeze-pump-thaw (FPT) with 0.3 equiv. DDQ was as effective as slow addition of nucleophile (entries 5 & 7) and both of these methods are more effective then their equivalent reaction without inert atmosphere or slow addition (entries 4 & 6 respectively). Our inference from these results was that undesired nucleophile – DDQ reactivity was occurring for pyrazole (see **Subsection 1.2.2**), and that minimising this reactivity by reducing the concentration of catalyst or effective concentration of nucleophile is needed. As previously demonstrated, reliability issues across substrates persist when the sub-stoichiometric FPT method is used and as such the slow addition method was adopted.

The scope of azoles subject to this method is detailed below (**Scheme 3.13**). As can be seen, reactivity is essentially limited to pyrazoles with triazoles (**103h**, **103i** and **103l**), indazole (**103k**), and imidazole (**103o**) proving ineffectual. The inability to use imidazole as a nucleophile is likely due to the imidazole – DDQ Michael addition problem observed by König (see **Subsection 1.2.2**). An easy explanation for the failure of the indazole and the triazoles reactions is less readily available. It is possibly due, once again, to the impact of subtle difference in

Table 3.9. *Optimisation table for the reaction of* ***103*** *with Pyrazole, to form* ***103b****, under 32 W blue light.*

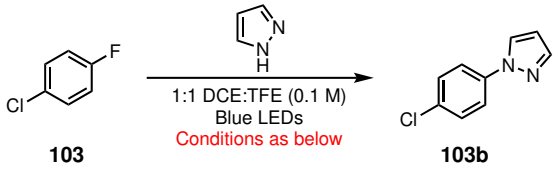

103 **103b**

Entry	[**103**] / M	DDQ equiv.	Pyrazole equiv.	**103** equiv.	Time / h	Atmo-sphere	Isolated Yield
1	0.1	1.2	10	1	48	Air	16%
2	0.1	1.2	2	1	48	Air	25%
3	0.1	1.2	1.2	1	48	Air	34%
4	0.1	1.2	1	2	48	Air	42%
5	0.1	1.2	1.2	1	14[a]	Air	62%
6	0.1	1.2	1.2	1	14	Air	35%
7	0.1	0.3	1.2	1	48	N_2[b]	61%

[a] 2.5 mL of a solution of pyrazole in 1:1 DCE:TFE was added over 12 h to a 2.5 ml solution of **103** and DDQ in 1:1 DCE:TFE suspended in the photoreactor. [b] O_2 removed *via* freeze-pump-thaw under N_2.

reactivity. In these cases, optimisation of the rate of addition of nucleophile in order to regain some reactivity, may be achievable (although this is not something we have yet investigated).

Of the pyrazoles studied, 4-substituted pyrazoles were generally higher yielding than 3-substituted pyrazoles, with moderate yields obtained for all of the 4-substituted pyrazoles under study (**103c**, **103d**, **103e** and **103g**) except for **103n** – although isolation of **103e** was complicated by hydrolysis of the boronic ester on silica gel column. The reason for observing no product with **103n** could simply be due to the increased acidity reducing the nucleophilicity of this pyrazole. Of the 3-substituted pyrazoles (**103f**, **103j** and **103m**), only **103f** gave a recordable yield and even this was only 5%. It is interesting that only one isomer of product (**103f** as drawn) was observed in this example, but this could easily be due to the fact that the reaction was so low yielding that the other isomer was not observed.

A final observation to make is that pyrazole gave an identical yield to methanol with 4–chloro-

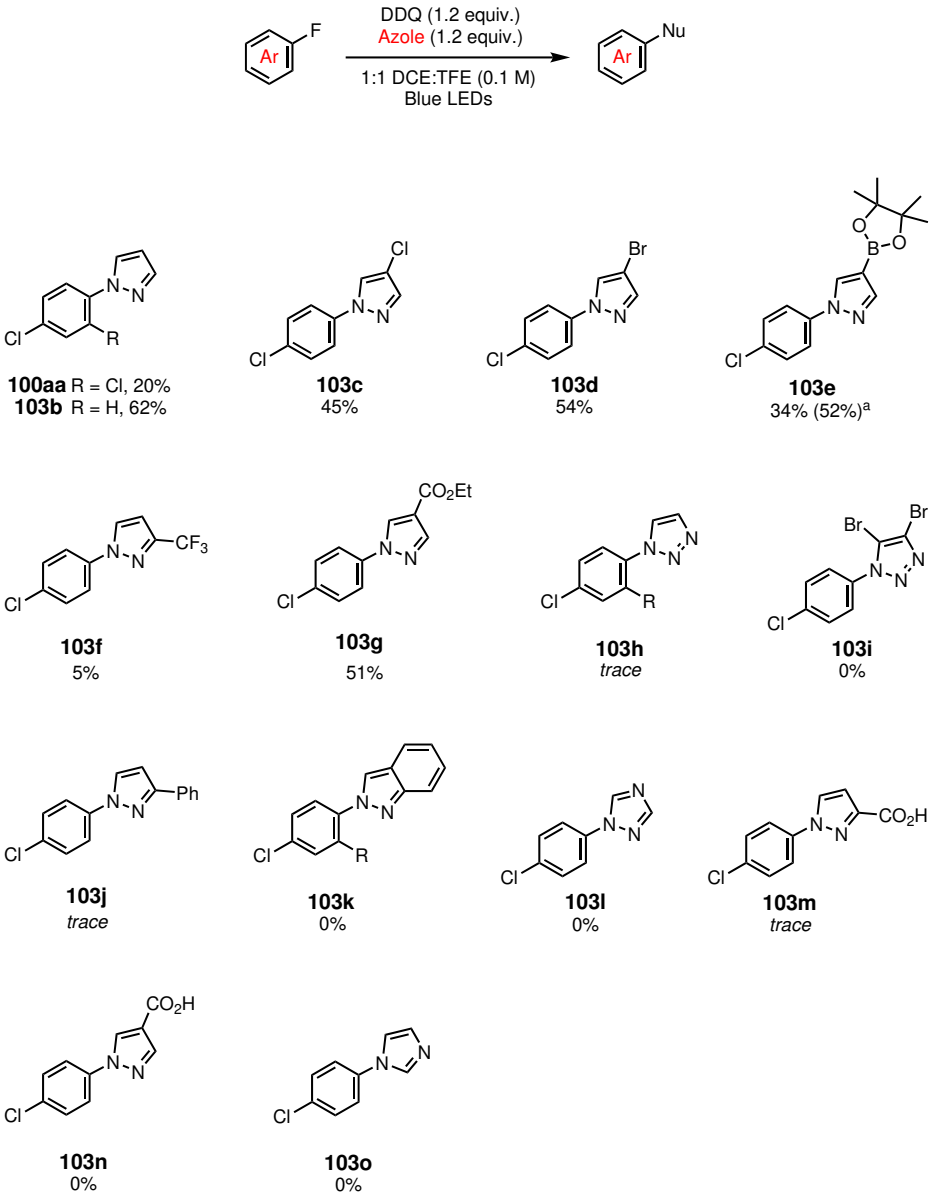

Scheme 3.13. *Azole nucleophile scope of the methodology.* [a]*NMR yield using 1,3,5–trimethoxybenzene as the internal standard.*

fluorobenzene (**103b**), but with 2,4–dichlorofluorobenzene (**100aa**) the yield was significantly worse. This is likely due to the optimisation of the rate of addition of pyrazole. **100** has higher oxidation potential than **103**, as a result the stead state concentration of the radical cation **100**$^{\bullet+}$ which will build up before the first addition of nucleophile will be lower. As the addition rate was the same for both **100** and **103**, the amount of excess nucleophile (relative to the radical cation) was higher for substrate **100**, meaning more opportunity for off cycle catalyst

deactivation as discussed above.

While improving the electrophilicity of our arenes did, until point where oxidation became slow, improve reaction performance we see no great benefit in improving the nucleophilicity of our nucleophile, as demonstrated by the yield of **103b** being the same as **103a**, 62%. Indeed the difficulties posed by off-cycle catalyst reactivity have been highlighted. This further suggests that it is loss of fluoride which is likely to be rate determining in this chemistry. While increasing arene electrophilicity did lead to improvement in yields in many cases this can be seen as relating back to our discussion of transition state stability (**Subsection 3.2.4**) the nucleophilicity of the nucleophile can be seen not to exert much of an effect here.

This completes the delineation of our photochemical S_NAr method.[108] To enable a balanced discussion of the advantages and disadvantages of this method, it would be germane to consider the method of Lambert *et al.* which was published shortly before this work.[107] There are a number of points of similarity between the two works, however, the important differences in method – particularly the use of electrophotochemistry by Lambert and coworker – result in some fascinating, as well as practical, differences between the two. This comparison is presented below.

3.2.8 Lambert method for electrophotochemical S_NAr

The recent work of Lambert and co-worker also uses photochemically excited DDQ to oxidise fluoroarenes to the corresponding aryl radical cations, to allow a radical cation accelerated S_NAr to take place (**Scheme 3.14**).[107] However, unlike other chemistry discussed this work uses an electrochemical (undivided) cell to complete the catalytic cycle (**Scheme 3.15**).

In this cycle, $DDQ^{\bullet -}$ is oxidised at the anode to DDQ and, at the cathode, the aryl radical formed upon nucleophilic addition to the aryl radical cation, is reduced to an aryl anion – a

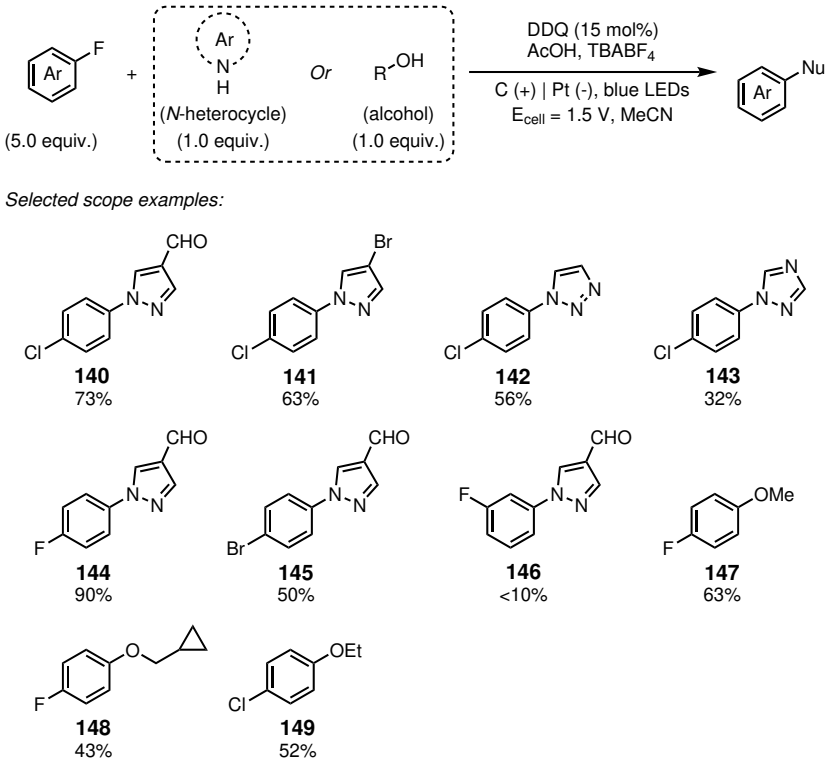

Scheme 3.14. *Electrophotochemical S_NAr of fluoroarenes developed by Lambert and co-workers.* [107]

Meisenheimer complex – which can spontaneously lose F^- to regain aromaticity and form product. The first advantage of this methodology over the work presented here is clear – a significantly lower DDQ loading is enabled by electrochemically induced turnover. Although, it should be noted that the authors recharge the reaction with DDQ after 24 h, an approach we had not attempted.

An additional advantage of the Lambert method is the nucleophile scope, which is an improvement on ours. This will be due to factors including the lower DDQ loading and the continual electrochemical turnover of the DDQ minimising its interaction with the nucleophile. Also the use of a solvent such as MeCN instead of the strongly H-bonding TFE, will also result in an effective increase in nucleophilicity of the nucleophiles used. Finally, the use of excess arene (5.0 equiv.) will help allow for greater conversions for a given nucleophile.

Conversely, however, many of these factors are also responsible for reducing arene com-

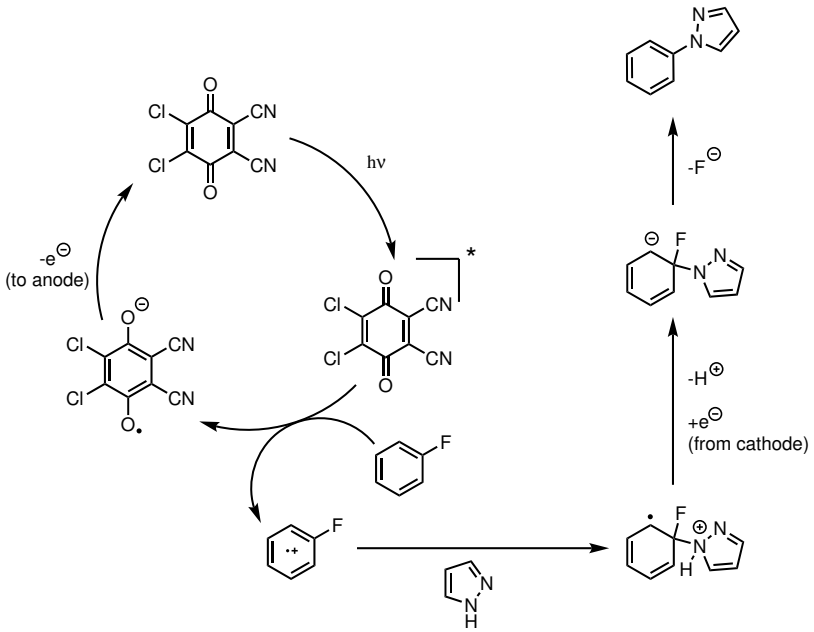

Scheme 3.15. *Mechanism proposed by Lambert and co-workers for the electrophotochemical S_NAr of fluoroarenes.*[107]

patibility, and while the arene scope of our method is not quite as broad as would be ideal, it is still slightly larger and slightly more diverse than that presented by Lambert and co-worker. Three points of difference seem important to this outcome. Firstly, the arene scope is highly sensitive to the DDQ loading, as was seen in trying to advance our FPT method. Secondly, solvent will be a significant factor here. While TFE will retard the nucleophilicity of the nucleophiles under study *via* H-bond donating effects, the same H-bond doing effects will help stabilise the radical anion of DDQ and its high dielectric constant will help stabilise the aryl radical cation of the arene. This dual effect will increase the number of arenes that can be effectively oxidised by DDQ. Finally, having the nucleophile in excess will allow more efficient trapping of the aryl radical cations that form, even if those aryl radical cations are inherently less reactive.

Operational simplicity is perhaps another area in which our method may be considered more favourable. Pure photochemical setups are relatively simple, while adding an electrochemical component adds complexity and additional factors to consider. It is possible that in

the case of a failed classical S_NAr reaction for a substrate with only mild activation, the barrier to attempting our method for a researcher may be lower than that of Lambert and coworker. This factor would be increased if the arene was a more valuable component than the nucleophile, and reduced if the opposite were true.

From the comparisons made above it can be seen that, while a number of features are shared by both methods, the subtle differences between the two have a significant effect on the ideal use cases for the methods. Factors including the relative value of the components, the nature of the arene and nucleophile desired for use, supply of DDQ, access to electrochemistry equipment, and practicality of catalyst recharging etc. To some extent the methods can be seen to complement each other, and both complement traditional S_NAr which tends to struggle for the type of mildly activated arenes and moderate nucleophiles that both these works address. Before progressing to the conclusion of this chapter, it is worth briefly examining another radical cation accelerated substitution. The following chemistry was observed during the study of our S_NAr chemistry.

3.3 Radical Cation Accelerated Deprotection of Tosylates

When discussing the attempts to optimise the S_NAr chemistry of pyridine substrates, an unexpected detosylation occurred returning pyridone (entry 13, **Table 3.4**). While it can be seen as only a minor anomaly, it was considered to be worth following up, particularly given the stability of the pyridyl triflate to the reaction conditions. It was suspected that this chemistry was photochemical in nature. To investigate this, the usual control reactions without light or without DDQ, were performed. As can be seen (**Scheme 3.16**), no reactivity was observed in these control reactions. Typically, apart from deprotection by acids and strong nucleophiles, tosylates are susceptible to reduction (not oxidation).

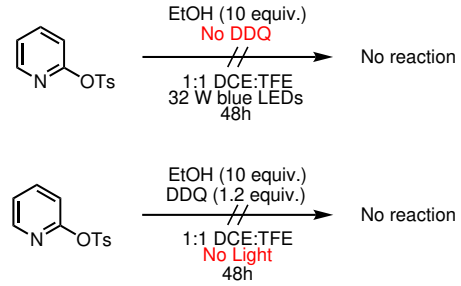

Scheme 3.16. *Control experiments for the observed deprotection of tosylates.*

However, in this case, we could be seeing reactivity due to a single electron oxidation enabling a weak nucleophile such as ethanol to effect the deprotection. This proposed mechanism is shown below (**Scheme 3.17**), and given that deprotection of tosylates by stronger nucleophiles such as Grignard reagents is known, this radical cation accelerated mechanism could well be operative. It seems very reasonable in this example, that the tosyl ring system would be oxidised in preference to the pyridyl ring system.

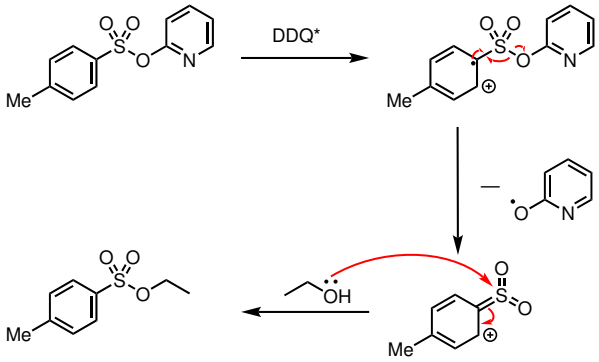

Scheme 3.17. *Proposed mechanism for the radical cation accelerated deprotection of tosylates.*

A quick optimisation of this reaction showed a strong dependence on DDQ loading, with super-stoichiometric loadings once again proving to be the most effective, although this is the only example where freeze-pump-thaw degassing was not also tested at lower catalyst loadings. Interestingly in this example, using an alcohol as solvent was just as effective as TFE:DCE with advantage that trace TFE tosylation was also avoided, as well as reducing reaction cost. Although not extensively studied, this curious deprotection method is somewhat

interesting although seemingly not high yielding enough to have much practical application (**Scheme 3.18**).

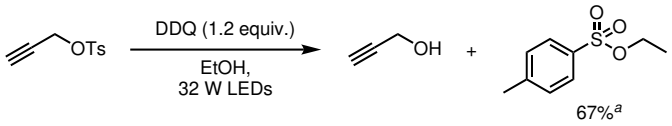

Scheme 3.18. *Photochemical deprotection of tosyl propagryl alcohol, over 48 h. [a]NMR yield (1,3,5-trimethoxybenzene internal standard).*

3.4 Chapter Summary

The above work describes our final application of DDQ as a photocatalyst, and the next chapter will present the conclusions and future work for this research as a whole. During the various chemistries under study in this thesis, the many advantages and disadvantages of this attempted application have been highlighted. Again, we find great possibility to affect powerful transformations by employing a photocatalyst with a redox potential of $E_{\mathrm{DDQ}^{\mathrm{T1}}/\mathrm{DDQ}^{\bullet-}} = +3.18$ V vs SCE, but encounter complications fully utilising it for desired reactivity. High (super-stoichiometric) loadings were often a feature of these chemistries. As the substitution chemistry would inherently be net redox neutral, this dependency on super-stoichiometric loadings was likely due to the need to generate high concentration of aryl radical cation given that our nucleophiles were either very mild, such as alcohols, or in very low concentrations, such as the pyrazoles. This is further exacerbated as the S_NAr chemistry proceeds. As while the product anisole is not reactive in the substitution, it is more reactive in the initial single electron oxidation (even if the back electron transfer is more rapid). Thereby lowering the effective catalyst loading as the reaction proceeds, as more and more catalyst molecules are tied up in endless non-productive redox transfers with the reaction product. This issue could be in part alleviated by stronger nucleophiles or possibly higher nucleophile concentration, however, this can be incompatible with the catalyst as shown. The solution of Lambert *et al.*, the

use of electrochemistry to keep DDQ constantly turning–over, is an effective one. Although, it does suffer from having a more complex reaction setup and the use of excess arene may play an important role in maximising desired single electron transfers with starting material over undesired, non-productive, shuttling events with product.

Despite these complexities, this chapter still describes the development of a photochemical S_NAr, with an inexpensive DDQ photocatalyst which can in some cases be used with a 30 mol% loading (although super-stoichiometric is more general), on mildly electron-poor fluoroarenes. These mildly electron poor fluoroarenes are often unreactive in classical S_NAr and if such a transformation had be designed for a synthesis and proved to be ineffective, these photochemical conditions could be trialed very expediently. A rough idea of arene suitability, with the caveats stated above, can also be gleaned for a range of arenes with the computational method outlined above.

Chapter 4

Conclusion and Future Work

Given the work presented in the preceding chapters, the opportunities and avenues for future work can now be adequately discussed. Further to this, reflection upon the findings of the work within this thesis can be undertaken. This can be measured against the aims set for this work at the outset. Such an examination can be found below in sections reflecting areas of work where appropriate.

4.1 Oxidative Functionalisation and Dual-Functionalisation of Arenes

The work on the hydroxylation of arenes met challenges surrounding generality. With subtly different arenes giving large differences in yields. While this does limit its application it does also allow for high selectivity. Regardless future work would likely focus on improving reactivity across the board. A possible way forward would be to use both TFE to increase the effective range of DDQ oxidation and set the nucleophile as the limiting reagent. This approach, based on the results of ours and other chemistry, should help level out the arene-to-arene differences in yield to some extent. Weather or not this would be enough of an effect would have to be seen. Additionally, a nucleophile of greater value than water may have to be used in that case, in order to justify the use of excess arene.

One of the key outcomes of this work was the development of the dual-functionalisation, hydroxylation-nitration, chemistry. This chemistry, while not truly broad in scope, was a marked improvement compared to the hydroxylation chemistry it was developed from, and allowed one pot one step access to a much more highly functionalised final product. This chemistry too may benefit from the future modifications suggested above. Indeed, there may be more value in investigating these changes in this case. Catalyst tuning could also be a viable option.

4.2 Radical Cation Accelerated S_NAr

The work on photochemically generated aryl radical cations as useful reactive intermediates in S_NAr chemistry, is perhaps our best demonstration of the use of DDQ as a photocatalyst. It demonstrates the application of the large $E_{DDQ^{T_1}/DDQ^{\bullet-}} = +3.18$ V vs SCE redox potential in a synthetically relevant context. The ability to enable S_NAr reactivity, under mild conditions, in arenes that would otherwise be unamenable or require forcing conditions to do so, does allow a moderate expansion of the chemical space of S_NAr reactivity. It achieves our original goal of harnessing the ubiquitous reagent DDQ as a powerful photocatalyst in real-world-relevant chemistry. However, there remains room for improvement in this method. Lambert *et al.* demonstrated a highly effective way to improve the nucleophile scope of such chemistry – the use of electrochemistry to ensure the turnover of the catalyst and allow for a lower loading. This marked improvement does, however, come at the cost of increasing the complexity of the reaction setup. Future work on this topic may therefore focus on chemical means to achieve the same effect. Would it, for example, be possible to find an efficient reoxidant for DDQ to increase the TON of the process? We already saw no large differences when TBN was used in our initial studies but a number of viable options exist, and if one were found to be appropriate for the chemistry then benefits of the electrophotochemical system could be had

with the simplicity of the purely photochemical one.

Additionally, it can be seen that while the ability to access aryl fluorides as substrates is useful, the ability to target other $C_{aryl}-X$ bonds would further extend the utility of the method. To effect such a change would most likely require a change in catalyst. As Nicewicz's work has shown the acridinium catalysts do not suffer from overly rapid electron transfer with the ARCs of anisoles - allowing substitution of OMe groups. One interesting and ambitious future aim would be the development of a powerfully oxidising catalyst, similar to DDQ, but with better tolerance of O-Aryl rings. Such a catalyst could enable the targeting of OMs or related groups allowing substitution of easily installable groups with significantly polarising effect enabling high yields with even moderate nucleophiles. While this would not be an easy goal, catalyst development could give significant benefits.

4.3 Other Chemistry with Aryl Radical Cations

In addition to the work shown previously in this thesis, we have begun initial exploration into other methods centered around photochemically generated aryl radical cations. The vast majority of that work could be termed: "internal trapping of photochemically generated aryl radical cations". This work sought to use tethered π-bonds for the initial aryl radical cation trapping event (e.g. **Scheme 4.1**). This is potentially more versatile than the direct trapping with external nucleophiles used in previous methods, as following trapping the π-bonds could be regenerated, or the newly generated radical cation my itself be trapped.

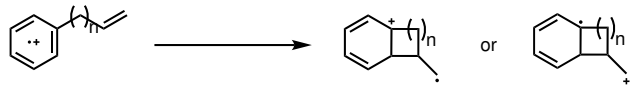

Scheme 4.1. *Example of internal trapping of an aryl radical cation.*

As of time of writing, the most developed process of this class is our initial investigation into radical cation analogs of 'cation-π' cyclisations. Cation-π cyclisation are very powerful

complexity generating transformations (e.g. progesterone synthesis, **Scheme 4.2**).[143] It was hoped we could utilise our radical cation generating chemistry to induce simple alkene trapping and perhaps even, *eventually*, cascades analogous to that in **Scheme 4.2**.

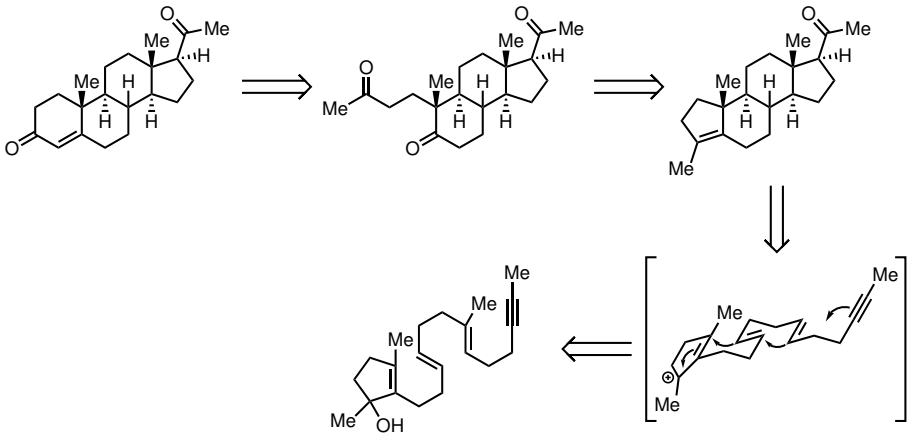

Scheme 4.2. *Cation-π rearrangement in progesterone synthesis.*[143]

To achieve this, a handle for oxidation was needed. A species that could be readily oxidised, and one which allowed diversification or removal. As such, electron rich imines of the type shown in **Figure 4.1** were hoped to act as a flexible starting point for the kinds of processes that could occur (**Scheme 4.3**). As well as being easily hydrolysed or otherwise transformed after the photochemical process, they offered both tractable oxidation potentials, as calculated by the author (**Figure 4.1**, see also **Subsection 5.3.2**) and the possibility for interesting chemistry (**Scheme 4.3**).

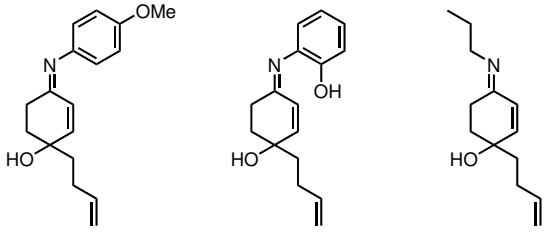

150 +0.616 V **151** +0.946 V **152** +1.432 V

Figure 4.1. *Potential model substrates and their computational redox potentials (vs SCE).*

While many appropriate imines could have been prepared, **151** was selected as the first

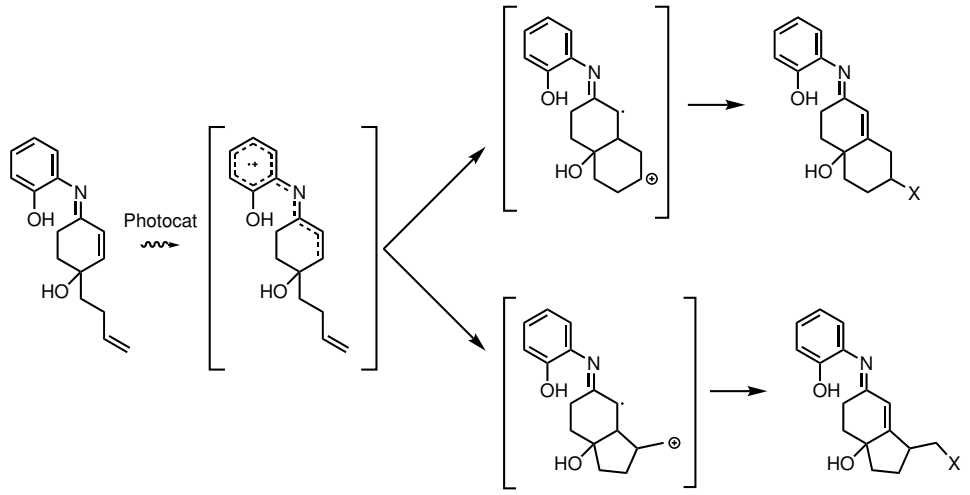

Scheme 4.3. *Possible reaction outcomes.*

model system. It was calculated to have a favourable oxidation potential of $E_{\mathbf{151/151^{\bullet-}}} = +0.946$ V (vs SCE, in MeCN), and the hydroxyl group on the 2-position of the arene was considered to be a possible trapping group potentially allowing additional chemistry to occur in the initial reactivity screens.

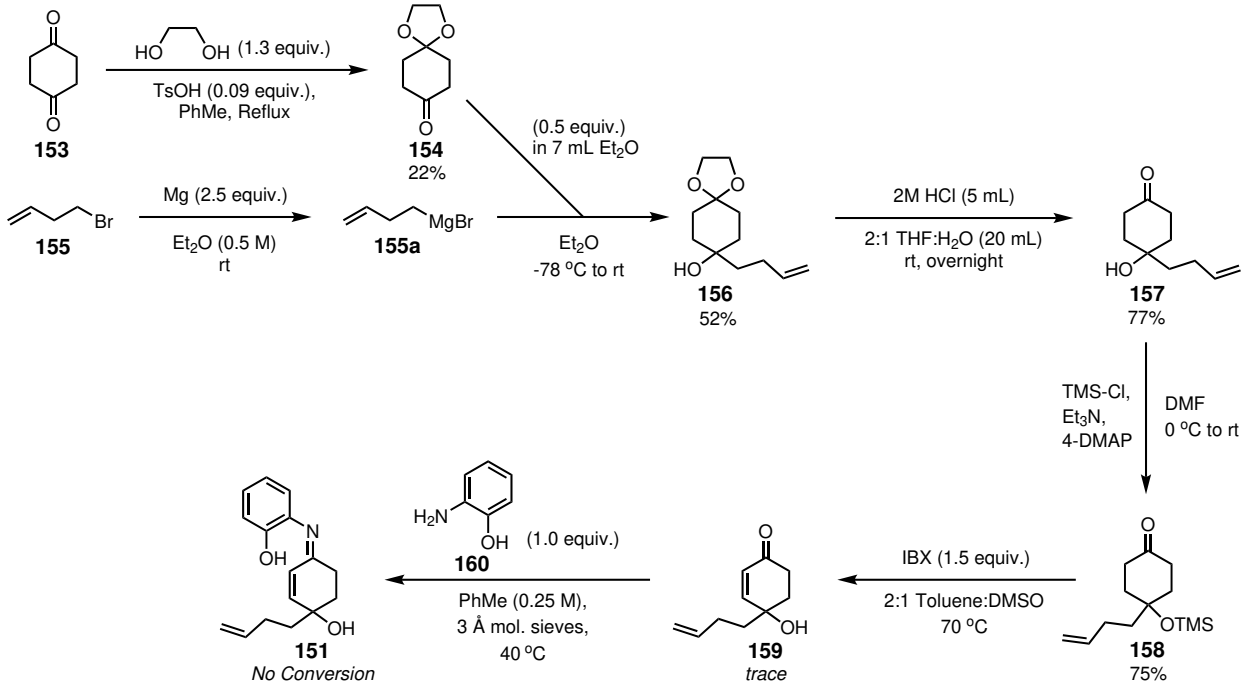

Scheme 4.4. *Synthesis of model substrate,* ***151****.*

The initial synthetic route to **151** is shown below (**Scheme 4.4**), and was not sufficient to

allow proper study of the envisaged transformation. A proposed improved route is also given (**Scheme 4.5**) although time did not allow for much progress to be made with this new route.

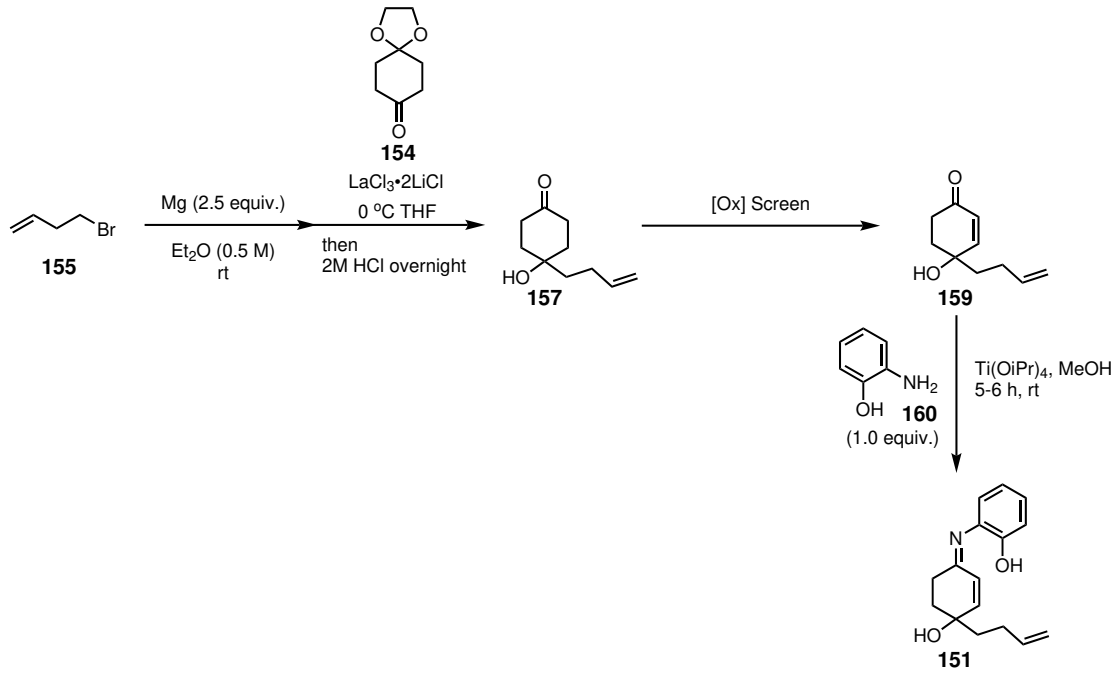

Scheme 4.5. *Proposed improved synthesis of model substrate,* ***151****.*

The work on internal trapping of aryl radical cations is thus a good examples of initial work that would heavily benefit form further development and research. As of this stage this work is in its infancy, but given the chemical principles involved and the experience of photochemistry gained, further examination of this would would hopefully bare fruit in the form of useful photochemical methods that provide a structural change to the starting materials.

4.4 Final Considerations

This work on the photochemical functionalisation of arenes and heteroarenes has mostly focused on the application of photoexcited DDQ to the generation of aryl radical cations *via* single electron oxidation. With these aryl radical cations we have studied a range of processes both net oxidative and net redox neutral, optimising these processes where it was felt appropriate.

In doing so we have developed an operationally simple photochemical S_NAr processes which extends S_NAr reactivity to the mildly electron-poor substrates which are incompatible with other methods. Additionally other smaller methods, such as the dual hydroxylation-nitration of arenes have also been refined. Still further methods have been begun and await later studies.

Chapter 5

Experimental Details

5.1 General Experimental Details

Reactions were carried in oven-dried glassware at room temperature (RT = approx. 25 ^{o}C) unless stated otherwise. Standard inert atmosphere techniques were used in handling all air and moisture sensitive reagents. Thin-layer chromatography (TLC) was performed using Merck aluminium backed sheets coated with Merck Kieselgel 60 F254 (230-400 mesh) fluorescent treated silica, which were visualised under UV light (λ_{max} = 254 nm) or $KMnO_4$. Flash column chromatography was performed using Merck Kieselgel (230-400 mesh). ^{1}H NMR, ^{13}C NMR and ^{19}F NMR spectra were recorded on Bruker AVIII HD 400 nanobay (400/101/376 MHz) and Bruker AVII 500 (500/126/471 MHz) spectrometers in deuterated solvents. Chemical shifts are reported in parts per million (ppm) to the nearest 0.01 ppm for ^{1}H NMR, ^{13}C NMR and ^{19}F NMR. ^{1}H NMR and ^{13}C NMR spectra were referenced relative to the solvent residual peak. Peak assignments were made on the basis of chemical shifts, integrations, coupling constants, and comparison to known compounds, using COSY, HSQC and HMBC experiments where appropriate. Multiplets are described as singlet (s), doublet (d), triplet (t), quartet (q), quintet (quint), septet (sept), multiplet (m), broad (br), or combinations thereof. Coupling constants

(*J*) are reported to the nearest 0.5 Hz. IR spectra were recorded on a Bruker Tensor 27 FT-IR spectrometer deposited as a thin film. Melting points were recorded using a Leica Galen III hot-stage microscope apparatus and are reported uncorrected in degrees Celsius (^{o}C). Low resolution mass spectra were recorded on a Waters LCT premier XE Micromass spectrometer (ESI). GC-MS analyses were performed on a 7890B GC system equipped with a HP 5MS column (30 m, 0.25 mm id, 0.25 μm film thickness), operated in split mode, with helium carrier gas. The detector was an Agilent 7200 quadrupole time of flight (Q-ToF) instrument equipped with a direct insertion probe supplied by Scientific Instrument Manufacturer (SIM) GmbH. Instrument control and data processing were performed using Agilent MassHunter software. Source conditions for EI were adjusted to maximise sensitivity. Light emission spectra measurements (UV-visible) were recorded using an Ocean Optics USB2000. Commercial grade reagents and solvents were used without purification, unless otherwise stated. 2,3-Dichloro-5,6-dicyano-p-benzoquinone (DDQ) was obtained commercially and purified by recrystallization from hot chloroform.

5.2 Photochemical Procedures

3 W LED information

ZFLIN Led Strip Lights Kit SMD 5050 Waterproof 32.8 Ft (10 M) 600 LEDs RGB 60 LEDs/m were purchased from Amazon and used for all 3 W photochemical experiments. Generic LED light strips are available from several manufacturers and would give similar results.

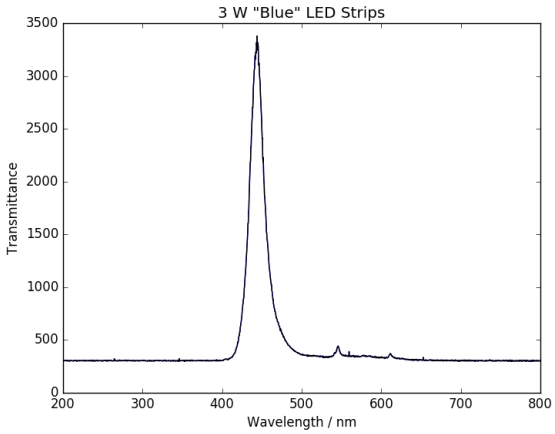

Figure 5.1. *UV-visible emission spectra of the 3 W LED strips, in the 'blue light' mode used in our study.*

32 W LED information

Kessil H150 LED Grow Lights were purchased from Amazon and used for all 32 W photochemical experiments. Alternative lamps are available from several manufacturers and would give similar results.

Initial Photoreactor Set-up

A continual strip of 3 W blue LEDs was placed around the inside of a crystallisation beaker, and a cardboard 'rack' placed on top so that vials may be held inside the reactor 2 cm away from the light source. A nitrogen line was placed into the reactor, to keep the light source cool and the reaction at approx. 30 ^{o}C.

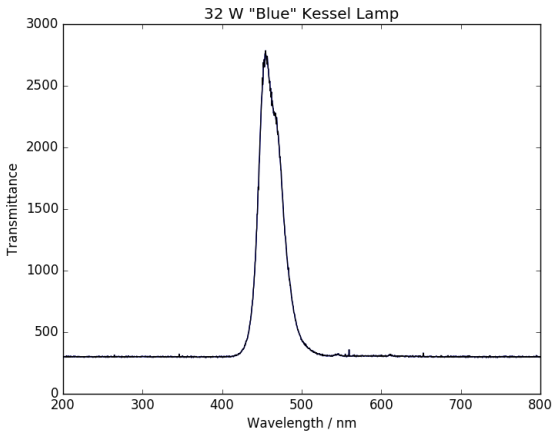

Figure 5.2. *UV-visible emission spectra of the 'blue light' 32 W LED lamp used in our study.*

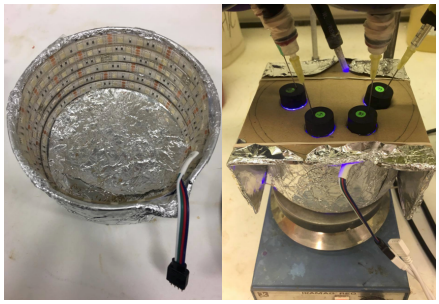

Figure 5.3. *The initial photoreactor set-up used in this project.*

Second Generation Photoreactor Set-up

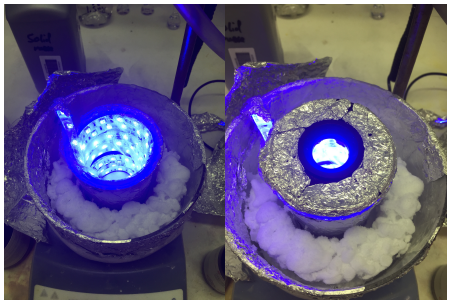

Figure 5.4. *The second generation photoreactor set-up used in this project.*

A continual strip of 3 W blue LEDs was placed around the inside of a 100 mL beaker, and a rubber Büchner ring placed on top so that a vial may be held inside the reactor. The reactor itself was then placed in the centre of a crystallisation beaker and the free space filled with dry ice pellets, to keep the light source cool and the reaction at approx. $-35\ ^{o}$C.

Flow Photoreactor Set-up

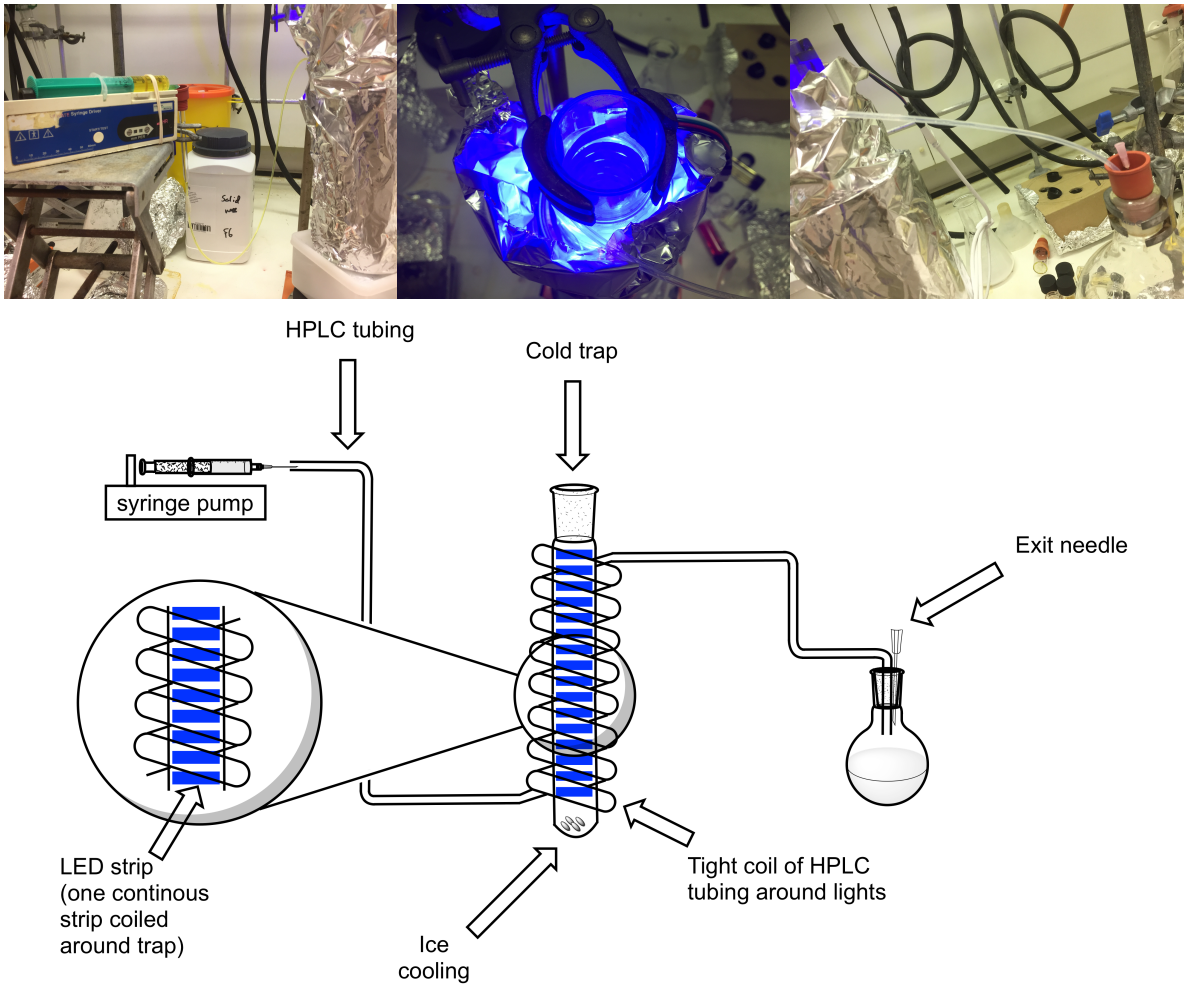

Figure 5.5. *The 'Flow' photoreactor set-up used in this project.*

A continual strip of 3 W blue LEDs was placed around the outside of a cold finger trap. 5 m of 1/16 × 1/8 × 1/32 inch FEP tubing (thermo scientific) was coiled around the lights. The cold trap itself was filed with ice and water for cooling of the lights (ice added at intervals to maintain cooling). A syringe pump was used to load and drive the reactor.

32 W Photoreactor Set-up

A 32 W LED lamp was held within a metal test tube rack and cooled with a strong flow of nitrogen gas. Reaction vials were installed into the slot 1 cm away from the front of the lamp.



Figure 5.6. *The 32 W photoreactor set-up used in this project.*

The reactor held a constant temperature of between 36-43 ^{o}C with the described cooling.

This simple setup proved to be very efficient. When later tested against some literature blue-light photochemistry it was found to approximately match or surpass the reported result in each case tested. For example, see Nicewicz demethoxylative S_NAr chemistry (**Scheme 5.1**) below.[23] This gave confidence that this setup would be a useful tool for our research.

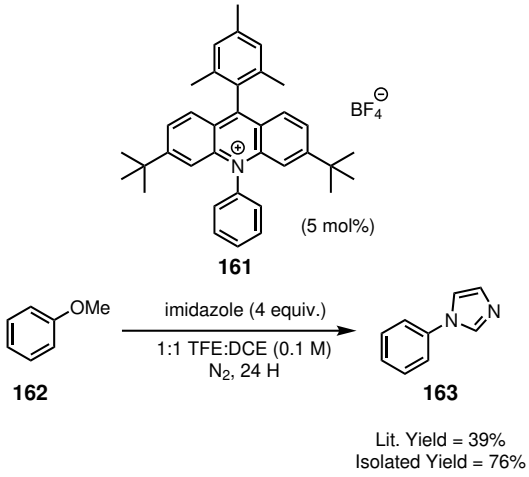

Scheme 5.1. *Comparison of the yield attained by this 32 W setup, for a literature example of Nicewicz and coworkers demethoxylative S_NAr methodology, to the recorded literature value.*[23]

5.3 Computational Methods

5.3.1 Natural Population Analysis

Density functional theory (DFT) calculations were performed with Gaussian16.[144] The most positive electronic charges on the carbon atoms in radical cations of chlorobenzene (**10**), fluo-

robenzene (**11**), 2,4-dichlorofluorobenzene (**100**) and 2,4-dichloroanisole (**100a**) are shown in **Figure 5.7** (more complete data from this analysis can be found in **Table 5.1**-**Table 5.7**). These are calculated using density functional theory at the B3LYP/6-31G(d,p) level, with natural population analysis.[41]

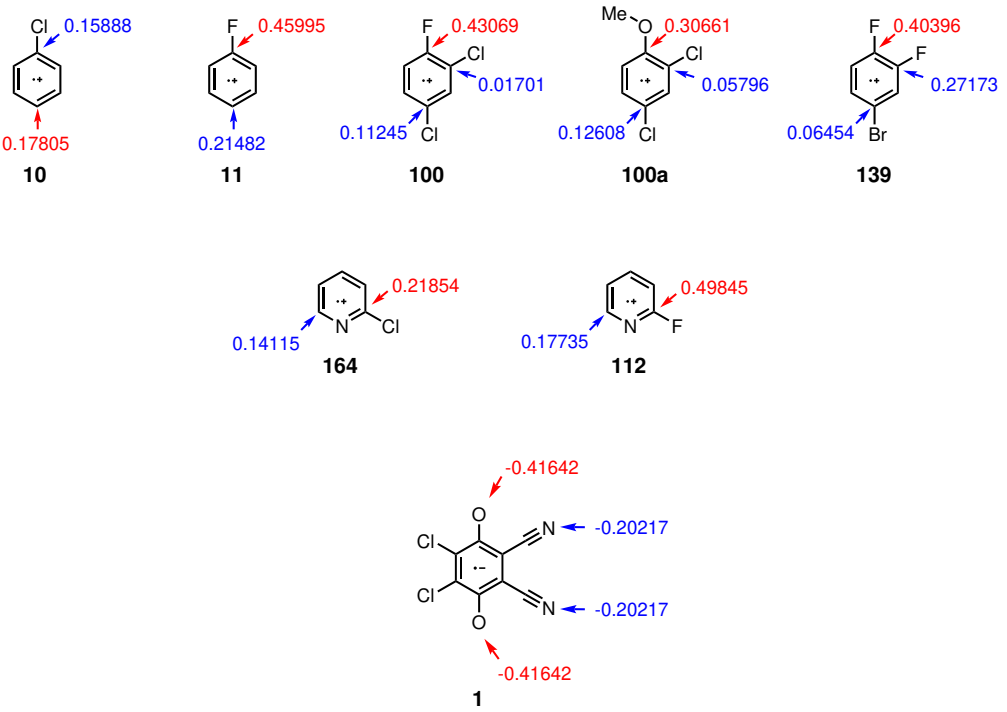

Figure 5.7. *NBO analysis of the most significant charge build ups, in the radical cations of relevant arenes from this thesis, and of the radical anion of DDQ (**1**).*

This analysis shows that charge build up is greatest at the para position for chlorobenzene (**10**), whilst, for simple fluoroarenes and anisoles, it is the *ipso* carbon which is the most positive site. Further, this analysis suggests that the *ipso* carbon of 2,4-dichlorofluorobenzene (**100**) bares a greater positive charge, than the equivalent position in 2,4-dichloroanisole (**100a**). In the case of 4-bromo-1,2-difluorobenzene **139**, it can be also be seen that the *ipso* carbon bares a much greater charge build up than *ortho* carbon which is also substituted with a fluorine atom. This is likely the origin of the high selectivity of defluorination under our reaction conditions.

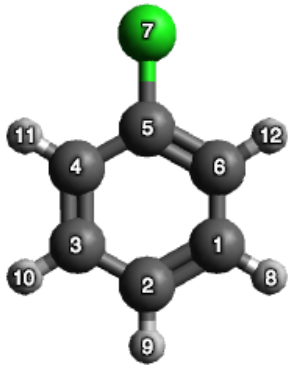

Table 5.1. *Natural population analysis results for the radical cation of chlorobenzene,* ***10****.*

		Cartesian Coordinates				Natural Population			
Atom	No.	X	Y	Z	Natural Charge	Core	Valence	Rydberg	Total
C	1	−1.544932	−1.239938	0.000000	−0.10740	0.99956	2.10094	0.00689	3.10740
C	2	−2.241337	−0.000001	0.000000	0.17805	0.99959	1.81601	0.00635	2.82195
C	3	−1.544931	1.239938	0.000000	−0.10739	0.99956	2.10094	0.00689	3.10739
C	4	−0.171569	1.251709	0.000000	−0.05208	0.99949	2.04480	0.00779	3.05208
C	5	0.524434	0.000002	0.000000	0.15888	0.99941	1.82957	0.01215	2.84112
C	6	−0.171570	−1.251707	0.000000	−0.05208	0.99949	2.04479	0.00779	3.05208
Cl	7	2.214243	−0.000001	0.000000	0.25610	4.99973	3.23320	0.01096	8.24390
H	8	−2.103026	−2.170015	0.000000	0.14731	0.00000	0.35212	0.00057	0.35269
H	9	−3.327389	0.000000	0.000000	0.13659	0.00000	0.36281	0.00060	0.36341
H	10	−2.103026	2.170014	0.000000	0.14731	0.00000	0.35212	0.00057	0.35269
H	11	0.395367	2.176051	0.000000	0.14736	0.00000	0.35194	0.00071	0.35264
H	12	0.395368	−2.176049	0.000000	0.14736	0.00000	0.35194	0.00071	0.35264

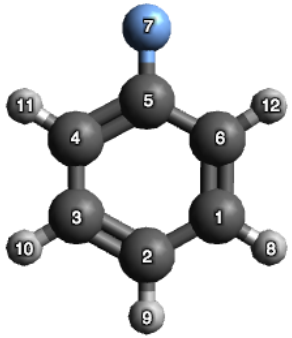

Table 5.2. *Natural population analysis results for the radical cation of fluorobenzene,* ***11****.*

		Cartesian Coordinates				Natural Population			
Atom	No.	X	Y	Z	Natural Charge	Core	Valence	Rydberg	Total
C	1	1.113124	1.246976	0.000000	−0.10106	0.99957	2.09462	0.00687	3.10106
C	2	1.810345	0.000000	0.000000	0.21482	0.99960	1.77934	0.00625	2.78518
C	3	1.113126	−1.246976	0.000000	−0.10106	0.99957	2.09462	0.00687	3.10106
C	4	−0.257880	−1.259174	0.000000	−0.07421	0.99952	2.06732	0.00738	3.07421
C	5	−0.931596	0.000000	0.000000	0.45995	0.99939	1.52671	0.01395	2.54005
C	6	−0.257882	1.259175	0.000000	−0.07422	0.99952	2.06733	0.00738	3.07422
F	7	−2.232454	−0.000001	0.000000	−0.05940	0.99996	3.55587	0.00356	4.55940
H	8	1.675428	2.174503	0.000000	0.14859	0.00000	0.35085	0.00056	0.35141
H	9	2.896451	0.000002	−0.000001	0.13652	0.00000	0.36290	0.00059	0.36348
H	10	1.675430	−2.174502	0.000000	0.14859	0.00000	0.35085	0.00056	0.35141
H	11	−0.845315	−2.171111	0.000000	0.15075	0.00000	0.34855	0.00070	0.34925
H	12	−0.845317	2.171111	0.000000	0.15075	0.00000	0.34855	0.00070	0.34925

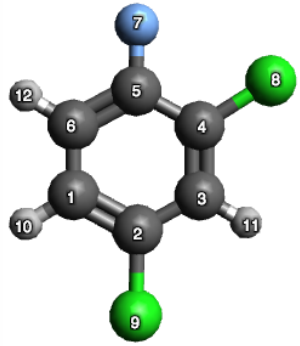

Table 5.3. *Natural population analysis results for the radical cation of 2,4-dichlorofluorobenzene,* ***100****.*

		Cartesian Coordinates				Natural Population			
Atom	No.	X	Y	Z	Natural Charge	Core	Valence	Rydberg	Total
C	1	−1.236559	1.414928	0.000000	0.01363	0.99951	1.97923	0.00763	2.98637
C	2	−1.443998	−0.009859	0.000000	0.11245	0.99938	1.87604	0.01213	2.88755
C	3	−0.370874	−0.916406	0.000000	−0.15261	0.99942	2.14440	0.00880	3.15261
C	4	0.920280	−0.417099	0.000000	0.01701	0.99931	1.97118	0.01250	2.98299
C	5	1.117097	1.014739	0.000000	0.43069	0.99929	1.55505	0.01497	2.56931
C	6	0.041682	1.919278	0.000000	−0.16779	0.99951	2.16097	0.00732	3.16779
F	7	2.337610	1.469872	0.000000	−0.07784	0.99996	3.57434	0.00354	4.57784
Cl	8	2.286858	−1.428729	0.000000	0.16017	4.99978	3.32851	0.01154	8.33983
Cl	9	−3.040002	−0.590967	0.000000	0.20441	4.99976	3.28481	0.01102	8.29559
H	10	−2.098152	2.073587	0.000000	0.14819	0.00000	0.35111	0.00070	0.35181
H	11	−0.548896	−1.985361	0.000000	0.15607	0.00000	0.34315	0.00078	0.34393
H	12	0.246247	2.984293	0.000000	0.15563	0.00000	0.34369	0.00068	0.34437

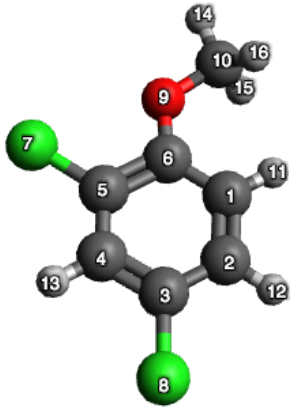

Table 5.4. *Natural population analysis results for the radical cation of 2,4-dichloroanisole,* ***100a****.*

		Cartesian Coordinates				Natural Population			
Atom	No.	X	Y	Z	Natural Charge	Core	Valence	Rydberg	Total
C	1	0.232928	−1.650555	0.000000	−0.12163	0.99952	2.11611	0.00600	3.12163
C	2	−1.130369	−1.509494	0.000000	−0.04996	0.99950	2.04261	0.00785	3.04996
C	3	−1.714527	−0.204906	0.000000	0.12608	0.99936	1.86243	0.01213	2.87392
C	4	−0.920017	0.952352	0.000000	−0.16585	0.99941	2.15781	0.00863	3.16585
C	5	0.456057	0.825777	0.000000	0.05796	0.99932	1.93014	0.01258	2.94204
C	6	1.065151	−0.495013	0.000000	0.30661	0.99944	1.68211	0.01184	2.69339
Cl	7	1.465111	2.204597	0.000000	0.12712	4.99979	3.36218	0.01091	8.37288
Cl	8	−3.415116	−0.065184	0.000000	0.16160	4.99977	3.32788	0.01075	8.33840
O	9	2.370321	−0.517153	0.000000	−0.09917	0.99985	3.09318	0.00614	4.09917
C	10	3.127744	−1.759166	0.000000	−0.17642	0.99969	2.17071	0.00602	3.17642
H	11	0.677504	−2.637939	−0.000001	0.14217	0.00000	0.35719	0.00064	0.35783
H	12	−1.778728	−2.378538	0.000000	0.14660	0.00000	0.35269	0.00071	0.35340
H	13	−1.378394	1.934192	0.000000	0.15385	0.00000	0.34534	0.00081	0.34615
H	14	4.168877	−1.445859	0.000004	0.13717	0.00000	0.36244	0.00040	0.36283
H	15	2.898232	−2.329316	−0.902717	0.12694	0.00000	0.37240	0.00066	0.37306
H	16	2.898227	−2.329319	0.902715	0.12694	0.00000	0.37241	0.00066	0.37306

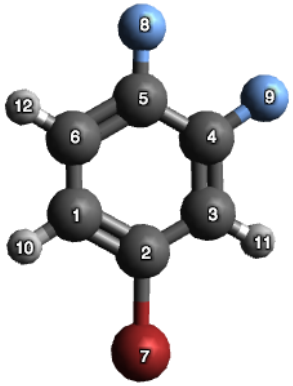

Table 5.5. *Natural population analysis results for the radical cation of 4-bromo-1,2-difluorobenzene,* ***139****.*

		Cartesian Coordinates				Natural Population			
Atom	No.	X	Y	Z	Natural Charge	Core	Valence	Rydberg	Total
C	1	−0.021143	−1.444928	0.000000	0.00451	0.99950	1.98815	0.00783	2.99549
C	2	−0.556261	−0.110099	0.000000	0.06454	0.99941	1.92437	0.01169	2.93546
C	3	0.274761	1.026846	0.000000	−0.17291	0.99944	2.16492	0.00855	3.17291
C	4	1.634300	0.823707	0.000000	0.27173	0.99926	1.71459	0.01441	2.72827
C	5	2.175024	−0.509784	0.000000	0.40396	0.99933	1.58246	0.01426	2.59604
C	6	1.341202	−1.639713	0.000000	−0.16635	0.99951	2.15941	0.00743	3.16635
Br	7	−2.390973	0.095780	0.000000	0.31712	13.99935	3.17344	0.01009	17.18288
F	8	3.472011	−0.634792	0.000000	−0.07521	0.99997	3.57148	0.00376	4.57521
F	9	2.488361	1.818630	0.000000	−0.10781	0.99997	3.60412	0.00372	4.60781
H	10	−0.703987	−2.286908	0.000000	0.14788	0.00000	0.35141	0.00071	0.35212
H	11	−0.129525	2.032381	0.000000	0.15711	0.00000	0.34211	0.00078	0.34289
H	12	1.786915	−2.628495	0.000000	0.15544	0.00000	0.34390	0.00067	0.34456

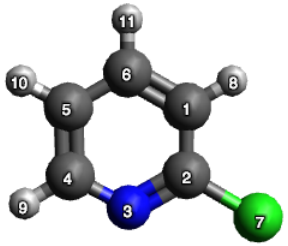

Table 5.6. *Natural population analysis results for the radical cation of 2-chloropyridine,* ***164****.*

		Cartesian Coordinates				Natural Population			
Atom	No.	X	Y	Z	Natural Charge	Core	Valence	Rydberg	Total
C	1	0.177131	1.201904	−0.000002	0.04229	0.99946	1.95127	0.00697	2.95771
C	2	−0.514799	−0.013506	−0.000001	0.21854	0.99936	1.76620	0.01590	2.78146
N	3	0.172668	−1.187504	−0.000003	−0.22593	0.99966	2.71518	0.01108	3.72593
C	4	1.532623	−1.218597	0.000003	0.14115	0.99959	1.84911	0.01015	2.85885
C	5	2.259588	−0.025237	−0.000002	0.11208	0.99956	1.88234	0.00602	2.88792
C	6	1.573899	1.191527	0.000001	−0.15167	0.99958	2.14480	0.00729	3.15167
Cl	7	−2.266710	−0.032779	0.000001	0.28605	4.99976	3.20469	0.00949	8.21395
H	8	−0.359635	2.141973	0.000004	0.14576	0.00000	0.35348	0.00076	0.35424
H	9	2.049207	−2.169078	0.000003	0.13958	0.00000	0.35965	0.00077	0.36042
H	10	3.341736	−0.043626	−0.000001	0.14090	0.00000	0.35845	0.00065	0.35910
H	11	2.123436	2.123961	0.000003	0.15122	0.00000	0.34824	0.00054	0.34878

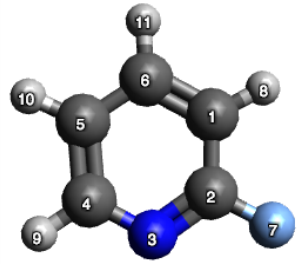

Table 5.7. *Natural population analysis results for the radical cation of 2-fluoropyridine,* ***112****.*

		Cartesian Coordinates				Natural Population			
Atom	No.	X	Y	Z	Natural Charge	Core	Valence	Rydberg	Total
C	1	−0.203022	1.240477	0.000003	0.05808	0.99952	1.93576	0.00665	2.94192
C	2	−0.905693	−0.024349	−0.000003	0.49845	0.99946	1.48458	0.01751	2.50155
N	3	−0.353333	−1.232744	0.000001	−0.24762	0.99968	2.73517	0.01277	3.74762
C	4	0.965268	−1.259508	0.000002	0.17735	0.99965	1.81234	0.01065	2.82265
C	5	1.790951	−0.063583	−0.000003	0.15625	0.99959	1.83825	0.00591	2.84375
C	6	1.179401	1.196867	0.000000	−0.16911	0.99957	2.16232	0.00722	3.16911
F	7	−2.199204	0.025403	−0.000001	−0.05855	0.99996	3.55477	0.00381	4.55855
H	8	−0.775530	2.162850	0.000004	0.14952	0.00000	0.34979	0.00070	0.35048
H	9	1.439262	−2.238982	0.000004	0.13905	0.00000	0.36016	0.00080	0.36095
H	10	2.871612	−0.169771	−0.000004	0.14201	0.00000	0.35741	0.00058	0.35799
H	11	1.769392	2.107060	0.000000	0.15457	0.00000	0.34491	0.00052	0.34543

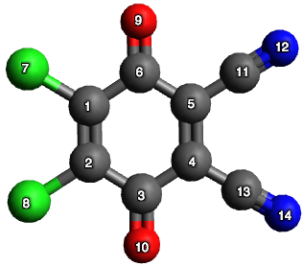

Table 5.8. *Natural population analysis results for the radical anion of DDQ,* ***1****.*

		Cartesian Coordinates				Natural Population			
Atom	No.	X	Y	Z	Natural Charge	Core	Valence	Rydberg	Total
C	1	−1.10665	−0.68254	0.00001	−0.07533	0.99919	2.06474	0.01140	3.07533
C	2	−1.10665	0.68254	0.00001	−0.07533	0.99919	2.06474	0.01140	3.07533
C	3	0.13516	1.48235	0.00001	0.19985	0.99952	1.78283	0.01780	2.80015
C	4	1.36547	0.70063	0.00000	−0.17235	0.99939	2.16558	0.00738	3.17235
C	5	1.36547	−0.70063	0.00001	−0.17235	0.99939	2.16558	0.00738	3.17235
C	6	0.13516	−1.48235	0.00001	0.19985	0.99952	1.78283	0.01798	2.80015
Cl	7	−2.58806	−1.60779	−0.00000	0.00494	4.99983	3.48444	0.01080	8.49506
Cl	8	−2.58806	1.60779	−0.00000	0.00494	4.99983	3.48444	0.01080	8.49506
O	9	0.12436	−2.72518	−0.00001	−0.41642	0.99991	3.40805	0.00846	4.41642
O	10	0.12436	2.72518	−0.00001	−0.41642	0.99991	3.40805	0.00846	4.41642
C	11	2.58651	−1.43742	0.00000	0.16149	0.99970	1.82096	0.01785	2.83851
N	12	3.58847	−2.03290	−0.00001	−0.20217	0.99982	2.69194	0.01041	3.70217
C	13	2.58651	1.43742	0.00000	0.16149	0.99970	1.82096	0.01785	2.83851
N	14	3.58847	2.03290	−0.00001	−0.20217	0.99982	2.69194	0.01041	3.70217

5.3.2 Computational Redox Potentials, E

Density functional theory (DFT) calculations were performed with Gaussian16.[144] All calculations of ground state redox potentials were performed with the PBEPBE/6-311+G level of theory, all solvents were modelled *implicitly*. This was selected for its closeness to know experimental values. The process used for calculating redox potentials is described below. **Table 5.9** shows the calculation and comparison of values from different levels of theory to the experimental value of DDQ, $E^o_{exp} = 0.49$ V,[71] and hence the selection of the PBEPBE/6-311G level of theory for use in this project. **Equation(s) 5.1-5.6** show how these values were reached (where G is the Gibbs free energy, SCF E is the self-consistent field energy calculated, n is the number of elections transferred (i.e. 1), F is the Faraday constant, and 4.67 V is the calculated *absolute* potential of the standard calomel electrode, *SCE*[145]). **Figure 5.8**, a Born-Haber cycle, gives these values physical meaning and emphasises the fact that equation 4.4 is merely a Hess's Law relationship. **Table 5.10** gives the result of the above calculation for arene substrates used in this methodology, and the result of plotting these values (bar pyridine results) vs experimental yield is shown in **Figure 5.9** below. This process as described was used to obtain all of the computational redox potienial values given in this thesis.

$$G_{(g)} = SCF_{(g)}\ E_{(method)} - \text{Gibbs Thermal Correction} \tag{5.1}$$

$$\Delta G_{solv} = SCF_{(sol)}\ E_{(method)} - SCF_{(g)}\ E_{(method)} \tag{5.2}$$

$$\Delta G_{red\ (g)} = G_{(g)}(DDQ^{\bullet -}) - G_{(g)}(DDQ) \tag{5.3}$$

$$\Delta G_{red\ (sol)} = -\Delta G_{(sol)}(DDQ) + \Delta G_{ox\ (g)} + \Delta G_{(sol)}(DDQ^{\bullet -}) \tag{5.4}$$

$$E^o_{abs} = \frac{\Delta G_{ox\ (sol)}}{-nF} \tag{5.5}$$

$$E^o_{cal} = E^o_{abs} - 4.67\ \text{V} \tag{5.6}$$

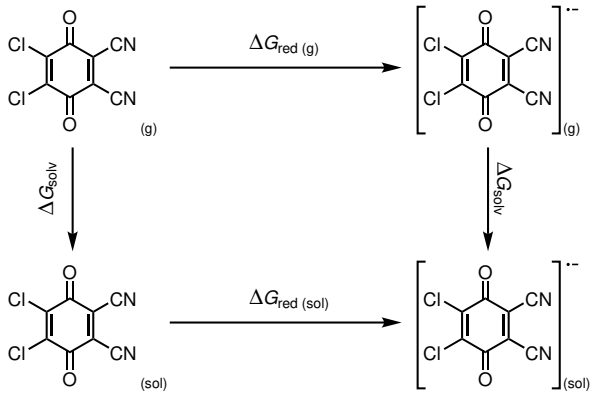

Figure 5.8. *Born-Haber cycle used for the calculation of redox potentials.*

Table 5.10. *Computational values of the $E_{Ar/Ar^{+\bullet}}$ redox potentials of key arenes used this project.*

Entry	Compound No.	Compound Name	Computational Redox Potential ($E_{Ar/Ar^{+\bullet}}$) relative to SCE / V
1	**100**	2,4-dichlorofluorobenzene	+2.316
2	**102**	4-bromo-2-chlorofluorobenzene	+2.156
3	**103**	4-chlorobenzene	+2.184
4	**104**	2,6-dichloro-4-bromofluorobenzene	+2.337
5	**105**	4-bromofluorobenzene	+2.026
6	**106**	2-chlorofluorobenzene	+2.322
7	**107**	5-methyl-2,4-dichlorofluorobenzene	+2.116
8	**108**	3-methyl-2,4-dichlorofluorobenzene	+2.213
9	**109**	1-fluoro-4-cyanonapthalene	+1.727
10	**110**	4-chloro-2-sulfonamide-fluorobenzene	+2.507
11	**111**	2-fluoro-5-chloropyridine	+2.594
12	**112**	2-fluoropyridine	+2.734
13	**113**	2-chloro-5-fluoropyridine	+2.612
14	**139**	4-bromo-1,2-difluorobenzene	+2.168

Table 5.9. *Computation of the E^o value of DDQ, relative to SCE, used to determine level of theory required for this project. Values in Hartrees unless otherwise stated.*

Method / Basis set		SCF (g) E(method)	SCF (sol) E(method)	Gibbs Thermal Correc-tion	$G_{(g)}$	ΔG_{solv}	$\Delta G_{red\ (sol)}$	E^o_{abs} / V	E^o_{cal} (relative to SCE) / V	$\lvert E^o_{cal} - E^o_{exp} \rvert$ / V
UB3LYP/ LANL2DZ										
	DDQ	−594.42234	−594.48161	0.0217	−594.40055	−0.0592708				
	$DDQ^{\bullet -}$	−594.55764	−594.68349	0.0205	−594.53714	−0.1258563				
							−85.7091	5.528	0.858	0.368
UB3LYP/ 6-311G										
	DDQ	−1485.0222	−1485.0878	0.0219	−1485.0002	−0.065639				
	$DDQ^{\bullet -}$	−1485.1571	−1485.2876	0.0206	−1485.1365	−0.130487				
							−126.2284	5.474	0.804	0.314
PBEPBE/ 6-31+G*										
	DDQ	−1484.0616	−1484.1192	0.0197	−1484.0418	−0.057591				
	$DDQ^{\bullet -}$	−1484.1936	−1484.2474	0.0189	−1484.1747	−0.053823				
							−81.0125	3.513	−1.157	1.647
PBEPBE/ 6-311G										
	DDQ	−1484.0294	−1484.0860	0.0195	−1484.0099	−0.056580				
	$DDQ^{\bullet -}$	−1484.1590	−1484.2744	0.0183	−1484.1406	−0.115375				
							−118.9471	5.158	0.488	0.002

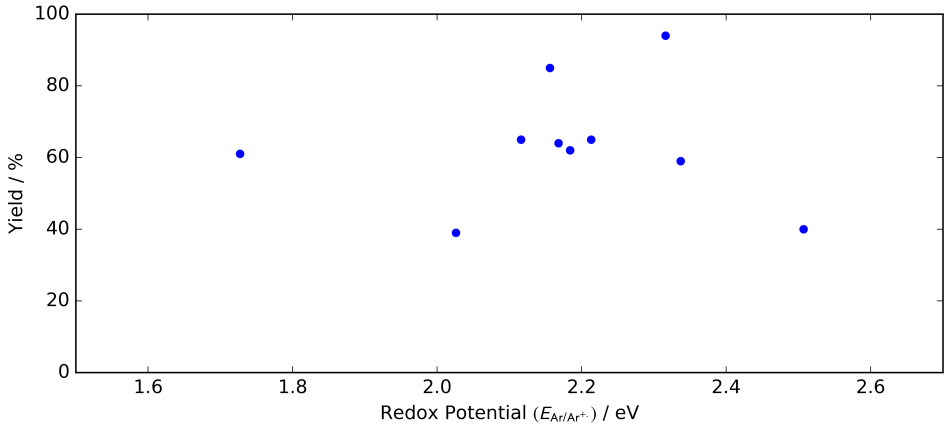

Figure 5.9. *Redox potential ($E_{Ar/Ar^{+\cdot}}$) vs yield of photochemical S_NAr reaction.*

5.3.3 Computational Electrophilicity Index, ω

The 'electrophilicity index' (ω), as the name would suggest is a measure of the electrophilicity of a species. There have been attempts at general experimental measurements with different levels of success. Computationally, it is derived from the electronegativity (χ) and 'hardness' (η) of the species. Both of these values themselves being easily obtained from electronic chemical potential (μ) and HOMO-LUMO gap of the species - i.e. readily computationally obtainable values.[138–142]

$$\omega = \frac{\mu^2}{2 \times \eta} \tag{5.7}$$

$$\mu = \frac{E_H + E_L}{2} \tag{5.8}$$

$$\eta = E_L - E_H \tag{5.9}$$

The equations relating these properties have been shown previously but are reproduced for convenience above (**Eqn. 5.7–6.9**). The first of these equations is how electrophilicity index was calculated in this thesis. It is one of the simplest expressions for electrophilicity index and

was chosen to allows others to quickly reproduced or expand upon this work. This expression of electrophilicity index (which can be thought of as 'electrophilic power') can be seen to be analogous to the classical mechanics calculation of power (W), $W = V^2/R$, where V is potential and R is resistance. In this analogy electronic chemical potential (μ) takes the place of potential (V) and resistance is replaced by 2η (hardness). Relevant values of ω determined in this work are shown below (**Table 5.11**), as is the result of plotting these values (bar pyridine results) vs experimental yield (**Figure 5.12**).

Table 5.11. *Computational values Electrophilicity Index (ω) of key arenes used this project.*

Entry	Compound No.	Compound Name	Computational Electrophilicity Index (ω)
1	**100**	2,4-dichlorofluorobenzene	1.704
2	**102**	4-bromo-2-chlorofluorobenzene	1.626
3	**103**	4-chlorobenzene	1.463
4	**104**	2,6-dichloro-4-bromofluorobenzene	1.942
5	**105**	4-bromofluorobenzene	1.388
6	**106**	2-chlorofluorobenzene	1.406
7	**107**	5-methyl-2,4-dichlorofluorobenzene	1.561
8	**108**	3-methyl-2,4-dichlorofluorobenzene	1.579
9	**109**	1-fluoro-4-cyanonapthalene	2.315
10	**110**	4-chloro-2-sulfonamide-fluorobenzene	2.240
11	**111**	2-fluoro-5-chloropyridine	1.983
12	**112**	2-fluoropyridine	1.640
13	**113**	2-chloro-5-fluoropyridine	1.997
14	**139**	4-bromo-1,2-difluorobenzene	1.555

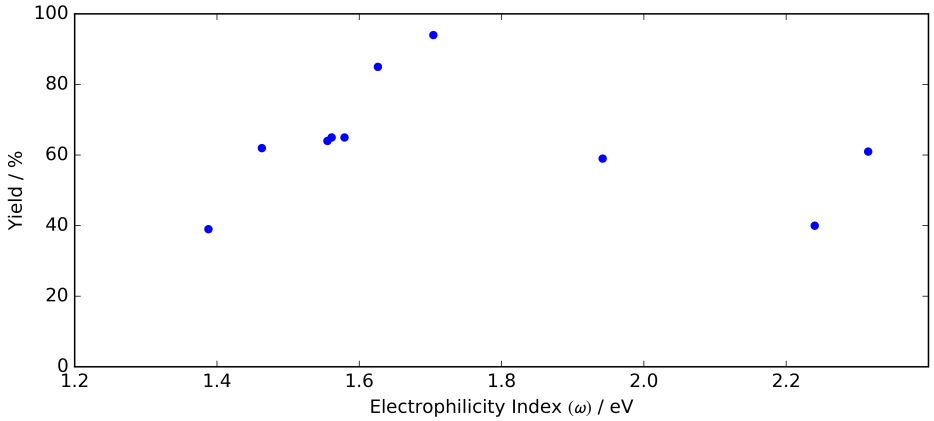

Figure 5.10. *Electrophilicity index (ω) vs yield of photochemical S_NAr reaction.*

5.3.4 The S_NAr parameter and linear parameter

The combination of redox potential ($E^o_{Ar/Ar^{\bullet+}}$) and electrophilicity index (ω) values – the values relevant to the efficency of the photochemical S_NAr process investigated – was termed the 'S_NAr parameter' and to the value of $\omega + \left(\frac{\omega + E^o_{Ox}}{2}\right)$. This form was chosen as it was seen empirically to give the best fit to the data. It may be possible to find a more refined fit, but this suited the needs of the project satisfactorily.

It should be noted that $E^o_{Ar/Ar^{\bullet+}}$ is calculated in volts (V), while ω is calculated in electron-volts (eV). Volts and electron-volts are related by the expression $V = \frac{E}{Q}$ where V is potential difference in volts, E is energy in electron-volts, and Q is the electric charge in 'elementary charge' (i.e. the charge of an electron or proton). Hence, as this is a one-electron process, $V = \frac{E}{1}$ meaning $E^o_{Ar/Ar^{\bullet+}}$ and ω can both be expressed in either unit. This in turn means they can undergo simple addition, giving S_NAr parameter value we can report in electron-volts.

Electronegativity index (ω) is given a higher waiting is this expression. This is reasonable given the better fit of the yield data to ω than $E^o_{Ar/Ar^{\bullet+}}$, and offers a much improved fit to the data than a simple $\omega + E^o_{Ox}$ combination (**Figure 5.11**).

The two tends obtained when plotting S_NAr parameter against yield are to be expected.

Table 5.12. *S_NAr parameter values of key arenes used this project.*

Entry	Compound No.	Compound Name	S_NAr parameter (eV)
1	**100**	2,4-dichlorofluorobenzene	3.715
2	**102**	4-bromo-2-chlorofluorobenzene	3.517
3	**103**	4-chlorobenzene	3.287
4	**104**	2,6-dichloro-4-bromofluorobenzene	4.081
5	**105**	4-bromofluorobenzene	3.095
6	**106**	2-chlorofluorobenzene	3.270
7	**107**	5-methyl-2,4-dichlorofluorobenzene	3.400
8	**108**	3-methyl-2,4-dichlorofluorobenzene	3.475
9	**109**	1-fluoro-4-cyanonapthalene	4.336
10	**110**	4-chloro-2-sulfonamide-fluorobenzene	4.614
11	**139**	4-bromo-1,2-difluorobenzene	3.417

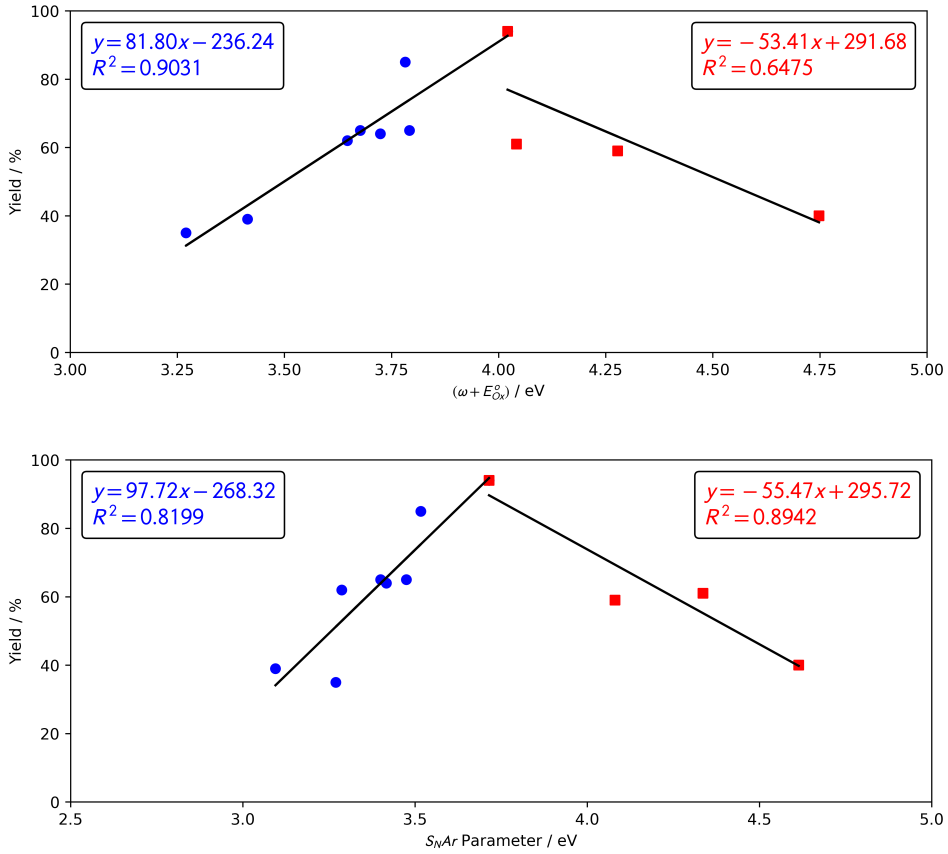

Figure 5.11. *Simple addition of ω and $E^o_{Ar/Ar^{\bullet+}}$ (top), and the chosen value of the S_NAr parameter (bottom).*

With a higher weighting given to electrophilicity index, yield increase as S_NAr parameter increases for the first half of the graph (**Figure 5.11**, bottom). However, as redox potentials increase yields lower on the latter half. Using the values obtained when both of these trends are submitted to linear regression, the results on the second trend line can be brought onto the first; i.e. $y = 97.94x_1 - 268.87 = -55.43x_2 + 295.54$ where x_1 would be the equivalent parameter value in trend 1. This allows a series of values referred to as the linear parameter to be generated. The reason for doing this is to simplify interpretation of these values from ”larger is better until a given value and then smaller is better” – which was the case with the S_NAr parameter, to simply ”larger is better”. It also allows for approximate bands to be delineated, allowing very quick rough prediction of approximate yield. Note from this point the values for **106a** are treated as the only outlier.

Table 5.13. *Linear parameter values of key arenes used this project.*

Entry	Compound No.	Compound Name	Linear parameter
1	**105**	4-bromofluorobenzene	3.095
2	**103**	4-chlorobenzene	3.287
3	**107**	5-methyl-2,4-dichlorofluorobenzene	3.400
4	**139**	4-bromo-1,2-difluorobenzene	3.417
5	**108**	3-methyl-2,4-dichlorofluorobenzene	3.475
6	**102**	4-bromo-2-chlorofluorobenzene	3.517
7	**100**	2,4-dichlorofluorobenzene	3.715
8	**104**	2,6-dichloro-4-bromofluorobenzene	3.453
9	**109**	1-fluoro-4-cyanonapthalene	3.309
10	**110**	4-chloro-2-sulfonamide-fluorobenzene	3.151

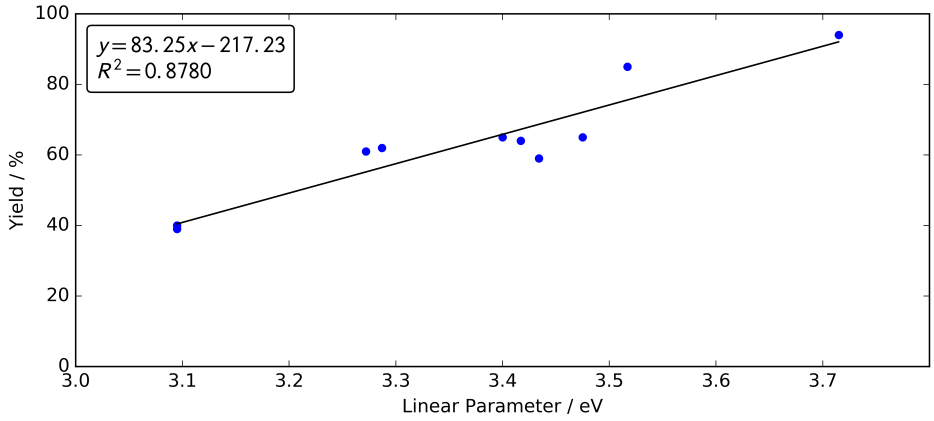

Figure 5.12. *Linear parameter vs yield of photochemical S_NAr reaction.*

Table 5.14. *A rough guide to yield for a given linear parameter value*

Entry	Parameter range	Yield range
1	<2.72	<10%
2	2.72-2.85	10-20%
3	2.85-2.97	20-30%
4	2.97-3.09	30-40%
5	3.09-3.21	40-50%
6	3.21-3.33	50-60%
7	3.33-3.45	60-70%
8	3.45-3.57	70-80%
9	3.57-3.69	80-90%
10	>3.69	>90%

5.4 Full Optimisation Details

5.4.1 Optimisation of Anisole Formation

Table 5.15. *S_NAr optimisation table for the reaction of **100** with methanol, to form **100a**, under 32 W blue light.*



100 **100a**

Entry	Scale / mmol	[**100**] / M	Solvent	Additive (equiv.)	DDQ equiv.	MeOH equiv.	Atmosphere	Isolated Yield
1	0.5	0.1	HFIP	-	1.2	10	Air	92%
2	1.0	0.2	HFIP	-	1.2	10	Air	90%
3	1.5	0.3	HFIP	-	1.2	10	Air	72%
4	0.5	0.1	MeOH	-	1.2	*solvent*	Air	10%
5	0.5	0.1	MeOH	HFIP (1)	1.2	*solvent*	Air	>10%[a]
6	0.5	0.1	MeOH	HFIP (2)	1.2	*solvent*	Air	>10%[a]
7	0.5	0.1	MeOH	HFIP (10)	1.2	*solvent*	Air	5%
8	0.5	0.1	TFE	-	1.2	10	Air	93%
9	0.5	0.1	1:1 DCE:TFE	-	1.2	10	Air	94%
10	0.5	0.1	DCE	-	1.2	10	Air	18%
11	0.5	0.1	DCE	TFA (2)	1.2	10	Air	37%
12	0.5	0.1	DCE	TFA (5)	1.2	10	Air	52%
13	0.5	0.1	MeCN	-	1.2	10	Air	44%[b]
14	0.5	0.1	1:1 MeCN:TFE	-	1.2	10	Air	85%
15	0.5	0.1	HFIP	-	1.2	5	Air	53%

Continued overleaf...

Entry	Scale / mmol	[**100**] / M	Solvent	Addi-tive (equiv.)	DDQ equiv.	MeOH equiv.	Atmo-sphere	Isolated Yield
16	0.5	0.1	HFIP	-	1.2	2	Air	18%
17	0.5	0.1	HFIP	-	1.2	1.2	Air	11%
18	0.5	0.1	HFIP	-	0.6	10	Air	81%
19	0.5	0.1	HFIP	-	0.3	10	Air	24%
20	0.5	0.1	HFIP	-	0.2	10	Air	23%
21	1.0	0.2	1:1 DCE:TFE	-	1.2	10	Air	95%
22	1.0	0.2	1:1 DCE:TFE	-	0.6	10	Air	82%
23	1.0	0.2	1:1 DCE:TFE	-	0.3	10	Air	81%
24	0.5	0.1	1:1 DCE:TFE	-	1.2	10	N_2 [c]	88%
25	0.5	0.1	1:1 DCE:TFE	-	0.3	10	N_2 [c]	74%
26	0.5	0.1	1:1 DCE:TFE	-	1.2	2	Air	93%
27	0.5	0.1	1:1 DCE:TFE	-	0.3	10	N_2 [d]	91%

[a] from analysis of the crude ^{1}H NMR spectrum. [b] 12% of the *para*-Cl substitution product. [c] solution sparged with N_2. [d] O_2 removed *via* Freeze-Pump-Thaw under N_2.

5.4.2 Optimisation for Fluoropyridines and Related Arenes

Table 5.16. *Optimisation for Fluoropyridine and Related Arenes*

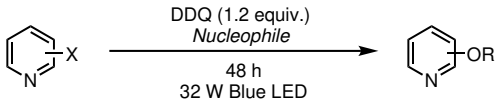

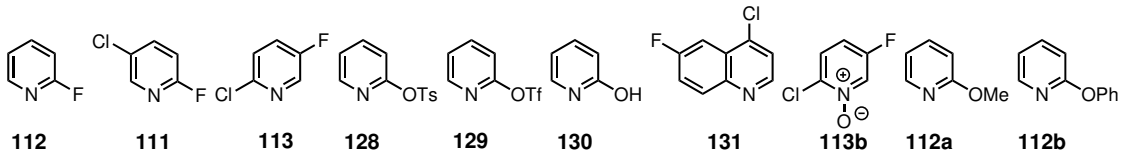

112 **111** **113** **128** **129** **130** **131** **113b** **112a** **112b**

Entry	SM	Nuc (10 eq.)	Solvent[a]	Additive (eq.)	Other	Result
1	**112**	MeOH	1:1 TFE:DCE			~5% conversion
2	**111**	MeOH	1:1 TFE:DCE			~10% conversion
3	**113**	MeOH	1:1 TFE:DCE			~5% conversion
4	**112**	MeOH	1:1 TFE:DCE		No Light	No conversion
5	**111**	MeOH	1:1 TFE:DCE		No Light	No conversion
6	**113**	MeOH	1:1 TFE:DCE		No Light	No conversion
7	**112**	TMSOEt	1:1 TFE:DCE			No conversion
8	**112**	TMSOEt	1:1 TFE:DCE			No conversion
9	**112**	TMSOEt	1:1 TFE:DCE			No conversion
10	**112**	MeOH	MeCN			No conversion
11	**112**	TMSOEt	MeCN			No conversion
12	**112a**	EtOH	1:1 TFE:DCE			No conversion
13	**128**	EtOH	1:1 TFE:DCE			Detosylation to give **130**
14	**129**	EtOH	1:1 TFE:DCE			No conversion
15	**131**	MeOH	1:1 TFE:DCE			Trace
16	**113b**	MeOH	1:1 TFE:DCE			No conversion
17	**112**	MeOH	1:1 TFE:DCE	DMAP (1.0 eq.)		No conversion

Continued overleaf...

Entry	SM	Nuc (10 eq.)	Solvent[a]	Additive (eq.)	Other	Result
18	**112**	MeOH[b]	MeOH			~50% conversion
19	**112**	MeOH	DCE			Trace
20	**112**	MeOH[f]	**112** (5 mL)			Significant conversion to **112a**[c]
21	**112**	MeOH	Ethyl acetate			No conversion
22	**112**	MeOH	Solvent free			~50% conversion[c]
23	**112**	MeOH[b]	MeOH		No Light	~40% conversion
24	**112**	MeOH	Solvent free		No Light	~5% conversion
25	**112**	TMSOEt	Solvent free			No conversion
26	**113**	MeOH[b]	MeOH			No conversion
27	**112**	MeOH	$PhNO_2$			No conversion
28	**112**	MeOH	1-Octanol			No conversion
29	**112**	MeOH	DIPC[e]			No conversion
30	**112**	MeOH	Phenol		45 °C	~30% conversion to **112b**
31	**112**	MeOH	Phenol	$Ti(OMe)_4$ (1.0 eq.)	45 °C	~55% conversion to **112b** and ~5% of **112a**[c]
32	**112**	MeOH	1:1 TFE:DCE	$Ti(OMe)_4$ (1.0 eq.)		No conversion
33	**112**	MeOH	DCE	$Ti(OMe)_4$ (1.0 eq.)		No conversion
34	**112**	MeOH	DCE	$Ti(OMe)_4$ (1.0 eq.)		No conversion
35	**112**	MeOH	1:4 TFE:DCE			No conversion
36	**112**	MeOH	1:4 TFE:DCE	$Ti(OMe)_4$ (1.0 eq.)		No conversion

Continued overleaf...

Entry	SM	Nuc (10 eq.)	Solvent[a]	Additive (eq.)	Other	Result
37	**112**	MeOH	Pyridine			No conversion
38	**112**	MeOH	1:1 Pyridine:TFE			No conversion
39	**112**	MeOH	DCE	$FeCl_3$ (2.0 eq.)		>40% conversion
40	**112**	MeOH	1:1 TFE:DCE	$FeCl_3$ (2.0 eq.)		No conversion
41	**112**	MeOH	1:1 DFE:DCE			No conversion
42	**112**	MeOH	DCE	$FeCl_3$ (2.0 eq.)	No Light	No conversion
43	**113**	MeOH	DCE	$FeCl_3$ (2.0 eq.)		trace
44	**112**	MeOH	1:1 TFE:DCE	β-Pinene (2.0 eq.)		No conversion[d]
45	**112**	MeOH	Solvent free		No DDQ	No conversion
46	**113**	MeOH	Solvent free			trace
47	**112**	MeOH	DCE			~40% conversion
48	**112**	MeOH	1:1 TFE:DCE			~30% conversion

[a]Concentration, with respect to arene, is kept at 0.1 M unless otherwise stated. [b]MeOH as solvent, not 10 eq. [c]Formation of byproduct with $M^{+\bullet}$ = 181 m/z was also observed. [d]Many isomers of pinene observed as well as OMe incorporation into the pinene structure. [e]Diisopropylcarbinol. [f]MeOH as limiting reagent (1 eq.), not 10 eq.

5.4.3 Optimisation for the Use of Azole Nucleophiles

Table 5.17. *Optimisation table for the reaction of* ***103*** *with Pyrazole, to form* ***103b****, under 32 W blue light.*

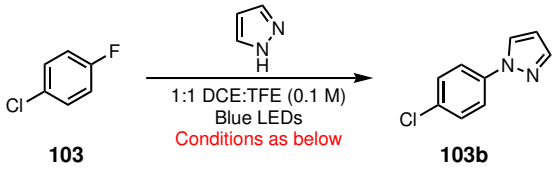

103 **103b**

Entry	[**103**] / M	DDQ equiv.	Pyrazole equiv.	**103** equiv.	Time / H	Atmo-sphere	Isolated Yield
1	0.1	1.2	10	1	48	Air	16%
2	0.1	1.2	2	1	48	Air	25%
3	0.1	1.2	1.2	1	48	Air	34%
4	0.1	1.2	1	2	48	Air	42%
5	0.1	1.2	1.2	1	14[a]	Air	62%
6	0.1	1.2	1.2	1	14	Air	35%
7	0.1	0.3	1.2	1	48	N_2[b]	61%

[a]2.5 mL of a solution of pyrazole in 1:1 DCE:TFE was added over 12 h to a 2.5 ml solution of **103** and DDQ in 1:1 DCE:TFE suspended in the photoreactor. [b]O_2 removed *via* freeze-pump-thaw under N_2.

5.5 Summary of Control Experiments

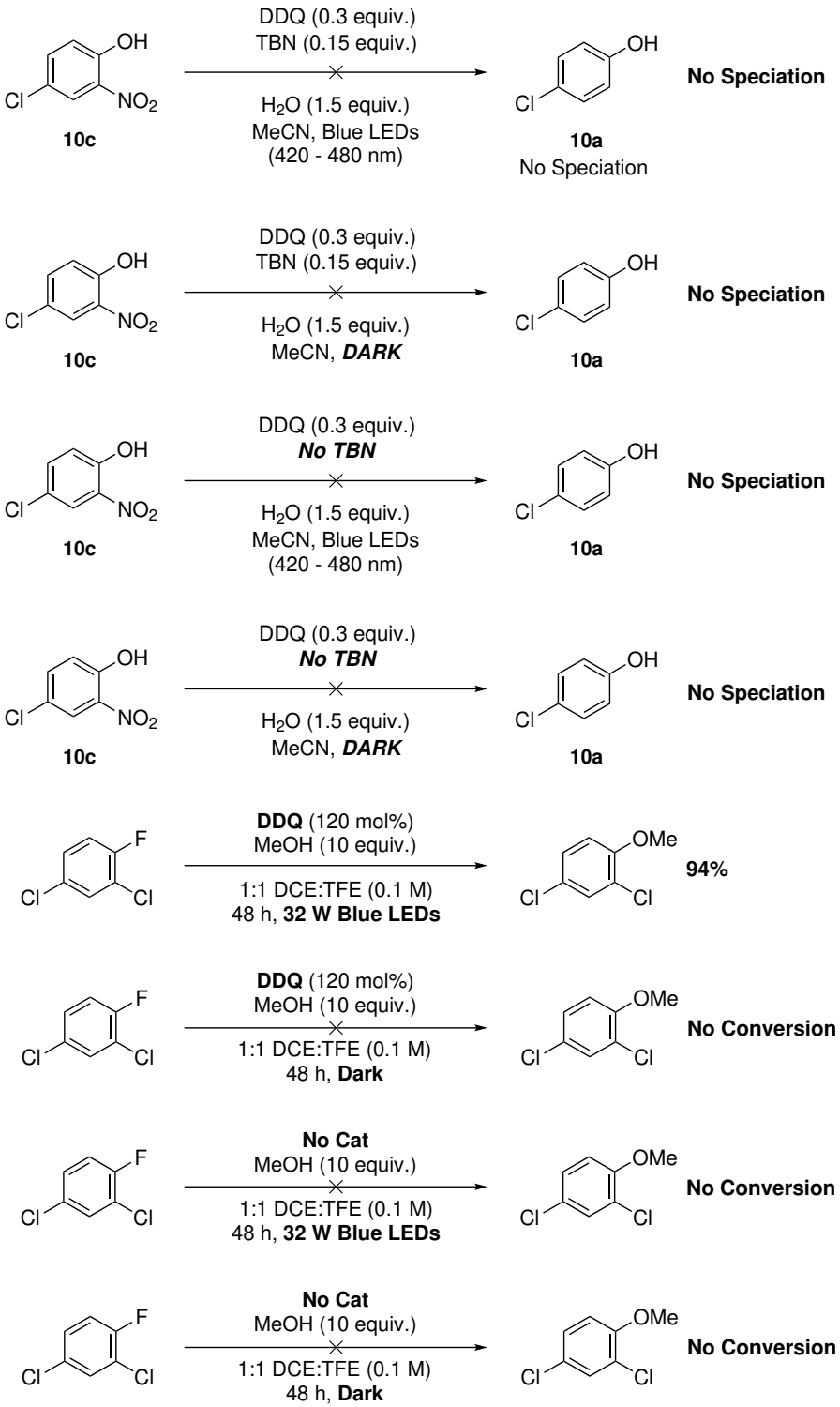

Scheme 5.2. *A summary of some of the control reactions carried out during this work [Part 1/2]*

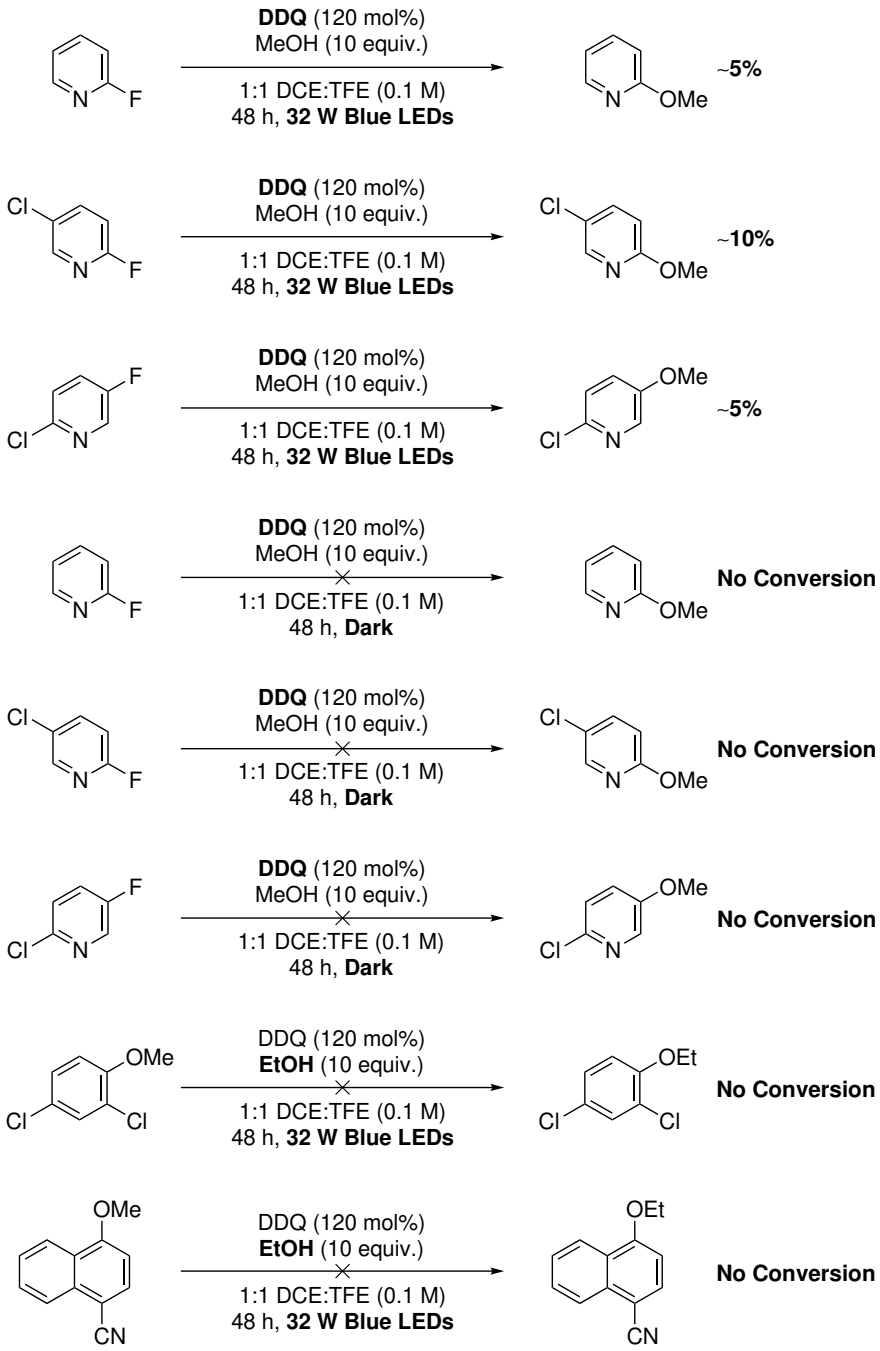

Scheme 5.3. *A summary of some of the control reactions carried out during this work [Part 2/2]*

5.6 General Experimental Procedures

General Procedure A: Arene hydroxylation-nitration conditions

To a clean, dry 10 mL vial containing a Teflon-coated magnetic stirrer bar was added 2,3-dichloro-5,6-dicyano-1,4-benzoquinone (DDQ, **1**) (34 mg, 0.15 mmol, 0.3 equiv.) and acetonitrile (5 mL, 0.1 M). The arene (0.5 mmol, 1.0 equiv.) was added, followed by H_2O (14 μL, 0.75 mmol, 1.5 equiv.), and finally *tert*-butyl nitrite (70 μL, 0.6 mmol, 1.2 equiv.). The reaction mixture was then left stirring under air, with irradiation from 3 W blue LEDs for 7 hr (*Second Generation Photoreactor Set-up*). The crude reaction mixture was then concentrated *in vacuo*, and purified via column chromatography (with the eluent described for each substrate).

General Procedure B: Arene Photochemical S_NAr with Alcohols

To a clean, dry 10 mL microwave vial containing a Teflon-coated magnetic stirrer bar was added 2,3-dichloro-5,6-dicyano-1,4-benzoquinone (DDQ, **1**) (136 mg, 0.6 mmol, 1.2 equiv.) and 1:1 DCE:TFE (5 mL, 0.1 M). The fluoroarene (0.5 mmol, 1.0 equiv.) was added, followed by nucleophile (5.0 mmol, 10 equiv.). The reaction mixture was then left stirring under air, with irradiation from 32 W blue LEDs for 48 hr (*32 W Photoreactor Set-up*). The crude reaction mixture was then concentrated *in vacuo*, and purified via column chromatography (with the eluent described for each substrate).

General Procedure C: Arene Photochemical S_NAr with Azoles

To a clean, dry 10 mL microwave vial containing a Teflon-coated magnetic stirrer bar, fluoroarene (0.5 mmol, 1.0 equiv.), 2,3-dichloro-5,6-dicyano-1,4-benzoquinone (DDQ, **1**) (136 mg, 0.6 mmol, 1.2 equiv.) in 2 mL 1:1 DCE:TFE under blue light irradiation (*32 W Photoreactor Set-up*), was added dropwise a solution azole (0.6 mmol, 1.2 equiv.) in 3 mL 1:1 DCE:TFE over 12

h. The reaction mixture was then left to stir under blue light irradiation for an additional 2 h. After which time $NaHCO_3$(aq) (15 mL) was added and washed with chloroform (3 × 15 mL). The organic layer was dried with Na_2SO_4 and solvent was removed *in vacuo*. Final purification was achieved via column chromatography (with the eluent described for each substrate).

5.7 Compound Synthesis and Characterisation

4-bromo-2-nitrophenol, 9c

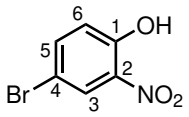

The title compound was prepared from bromobenzene **9** in accordance with **General Procedure A**. The crude residue was purified via silica gel column chromatography (30% toluene in pentane) yielding a yellow oil (24% yield).

$\mathbf{R}_f$ 0.30 (30% toluene in pentane). **^{1}H NMR** (400 MHz, $CDCl_3$) δ 10.49 (s 1H, O**H**), 8.26 (d 1H, *J* = 2.5 Hz, C{3}–**H**), 7.67 (dd 1H, *J* = 9,2.5 Hz, C{5}–**H**), 7.08 (d 1H, *J* = 9 Hz, C{6}–**H**). **^{13}C NMR** (101 MHz, $CDCl_3$) δ 154.28 (**C**{1}), 140.50 (**C**{5}), 127.49 (**C**{3}), 121.90 (**C**{6}), 111.87 (**C**{4}). **GCMS** (EI) m/z 77 100%, 156 63% [$M^{+\bullet}$]. All data in accordance with literature.[146]

4-chloro-2-nitrophenol, 10c

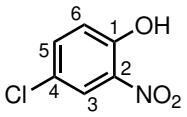

The title compound was prepared from chlorobenzene **10** in accordance with **General Procedure A**. The crude residue was purified via silica gel column chromatography (30% toluene in pentane) yielding a yellow solid (74% yield).

$\mathbf{R}_f$ 0.52 (30% toluene in pentane). **m.p.** 85-88 °C (lit.[147] 88-89 °C). **^{1}H NMR** (400 MHz, $CDCl_3$) δ 10.48 (s 1H, O**H**), 8.11 (s 1H, C{3}−**H**), 7.54 (d 1H, *J* = 8 Hz, C{5}−**H**), 7.14 (d 1H, *J* = 8 Hz, C{6}−**H**). **^{13}C NMR** (101 MHz, $CDCl_3$) δ 153.83 (**C**{1}), 137.78 (**C**{5}), 125.37 (**C**{4}), 124.48 (**C**{3}), 121.57 (**C**{6}). **GCMS** (EI) m/z 173 100% [$M^{+\bullet}$]. All data in accordance with literature.[147]

4-fluoro-2-nitrophenol, 11a

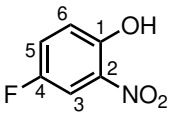

The title compound was prepared from fluorobenzene **11** in accordance with **General Procedure A**. The crude residue was purified via silica gel column chromatography (30% toluene in pentane) yielding a yellow solid as a mixture of product and 4-nitrophenol **11c** (24% yield).

R$_f$ 0.36 (30% toluene in pentane). **m.p.** 66-69 ^{o}C (lit.[148] 70-72 ^{o}C). **^{1}H NMR** (400 MHz, $CDCl_3$) δ 10.35 (s 1H, O**H**), 7.82 (dd 1H, *J* = 8,3 Hz, C{3}−**H**), 7.37 (ddd 1H, *J* = 9,7,3 Hz, C{5}−**H**), 7.16 (dd 1H, *J* = 9,4 Hz, C{6}−**H**). **^{13}C NMR** (101 MHz, $CDCl_3$) δ 137.67 (**C**{2}), 125.83 (d, *J* = 24 Hz, **C**{5}), 121.47 (d, *J* = 8 Hz, **C**{6}), 110.90 (d, *J* = 27 Hz, **C**{3}). **^{19}F NMR** (376 MHz, $CDCl_3$) δ −120.65 (m 1F, C{4}−**F**). **GCMS** (EI) m/z 32 100%, 157 19% [$M^{+\bullet}$]. All data in accordance with literature.[149]

4-nitrophenol, 11b

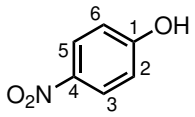

The title compound was prepared from benzene **165** in accordance with **General Procedure A**. The crude residue was purified via silica gel column chromatography (once 30% toluene in pentane, then 5% ethyl acetate in chloroform) yielding a yellow solid (49 % yield).

$\mathbf{R}_f$ 0.11 (5% ethyl acetate in chloroform). **m.p.** 109-112 °C (lit.[147] 112-114 °C). **^{1}H NMR** (400 MHz, $CDCl_3$) δ 8.17 (d 2H, *J* = 8 Hz, C{3+5}–**H**), 6.91 (d 2H, *J* = 8 Hz, C{2+6}–**H**), 6.32 (bs 1H, O**H**). **^{13}C NMR** (101 MHz, $CDCl_3$) δ 126.44 (**C**{3+5}), 115.74 (**C**{2+6}). **GCMS** (EI) m/z 139 100% [$M^{+\bullet}$]. All data in accordance with literature.[147]

2-nitrophenol, 11c

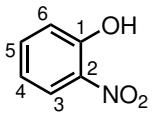

The title compound was prepared from benzene **165** in accordance with **General Procedure A**. The crude residue was purified via silica gel column chromatography (30% toluene in pentane) yielding a yellow solid (31% yield).

R$_f$ 0.33 (30% toluene in pentane). **m.p.** 40-43 ^{o}C (lit.[150] 42-44 ^{o}C). **^{1}H NMR** (400 MHz, $CDCl_3$) δ 10.60 (s 1H, O**H**), 8.12 (d 1H, *J* = 9 Hz, C{3}–**H**), 7.59 (dd 1H, *J* = 8.5,8 Hz, C{5}–**H**), 7.17 (d 1H, *J* = 9 Hz, C{6}–**H**), 7.00 (dd 1H, *J* = 8.5,8 Hz, C{4}–**H**). **^{13}C NMR** (101 MHz, $CDCl_3$) δ 137.71 (**C**{3/5}), 125.24 (**C**{3/5}), 120.13 (**C**{4/6}), 120.38 (**C**{4/6}). **GCMS** (EI) m/z 139 100% [$M^{+\bullet}$]. All data in accordance with literature.[150]

2,4-dichloroanisole, 100a

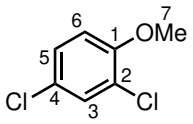

The title compound was prepared from 2,4-dichlorofluorobenzene **100** and methanol in accordance with **General Procedure B**. The crude residue was purified via silica gel column chromatography (3% chloroform in pentane) yielding a clear oil (94% yield).

$\mathbf{R}_f$ 0.27 (3% chloroform in pentane). **^{1}H NMR** (400 MHz, $CDCl_3$) δ 7.33 (d 1H, *J* = 2.5 Hz, C{3}–**H**), 7.16 (dd 1H, *J* = 9, 2.5 Hz, C{5}–**H**), 6.81 (d 1H, *J* = 9 Hz, C{6}–**H**), 3.85 (s 3H, C{7}–**H**). **^{13}C NMR** (101 MHz, $CDCl_3$) δ 153.92 (**C**{1}), 129.94 (**C**{3}), 127.63 (**C**{5}), 125.62 (**C**{2}), 123.25 (**C**{4}), 112.79 (**C**{6}), 56.35 (**C**{7}). **GCMS** (EI) m/z 176 100% [$M^{+\bullet}$]. All data in accordance with literature.[151]

2-chloro-4-bromoanisole, 102a

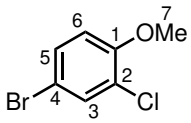

The title compound was prepared from 2-chloro-4-bromofluorobenzene **102** and methanol in accordance with **General Procedure B**. The crude residue was purified via silica gel column chromatography (3% chloroform in pentane) yielding a clear oil (85 % yield).

$\mathbf{R}_f$ 0.42 (3% chloroform in pentane). **^{1}H NMR** (400 MHz, $CDCl_3$) δ 7.49 (d 1H, *J* = 2.5 Hz, C{3}–**H**), 7.32 (dd 1H, *J* = 9,2.5 Hz, C{5}–**H**), 6.79 (d 1H, *J* = 9 Hz, C{6}–**H**), 3.87 (s 3H, C{7}–**H**). **^{13}C NMR** (101 MHz, $CDCl_3$) δ 154.51 (**C**{1}), 133.63 (**C**{5}), 132.78 (**C**{3}), 123.76 (**C**{2}), 113.45 (**C**{6}), 112.62 (**C**{4}), 56.43 (**C**{8}). **GCMS** (EI) m/z 220 77% [$M^{+\bullet}$], 222 100% [M+2]. All data in accordance with literature.[151]

4-chloroanisole, 103a

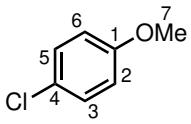

The title compound was prepared from 4-chlorofluorobenzene **103** and methanol in accordance with **General Procedure B**. The crude residue was purified via silica gel column chromatography (3% chloroform in pentane) yielding a clear oil (62% yield).

$\mathbf{R}_f$ 0.38 (3% chloroform in pentane). **^{1}H NMR** (400 MHz, $CDCl_3$) δ 7.22 - 7.14 (m 2H, C{3+5}−**H**), 6.82 - 6.73 (m 2H, C{2+6}−**H**), 3.72 (s 3H, C{7}−**H**). **^{13}C NMR** (101 MHz, $CDCl_3$) δ 158.33 (**C**{1}), 129.40 (**C**{3+5}), 125.64 (**C**{4}), 115.30 (**C**{2+6}), 55.57 (**C**{7}). **GCMS** (EI) m/z 142 100% [$M^{+\bullet}$]. All data in accordance with literature.[151]

2,6-dichloro-4-bromoanisole, 104a

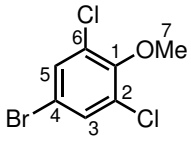

The title compound was prepared from 2,6-dichloro-4-bromofluorobenzene **104** and methanol in accordance with **General Procedure B**. The crude residue was purified via silica gel column chromatography (3% chloroform in pentane) yielding a clear oil (59 % yield).

R$_f$ 0.58 (3% chloroform in pentane). **^{1}H NMR** (400 MHz, $CDCl_3$) δ 7.40 (s 2H, C{3+5}−**H**), 3.84 (s 3H, C{7}−**H**). **^{13}C NMR** (101 MHz, $CDCl_3$) δ 151.97 (**C**{1}), 131.68 (**C**{3+5}), 130.46 (**C**{2+6}), 116.57 (**C**{4}), 60.97 (**C**{7}). **GCMS** (EI) m/z 254 63% [$M^{+\bullet}$], 256 100% [M+2]. All data in accordance with literature.[152]

4-bromoanisole, 105a

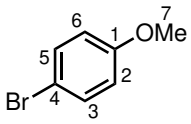

The title compound was prepared from 4-bromofluorobenzene **105** and methanol in accordance with **General Procedure B**. The crude residue was purified via silica gel column chromatography (3% chloroform in pentane) yielding a clear oil (39% yield).

$\mathbf{R}_f$ 0.42 (3% chloroform in pentane). **^{1}H NMR** (400 MHz, $CDCl_3$) δ 7.42 – 7.33 (m 2H, C{3+5}–**H**), 6.87 – 6.73 (m 2H, C{2+6}–**H**), 3.78 (s 3H, C{7}–**H**). **^{13}C NMR** (101 MHz, $CDCl_3$) δ 158.80 (**C**{1}), 132.35 (**C**{3+5}), 115.83 (**C**{2+6}), 115.29 (**C**{4}), 55.56 (**C**{7}). **GCMS** (EI) m/z 186 100% [$M^{+\bullet}$]. All data in accordance with literature.[151]

2-chloroanisole, 106a

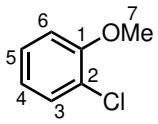

The title compound was prepared from 2-chlorofluorobenzene **106** and methanol in accordance with **General Procedure B**. The crude residue was purified via silica gel column chromatography (3% chloroform in pentane) yielding a clear oil (32% yield).

$\mathbf{R}_f$ 0.83 (3% chloroform in pentane). **^{1}H NMR** (400 MHz, $CDCl_3$) δ 7.36 (dd 1H, *J* = 8, 1.5 Hz, C{3}–**H**), 7.23 (ddd 1H, *J* = 8, 7.5, 1.5 Hz, C{5}–**H**), 6.95 - 6.87 (m 2H, C{4+6}–**H**), 3.90 (s 3H, C{7}–**H**). **^{13}C NMR** (101 MHz, $CDCl_3$) δ 155.10 (**C**{1}), 130.37 (**C**{3}), 127.87 (**C**{5}), 122.53 (**C**{2}), 121.42 (**C**{4}), 112.17 (**C**{6}), 56.13 (**C**{7}). **GCMS** (EI) m/z 142 100% [$M^{+\bullet}$]. All data in accordance with literature.[153]

1,5-dichloro-2-methoxy-4-methylbenzene, 107a / 1,3-dichloro-4-methoxy-2-methylbenzene, 108a

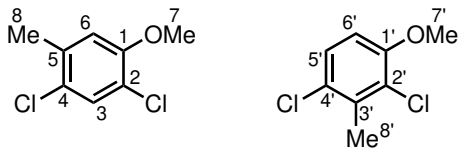

The title compounds was prepared from a comercial sample of 1,5-dichloro-2-fluoro-4-methylbenzene **107** (which was later deduced to be an approximately 1:1 mixture of 1,5-dichloro-2-fluoro-4-methylbenzene and 1,3-dichloro-4-fluoro-2-methylbenzene) and methanol in accordance with **General Procedure B**. The crude residue was purified via silica gel column chromatography (3% chloroform in pentane) with the title compounds collected as an inseparable oil, in the same ratio as starting material (65% yield).

$\mathbf{R}_f$ 0.28 (3% chloroform in pentane). **^{1}H NMR** (400 MHz, $CDCl_3$) δ 7.32 (s 1H, C{3}–**H**), 7.21 (d 1H, *J* = 9 Hz, C{5'}–**H**), 6.76 (s 1H, C{6}–**H**), 6.72 (d 1H, *J* = 9 Hz, C{6'}–**H**), 3.87 (s 3H, C{7'}–**H**), 3.87 (s 3H, C{7}–**H**), 2.46 (s 3H, C{8'}–**H**), 2.33 (s 3H, C{8}–**H**). **^{13}C NMR** (101 MHz, $CDCl_3$) δ 154.07 (**C**{1/1'}), 153.65 (**C**{1/1'}), 135.65, 135.62, 130.03 (**C**{3}), 127.38 (**C**{5'}), 126.67, 125.74, 123.92, 120.39, 114.30 (**C**{6}), 109.93 (**C**{6'}), 56.45 (**C**{7+7'}), 20.22 (**C**{8}), 17.87 (**C**{8'}). **GCMS** (EI) m/z 190 100% [$M^{+\bullet}$].

4-methoxy-1-naphthonitrile, 109a

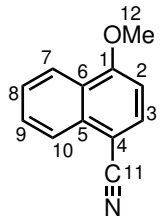

The title compound was prepared from 4-fluoro-1-naphthonitrile **109** and methanol in accordance with **General Procedure B**. The crude residue was purified via silica gel column chromatography (3% to 20% chloroform in pentane) yielding a white solid (61 % yield).

$\mathbf{R}_f$ 0.10 (3% chloroform in pentane). **m.p.** 98-99 °C (lit.[154] 100-102 °C). **^{1}H NMR** (400 MHz, $CDCl_3$) δ 8.26 (d 1H, *J* = 8.5 Hz, C{7/10}–**H**), 8.11 (d 1H, *J* = 8.5 Hz, C{7/10}–**H**), 7.80 (d 1H, *J* = 8 Hz, C{3}–**H**), 7.65 (dd 1H, *J* = 8, 8 Hz, C{8/9}–**H**), 7.55 (dd 1H, *J* = 8, 8 Hz, C{8/9}–**H**), 6.77 (d 1H, *J* = 8 Hz, C{2}–**H**), 4.03 (s 3H, C{12}–**H**). **^{13}C NMR** (101 MHz, $CDCl_3$) δ 159.35 (**C**{1}), 134.07 (**C**{3}), 133.40 (**C**{5/6}), 128.93 (**C**{8/9}), 126.69 (**C**{7/10}), 125.15 (**C**{5/6}), 124.83 (**C**{8/9}), 122.78 (**C**{7/10}), 118.51 (**C**{11}), 103.38 (**C**{2/4}), 101.76 (**C**{2/4}), 55.85 (**C**{12}). **GCMS** (EI) m/z 140 100%, 183 85% [$M^{+\bullet}$]. All data in accordance with literature.[154]

N-Boc-5-fluoroindole, 120

Prepared by modified procedure of Mongin *et al.* [155]

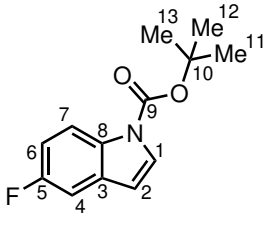

To a stirred solution of 5-fluoroindole **166** (250 mg, 1.85 mmol) in THF (15 mL) were successively added Boc_2O (0.8 g, 3.7 mmol), and DMAP (0.34 g, 2.8 mmol). The mixture was stirred for 4 h at r.t. before addition of sat. aq NH_4Cl (20 mL) and extraction with EtOAc (3×15 mL). The combined organic layers were dried (Na_2SO_4), filtered, and concentrated under reduced pressure. The residue was purified by chromatography on silica gel (3% chloroform in pentane).

$\mathbf{R}_f$ 0.21 (3% chloroform in pentane). **m.p.** 93-95 °C. **^{1}H NMR** (400 MHz, $CDCl_3$) δ 8.16 – 8.04 (m 1H, C{7} – **H**), 7.63 (d 1H, *J* = 3.5 Hz, C{1} – **H**), 7.21 (dd 1H, *J* = 9, 2.5 Hz, C{4} – **H**), 7.04 (ddd 1H, *J* = 9, 9, 2.5 Hz, C{6} – **H**), 6.52 (dd 1H, *J* = 3.5, 0.5 Hz, C{2} – **H**), 1.68 (s 9H, C{11+12+13} – **H**). **^{13}C NMR** (101 MHz, $CDCl_3$) δ 159.61 (d, *J* = 238.5 Hz, **C**{5}), 149.65 (**C**{9}), 131.74 (**C**{8}), 116.16 (d, *J* = 10 Hz, **C**{3}), 127.55 (**C**{1}), 116.16 (d, *J* = 9.5 Hz, **C**{7}), 112.07 (d, *J* = 25 Hz, **C**{6}), 107.09 (d, *J* = 4 Hz, **C**{2}), 106.43 (d, *J* = 24 Hz, **C**{4}), 84.02 (**C**{10}), 28.30 (**C**{11+12+13}). **GCMS** (EI) m/z 57 100%, 135 66% [$M^{+\bullet}$ – Boc], 253 11% [$M^{+\bullet}$]. All data in accordance with literature. [155]

3,5-dibromo-4-chloroanisole, 132a

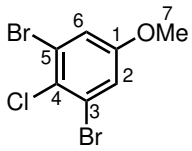

The title compound was prepared from 3,5-dibromo-4-chlorofluorobenzene **132** and methanol in accordance with **General Procedure B**. The crude residue was purified via silica gel column chromatography (3% chloroform in pentane) white solid (33% yield).

R$_f$ 0.36 (3% chloroform in pentane). **m.p.** 66-68 ^{o}C (lit.[156] 69-71 ^{o}C). **^{1}H NMR** (400 MHz, $CDCl_3$) δ 7.15 (s 2H, C{2+6}–**H**), 3.78 (s 3H, C{7}–**H**). **GCMS** (EI) m/z 298 44% [$M^{+\bullet}$]. All data in accordance with literature.[156]

3,4-dichloroanisole, 133a

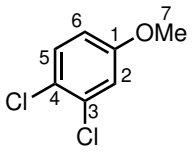

The title compound was prepared from 3,4-dichlorofluorobenzene **133** and methanol in accordance with **General Procedure B**. The crude residue was purified via silica gel column chromatography (3% chloroform in pentane) clear oil (74% yield).

$\mathbf{R}_f$ 0.56 (3% chloroform in pentane). **^{1}H NMR** (400 MHz, $CDCl_3$) δ 7.32 (d 1H, *J* = 9 Hz, C{5}–**H**), 6.99 (d 1H, *J* = 3 Hz, C{2}–**H**), 6.76 (dd 1H, *J* = 9,3 Hz, C{6}–**H**), 3.79 (s 3H, C{7}–**H**). **^{13}C NMR** (101 MHz, $CDCl_3$) δ 158.80 (**C**{1}), 133.01 (**C**{3/4}), 130.81 (**C**{5}), 124.07 (**C**{3/4}), 115.87 (**C**{2}), 114.27 (**C**{6}), 55.89 (**C**{7}). **GCMS** (EI) m/z 176 100% [$M^{+\bullet}$]. All data in accordance with literature.[157]

2,4-dichloro-5-bromoanisole, 134a

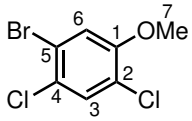

The title compound was prepared from 2,4-dichloro-5-bromofluorobenzene **134** and methanol in accordance with **General Procedure B**. The crude residue was purified via silica gel column chromatography (3% chloroform in pentane) clear oil (61% yield).

$\mathbf{R}_f$ 0.33 (3% chloroform in pentane). **^{1}H NMR** (500 MHz, $CDCl_3$) δ 7.45 (s 1H, C{6}–**H**), 7.14 (s 1H, C{3}–**H**), 3.89 (s 3H, C{7}–**H**). **^{13}C NMR** (126 MHz, $CDCl_3$) δ 154.26 (**C**{1}), 130.91 (**C**{3}), 126.27 (**C**{2/4/5}), 122.61 (**C**{2/4/5}), 120.80 (**C**{2/4/5}), 116.89 (**C**{6}), 56.80 (**C**{7}). **GCMS** (EI) m/z 254 64% [$M^{+\bullet}$].

4-bromo-2-fluoroanisole, 139a

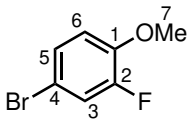

The title compound was prepared from 4-bromo-1,2-difluorobenzene **139** and methanol in accordance with **General Procedure B**. The crude residue was purified via silica gel column chromatography (3% chloroform in pentane) yielding a clear oil (64% yield).

$\mathbf{R}_f$ 0.37 (3% chloroform in pentane). **^{1}H NMR** (400 MHz, $CDCl_3$) δ 7.22 (dd 1H, *J* = 10.5, 2.5 Hz, C{3}–**H**), 7.19 (ddd 1H, *J* = 9, 2.5, 1.5 Hz, C{5}–**H**), 6.83 (dd 1H, *J* = 9, 9 Hz, C{6}–**H**), 3.86 (s 3H, C{7}–**H**). **^{13}C NMR** (101 MHz, $CDCl_3$) δ 152.39 (d, *J* = 250.5 Hz, **C**{2}), 147.12 (d, *J* = 10.5 Hz, **C**{1}), 127.31 (d, *J* = 5 Hz, **C**{5}), 119.67 (d, *J* = 21.5 Hz, **C**{3}), 114.66 (d, *J* = 2.5 Hz, **C**{6}), 111.97 (d, *J* = 8.5 Hz, **C**{4}), 56.47 (**C**{7}). **^{19}F NMR** (376 MHz, $CDCl_3$) δ −132.11 (m 1F, C{2}–**F**). **GCMS** (EI) m/z 81 100%, 161 93%, 204 95% [$M^{+\bullet}$]. All data in accordance with literature.[158]

2,4-dichloro-1-ethoxybenzene, 100b

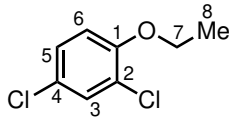

The title compound was prepared from 2,4-dichlorofluorobenzene **100** and ethanol in accordance with **General Procedure B**. The crude residue was purified via silica gel column chromatography (3% chloroform in pentane) yielding a clear oil (87% yield).

$\mathbf{R}_f$ 0.52 (3% chloroform in pentane). **^{1}H NMR** (400 MHz, $CDCl_3$) δ 7.35 (d 1H, *J* = 2.5 Hz, C{3}–**H**), 7.15 (dd 1H, *J* = 9, 2.5 Hz, C{5}–**H**), 6.82 (d 1H, *J* = 9 Hz, C{6}–**H**), 4.06 (q 2H, *J* = 7 Hz, C{7}–**H**), 1.46 (t 3H, *J* = 7 Hz, C{8}–**H**). **^{13}C NMR** (101 MHz, $CDCl_3$) δ 153.41 (**C**{1}), 130.01 (**C**{3}), 127.63 (**C**{5}), 125.55 (**C**{2/4}), 123.70 (**C**{2/4}), 114.05 (**C**{6}), 65.23 (**C**{7}), 14.73 (**C**{8}). **GCMS** (EI) m/z 190 100% [$M^{+\bullet}$]. All data in accordance with literature.[159]

2,4-dichloro-1-isopropoxybenzene, 100c

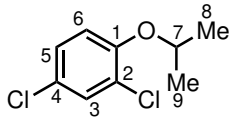

The title compound was prepared from 2,4-dichlorofluorobenzene **100** and *iso*-propanol in accordance with **General Procedure B**. The crude residue was purified via silica gel column chromatography (3% chloroform in pentane) yielding a clear oil (89% yield).

$\mathbf{R}_f$ 0.47 (3% chloroform in pentane). **^{1}H NMR** (400 MHz, $CDCl_3$) δ 7.35 (d 1H, *J* = 2.5 Hz, C{3}−**H**), 7.15 (dd 1H, *J* = 9, 2.5 Hz, C{5}−**H**), 6.86 (d 1H, *J* = 9 Hz, C{6}−**H**), 4.50 (sept 1H, *J* = 6 Hz, C{7}−**H**), 1.36 (d 6H, *J* = 6 Hz, C{8+9}−**H**). **^{13}C NMR** (101 MHz, $CDCl_3$) δ 152.61 (**C**{1}), 130.17 (**C**{3}), 127.56 (**C**{5}), 125.86 (**C**{2/4}), 125.22 (**C**{2/4}), 116.89 (**C**{6}), 72.71 (**C**{7}), 22.04 (**C**{8+9}). **GCMS** (EI) m/z 161 100% [$M^{+\bullet} - C_3H_7$], 204 5% [$M^{+\bullet}$]. All data in accordance with literature.[160]

2,4-dichloro-1-(2,2,2-trifluoroethoxy)benzene, 100d

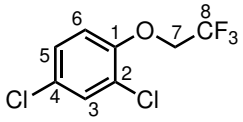

The title compound was prepared from 2,4-dichlorofluorobenzene **100** and *tert*-butanol in accordance with **General Procedure B**. The crude residue was purified via silica gel column chromatography (3% chloroform in pentane) yielding a clear oil (3% yield).

$\mathbf{R}_f$ 0.56 (3% chloroform in pentane). **^{1}H NMR** (400 MHz, $CDCl_3$) δ 7.42 (d 1H, *J* = 2.5 Hz, C{3}–**H**), 7.21 (dd 1H, *J* = 9, 2.5 Hz, C{5}–**H**), 6.92 (d 1H, *J* = 9 Hz, C{6}–**H**), 4.38 (q 2H, *J* = 9 Hz, C{7}–**H**). **^{19}F NMR** (376 MHz, $CDCl_3$) δ −73.95 (t 3F, *J* = 9 Hz, C{8}–**F**). **GCMS** (EI) m/z 161 100% [$M^{+\bullet} - CH_2CF_3$], 244 83% [$M^{+\bullet}$]. All data in accordance with literature.[161]

2,4-dichloro-1-(((1*R*,2*S*,5*R*)-2-isopropyl-5-methylcyclohexyl)oxy)benzene, 100e

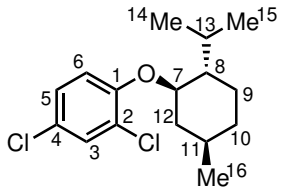

The title compound was prepared from 2,4-dichlorofluorobenzene **100** and (-)-menthol (5 equiv.) in accordance with **General Procedure B**. The crude residue was purified via silica gel column chromatography (100% pentane) yielding a white solid (21% yield).

R$_f$ 0.48 (100% pentane). **m.p.** 44-46 °C. **^{1}H NMR** (500 MHz, $CDCl_3$) δ 7.35 (d 1H, *J* = 2.5 Hz, C{3}–**H**), 7.14 (dd 1H, *J* = 9, 2.5 Hz, C{5}–**H**), 6.86 (d 1H, *J* = 9 Hz, C{6}–**H**), 4.02 (td 1H, *J* = 10.5, 4 Hz, C{7}–**H**), 2.25 (m 1H, C{11}–**H**), 2.07 (dtd 1H, *J* = 12.5, 4, 2 Hz, C{12}–**H'**), 1.77 - 1.69 (m 2H, C{9+10}–**H'**), 1.61 (ddt 1H, *J* = 16, 10.5, 3.5 Hz, C{8}–**H**), 1.44 (m 1H, C{13}–**H**), 1.15 - 1.03 (m 2H, C{12+9}–**H"**), 1.00 - 0.95 (m 1H, C{10}–**H"**), 0.94 (d 3H, *J* = 6.5 Hz, C{14/15}–**H**), 0.92 (d 3H, *J* = 6.5 Hz, C{14/15}–**H**), 0.76 (d 3H, *J* = 7 Hz, C{16}–**H**). **^{13}C NMR** (126 MHz, $CDCl_3$) δ 152.91 (**C**{1}), 130.24 (**C**{3}), 127.57 (**C**{5}), 125.28 (**C**{2/4}), 124.84 (**C**{2/4}), 115.61 (**C**{6}), 79.77 (**C**{7}), 47.98 (**C**{8}), 40.19 (**C**{12}), 34.48 (**C**{10}), 31.61 (**C**{13}), 26.16 (**C**{11}), 23.78 (**C**{9}), 22.24 (**C**{14/15}), 20.89 (**C**{14/15}), 16.73 (**C**{16}). **HRMS** (EI) m/z found 300.1048, $C_{16}H_{22}OCl_2^{+\bullet}$ requires 300.1042. ν_{max} / cm^{-1} 2928, 2360, 1477, 1387, 1287, 1251, 1152, 1101, 1059, 744. $[\alpha]_{\mathbf{D}}^{25} = -122.0$ (*c* = 0.96, EtOH).

2,4-dichloro-1-(cyclohexyloxy)benzene, 100f

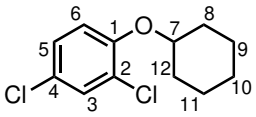

The title compound was prepared from 2,4-dichlorofluorobenzene **100** and cyclohexanol in accordance with **General Procedure B**. The crude residue was purified via silica gel column chromatography (2% chloroform in pentane) yielding a white soild (64% yield).

$\mathbf{R}_f$ 0.33 (3% chloroform in pentane). **^{1}H NMR** (400 MHz, $CDCl_3$) δ 7.35 (d 1H, *J* = 2.5 Hz, C{3}–**H**), 7.14 (dd 1H, *J* = 9, 2.5 Hz, C{5}–**H**), 6.87 (d 1H, *J* = 9 Hz, C{6}–**H**), 4.28 – 4.21 (m 1H, C{7}–**H**), 1.97 – 1.88 (m 2H, C{8+12/8'+12'}–**H**), 1.86 – 1.76 (m 2H, C{9+11/9'+11'}–**H**), 1.68 – 1.58 (m 2H, C{8+12/8'+12'}–**H**), 1.58 – 1.51 (m 1H, C{10/10'}–**H**), 1.42 – 1.31 (m 3H, C{(9+11/9'+11')+(10/10')}–**H**). **^{13}C NMR** (101 MHz, $CDCl_3$) δ 152.45 (**C**{1}), 130.22 (**C**{3}), 127.52 (**C**{5}), 125.80 (**C**{2/4}), 125.35 (**C**{2/4}), 117.04 (**C**{6}), 77.62 (**C**{7}), 31.64 (**C**{8+12}), 25.67 (**C**{10}), 22.04 (**C**{9+11}). **GCMS** (EI) m/z 162 100% [$M^{+\bullet} - C_6H_{10}$], 244 2% [$M^{+\bullet}$]. All data in accordance with literature.[162]

2,4-dichloro-1-(cyclopropylmethoxy)benzene, 100g

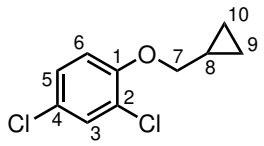

The title compound was prepared from 2,4-dichlorofluorobenzene **100** and cyclopropylmethanol in accordance with **General Procedure B**. The crude residue was purified via silica gel column chromatography (2% chloroform in pentane) yielding a clear oil (87% yield).

$\mathbf{R}_f$ 0.44 (3% chloroform in pentane). **^{1}H NMR** (400 MHz, $CDCl_3$) δ 7.35 (d 1H, *J* = 2.5 Hz, C{3}–**H**), 7.14 (dd 1H, *J* = 9, 2.5 Hz, C{5}–**H**), 6.81 (d 1H, *J* = 9 Hz, C{6}–**H**), 3.85 (d 2H, *J* = 7 Hz, C{7}–**H**), 1.35-1.22 (m 1H, C{8}–**H**), 0.67-0.62 (m 2H, C{9+10/9'+10'}–**H**), 0.38 (dt 3H, *J* = 6.5, 5 Hz, C{9+10/9'+10'}–**H**). **^{13}C NMR** (101 MHz, $CDCl_3$) δ 153.54 (**C**{1}), 130.04 (**C**{3}), 127.58 (**C**{5}), 125.78 (**C**{2/4}), 124.13 (**C**{2/4}), 114.84 (**C**{6}), 74.31 (**C**{7}), 10.22 (**C**{8}), 3.36 (**C**{9+10}). **HRMS** (EI) m/z found 216.0109, $C_{10}H_{10}O^{35}Cl_2^{+\bullet}$ requires 216.0103. ν_{max} / cm^{-1} 3085, 3009, 2919, 1587, 1483, 1466, 1407, 1390, 1289, 1248, 1103, 1060, 1023, 1004, 801, 736, 654.

(*R*)-1-(3-bromo-2-methylpropoxy)-2,4-dichlorobenzene, 100h

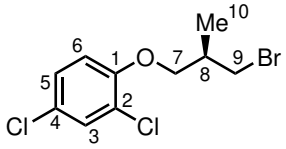

The title compound was prepared from 2,4-dichlorofluorobenzene **100** and (*R*)-3-bromo-2-methylpropan-1-ol **167** in accordance with **General Procedure B**. The crude residue was purified via silica gel column chromatography (100% pentane) yielding The title compound as a colourless oil (36% yield).

$\mathbf{R}_f$ 0.46 (2% diethyl ether in pentane). **^{1}H NMR** (500 MHz, $CDCl_3$) δ 7.36 (d 1H, *J* = 2.5 Hz, C{3}−**H**), 7.17 (d 1H, *J* = 9, 2.5 Hz, C{5}−**H**), 6.85 (d 1H, *J* = 9 Hz, C{6}−**H**), 4.01-3.89 (m 2H, C{7+7'}−**H**), 3.67-3.55 (m 2H, C{9+9'}−**H**), 2.43-2.31 (m 1H, C{8}−**H**), 1.17 (d 3H, *J* = 7 Hz, C{10}−**H**). **^{13}C NMR** (126 MHz, $CDCl_3$) δ 153.23 (**C**{1}), 130.08 (**C**{3}), 127.69 (**C**{5}), 126.03 (**C**{2/4}), 124.01 (**C**{2/4}), 114.31 (**C**{6}), 71.48 (**C**{7}), 37.19 (**C**{9}), 35.36 (**C**{8}), 15.89 (**C**{10}). **HRMS** (EI) m/z found 295.9370, $C_{10}H_{11}BrCl_2O^{+\bullet}$ requires 295.9365. ν_{max} / cm^{-1} 2968, 1587, 1484, 1463, 1389, 1288, 1254, 1103, 1062, 907, 803, 732, 653

(*R*)-4-(2,4-dichlorophenoxy)butan-2-ol, 100i / (*R*)-3-(2,4-dichlorophenoxy)butan-1-ol, 100j

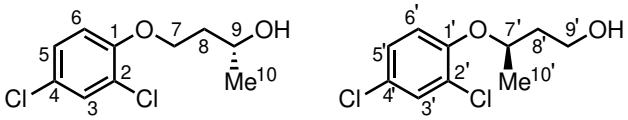

The title compounds was prepared from 2,4-dichlorofluorobenzene **100** and butane-1,3-diol in accordance with **General Procedure B**. The crude residue was purified via silica gel column chromatography (5% ethyl acetate in pentane) with the title compounds collected as an inseparable oil, in a 3:1 ratio of **100i** to **100j** as assigned by HMBC (80% combined yield).

$\mathbf{R}_f$ 0.10 (10% ethyl acetate in pentane). **^{1}H NMR** (400 MHz, $CDCl_3$) δ 7.37 – 7.35 (m 1H, C{3+3'}–**H**), 7.21 – 7.14 (m 1H, C{5+5'}–**H**), 6.91 (d 0H, *J* = 9 Hz, C{6'}–**H**), 6.86 (d 1H, *J* = 9 Hz, C{6}–**H**), 4.67 – 4.56 (m 0H, C{7'}–**H**), 4.26 – 4.19 (m 1H, C{9}–**H**), 4.16 – 4.08 (m 2H, C{7}–**H**), 3.95 – 3.76 (m 1H, C{9'}–**H**), 2.03 – 1.90 (m 2H, C{8+8'}–**H**), 1.35 (d 1H, *J* = 6 Hz, C{10'}–**H**), (d 3H, *J* = 6.5 Hz, C{10}–**H**). **^{13}C NMR** (101 MHz, $CDCl_3$) δ 153.16, 152.31, 130.24, 130.07, 127.76, 127.73, 126.09, 123.72, 116.47, 113.93, 74.78, 67.70, 66.40, 59.80, 39.06, 37.91, 19.68. **GCMS** (EI) m/z 162 100% [$M^{+\bullet} - C_4H_8O$].

1-(2,4-dichlorophenyl)-1*H*-pyrazole, 100aa

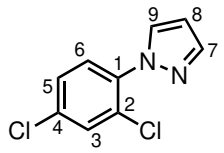

The title compound was prepared from 2,4-dichlorofluorobenzene **100** and pyrazole **41** in accordance with **General Procedure C**. The crude residue was purified via silica gel column chromatography (2% ethyl acetate in pentane) yielding The title compound as a pale yellow solid (20% yield).

R$_f$ 0.39 (10% ethyl acetate in pentane). **m.p.** 40-42 ^{o}C (lit.[163] 47-48 ^{o}C). **^{1}H NMR** (400 MHz, $CDCl_3$) δ 7.87 (d 1H, *J* = 2.5 Hz, C{9}–**H**), 7.75 (d 1H, *J* = 2 Hz, C{7}–**H**), 7.54 (d 1H, *J* = 9 Hz, C{6}–**H**), 7.54 (d 1H, *J* = 2.5 Hz, C{3}–**H**), 7.36 (dd 1H, *J* = 9,2.5 Hz, C{5}–**H**), 6.48 (dd 1H, *J* = 2.5,2 Hz, C{8}–**H**). **^{13}C NMR** (101 MHz, $CDCl_3$) δ 141.34 (**C**{7}), 137.01 (**C**{1}), 134.24 (**C**{4}), 131.36 (**C**{9}), 130.52 (**C**{3}), 129.00 (**C**{2}), 128.62 (**C**{6}), 128.12 (**C**{5}), 107.21 (**C**{8}). **LRMS** (ESI) m/z 213 100% [M+H]. All data in accordance with literature.[23,163]

1-(4-chlorophenyl)-1*H*-pyrazole, 103b

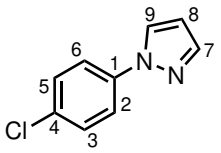

The title compound was prepared from 4-chlorofluorobenzene **103** and pyrazole **41** in accordance with **General Procedure C**. The crude residue was purified via silica gel column chromatography (2% ethyl acetate in pentane) yielding The title compound as a pale yellow solid (62% yield).

$\mathbf{R}_f$ 0.48 (10% ethyl acetate in pentane). **m.p.** 49-52 ^{o}C (lit.[164] 52-54 ^{o}C). **^{1}H NMR** (400 MHz, $CDCl_3$) δ 7.88 (dd 1H, *J* = 2.5, 0.5 Hz, C{9}–**H**), 7.72 (dd 1H, *J* = 2, 0.5 Hz, C{7}–**H**), 7.67 - 7.60 (m 2H, C{2+6/3+5}–**H**), 7.44 - 7.36 (m 2H, C{2+6/3+5}–**H**), 6.47 (dd 1H, *J* = 2.5, 2 Hz, C{8}–**H**). **^{13}C NMR** (101 MHz, $CDCl_3$) δ 141.47 (**C**{7}), 138.88 (**C**{1}), 132.01 (**C**{4}), 129.62 (**C**{2+4/3+5}), 126.80 (**C**{9}), 120.42 (**C**{2+4/3+5}), 108.10 (**C**{8}). **LRMS** (ESI) m/z 179 100% [M+H]. All data in accordance with literature.[164]

4-chloro-1-(4-chlorophenyl)-1*H*-pyrazole, 103c

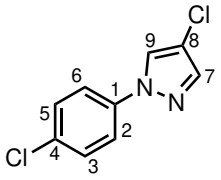

The title compound was prepared from 4-chlorofluorobenzene **103** and 4-chloropyrazole **168** in accordance with **General Procedure C**. The crude residue was purified via silica gel column chromatography (2% diethyl ether in pentane) yielding The title compound as a colourless oil (45% yield).

$\mathbf{R}_f$ 0.50 (20% diethyl ether in pentane). **m.p.** 57-59 ^{o}C. **^{1}H NMR** (400 MHz, $CDCl_3$) δ 7.87 (d 1H, *J* = 0.5 Hz, C{9}–**H**), 7.67 (d 1H, *J* = 0.5 Hz, C{7}–**H**), 7.60-7.55 (m 2H, C{2+6/3+5}–**H**), 7.45-7.39 (m 2H, C{2+6/3+5}–**H**). **^{13}C NMR** (101 MHz, $CDCl_3$) δ 139.92 (**C**{7}), 138.39 (**C**{1}), 132.69 (**C**{4}), 129.79 (**C**{2+6/3+5}), 124.87 (**C**{9}), 120.22 (**C**{2+6/3+5}), 112.96 (**C**{8}). **HRMS** (ESI^+) found 212.9983, $C_9H_7N_2{}^{35}Cl_2{}^+$ requires 212.9981. ν_{max} / cm^{-1} 1596, 1535, 1433, 1385, 1345, 1245, 1155, 1091, 1029, 971, 946, 849, 800, 778, 648.

4-bromo-1-(4-chlorophenyl)-1*H*-pyrazole, 103d

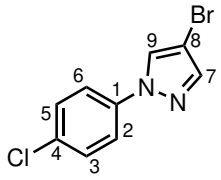

The title compound was prepared from 4-chlorofluorobenzene **103** and 4-bromopyrazole **169** in accordance with **General Procedure C**. The crude residue was purified via silica gel column chromatography (2% diethyl ether in pentane) yielding The title compound as a pale yellow solid (20% yield).

$\mathbf{R}_f$ 0.17 (2% diethyl ether in pentane). **m.p.** 63-64 °C. **^{1}H NMR** (500 MHz, $CDCl_3$) δ 7.90 (d 1H, *J* = 0.5 Hz, C{9}–**H**), 7.67 (d 1H, *J* = 0.5 Hz, C{7}–**H**), 7.60-7.56 (m 2H, C{2+6/3+5}–**H**), 7.45-7.40 (m 2H, C{2+6/3+5}–**H**). **^{13}C NMR** (126 MHz, $CDCl_3$) δ 141.95 (**C**{7}), 138.28 (**C**{1}), 132.72 (**C**{4}), 129.79 (**C**{2+6/3+5}), 127.07 (**C**{9}), 120.27 (**C**{2+6/3+5}), 96.20 (**C**{8}). **HRMS** (ESI^+) found 256.9478, $C_9H_7N_2{}^{79}Br^{35}Cl^+$ requires 256.9476. All data in accordance with literature.[42]

1-(4-chlorophenyl)-4-(4,4,5,5-tetramethyl-1,3,2-dioxaborolan-2-yl)-1*H*-pyrazole, 103e

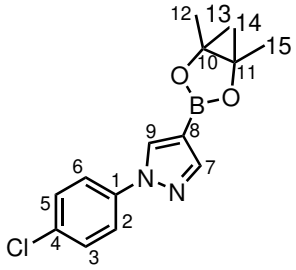

The title compound was prepared from 4-chlorofluorobenzene **103** and 4-(BPin)pyrazole **170** in accordance with **General Procedure C**. The crude residue was purified via silica gel column chromatography (20% diethyl ether in pentane) yielding The title compound as a white solid (45% yield).

$\mathbf{R}_f$ 0.36 (30% diethyl ether in pentane). **^{1}H NMR** (400 MHz, $CDCl_3$) δ 8.20 (d 1H, *J* = 0.5 Hz, C{9}−**H**), 7.96 (d 1H, *J* = 0.5 Hz, C{7}−**H**), 7.68-7.61 (m 2H, C{2+6/3+5}−**H**), 7.44-7.38 (m 2H, C{2+6/3+5}−**H**), 1.34 (s 12H, C{12+13+14+15}−**H**). **^{13}C NMR** (101 MHz, $CDCl_3$) δ 147.11 (**C**{7}), 138.54 (**C**{1}), 133.73 (**C**{9}), 132.36 (**C**{4}), 129.71 (**C**{2+6/3+5}), 120.66 (**C**{2+6/3+5}), 83.78 (**C**{10+11}), 24.96 (**C**{12+13+14+15}). **HRMS** (ESI^+) found 304.1261, $C_{15}H_{19}O_2N_2\,^{10}B^{35}Cl^+$ requires 304.1259. ν_{max} / cm^{-1} 2361, 1558, 1383, 1251, 1149, 1073, 953, 856, 691.

1-(4-chlorophenyl)-3-(trifluoromethyl)-1*H*-pyrazole, 103f

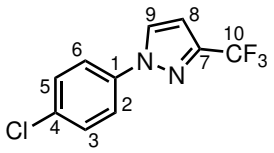

The title compound was prepared from 4-chlorofluorobenzene **103** and 3-(trifluoromethyl)pyrazole **171** in accordance with **General Procedure C**. The crude residue was purified via silica gel column chromatography (20% diethyl ether in pentane) yielding The title compound as a pale yellow solid (5% yield).

$\mathbf{R}_f$ 0.32 (30% diethyl ether in pentane). **^{1}H NMR** (500 MHz, $CDCl_3$) δ 7.95-7.90 (m 1H, C{9}–**H**), 7.68-7.64 (m 2H, C{2+6/3+5}–**H**), 7.49-7.42 (m 2H, C{2+6/3+5}–**H**), 6.37 (d 1H, *J* = 2.5 Hz, C{8}–**H**). **^{13}C NMR** (126 MHz, $CDCl_3$) δ 144.43 (q, *J* = 38.6 Hz, **C**{7}), 138.06 (**C**{1}), 133.58 (**C**{4}), 129.88 (**C**{2+6/3+5}), 128.39 (**C**{9}), 121.16 (**C**{2+6/3+5}), 121.19 (q, *J* = 264 Hz, **C**{10}), 107.21 (d, *J* = 2.5 Hz, **C**{8}). **^{19}F NMR** (470 MHz, $CDCl_3$) δ −62.24 (s 3F, C{10}–**F**). **HRMS** (ESI^+) found 247.0245, $C_{10}H_7N_2{}^{35}ClF_3{}^+$ requires 247.0244. ν_{max} / cm^{-1} 1708, 1562, 1462, 1383, 1263, 1154, 1089, 954, 825, 765.

Ethyl 1-(4-chlorophenyl)-1*H*-pyrazole-4-carboxylate, 103g

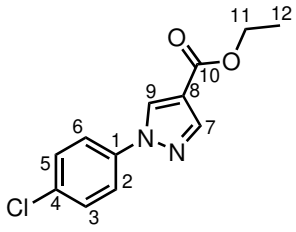

The title compound was prepared from 4-chlorofluorobenzene **103** and ethyl pyrazole-4-carboxylate **172** in accordance with **General Procedure C**. The crude residue was purified via silica gel column chromatography (5% diethyl ether in pentane) yielding The title compound as a white solid (51% yield).

$\mathbf{R}_f$ 0.15 (10% diethyl ether in pentane). **m.p.** 129-130 °C (lit.[165] 122-124 °C). **^{1}H NMR** (500 MHz, $CDCl_3$) δ 8.37 (s 1H, C{9}–**H**), 8.09 (s 1H, C{7}–**H**), 7.67-7.63 (m 2H, C{2+6/3+5}–**H**), 7.46-7.43 (m 2H, C{2+6/3+5}–**H**), 4.43 (q 2H, *J* = 7 Hz, C{11}–**H**), 1.37 (t 3H, *J* = 7 Hz, C{12}–**H**). **^{13}C NMR** (126 MHz, $CDCl_3$) δ 162.77 (**C**{10}), 142.51 (**C**{7}), 138.06 (**C**{1}), 133.29 (**C**{4}), 130.04 (**C**{2+6/3+5}), 129.85 (**C**{9}), 120.85 (**C**{2+6/3+5}), 117.42 (**C**{8}), 60.67 (**C**{11}), 14.52 (**C**{12}). **GCMS** (EI) m/z 205 100% [$M^{+\bullet} - C_2H_5O$], 250 33% [$M^{+\bullet}$]. All data in accordance with literature.[165]

1,4-dioxaspiro[4.5]decan-8-one, 154

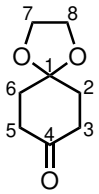

To a round bottomed flask charged with 1,4-cyclohexadiene **153** (4.5 g, 40 mmol, 1.0 equiv.) was added toluene (100 mL), tosic acid (310 mg, 3.6 mmol, 0.09 equiv.) and ethylene glycol (1.45 mL, 52 mmol, 1.3 equiv.). The reaction was heated to reflux and water was removed via a Dean-Stark apparatus. After 4 hours the reaction mixture was allowed to cool to room temperature and the starting material separated by decantation. Upon further cooling over ice monoprotected product was precipitated out allowing recycling of diprotected byproduct and starting material. Following ether-hexane (2:1) recrystallisation the title compound was obtained as a white crystalline solid (22% yield from one cycle).

$\mathbf{R}_f$ 0.24 (50% diethyl ether in pentane). **^{1}H NMR** (500 MHz, $CDCl_3$) δ 4.03 (s 4H, C{7+8}–**H**), 2.57-2.46 (m 4H, C{2+6/3+5}–**H**), 2.04-1.96 (m 4H, C{2+6/3+5}–**H**). **^{13}C NMR** (126 MHz, $CDCl_3$) δ 210.38 (**C**{4}), 107.15 (**C**{1}), 64.67 (**C**{7+8}), 38.19 (**C**{2+6/3+5}), 33.89 (**C**{2+6/3+5}). All data in accordance with literature.[151]

8-(but-3-en-1-yl)-1,4-dioxaspiro[4.5]decan-8-ol, 156

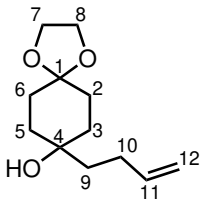

To a flame-dried 3-necked round bottom flask fitted with a septum and reflux condenser under a nitrogen atmosphere was added magnesium turnings (1.8 g, 44 mmol, 2.5 equiv) and dry diethyl ether (40 mL, 0.5 M). 4-bromobutene **155** (1.77 mL, 10 mmol, 1.0 equiv) was added to the reactor dropwise. The solution was allowed to stir at room temperature (10 mins). After this time, the reaction mixture was cooled to $-78\ ^{o}$C, and monoprotected 1,4-cyclohexadione **154** (1.36 g, 8.7 mmol, 0.5 equiv) dissolved in dry diethyl ether (7 mL) was dropwise. The resulting solution was allowed to slowly warm to room temperature and stirred for 1 h before diluting with diethyl ether (50 mL) and quenched with satd. aq. NH_4Cl (100 mL) [CAREFULLY]. The layers were separated, and the aqueous phase extracted diethyl ether (2×100 mL). The organic extracts were combined, dried over Na_2SO_4, filtered and concentrated under reduced pressure. The crude residue was purified via silica gel column chromatography (10-20% acetone in pentane) yielding a clear oil (52% yield).

$\mathbf{R}_f$ 0.10 (10% acetone in pentane). **^{1}H NMR** (500 MHz, $CDCl_3$) δ 5.84 (ddt 1H, *J* = 17,10,6.5 Hz, C{11}–**H**), 5.03 (dd 1H, *J* = 17,1.5 Hz, C{12 'trans'}–**H**), 4.94 (dd 1H, *J* = 10,1.5 Hz, C{12 'cis'}–**H**), 3.97-3.86 (m 4H, C{7+8}–**H**), 2.15 (dddd 2H, *J* = 13,6.5,3 Hz, C{10}–**H**), 1.87 (dt 2H, *J* = 13,8 Hz, C{9}–**H**), 1.64 (dd 4H, *J* = 8,4.5 Hz, C{2+6/3+5}–**H**), 1.61-1.50 (m 4H, C{2+6/3+5}–**H**). **^{13}C NMR** (126 MHz, $CDCl_3$) δ 139.13 (**C**{11}), 115.23 (**C**{12}), 108.91 (**C**{1}), 70.61 (**C**{4}), 64.36 (**C**{7+8}), 37.82 (**C**{10}), 34.82 (**C**{2+6/3+5}), 30.58 (**C**{2+6/3+5}), 27.92 (**C**{9}). All data in accordance with literature.[151]

4-(but-3-en-1-yl)-4-hydroxycyclohexan-1-one, 157

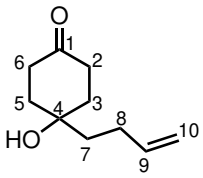

To a solution of acetal **156** (853 mg, 4 mmol, 1.0 equiv.) in 2:1 THF:H2O (20 mL) in an round bottomed flask was added 2M HCl (5 mL). The resulting solution was allowed to stir at rt overnight (18 hr). After which time, the reaction was diluted with ethyl acetate (20 mL) and sat. aq. sodium bicarbonate (10 mL) was added. The layers were separated and the aqueous layer was washed with ethyl acetate (3 × 20 mL). The combined organic layer was washed with brine (50 mL) and dried with Na_2SO_4. Solvent was removed under reduced pressure. The crude residue was purified via silica gel column chromatography (20-50% ethyl acetate in pentane) yielding a clear oil (77% yield).

$\mathbf{R}_f$ 0.12 (20% ethyl acetate in pentane). **^{1}H NMR** (500 MHz, $CDCl_3$) δ 5.86 (ddt 1H, *J* = 17,10,6.5 Hz, C{9}–**H**), 5.07 (dd 1H, *J* = 17,1.5 Hz, C{10 'trans'}–**H**), 5.00 (dd 1H, *J* = 10,1.5 Hz, C{10 'cis'}–**H**), 2.79-2.64 (m 2H, C{2+6}–**H**), 2.28-2.14 (m 4H, C{2'+6'+8}–**H**), 1.98 (ddt 2H, *J* = 15,6.5,3 Hz, C{3+5}–**H**), 1.79 (td 2H, *J* = 13.5,5 Hz, C{3'+5'}–**H**), 1.68-1.63 (m 2H, C{7}–**H**), 1.57 (s 1H, O**H**). **^{13}C NMR** (126 MHz, $CDCl_3$) δ 212.27 (**C**{1}), 138.59 (**C**{9}), 115.26 (**C**{10}), 70.44 (**C**{4}), 41.51 (**C**{7}), 37.06 (**C**{2+6/3+5}), 37.02 (**C**{2+6/3+5}), 28.09 (**C**{8}). All data in accordance with literature.[151]

1-phenyl-1*H*-imidazole, 163

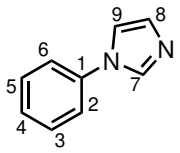

To a clean, dry microwave vial containing a Teflon-coated magnetic stirrer bar was added 9-mesityl-3,6-di-tert-butyl-10-phenylacridinium tetrafluoroborate **161** (14 mg, 0.025 mmol, 5 mol%), imidazole (137 mg, 4 equiv.), anisole **162** (54 μL, 1 equiv.) followed by solvent 1:1 DCE:TFE (5 mL). The vial was sealed with suba seal and degassed with a flow of N_2 gas. After degassing (30 min), the reaction was stirred under irradiation by 32 W lamp for 24 hours. Solvent removed in vacuo, and purified via column chromatography (in 80% ethyl acetate in pentane) yielding a yellow oil (76% yield).

$\mathbf{R}_f$ 0.36 (80% ethyl acetate in pentane). **^{1}H NMR** (400 MHz, $CDCl_3$) δ 7.87 (bs 1H, C{7}–**H**), 7.54-7.42 (m 2H, C{3+5}–**H**), 7.40-7.33 (m 3H, *J* = 2+4+6 Hz), 7.30 (bs 1H, *J* = 8/9 Hz), 7.22 (bs 1H, *J* = 8/9 Hz). **^{13}C NMR** (101 MHz, $CDCl_3$) δ 129.99 (**C**{3+5}), 127.61 (**C**{2+6/4}), 121.62 (**C**{2+6/4}). **GCMS** (EI) m/z 144 100% [$M^{+\bullet}$]. All data in accordance with literature.[23]

1D NMR SPECTRA

4-bromo-2-nitrophenol, 9c

400 MHz ^{1}H NMR spectrum ($CDCl_3$)

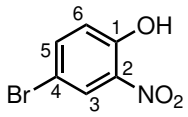

101 MHz ^{13}C NMR spectrum ($CDCl_3$)

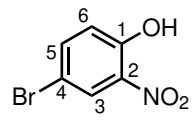

4-chloro-2-nitrophenol, 10c

400 MHz ^{1}H NMR spectrum ($CDCl_3$)

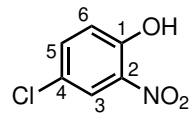

101 MHz ^{13}C NMR spectrum ($CDCl_3$)

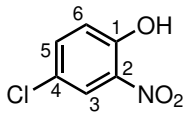

4-fluoro-2-nitrophenol, 11a

400 MHz ^{1}H NMR spectrum ($CDCl_3$)

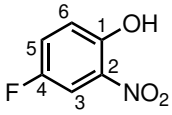

101 MHz ^{13}C NMR spectrum ($CDCl_3$)

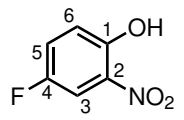

376 MHz ^{19}F NMR spectrum ($CDCl_3$)

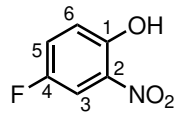

4-nitrophenol, 11b

400 MHz ^{1}H NMR spectrum ($CDCl_3$)

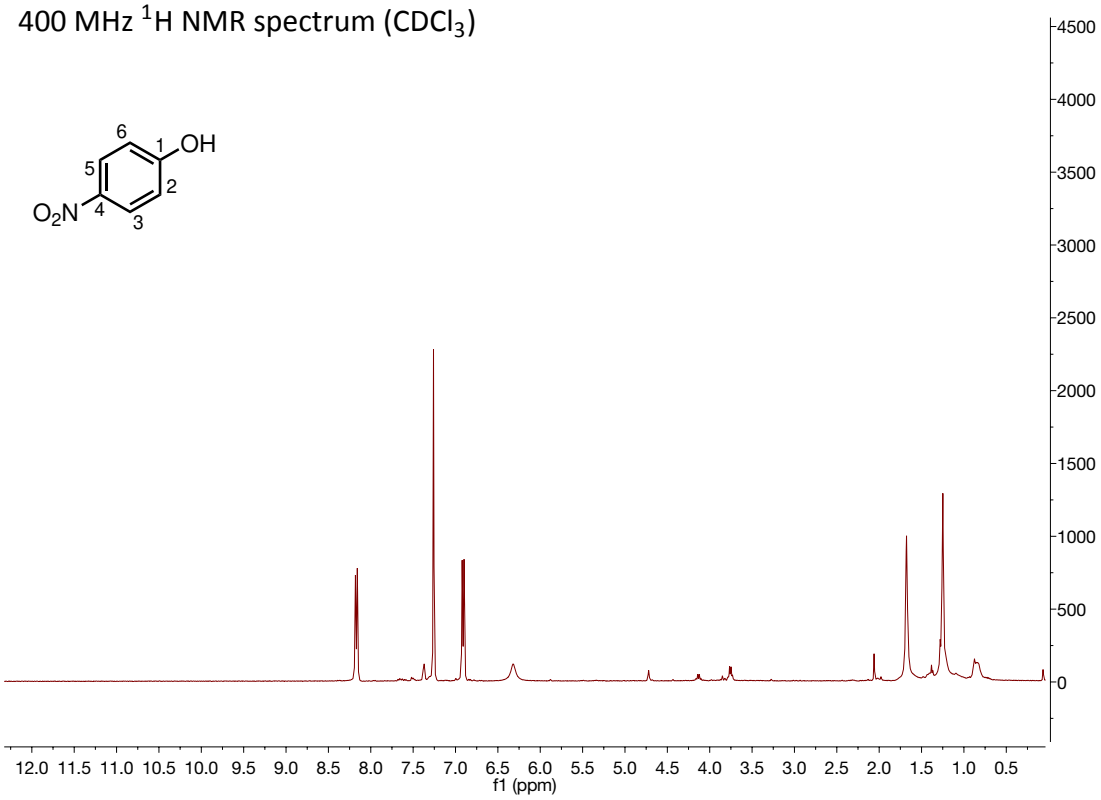

101 MHz ^{13}C NMR spectrum ($CDCl_3$)

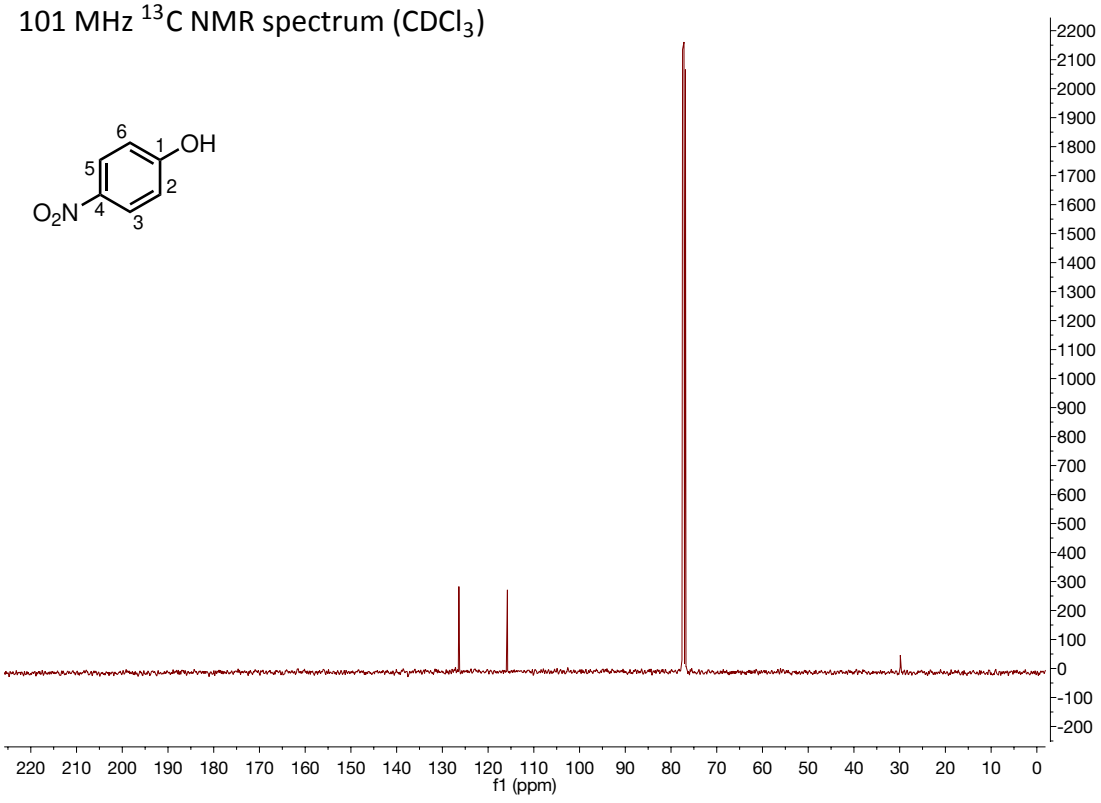

2-nitrophenol, 11c

400 MHz ^{1}H NMR spectrum ($CDCl_3$)

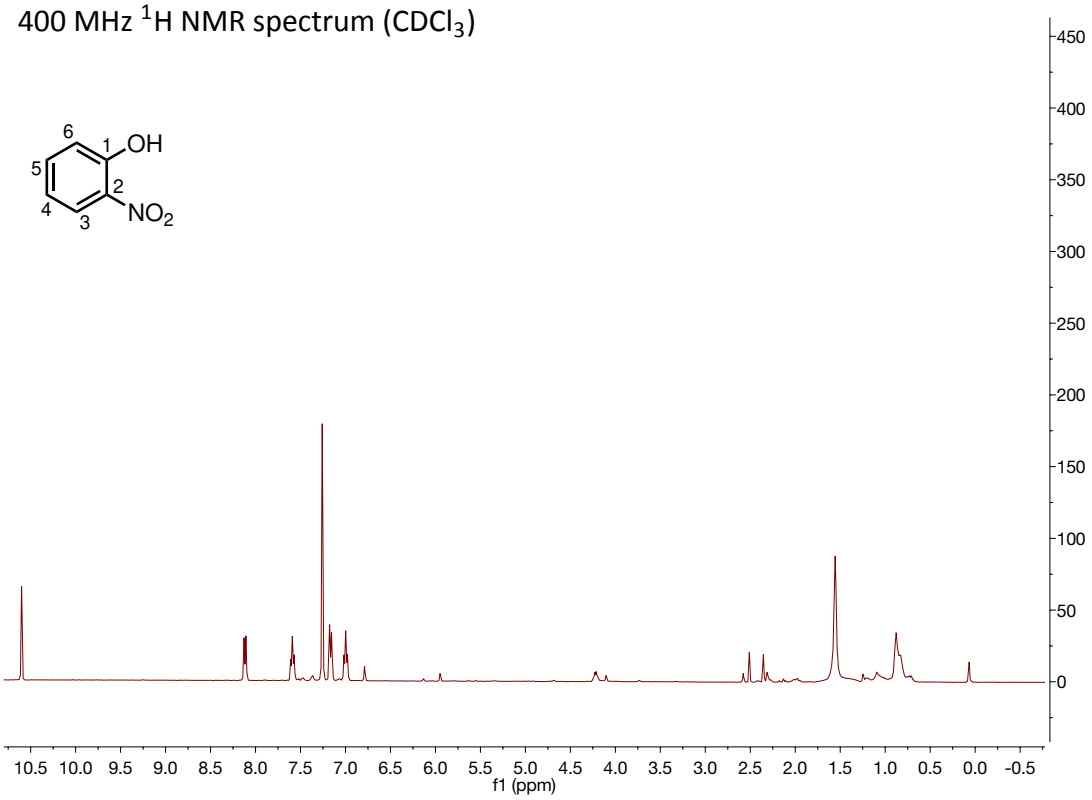

101 MHz ^{13}C NMR spectrum ($CDCl_3$)

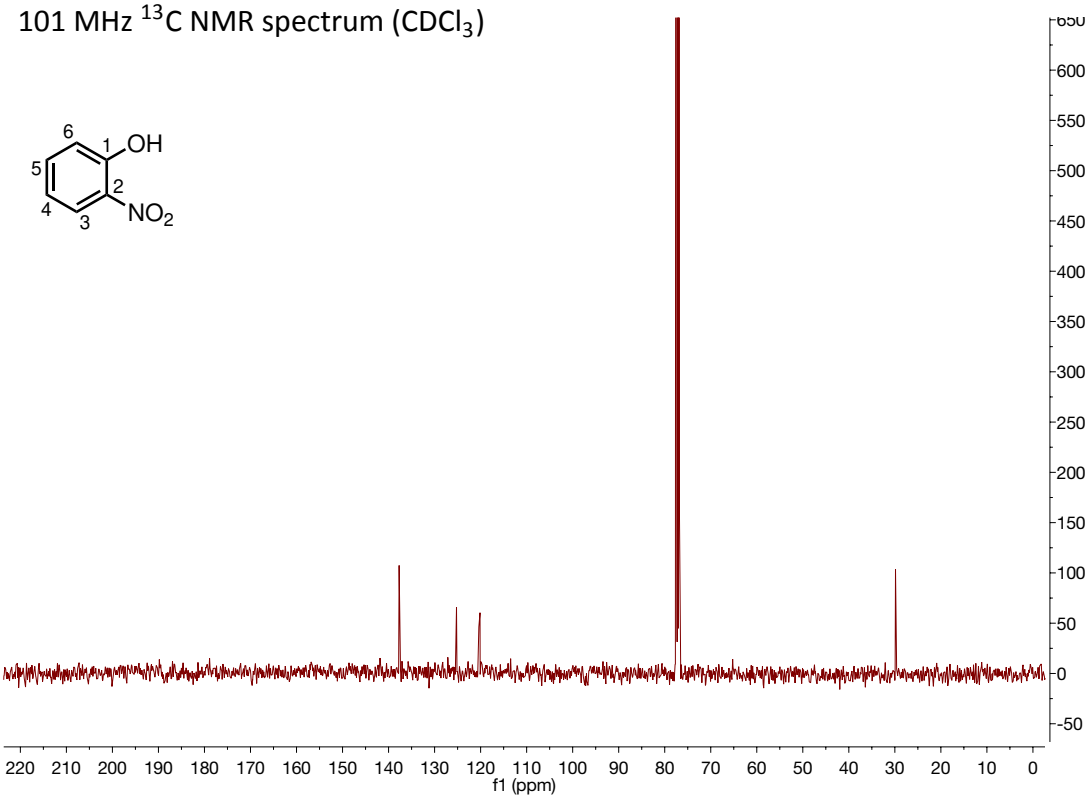

2,4-dichloroanisole, 100a

400 MHz ^{1}H NMR spectrum ($CDCl_3$)

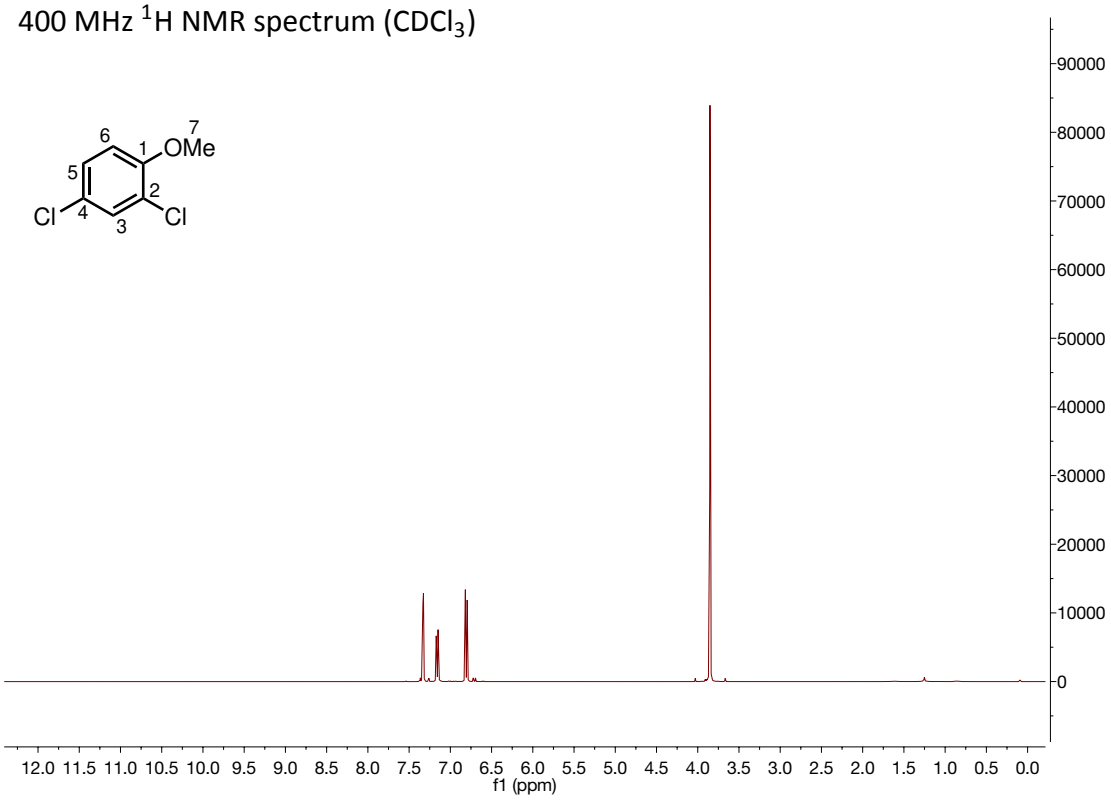

101 MHz ^{13}C NMR spectrum ($CDCl_3$)

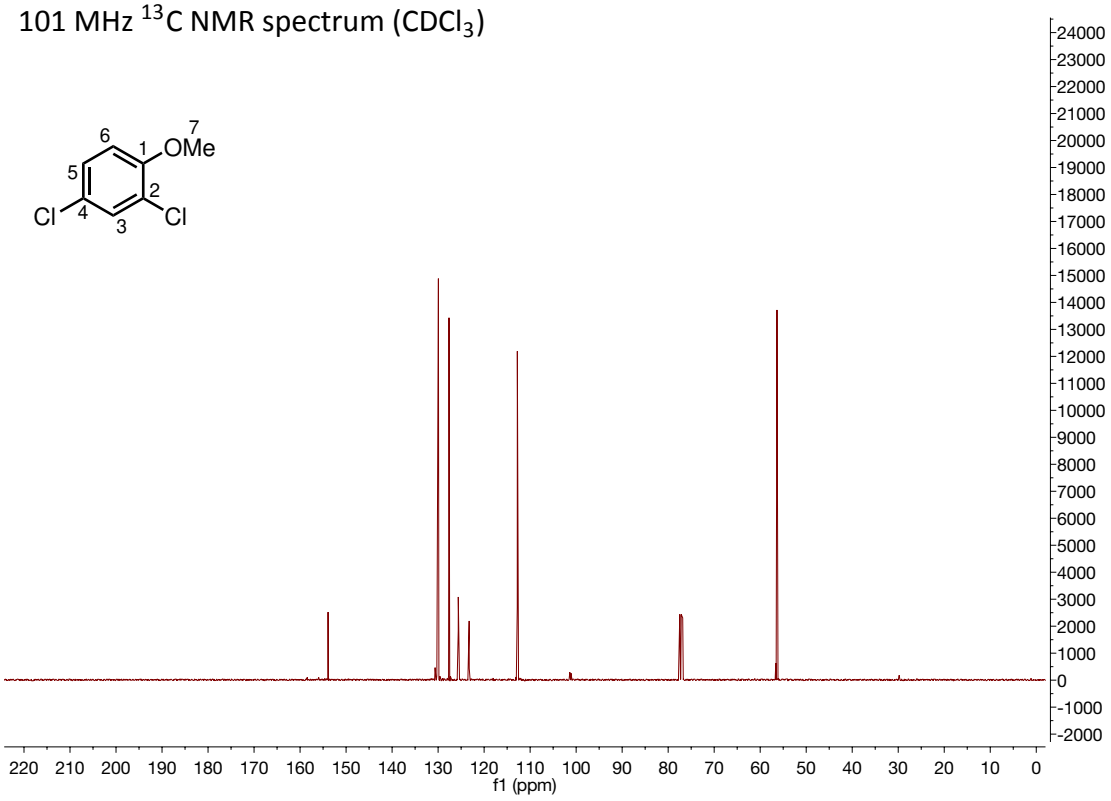

2-chloro-4-bromoanisole, 102a

400 MHz ^{1}H NMR spectrum ($CDCl_3$)

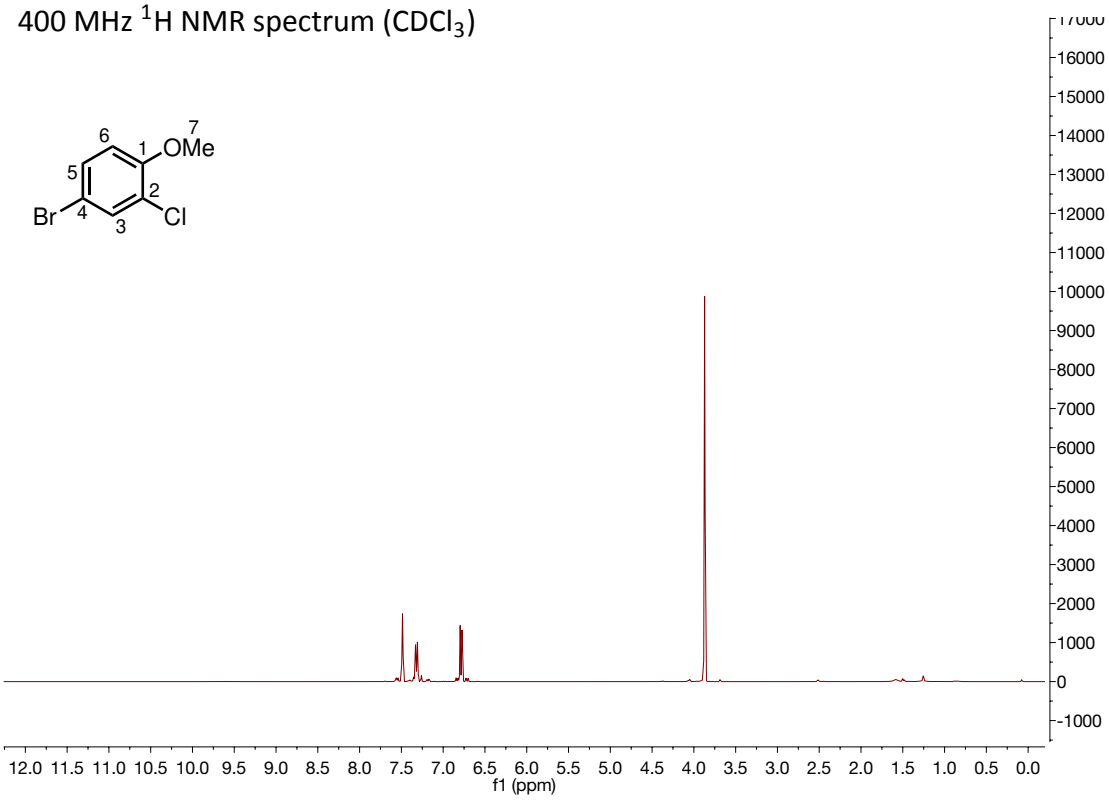

101 MHz ^{13}C NMR spectrum ($CDCl_3$)

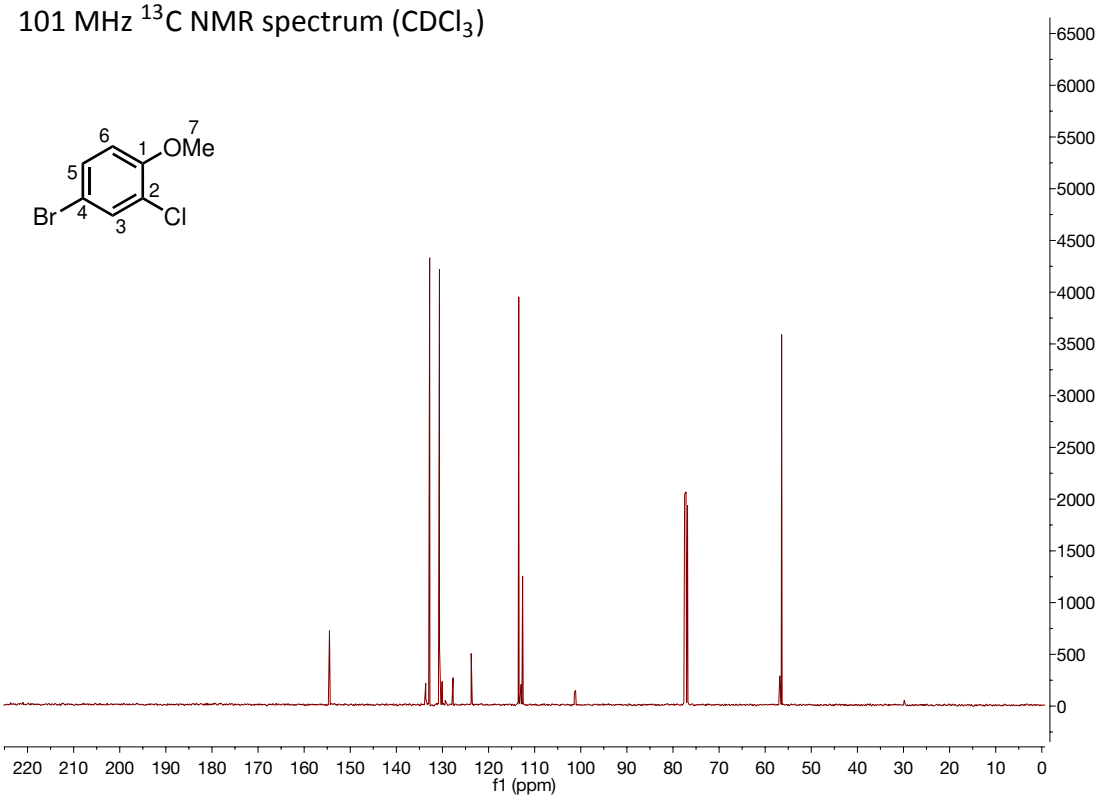

4-chloroanisole, 103a

400 MHz ^{1}H NMR spectrum ($CDCl_3$)

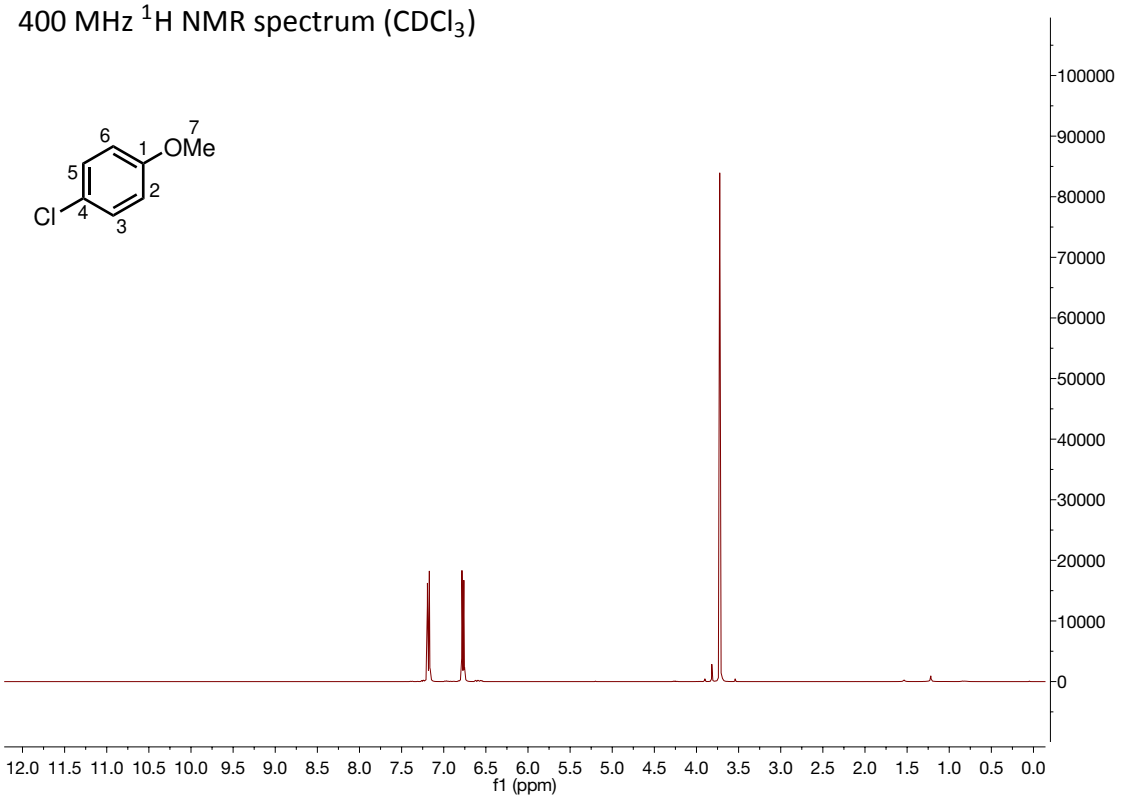

101 MHz ^{13}C NMR spectrum ($CDCl_3$)

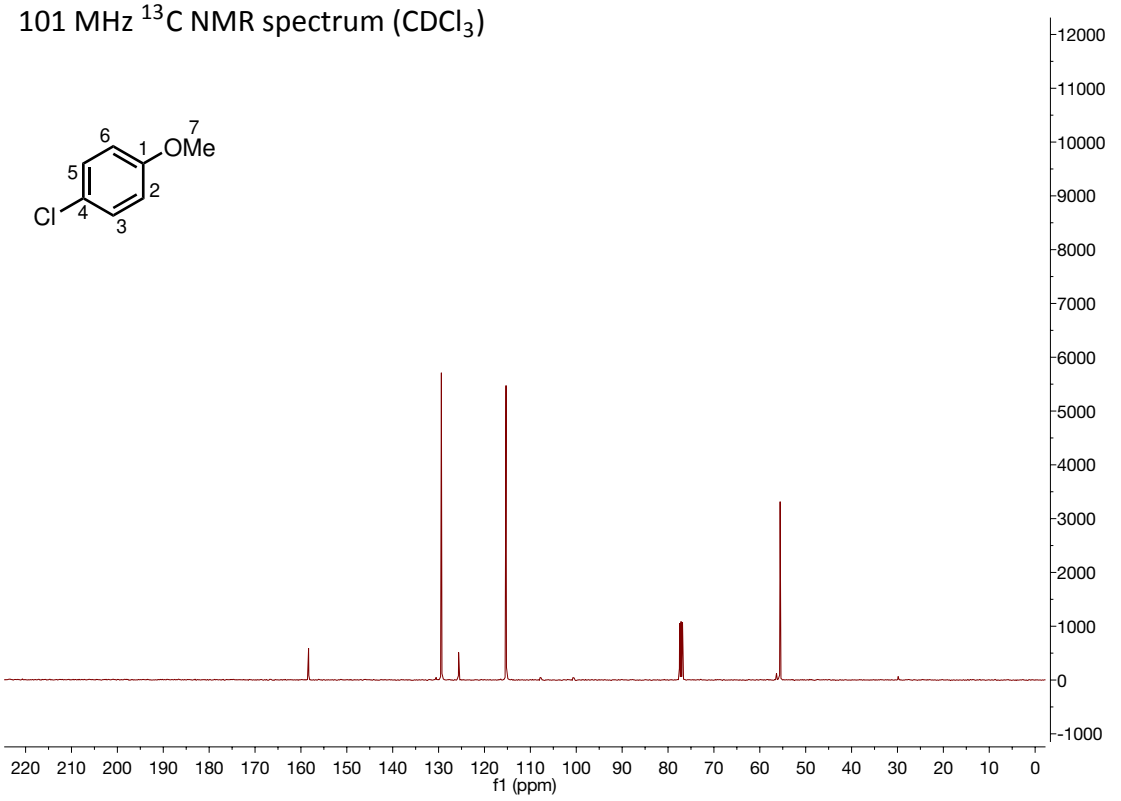

2,6-dichloro-4-bromoanisole, 104a

400 MHz ^{1}H NMR spectrum ($CDCl_3$)

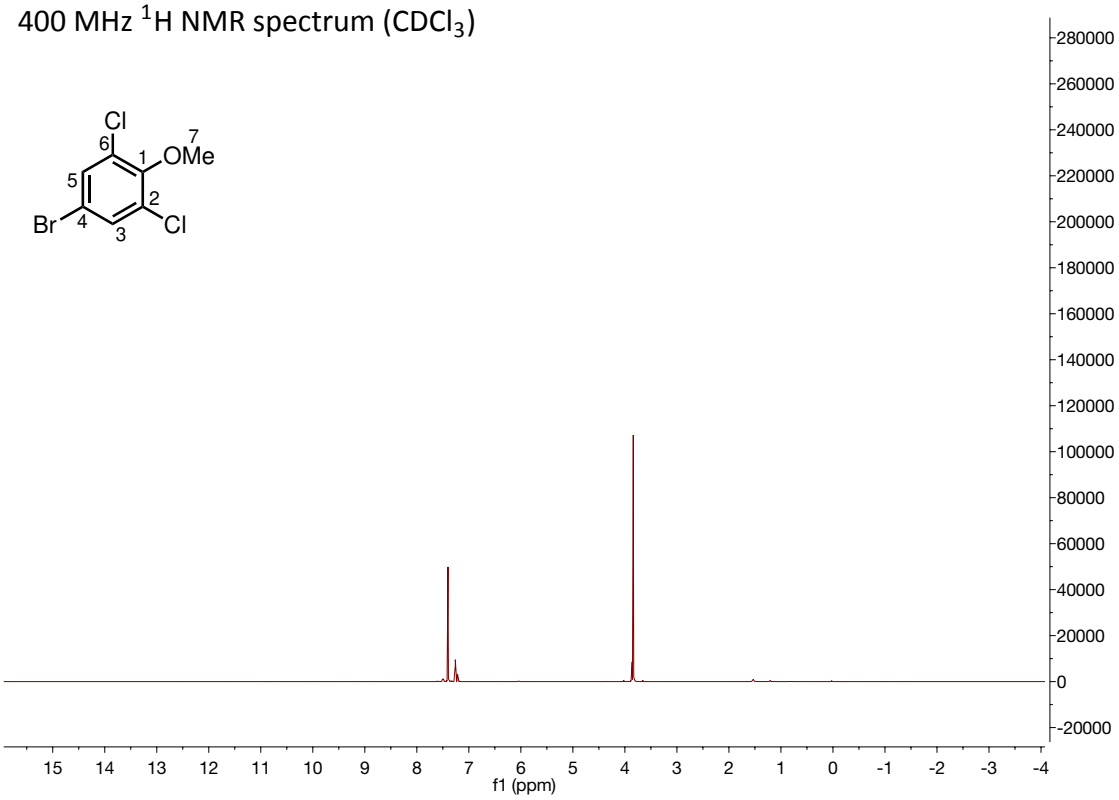

101 MHz ^{13}C NMR spectrum ($CDCl_3$)

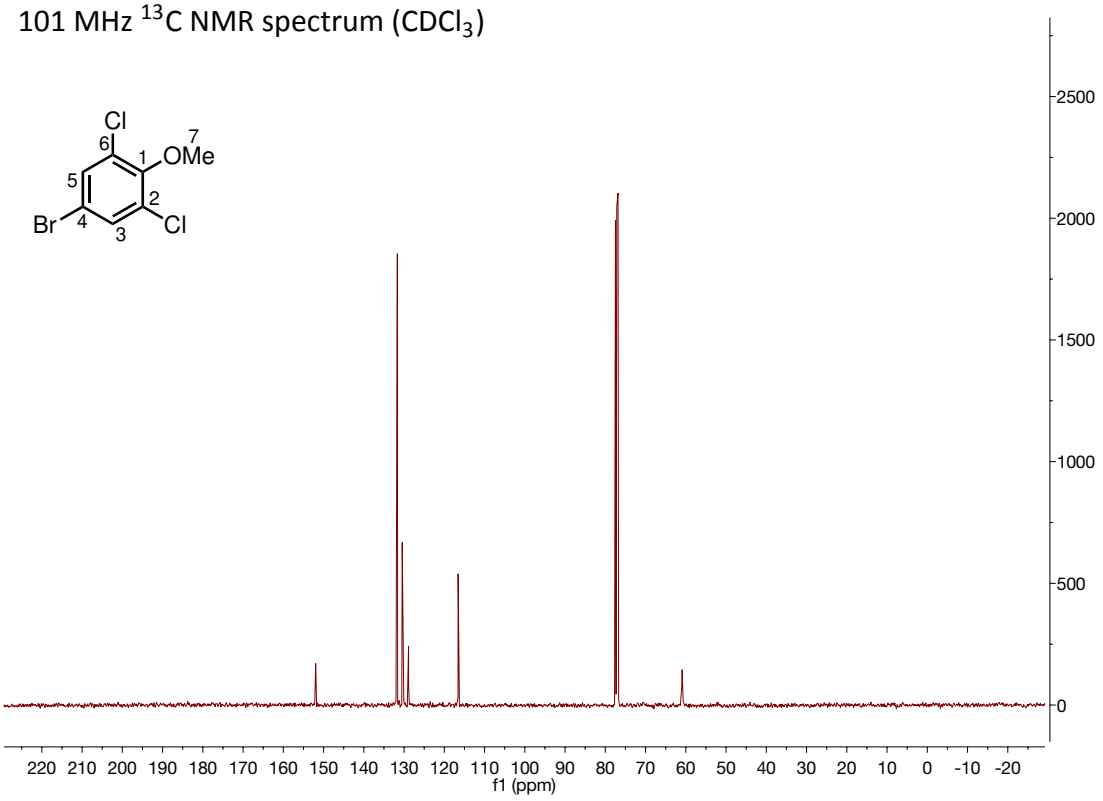

4-bromoanisole, 105a

400 MHz ^{1}H NMR spectrum ($CDCl_3$)

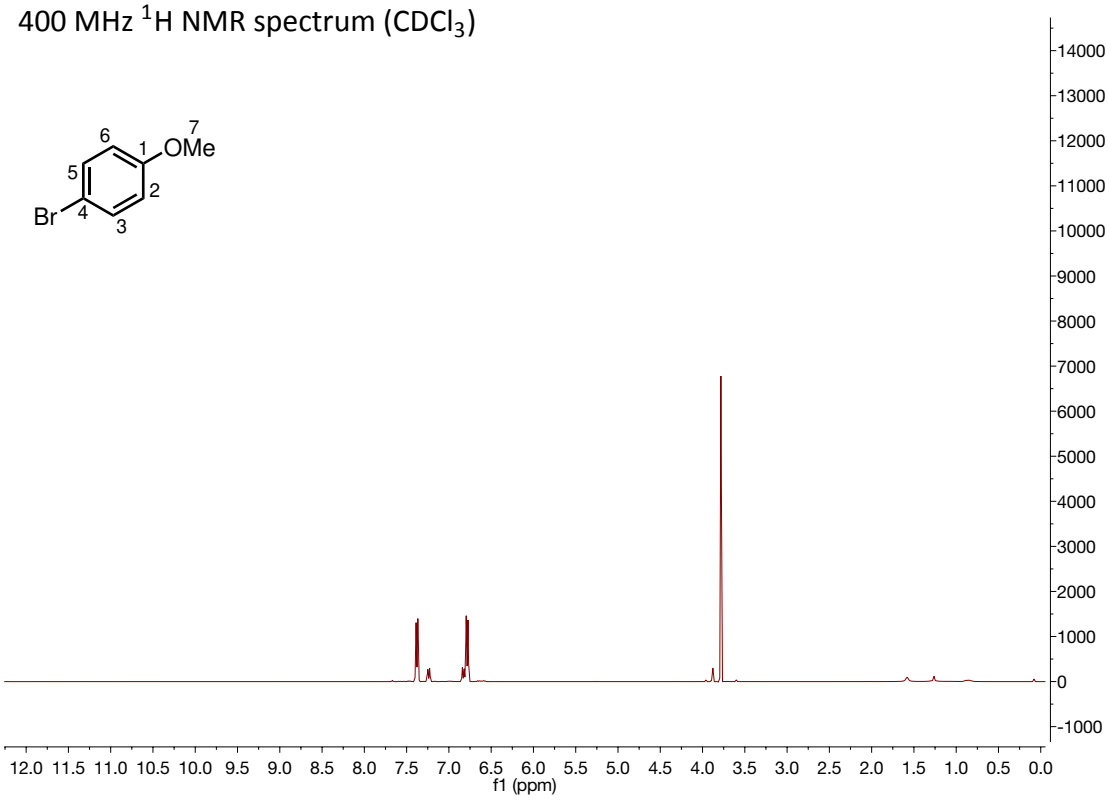

101 MHz ^{13}C NMR spectrum ($CDCl_3$)

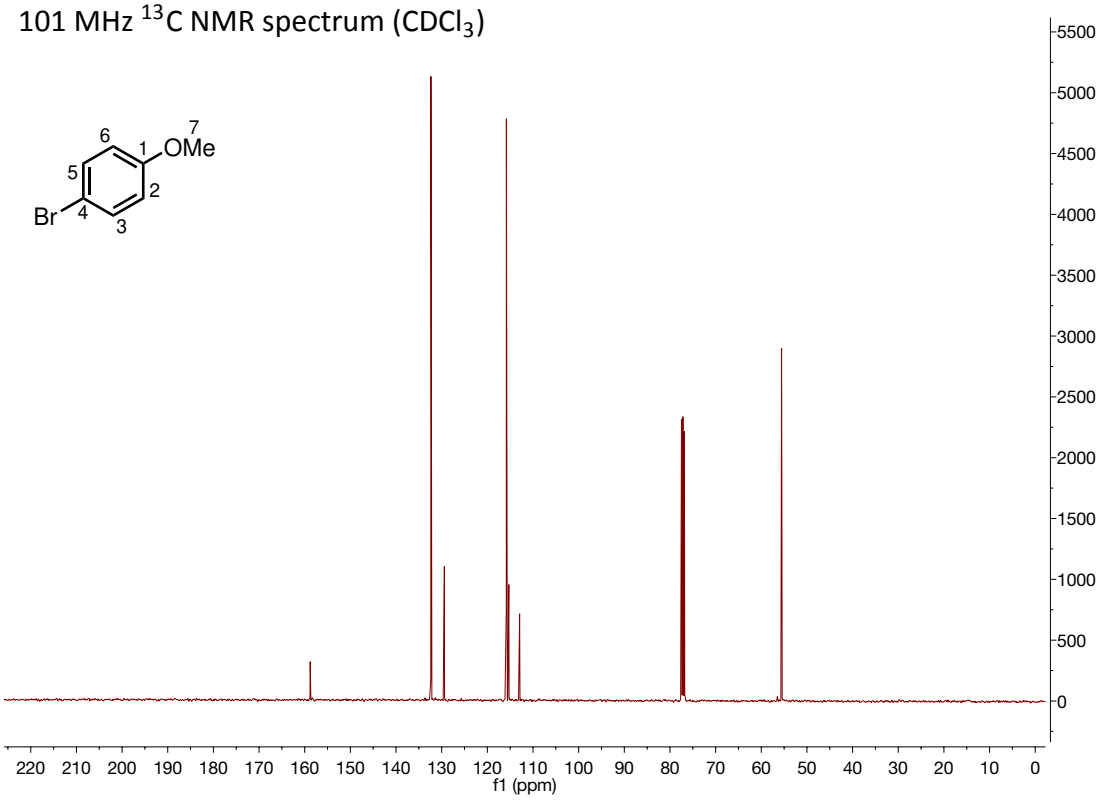

2-chloroanisole, 106a

400 MHz ^{1}H NMR spectrum ($CDCl_3$)

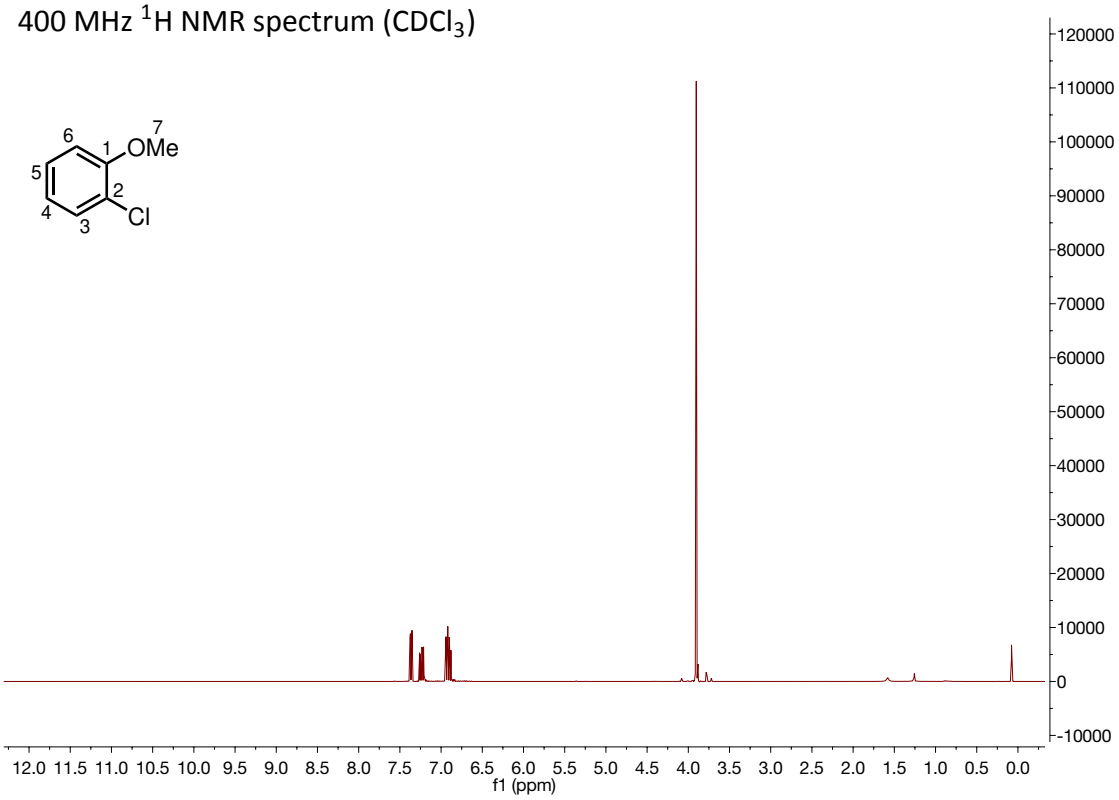

101 MHz ^{13}C NMR spectrum ($CDCl_3$)

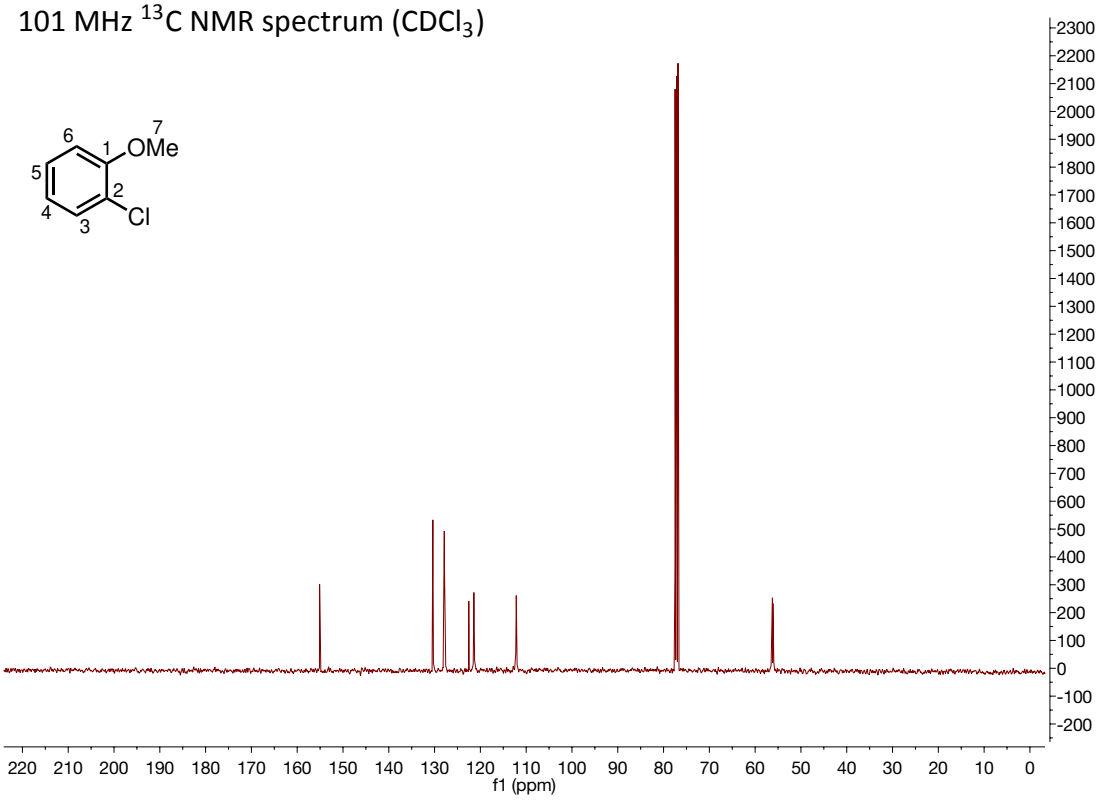

1,5-dichloro-2-methoxy-4-methylbenzene, 107a / 1,3-dichloro-4-methoxy-2-methylbenzene, 108a

400 MHz ^{1}H NMR spectrum ($CDCl_3$)

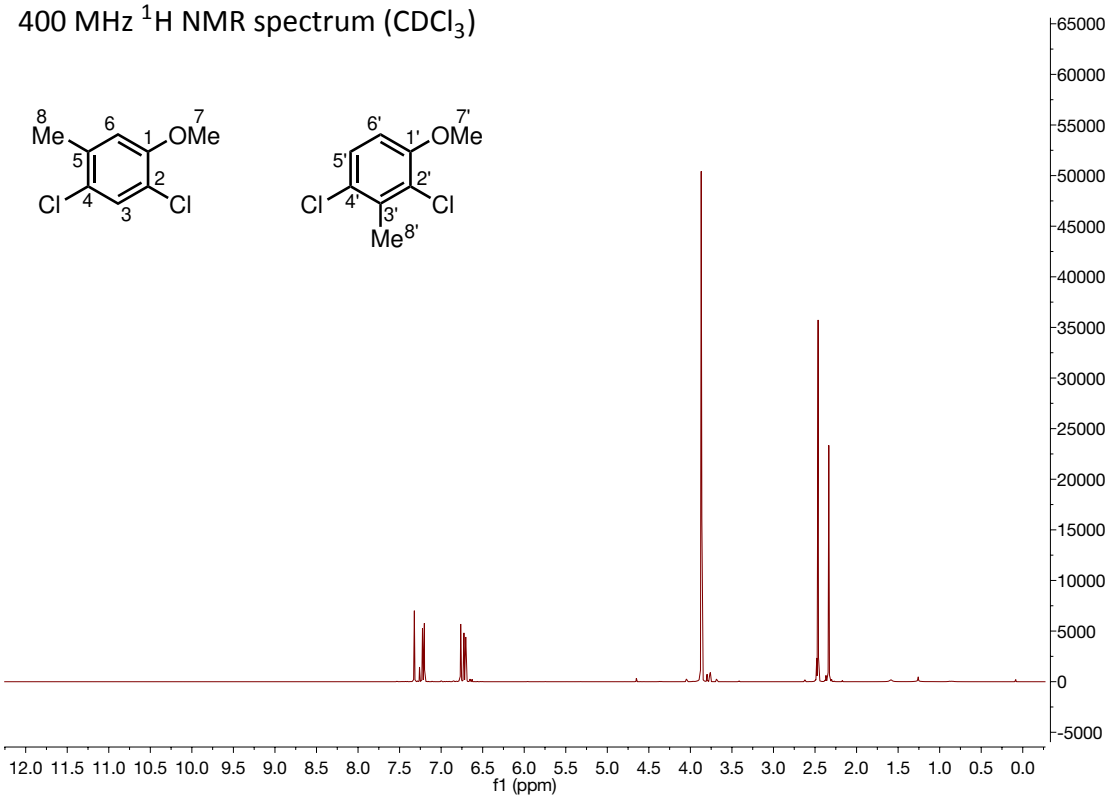

101 MHz ^{13}C NMR spectrum ($CDCl_3$)

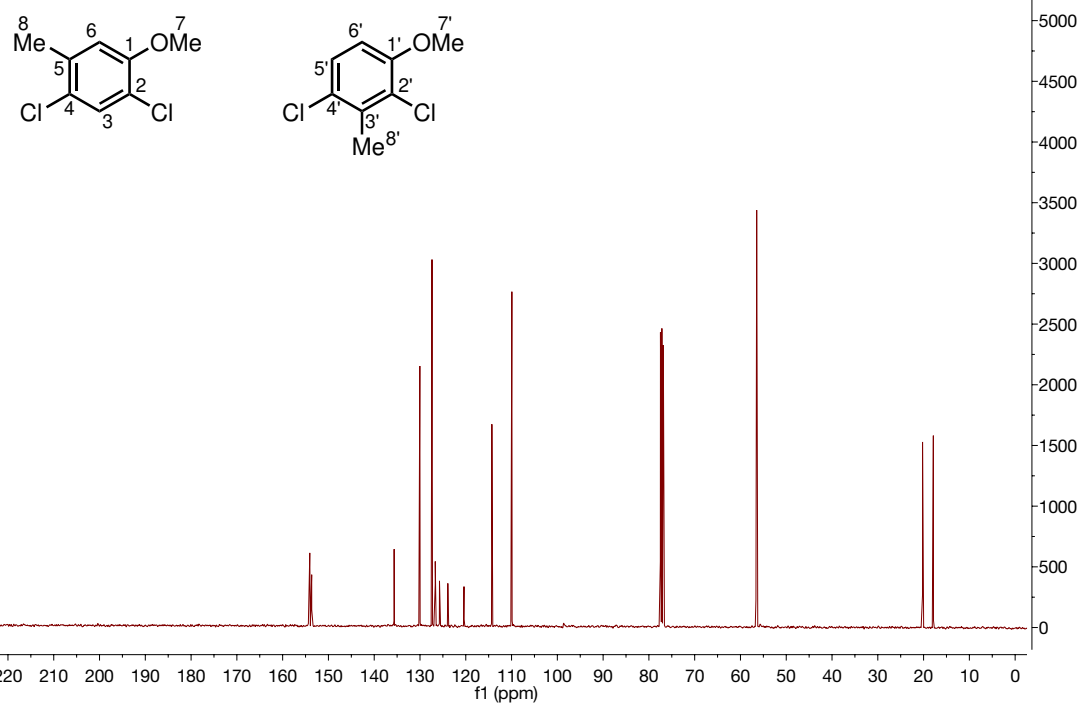

4-methoxy-1-naphthonitrile, 109a

400 MHz ^{1}H NMR spectrum ($CDCl_3$)

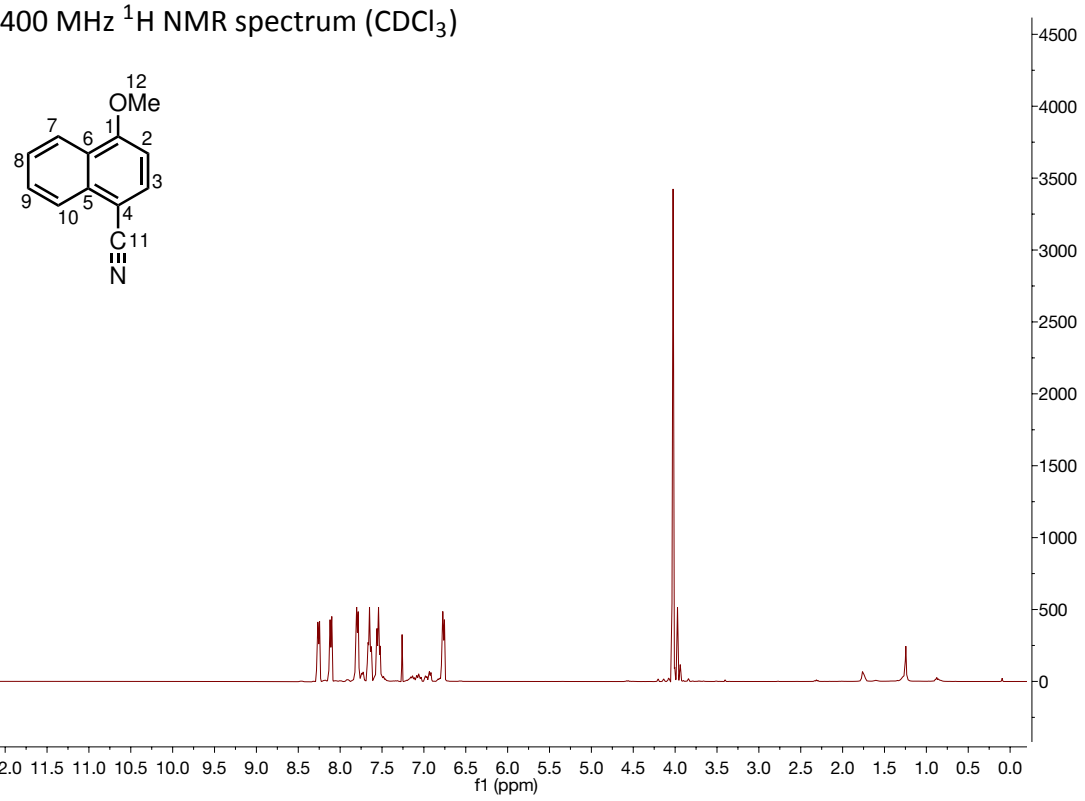

101 MHz ^{13}C NMR spectrum ($CDCl_3$)

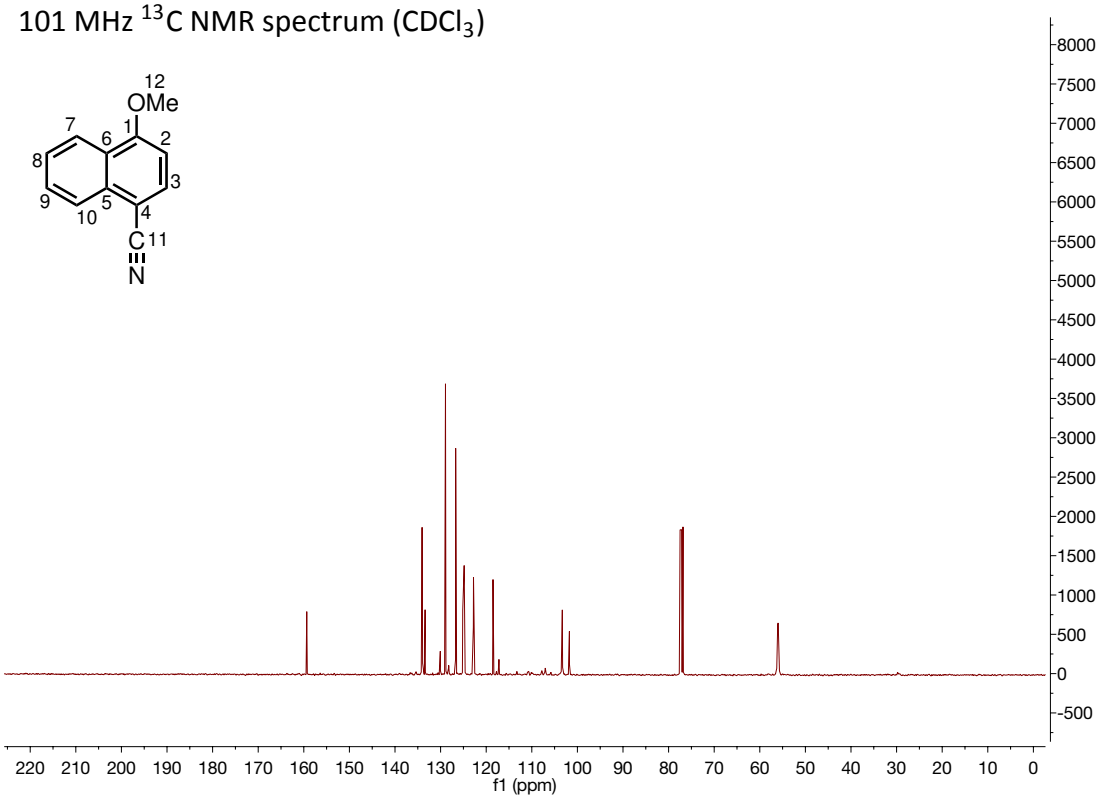

N-Boc-5-fluoroindole, 120

400 MHz ^{1}H NMR spectrum ($CDCl_3$)

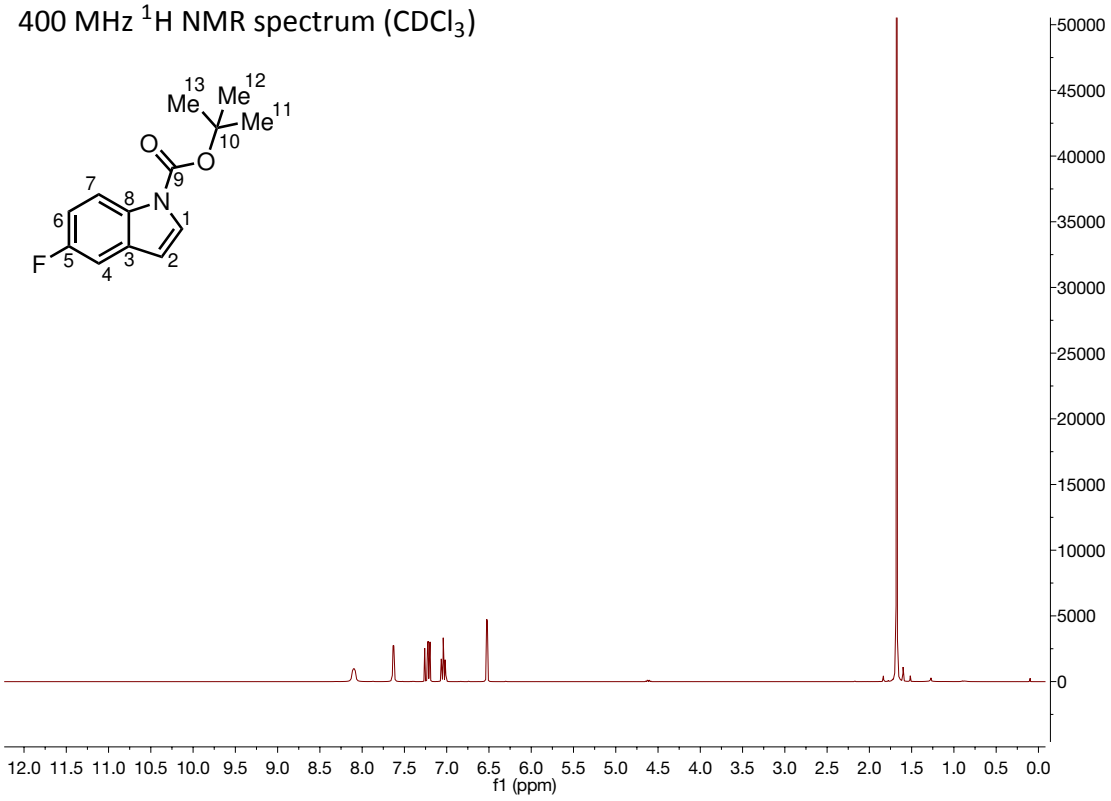

101 MHz ^{13}C NMR spectrum ($CDCl_3$)

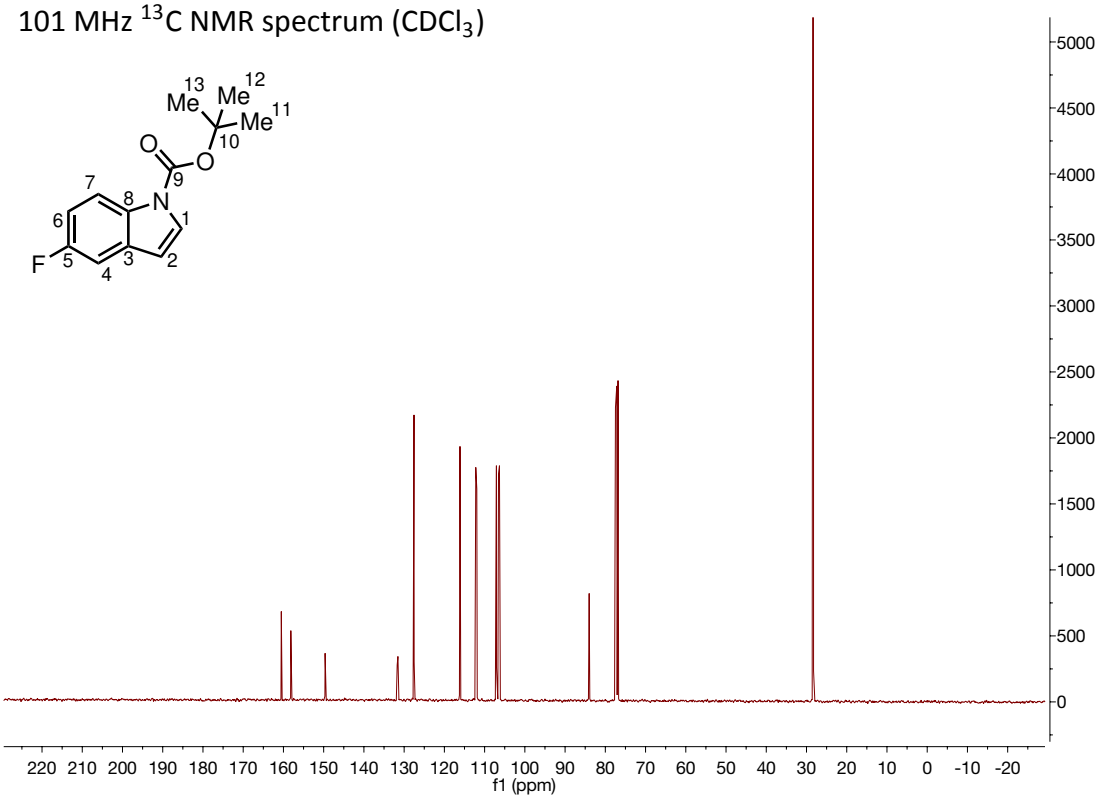

376 MHz ^{19}F NMR spectrum ($CDCl_3$)

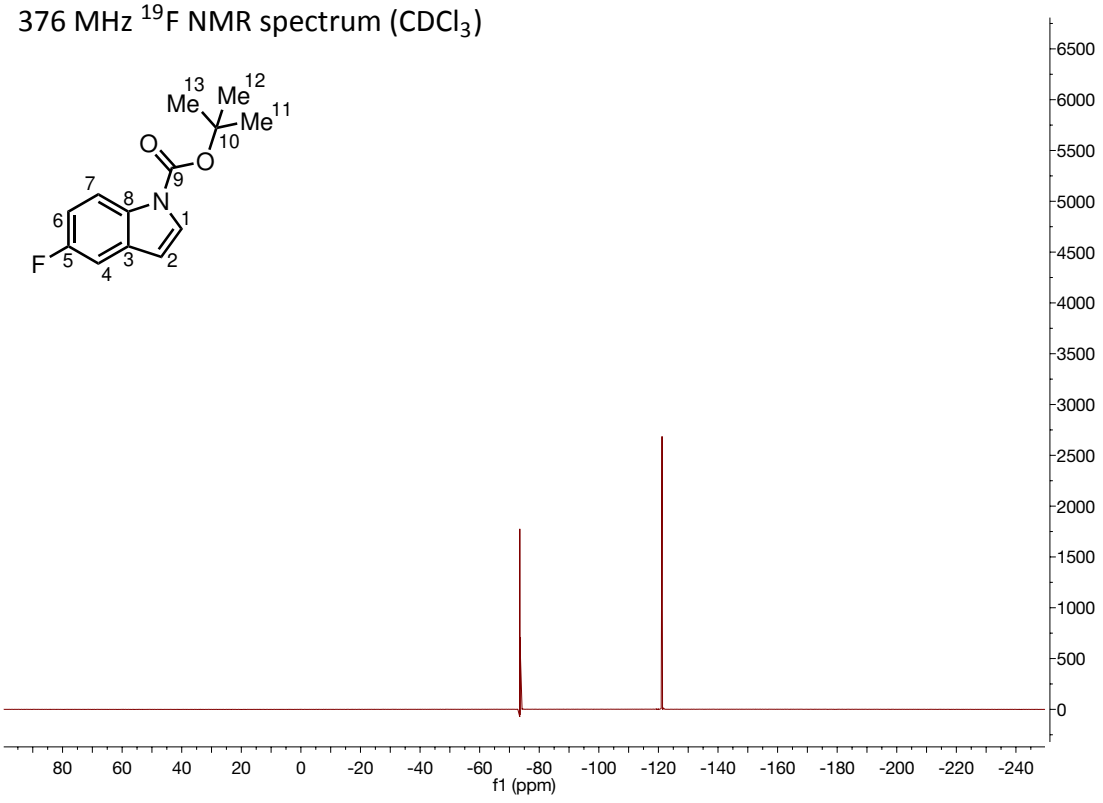

3,5-dibromo-4-chloroanisole, 132a

400 MHz ^{1}H NMR spectrum ($CDCl_3$)

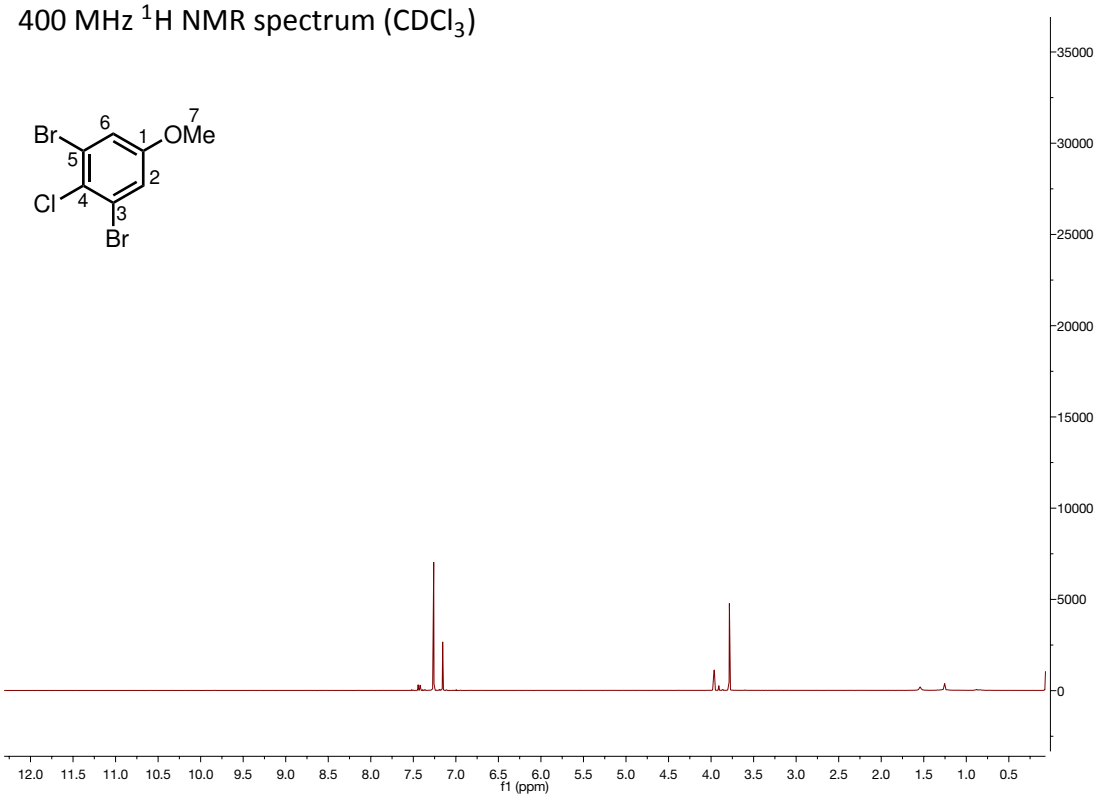

3,4-dichloroanisole, 133a

400 MHz ^{1}H NMR spectrum ($CDCl_3$)

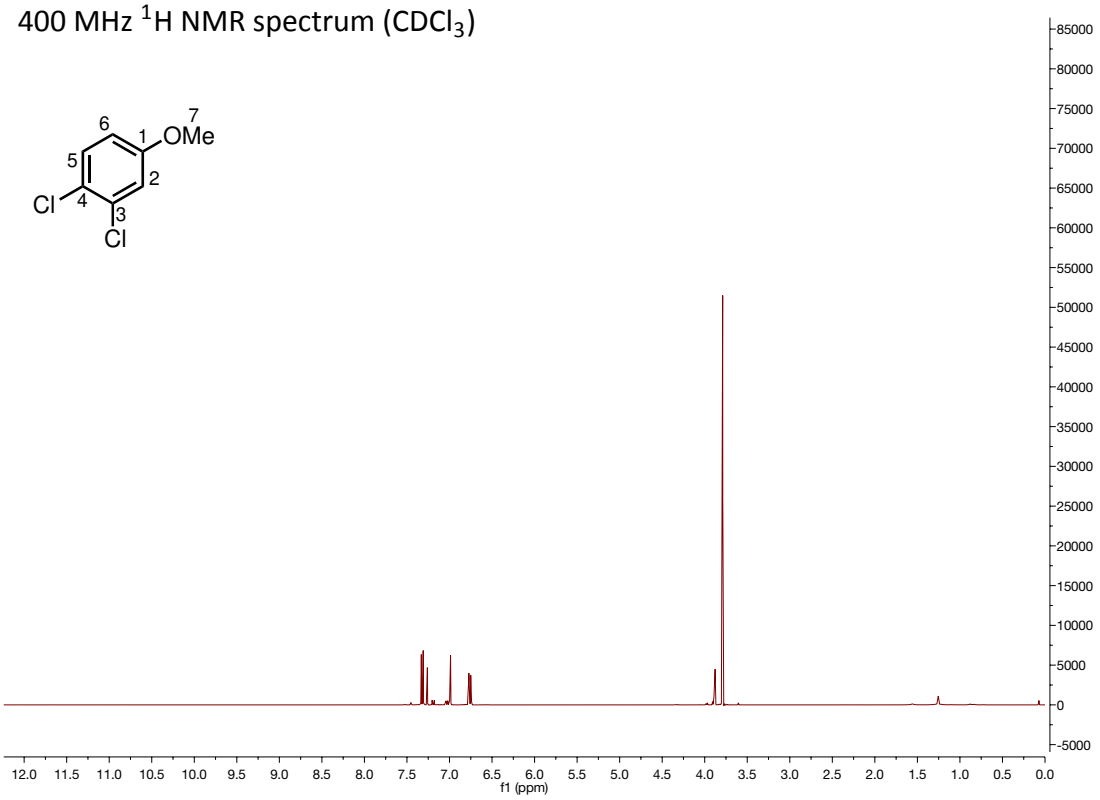

101 MHz ^{13}C NMR spectrum ($CDCl_3$)

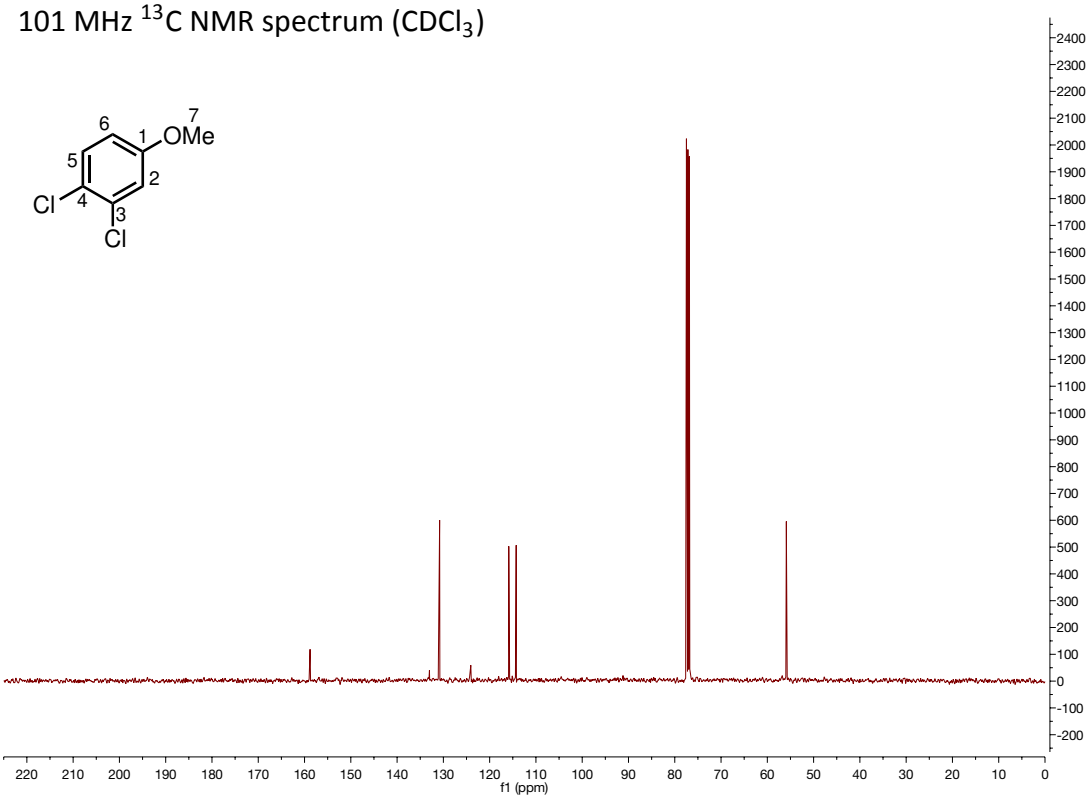

2,4-dichloro-5-bromoanisole, 133a

500 MHz ^{1}H NMR spectrum ($CDCl_3$)

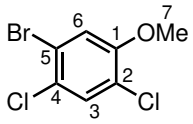

126 MHz ^{13}C NMR spectrum ($CDCl_3$)

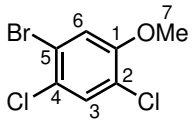

4-bromo-2-fluoroanisole, 139a

400 MHz ^{1}H NMR spectrum ($CDCl_3$)

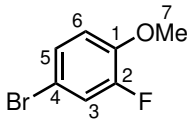

101 MHz ^{13}C NMR spectrum ($CDCl_3$)

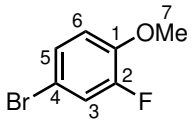

376 MHz ^{19}F NMR spectrum ($CDCl_3$)

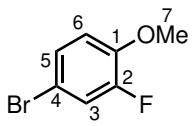

2,4-dichloro-1-ethoxybenzene, 100b

400 MHz ^{1}H NMR spectrum ($CDCl_3$)

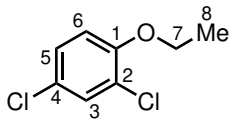

101 MHz ^{13}C NMR spectrum ($CDCl_3$)

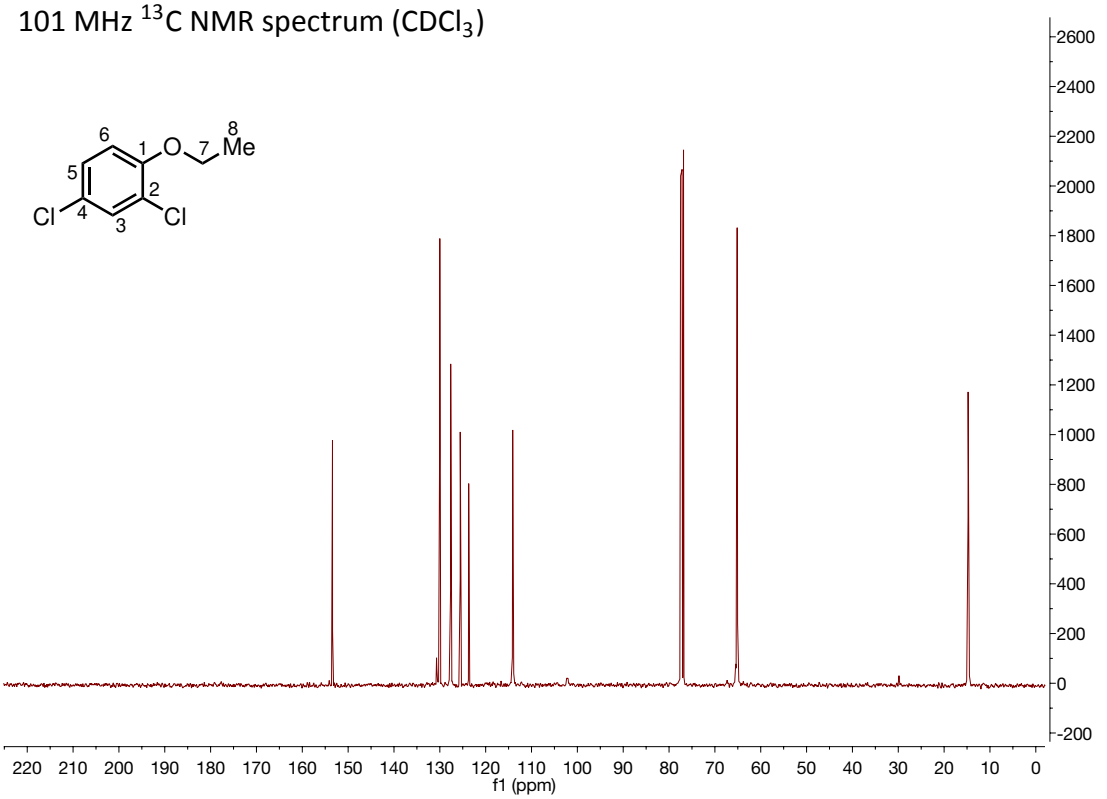

2,4-dichloro-1-isopropoxybenzene, 100c

400 MHz ^{1}H NMR spectrum ($CDCl_3$)

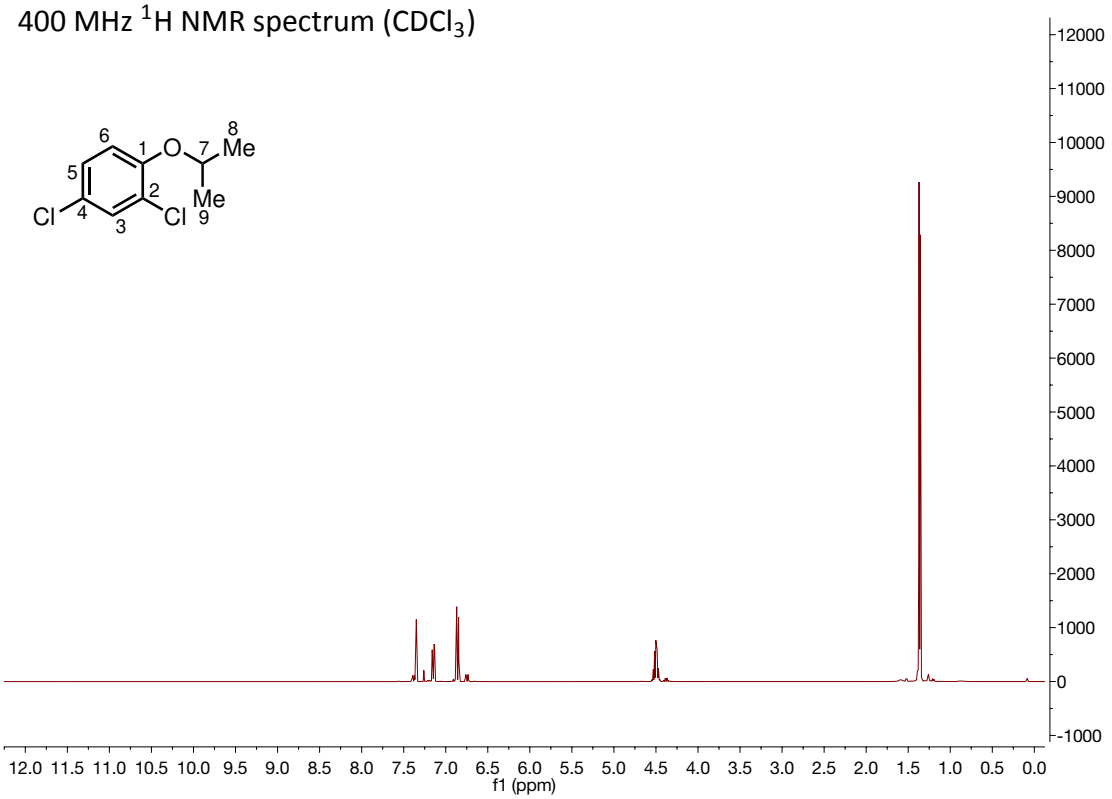

101 MHz ^{13}C NMR spectrum ($CDCl_3$)

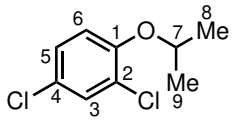

2,4-dichloro-1-(2,2,2-trifluoroethoxy)benzene, 100d

400 MHz ^{1}H NMR spectrum ($CDCl_3$)

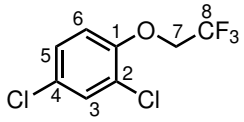

376 MHz ^{19}F NMR spectrum ($CDCl_3$)

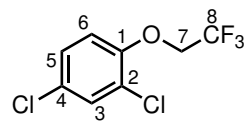

2,4-dichloro-1-(((1R,2S,5R)-2-isopropyl-5-methylcyclohexyl)oxy)benzene, 100e

500 MHz ^{1}H NMR spectrum ($CDCl_3$)

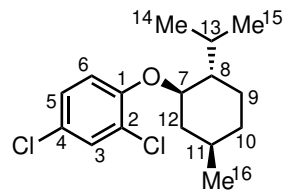

126 MHz ^{13}C NMR spectrum ($CDCl_3$)

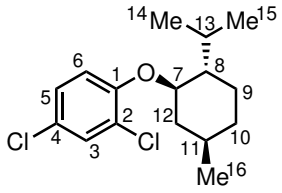

2,4-dichloro-1-(cyclohexyloxy)benzene, 100f

500 MHz ^{1}H NMR spectrum ($CDCl_3$)

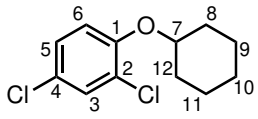

126 MHz ^{13}C NMR spectrum ($CDCl_3$)

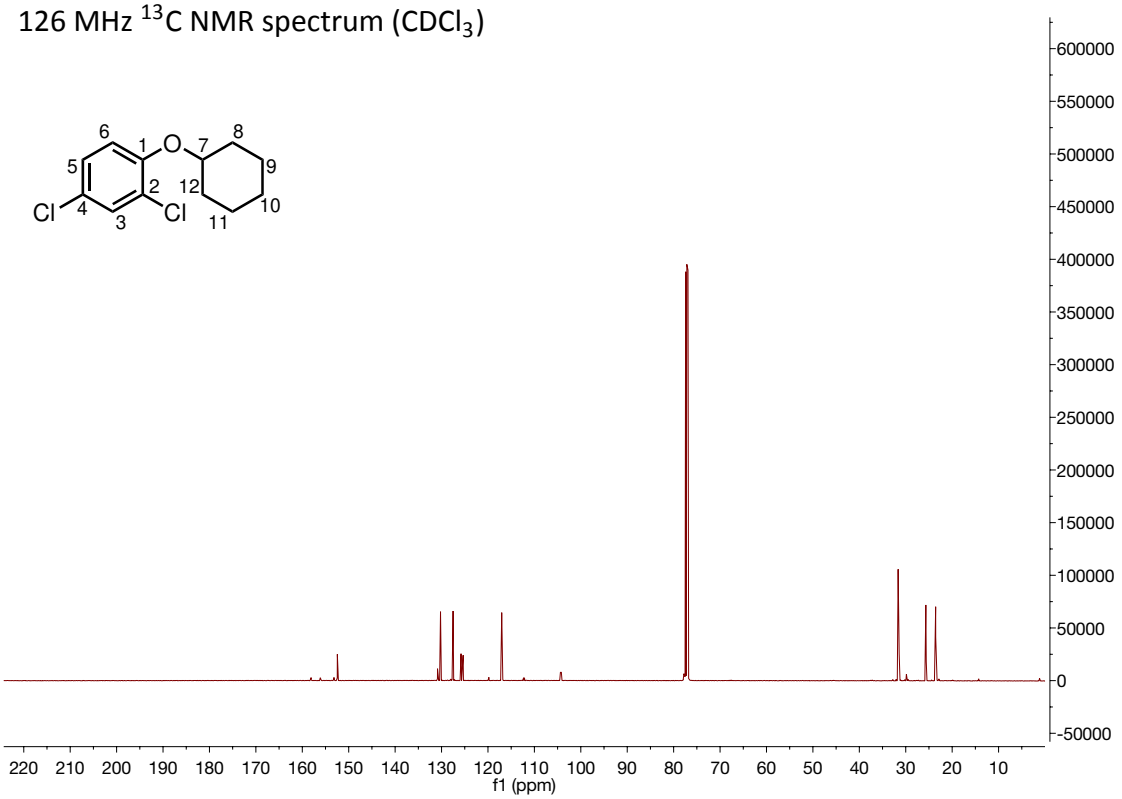

2,4-dichloro-1-(cyclopropylmethoxy)benzene, 100g

500 MHz ^{1}H NMR spectrum ($CDCl_3$)

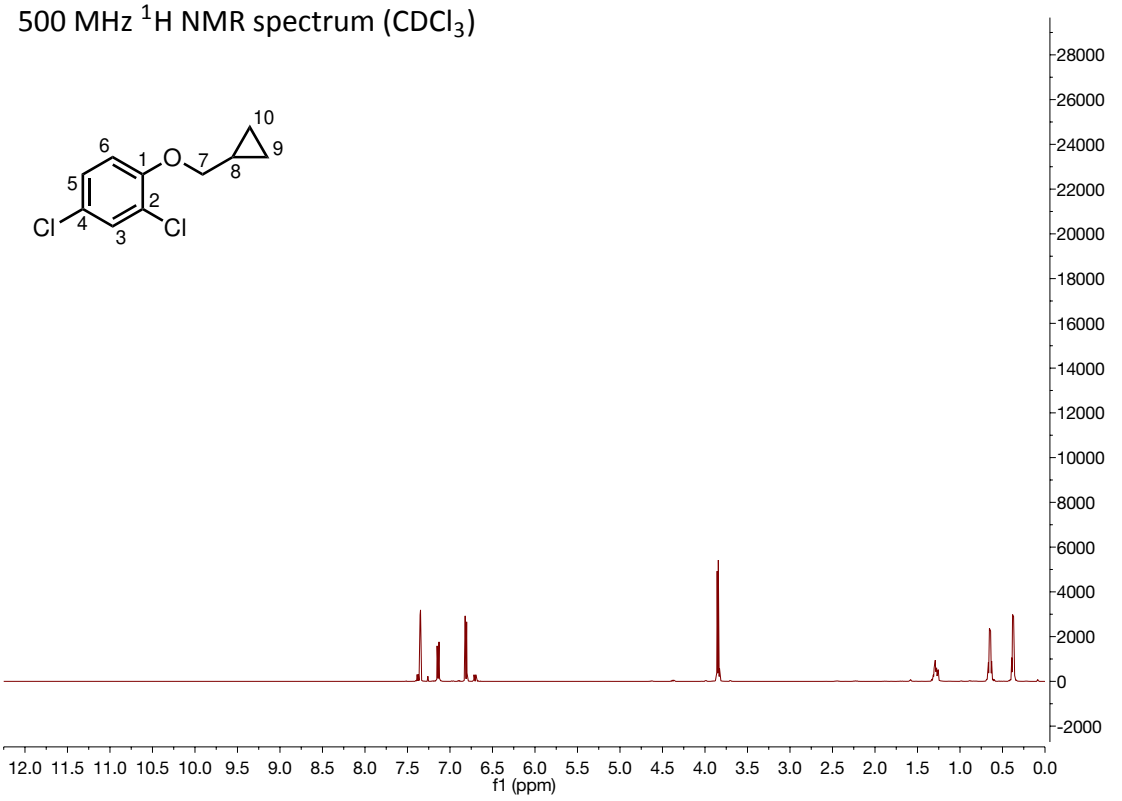

126 MHz ^{13}C NMR spectrum ($CDCl_3$)

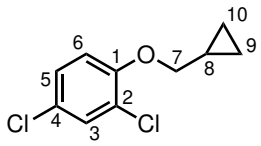

(*R*)-1-(3-bromo-2-methylpropoxy)-2,4-dichlorobenzene, 100h

500 MHz ^{1}H NMR spectrum ($CDCl_3$)

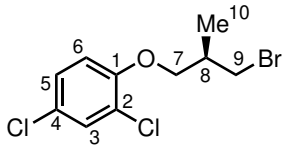

126 MHz ^{13}C NMR spectrum ($CDCl_3$)

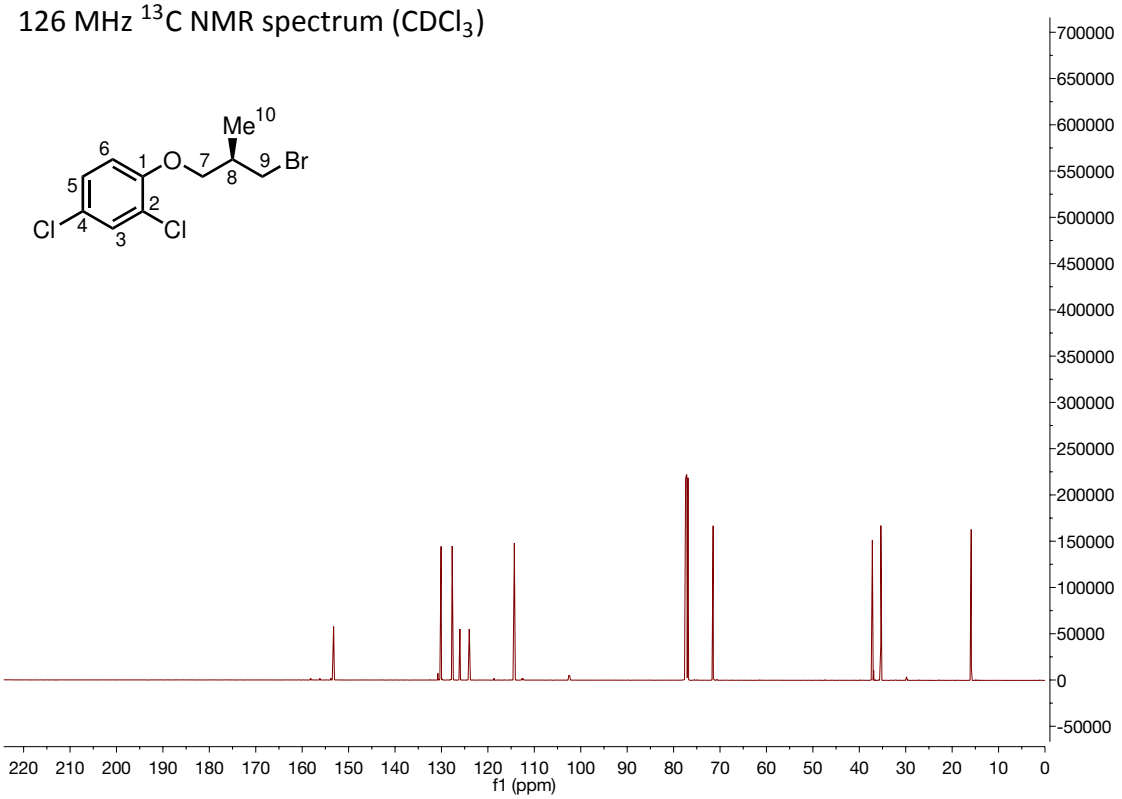

(R)-4-(2,4-dichlorophenoxy)butan-2-ol, 100i / (R)-3-(2,4-dichlorophenoxy)butan-1-ol, 100j

400 MHz ^{1}H NMR spectrum ($CDCl_3$)

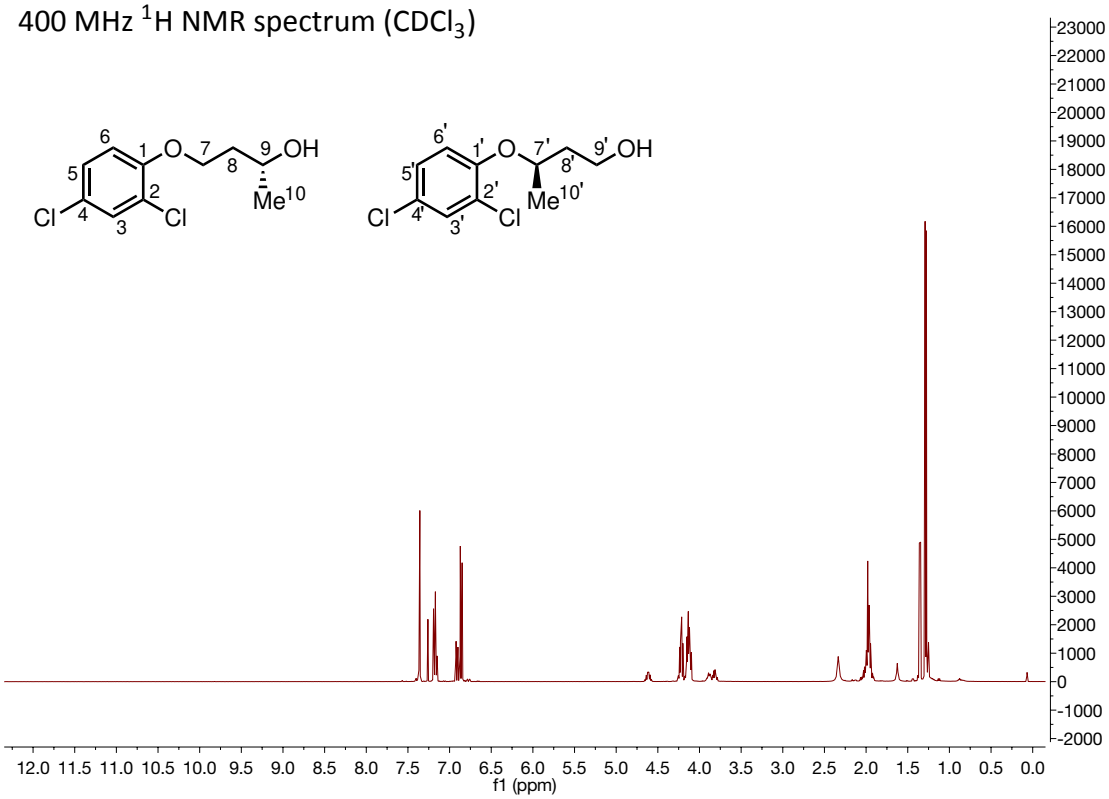

101 MHz ^{13}C NMR spectrum ($CDCl_3$)

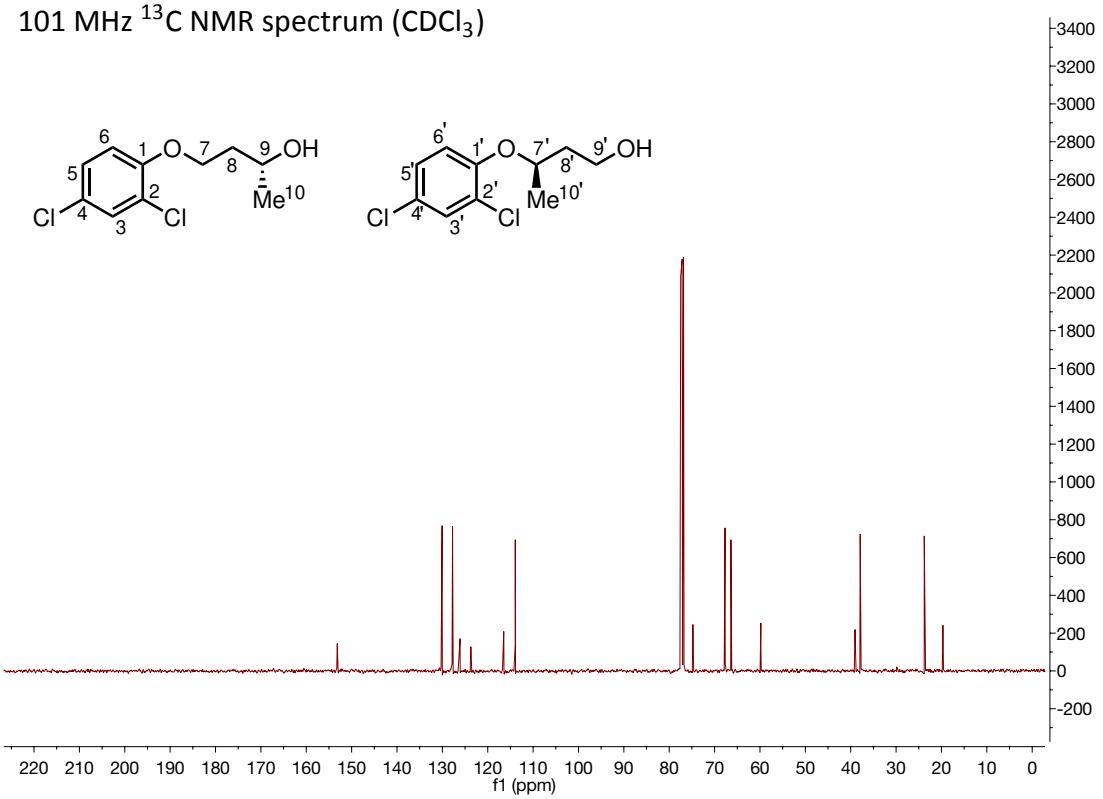

1-(2,4-dichlorophenyl)-1*H*-pyrazole, 100aa

400 MHz ^{1}H NMR spectrum ($CDCl_3$)

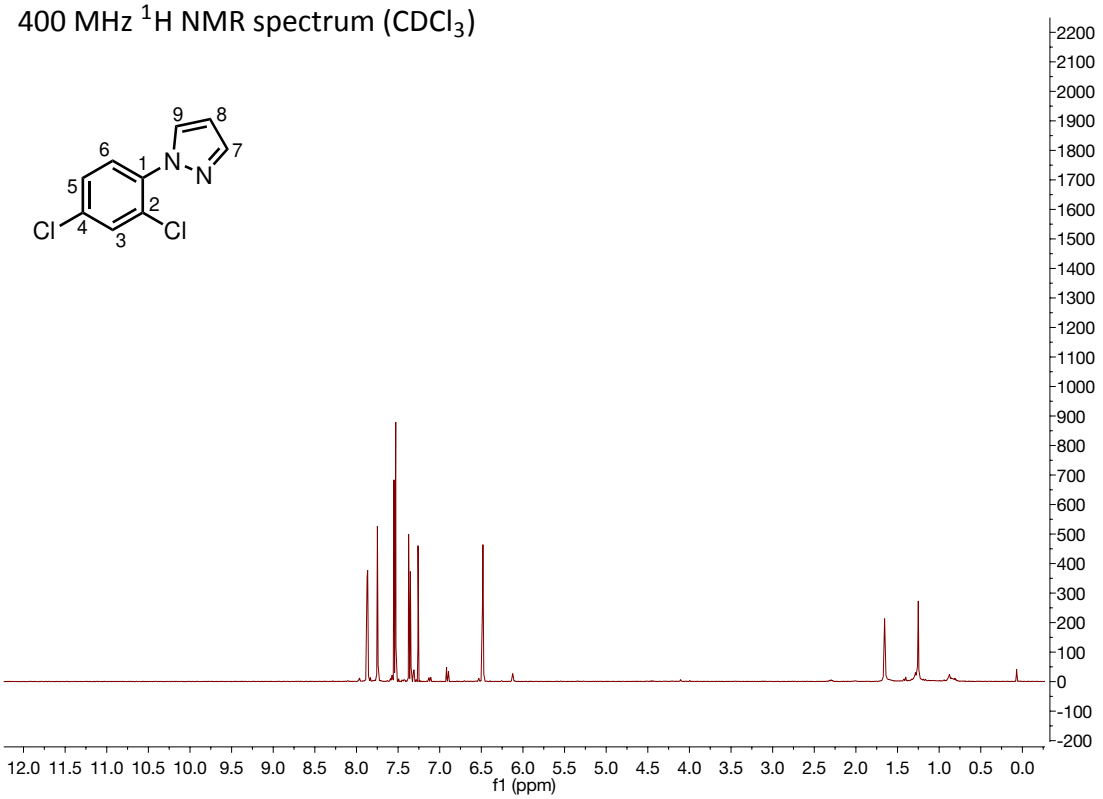

101 MHz ^{13}C NMR spectrum ($CDCl_3$)

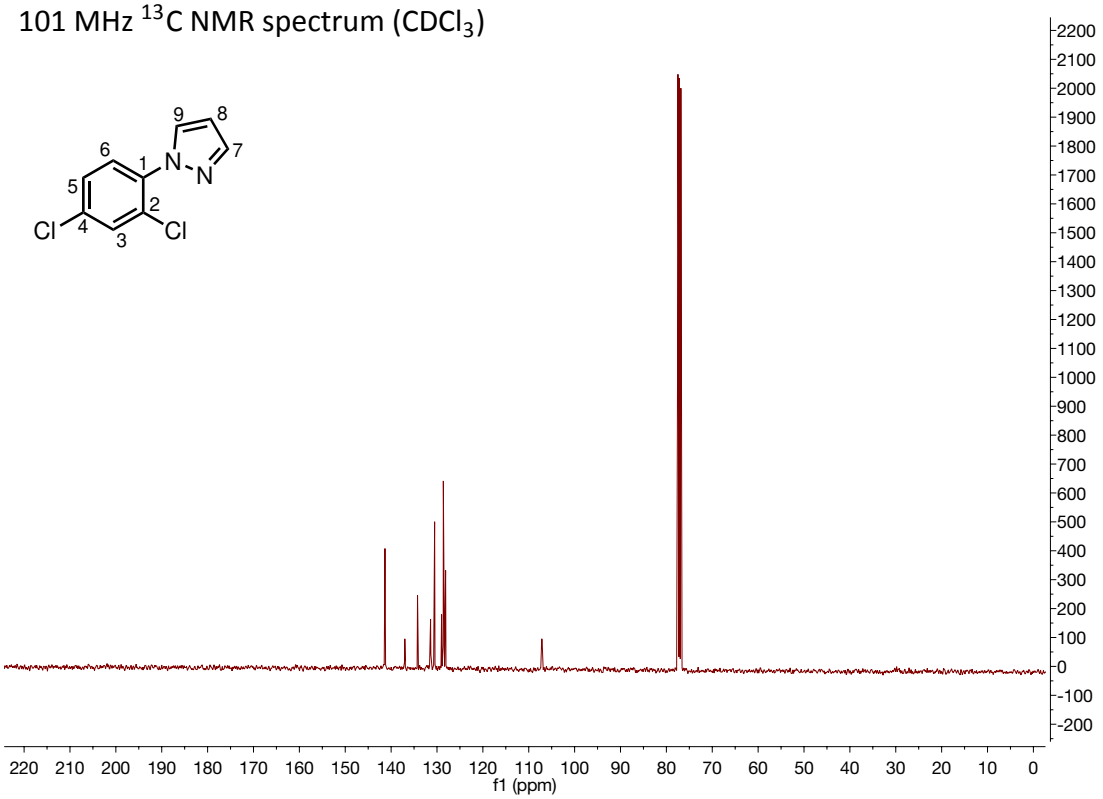

1-(4-chlorophenyl)-1*H*-pyrazole, 103b

400 MHz ^{1}H NMR spectrum ($CDCl_3$)

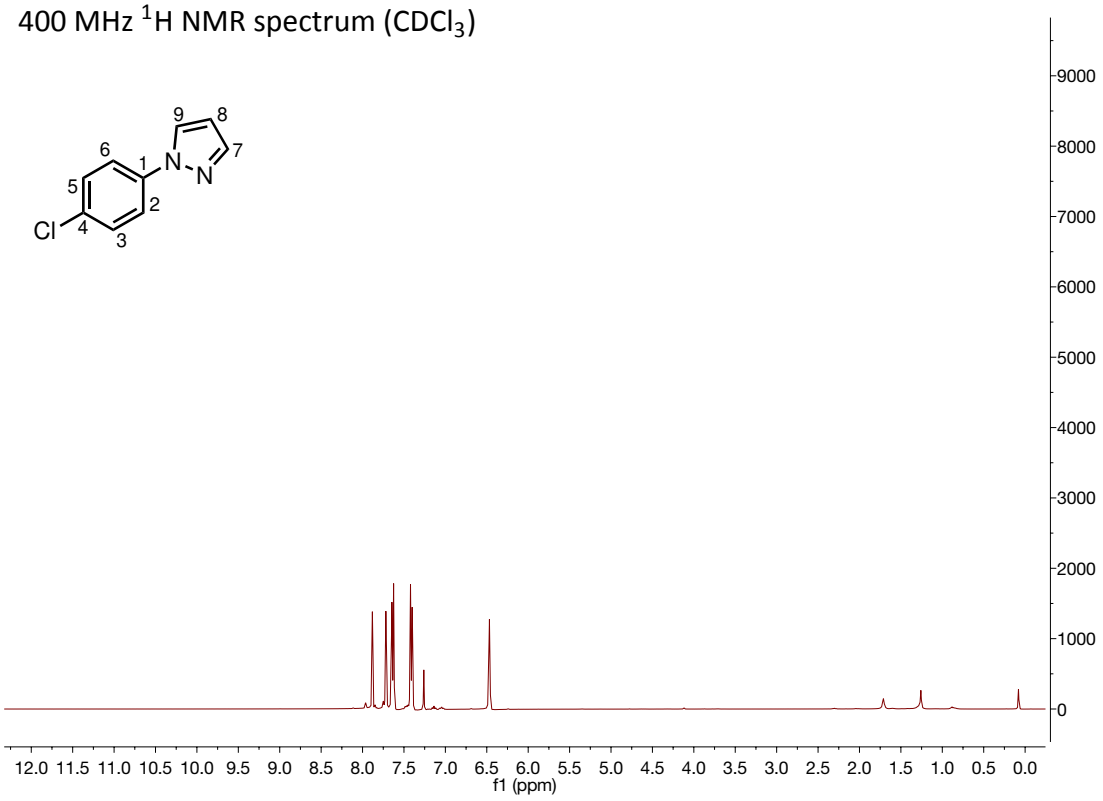

101 MHz ^{13}C NMR spectrum ($CDCl_3$)

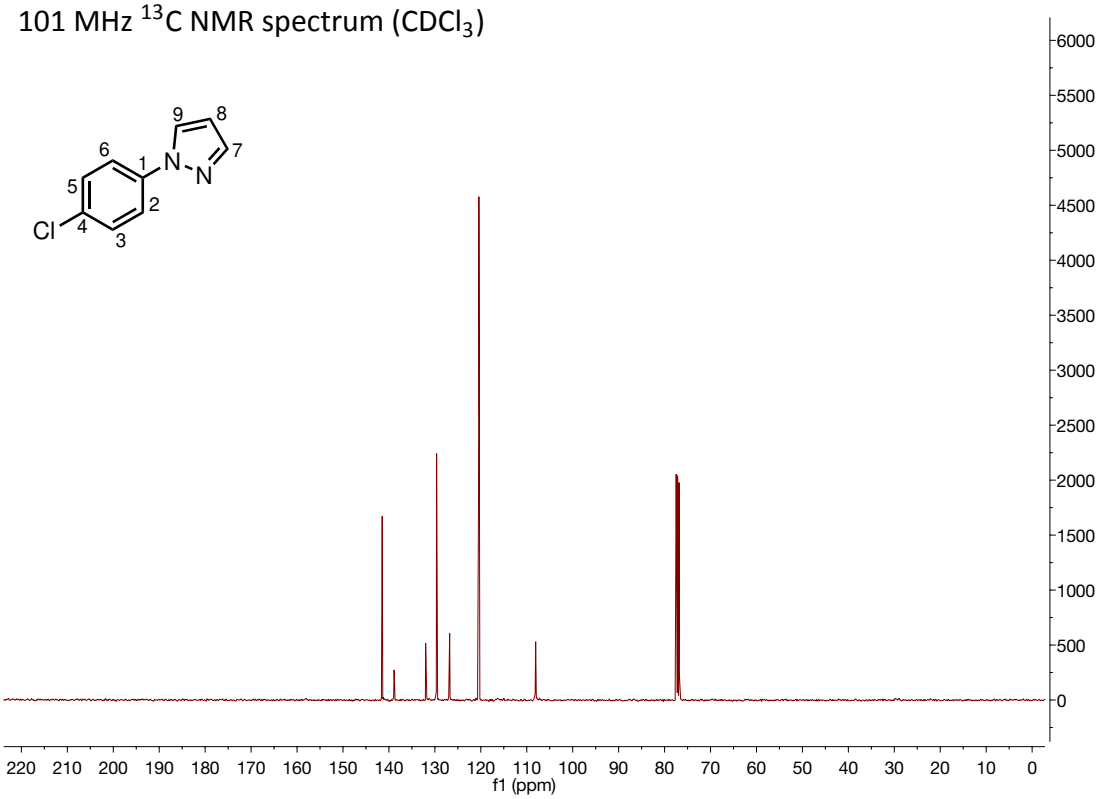

4-chloro-1-(4-chlorophenyl)-1*H*-pyrazole, 103c

500 MHz ^{1}H NMR spectrum ($CDCl_3$)

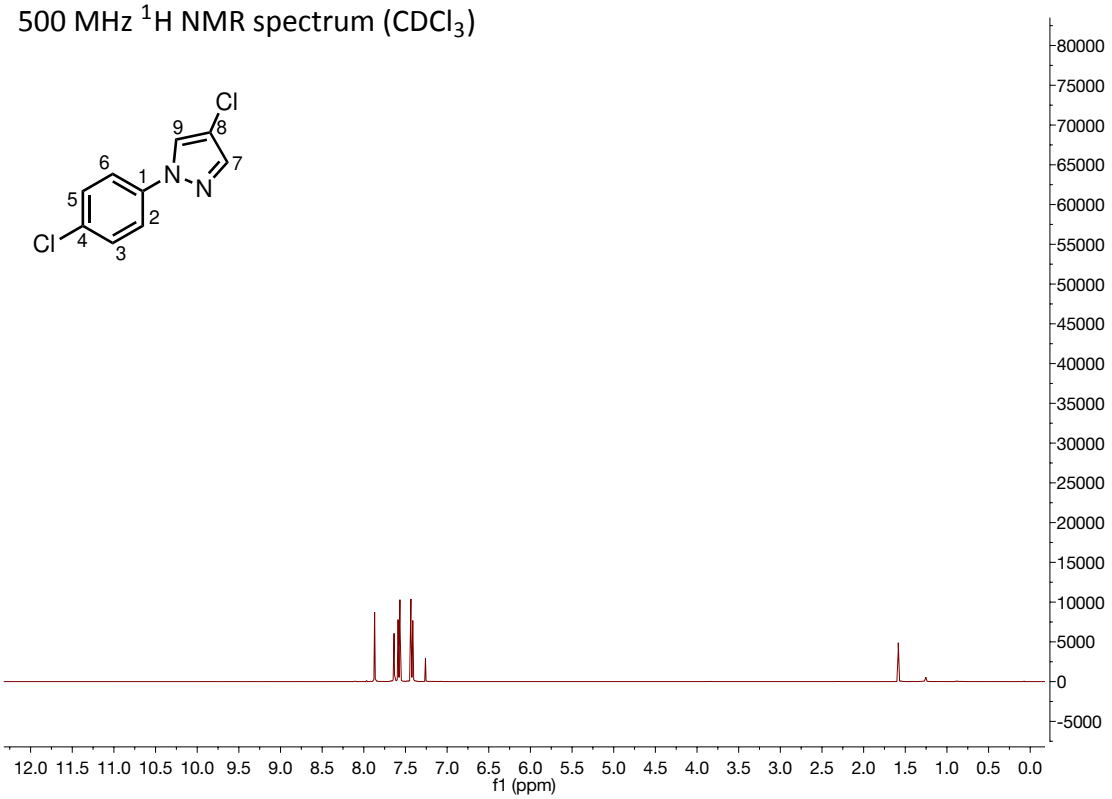

126 MHz ^{13}C NMR spectrum ($CDCl_3$)

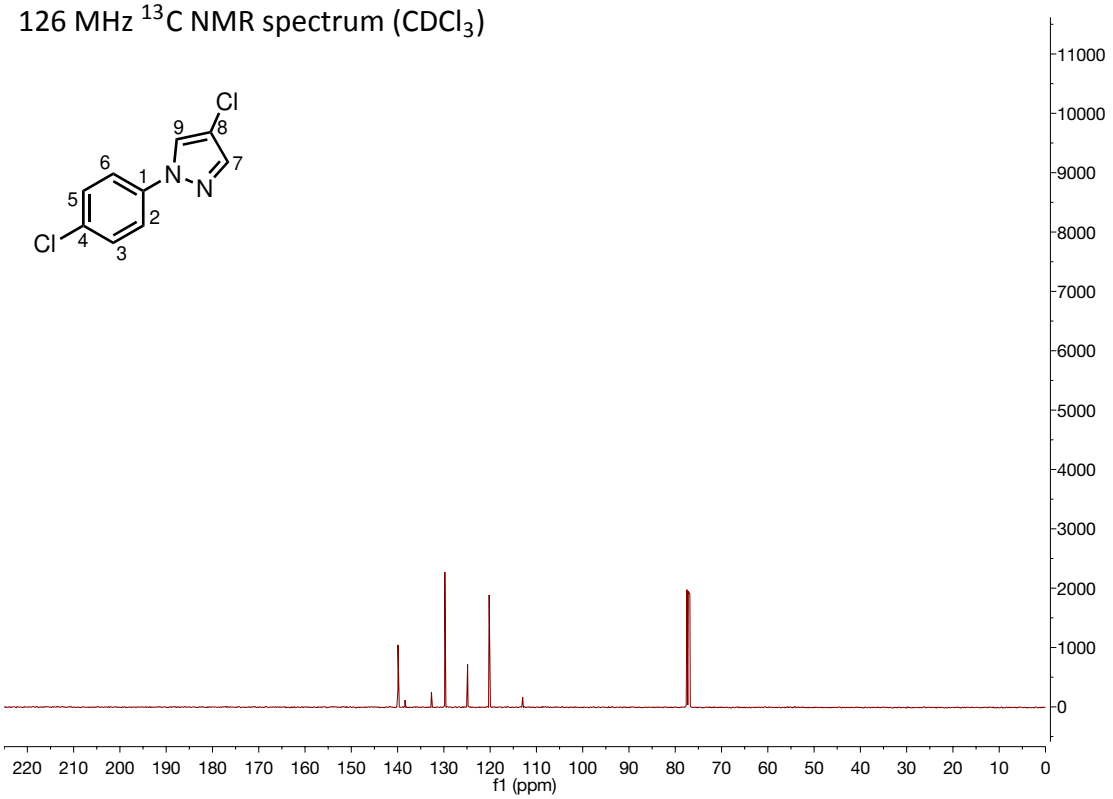

4-bromo-1-(4-chlorophenyl)-1*H*-pyrazole, 103d

500 MHz ^{1}H NMR spectrum ($CDCl_3$)

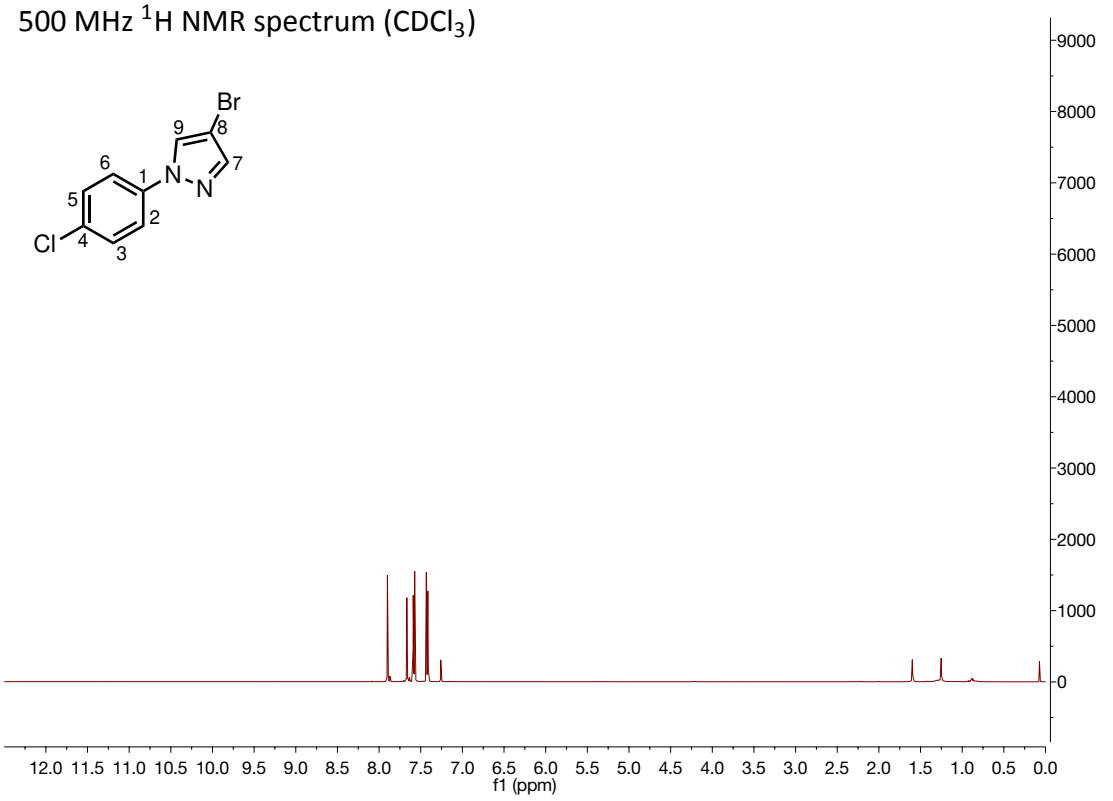

126 MHz ^{13}C NMR spectrum ($CDCl_3$)

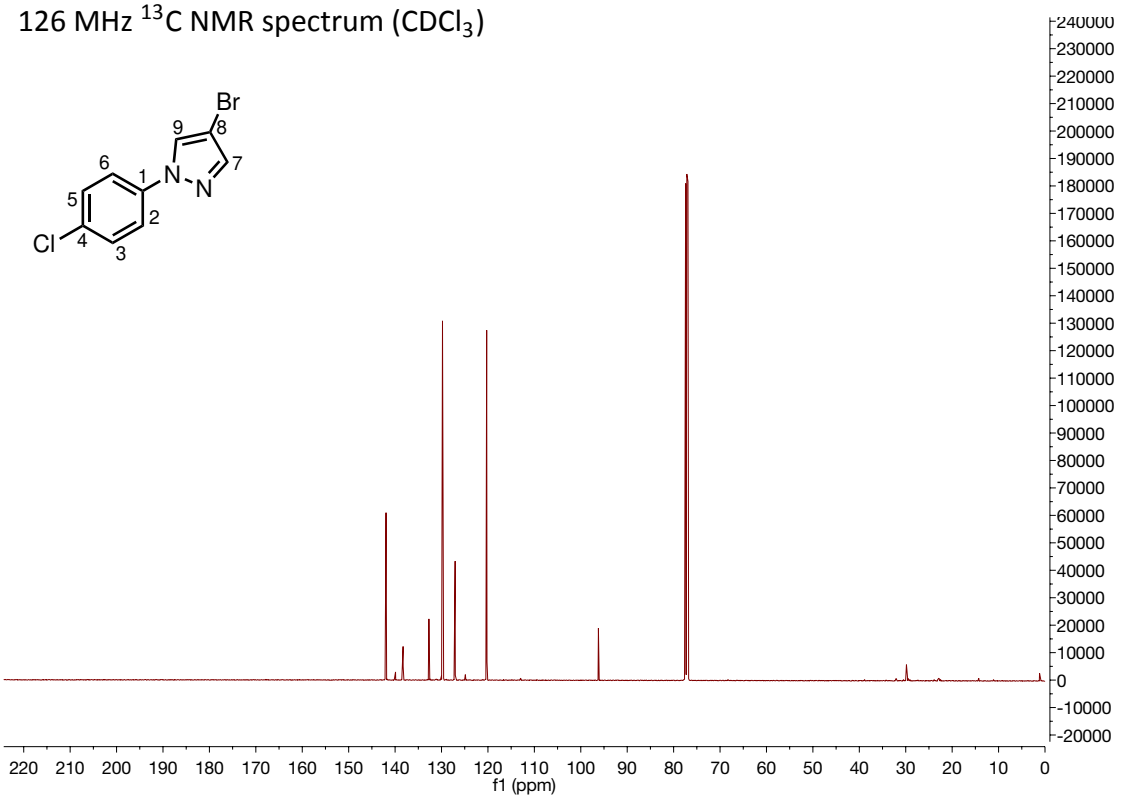

1-(4-chlorophenyl)-4-(4,4,5,5-tetramethyl-1,3,2-dioxaborolan-2-yl)-1*H*-pyrazole, 103e

400 MHz ^{1}H NMR spectrum ($CDCl_3$)

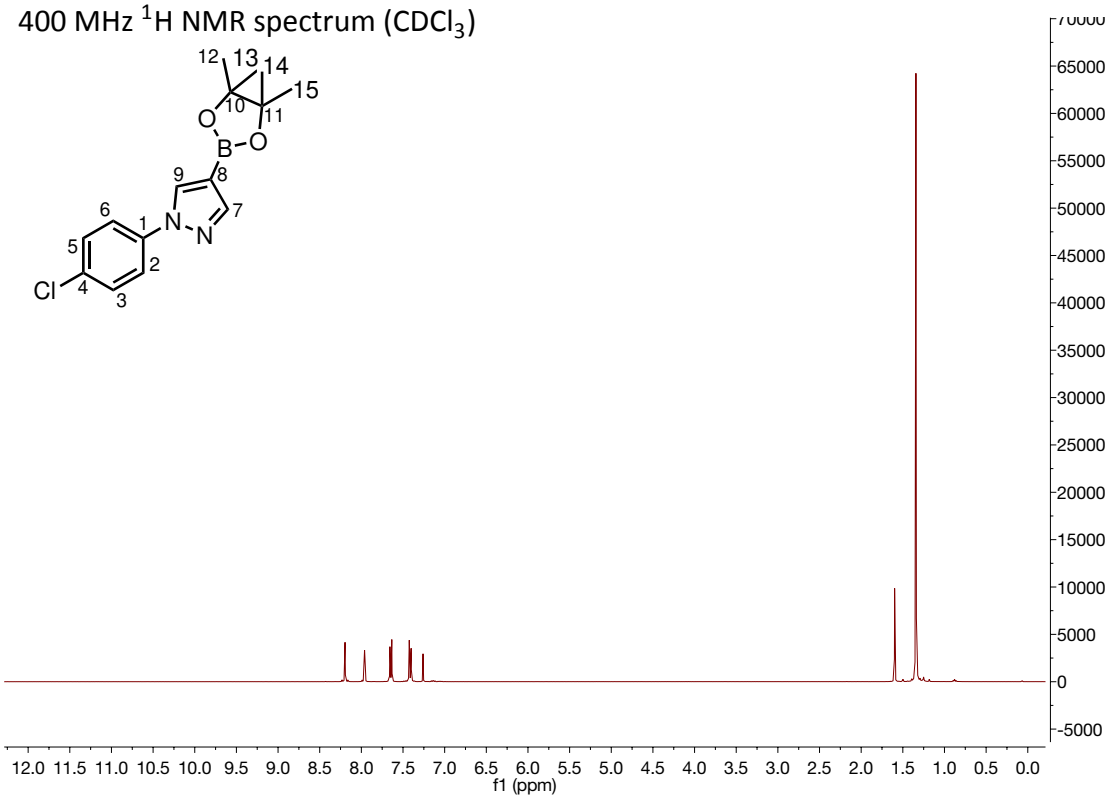

101 MHz ^{13}C NMR spectrum ($CDCl_3$)

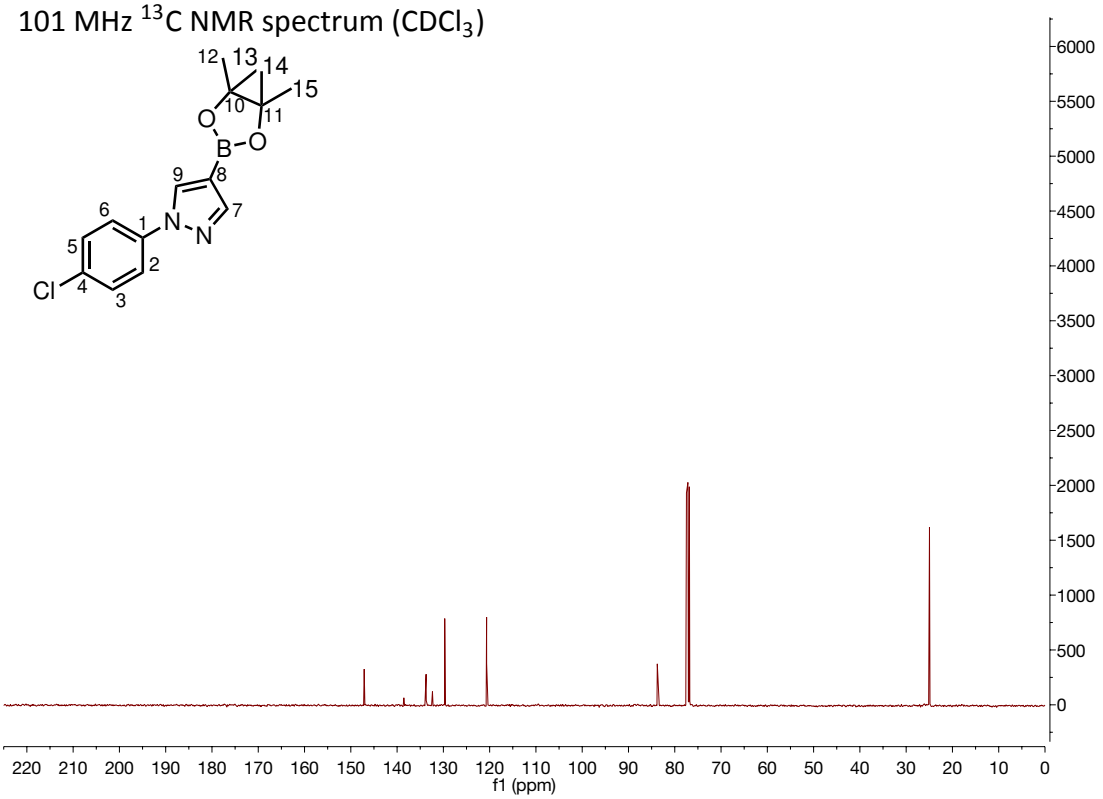

1-(4-chlorophenyl)-3-(trifluoromethyl)-1H-pyrazole, 103f

500 MHz ^{1}H NMR spectrum ($CDCl_3$)

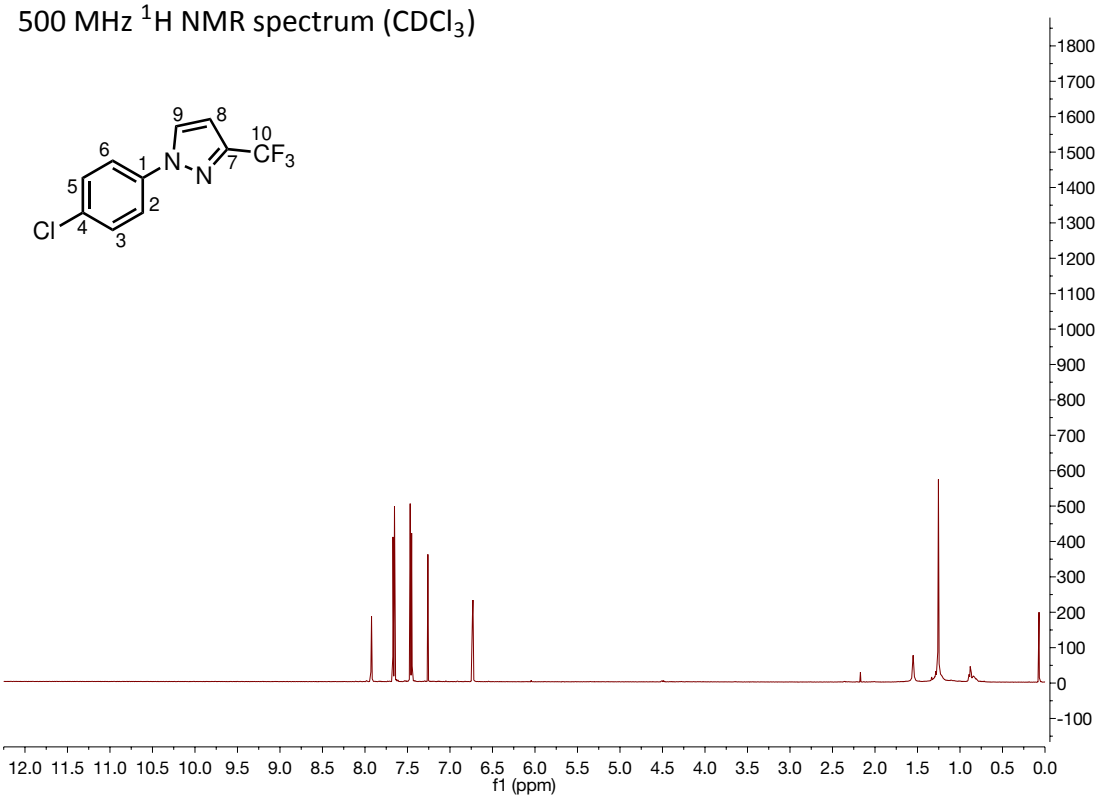

126 MHz ^{13}C NMR spectrum ($CDCl_3$)

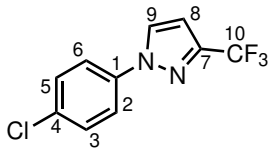

470 MHz ^{19}F NMR spectrum ($CDCl_3$)



ethyl 1-(4-chlorophenyl)-1*H*-pyrazole-4-carboxylate, 103g

500 MHz ^{1}H NMR spectrum ($CDCl_3$)

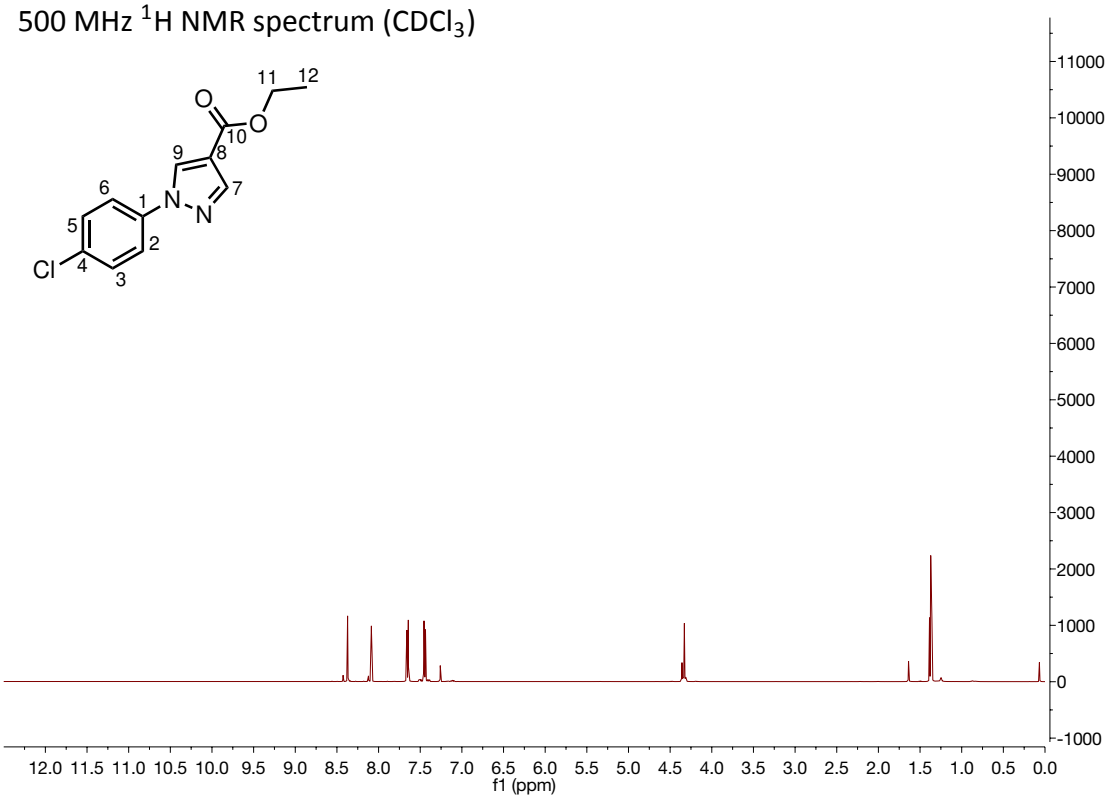

126 MHz ^{13}C NMR spectrum ($CDCl_3$)

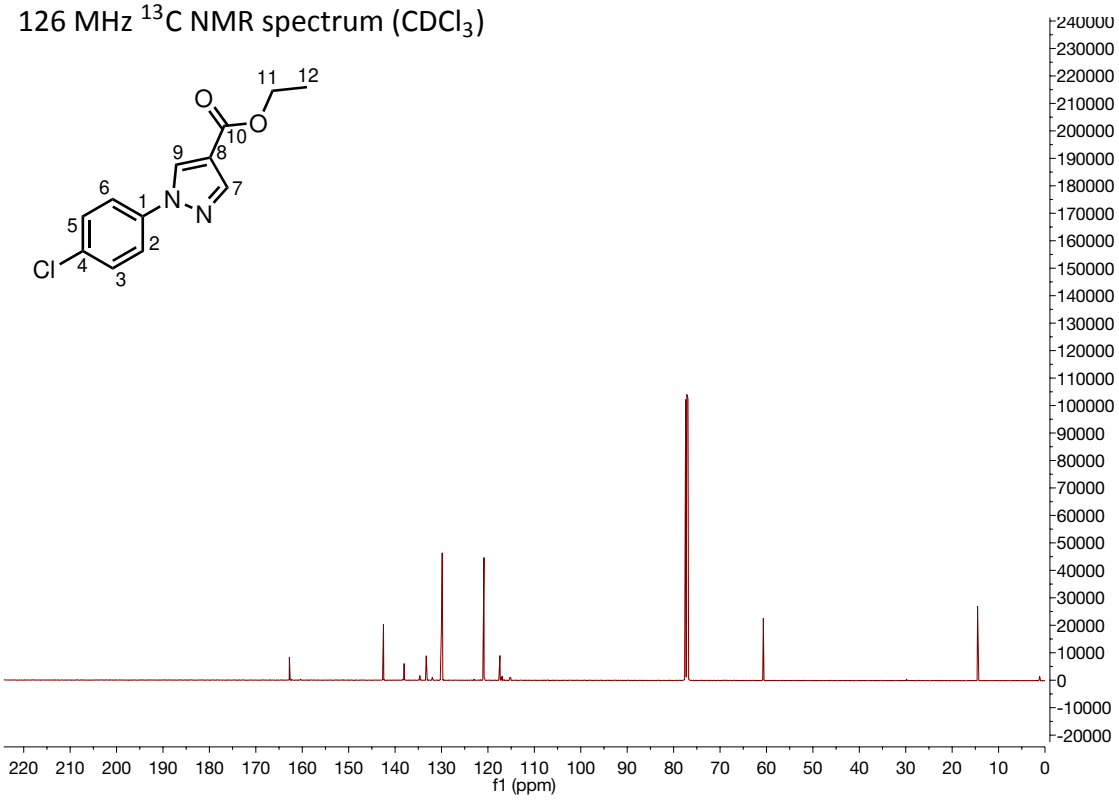

1,4-dioxaspiro[4.5]decan-8-one, 154

500 MHz ^{1}H NMR spectrum ($CDCl_3$)

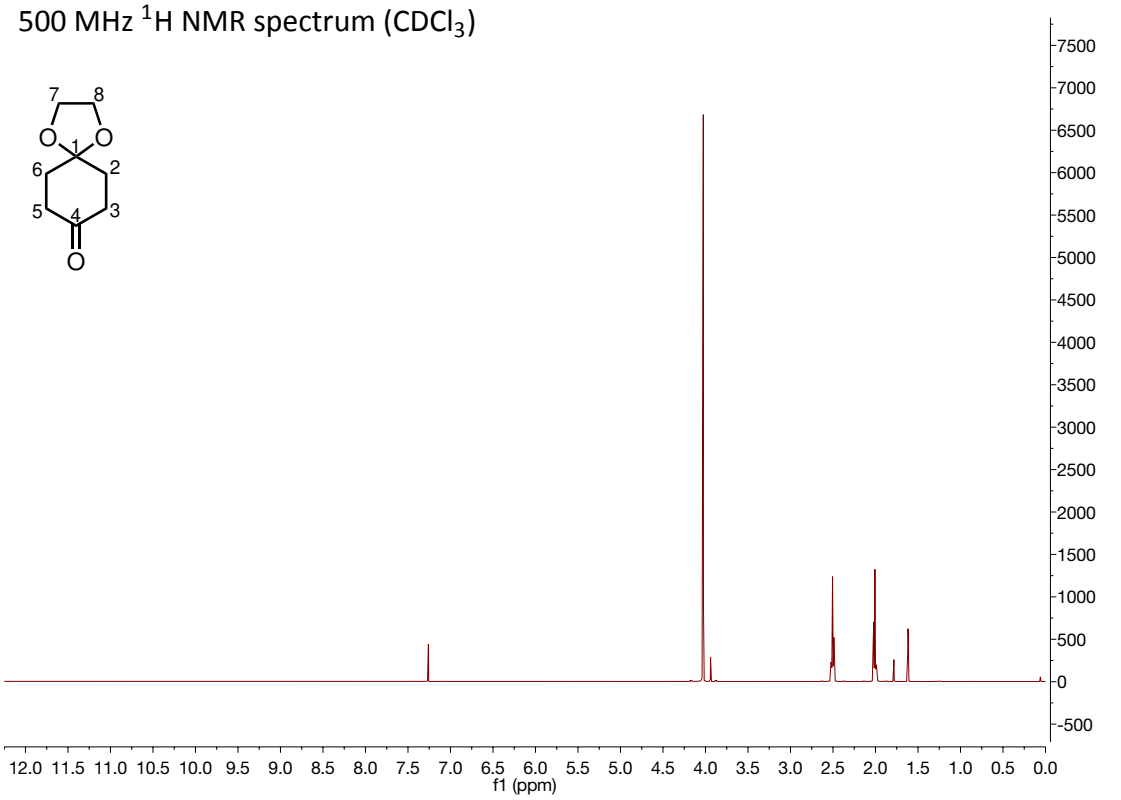

126 MHz ^{13}C NMR spectrum ($CDCl_3$)

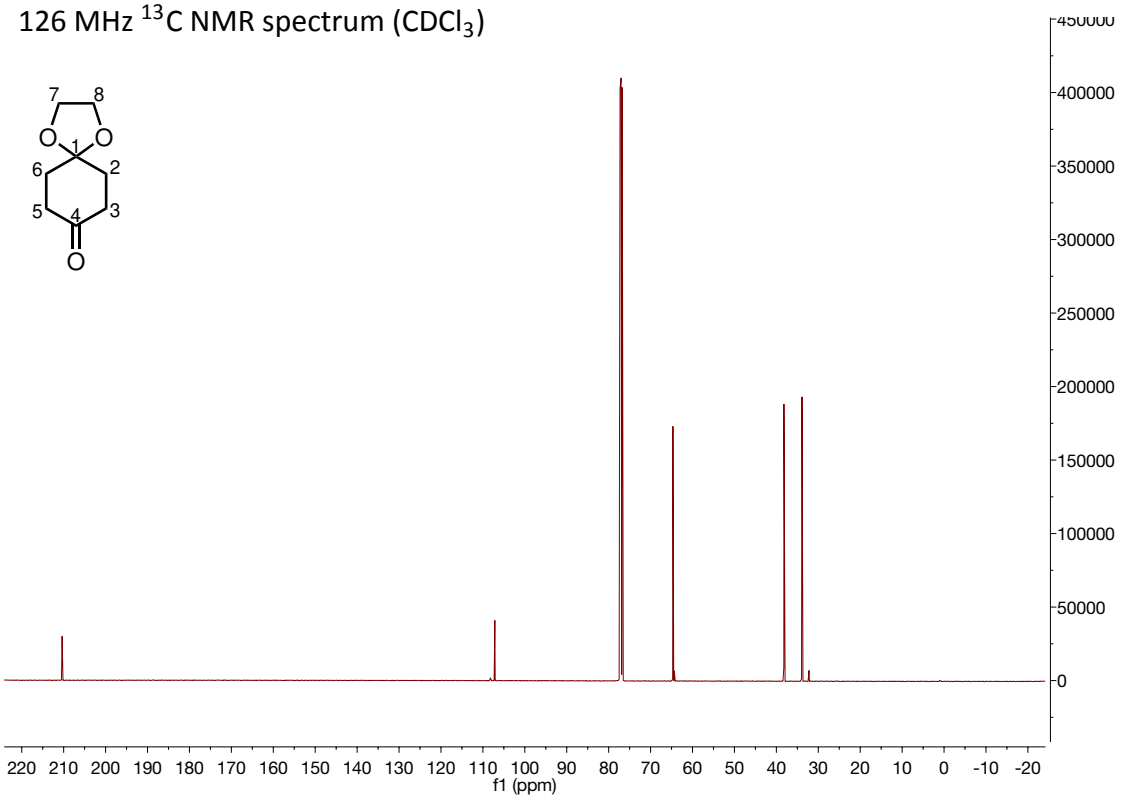

8-(but-3-en-1-yl)-1,4-dioxaspiro[4.5]decan-8-ol, 156

500 MHz ^{1}H NMR spectrum ($CDCl_3$)

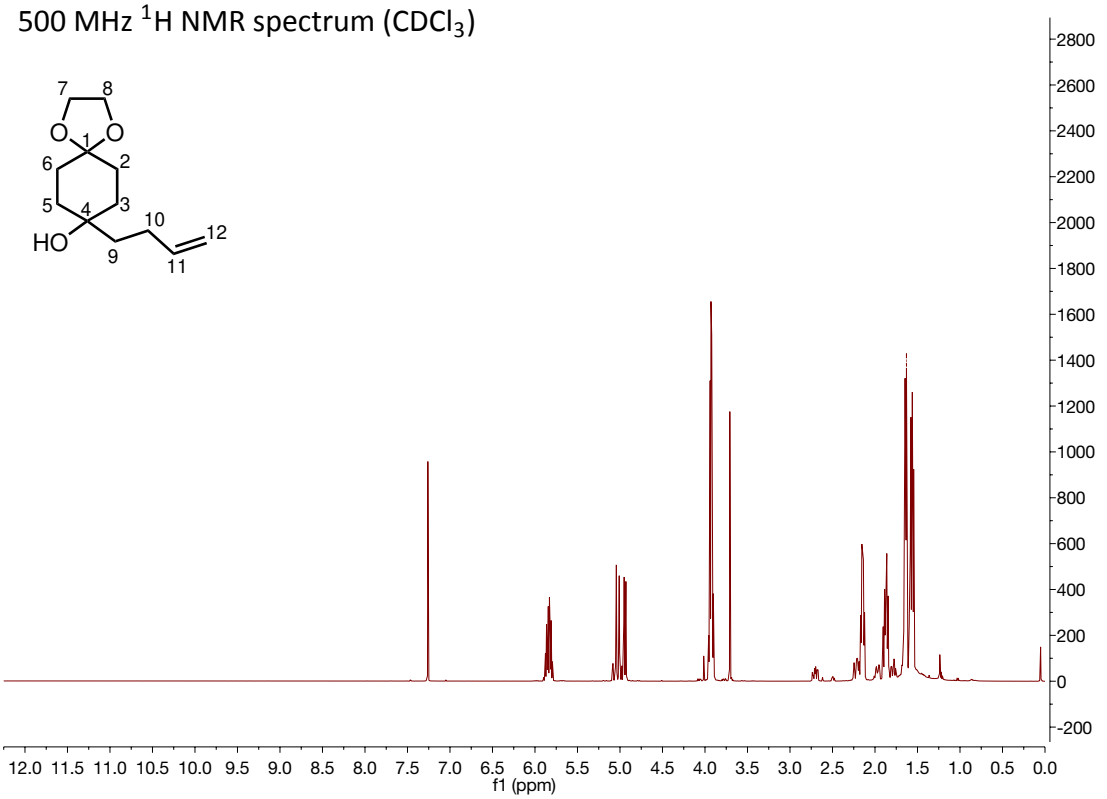

126 MHz ^{13}C NMR spectrum ($CDCl_3$)

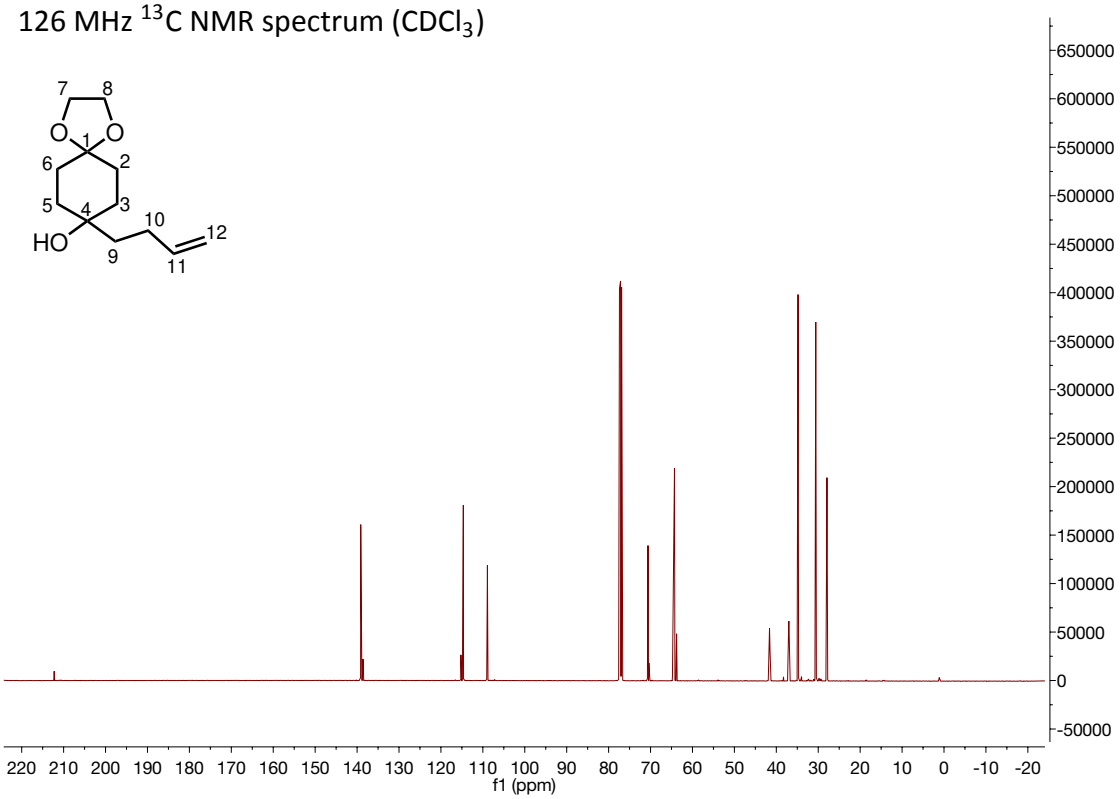

4-(but-3-en-1-yl)-4-hydroxycyclohexan-1-one, 157

500 MHz ^{1}H NMR spectrum ($CDCl_3$)

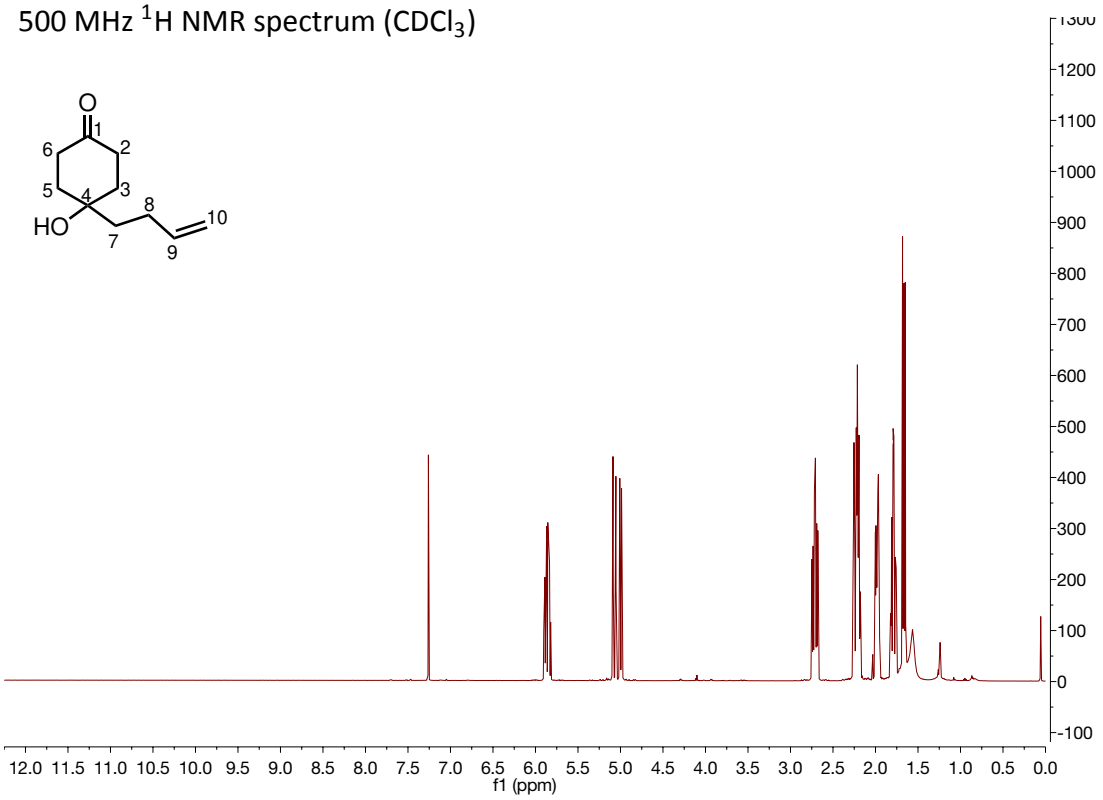

126 MHz ^{13}C NMR spectrum ($CDCl_3$)

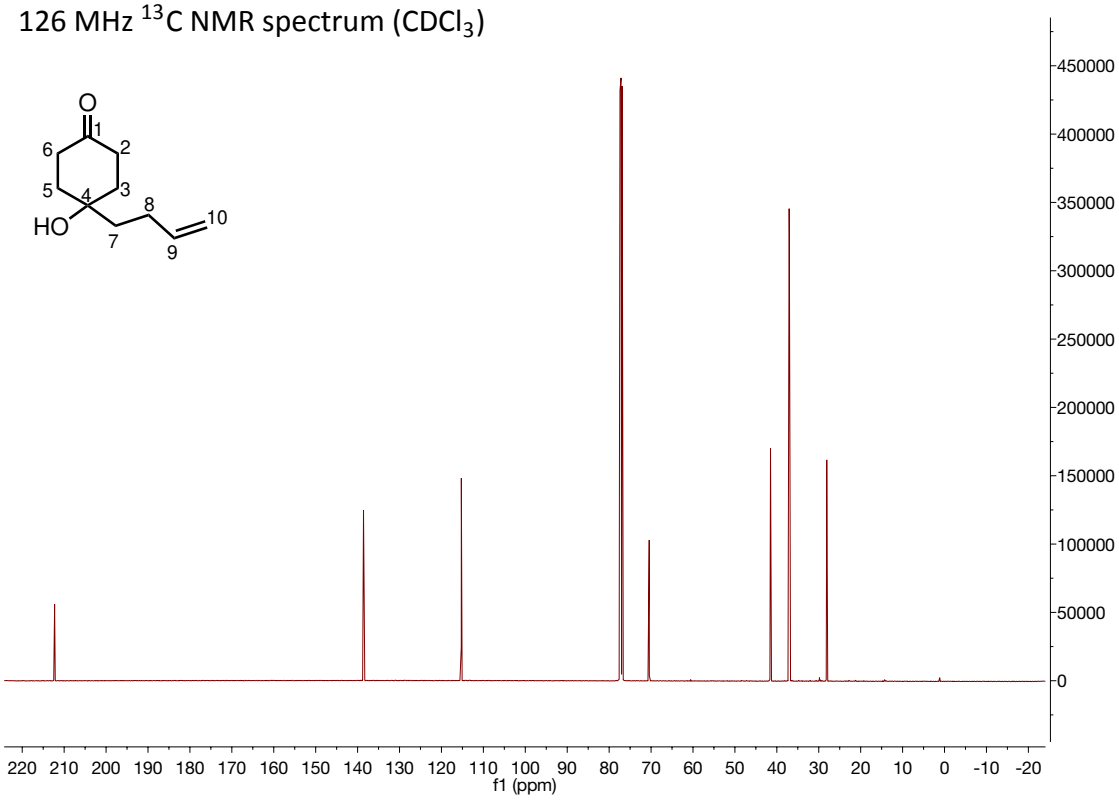

1-phenyl-1*H*-imidazolel, 163

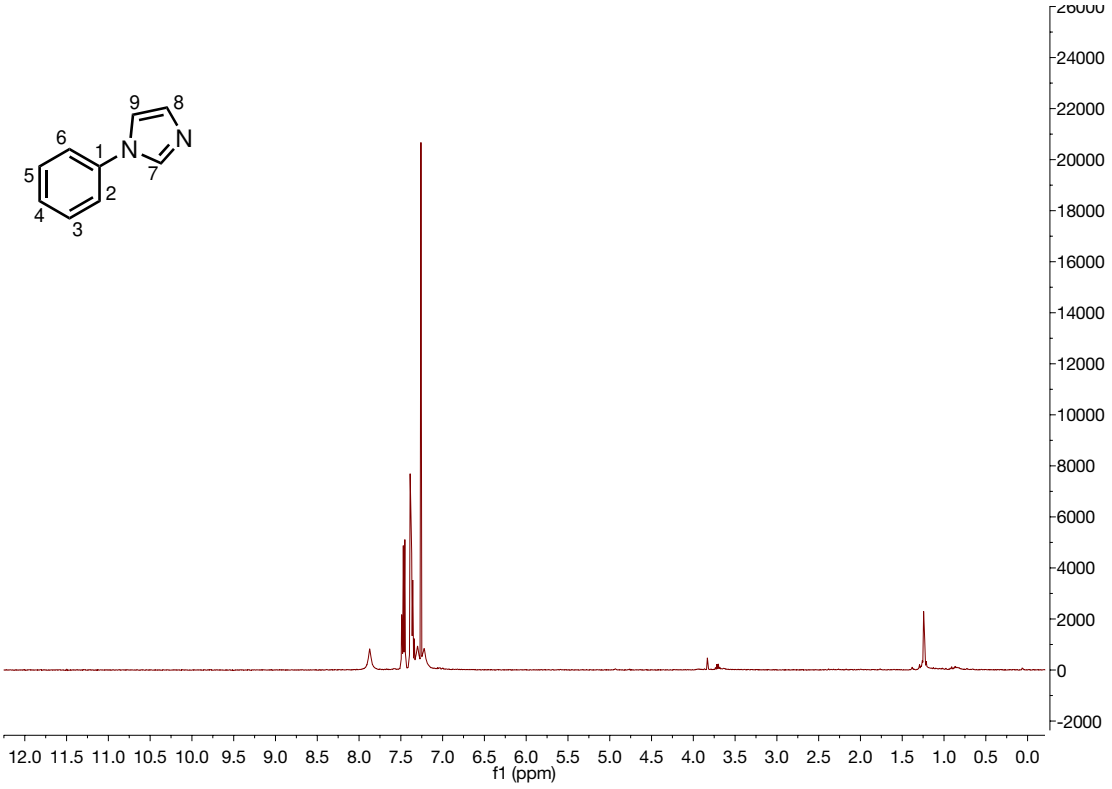

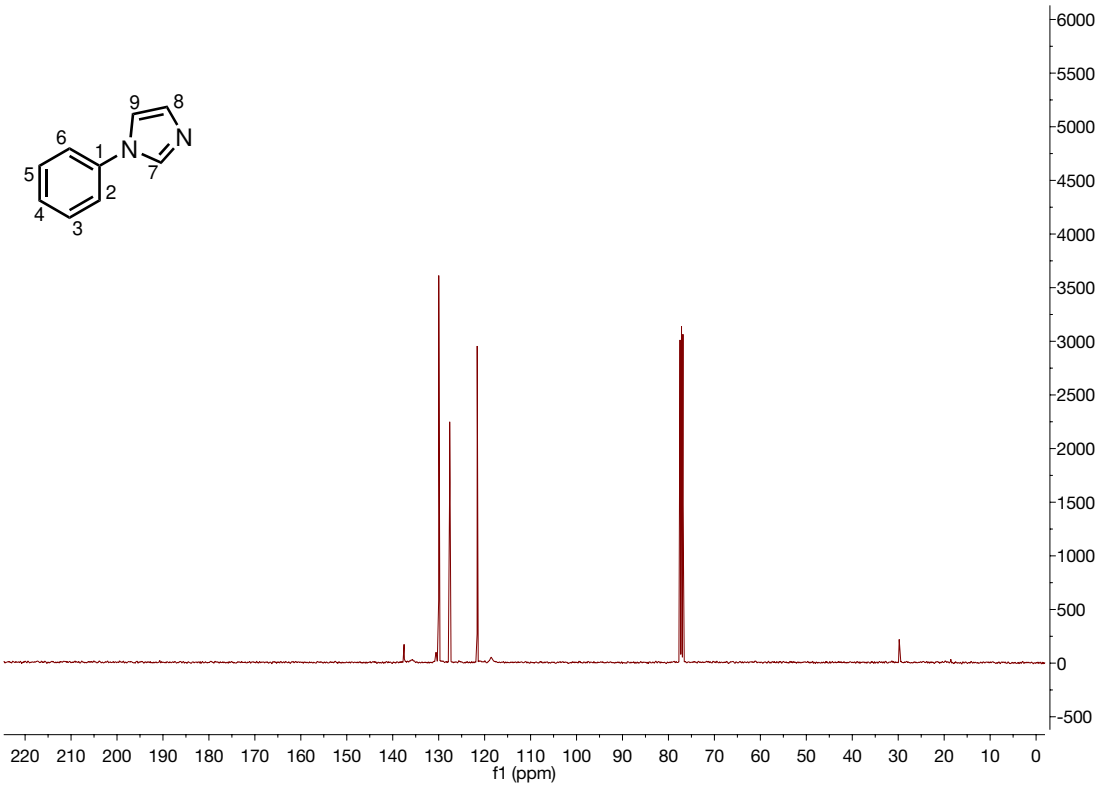

SELECTED GC-MS TRACES

GC Calibration Data

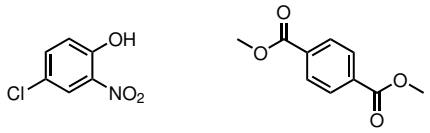

CMPD **10c** IS **173**

Figure 5.13. *CMPD and IS used in the following GC calibration.*

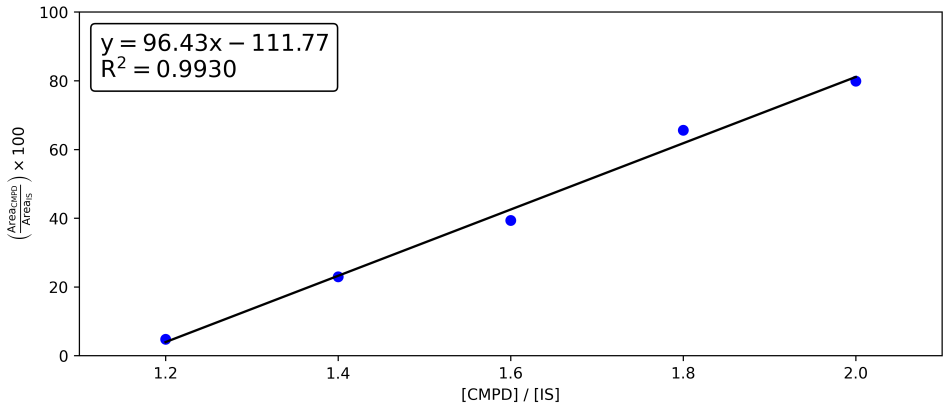

Calibration for GC yields of ***10c***

$$R_A = \left(\frac{\text{CMPD Peak Area}}{\text{IS Peak Area}}\right) \times 100$$

$$[\text{CMPD}] = [\text{IS}] \times \left(\frac{R_A + 111.77}{96.43}\right)$$

[**10c**]/[IS] = 1.2

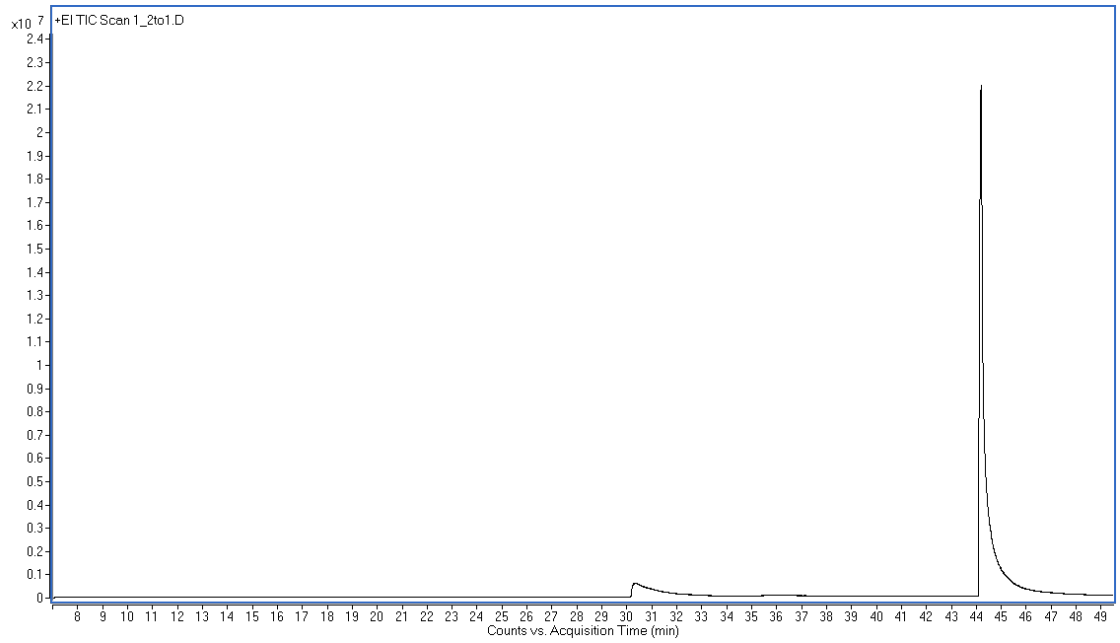

[**10c**]/[IS] = 1.4

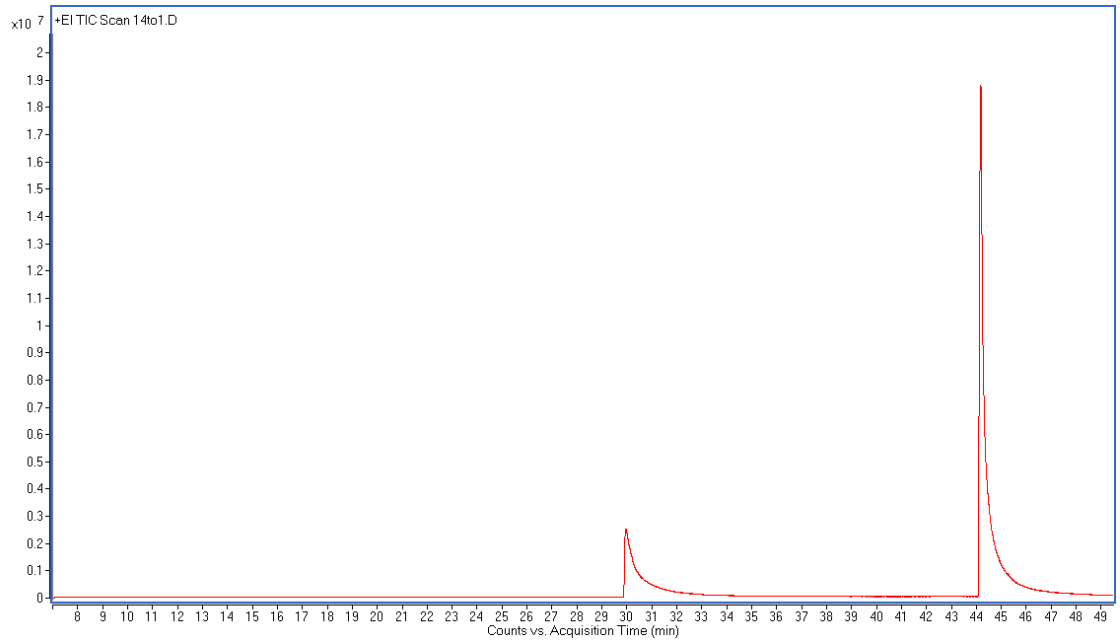

[**10c**]/[IS] = 1.6

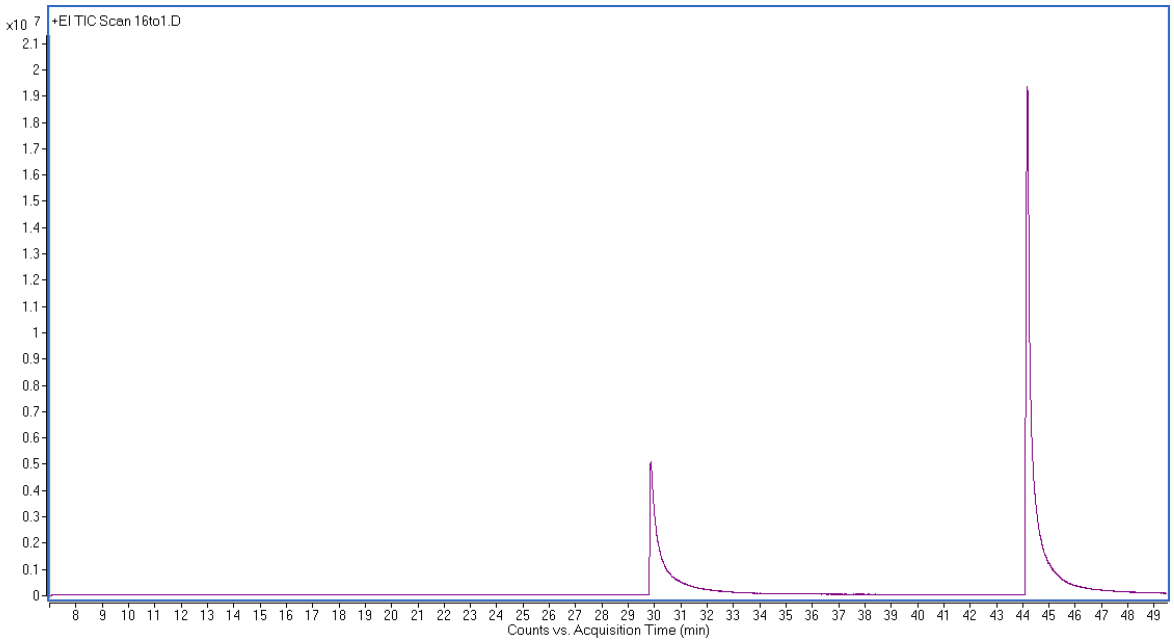

[**10c**]/[IS] = 1.8

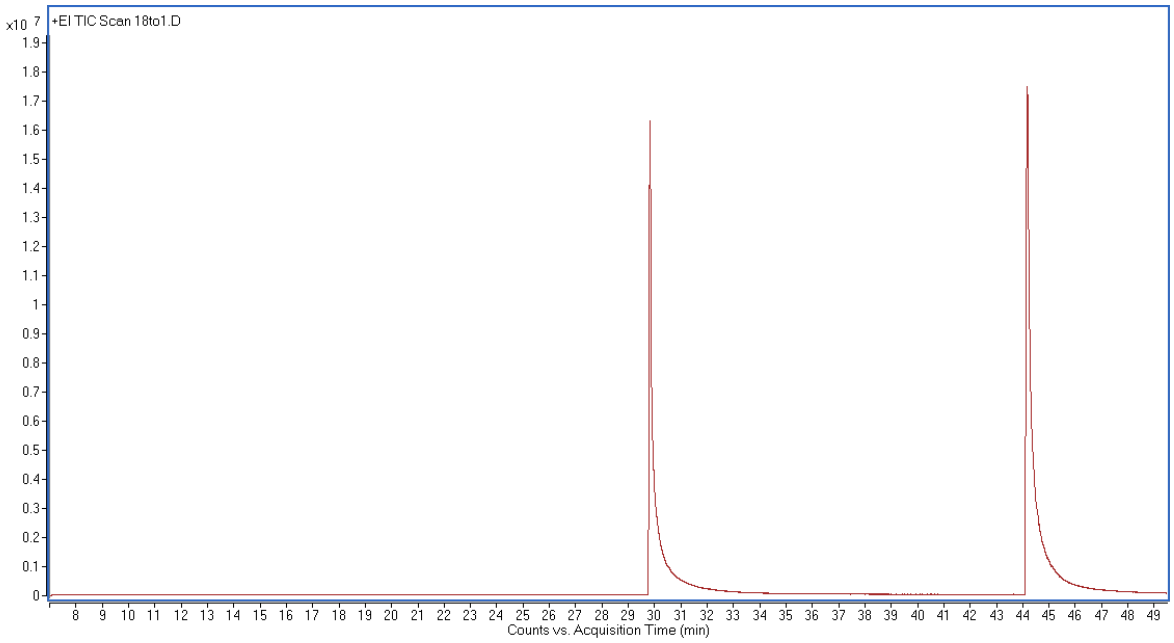

[**10c**]/[IS] = 2

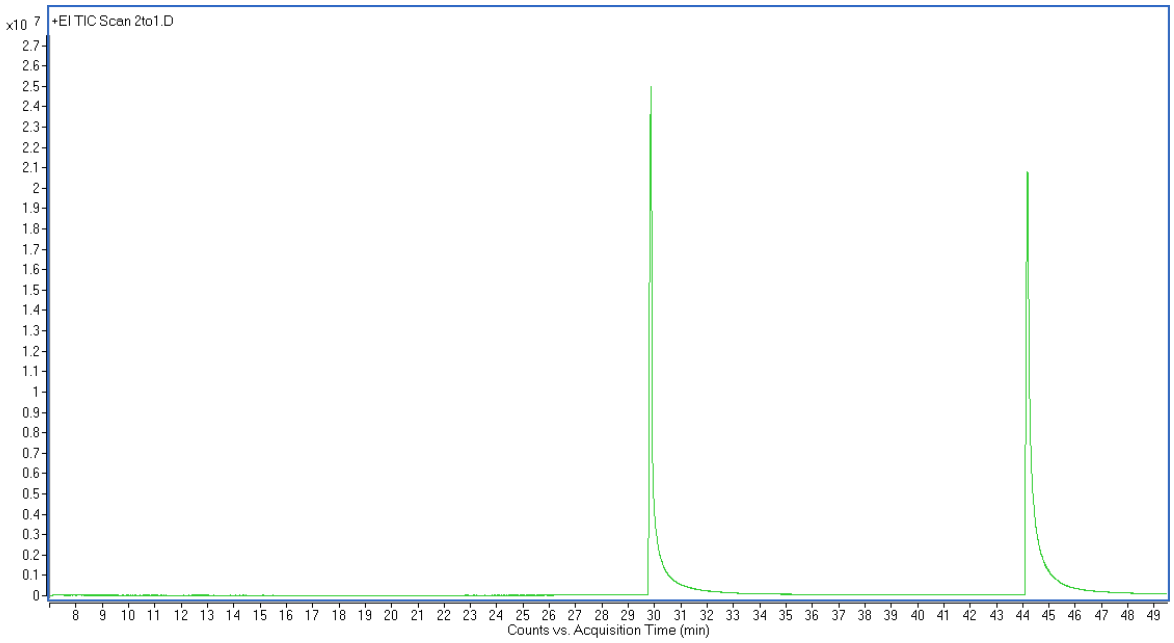

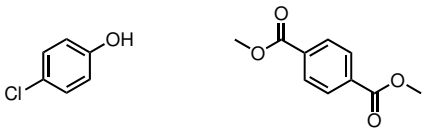

CMPD **10a** IS **173**

Figure 5.15. *CMPD and IS used in the following GC calibration.*

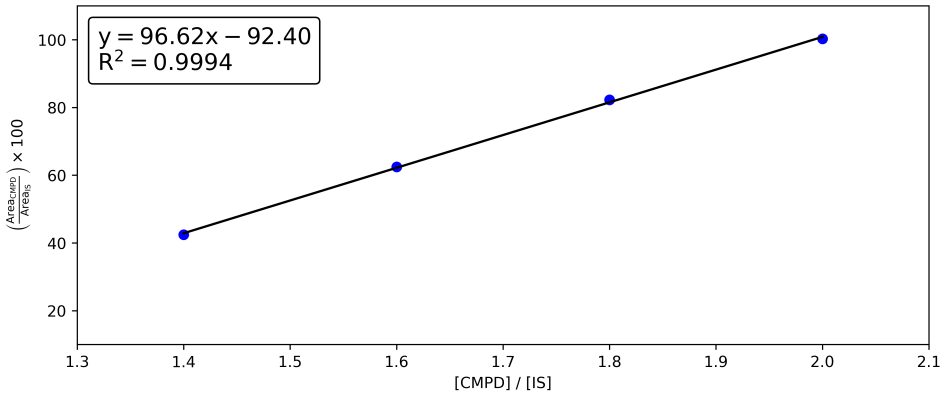

Figure 5.16. *Calibration for GC yields of* ***10a***

$$R_A = \left(\frac{\text{CMPD Peak Area}}{\text{IS Peak Area}}\right) \times 100$$

$$[\text{CMPD}] = [\text{IS}] \times \left(\frac{R_A + 92.40}{96.62}\right)$$

[**10a**]/[IS] = 1.2

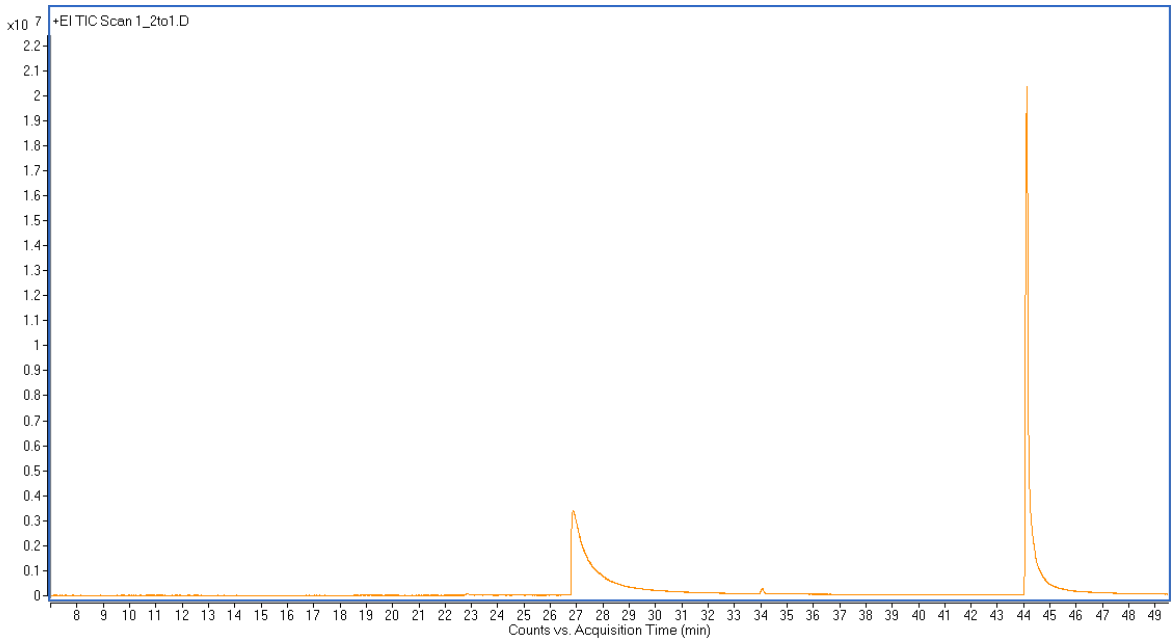

[**10a**]/[IS] = 1.4

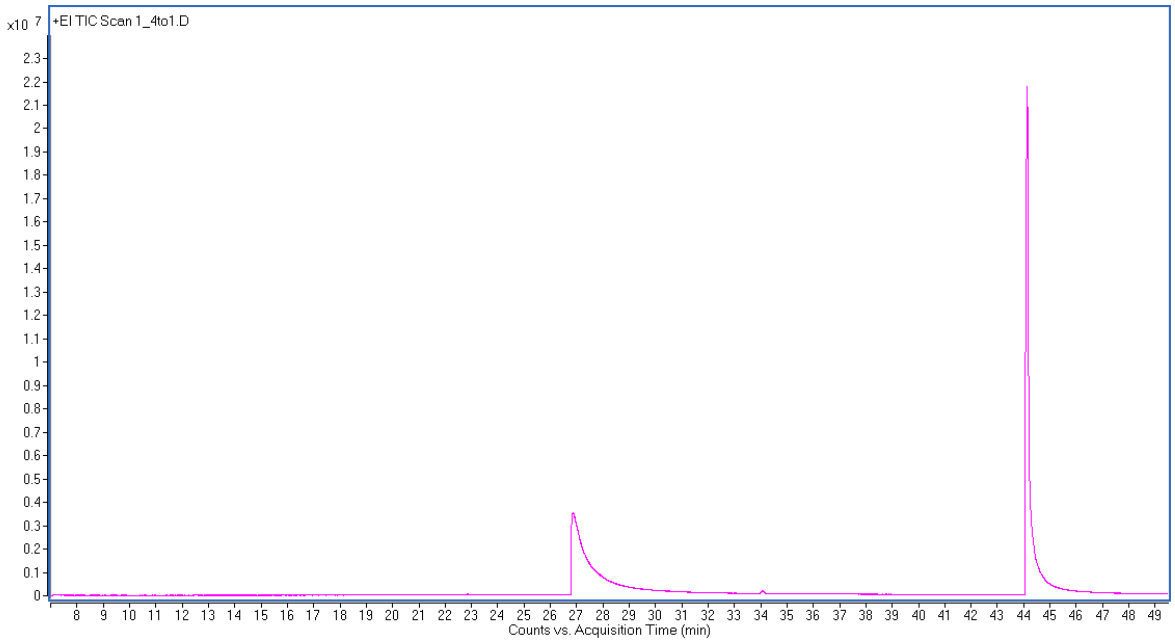

[**10a**]/[IS] = 1.6

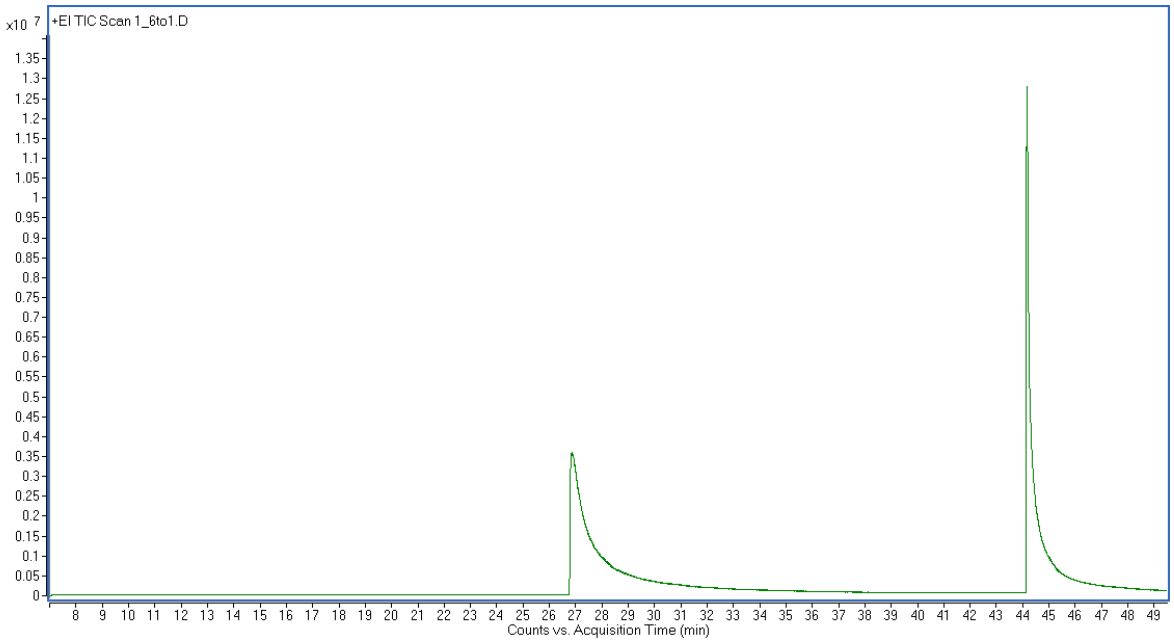

[**10a**]/[IS] = 1.8

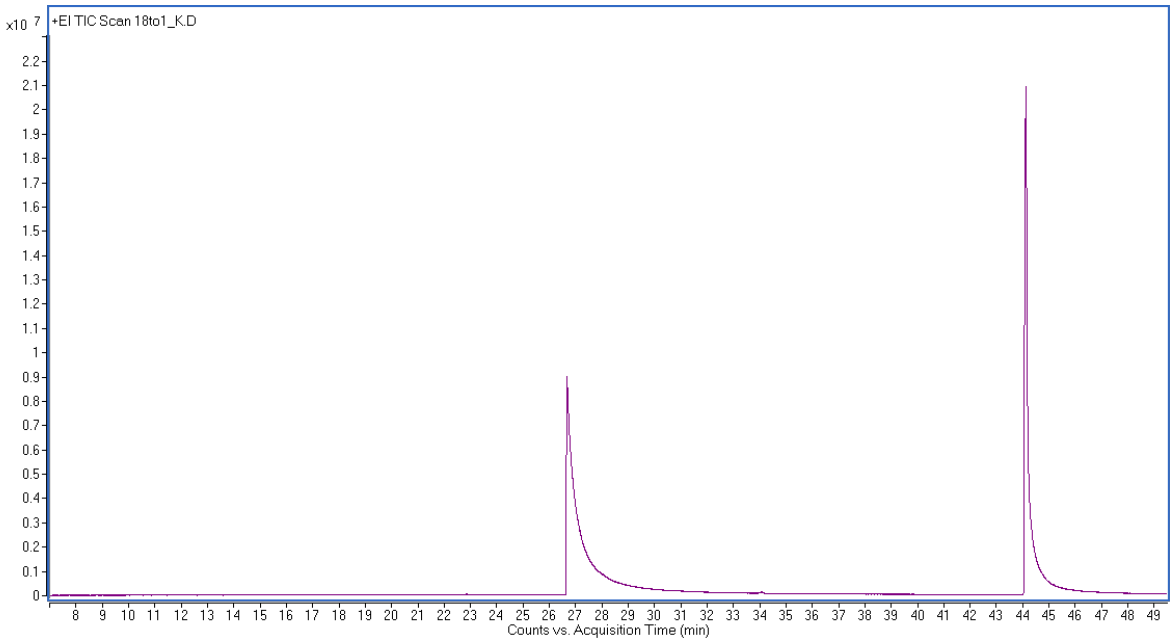

[**10a**]/[IS] = 2

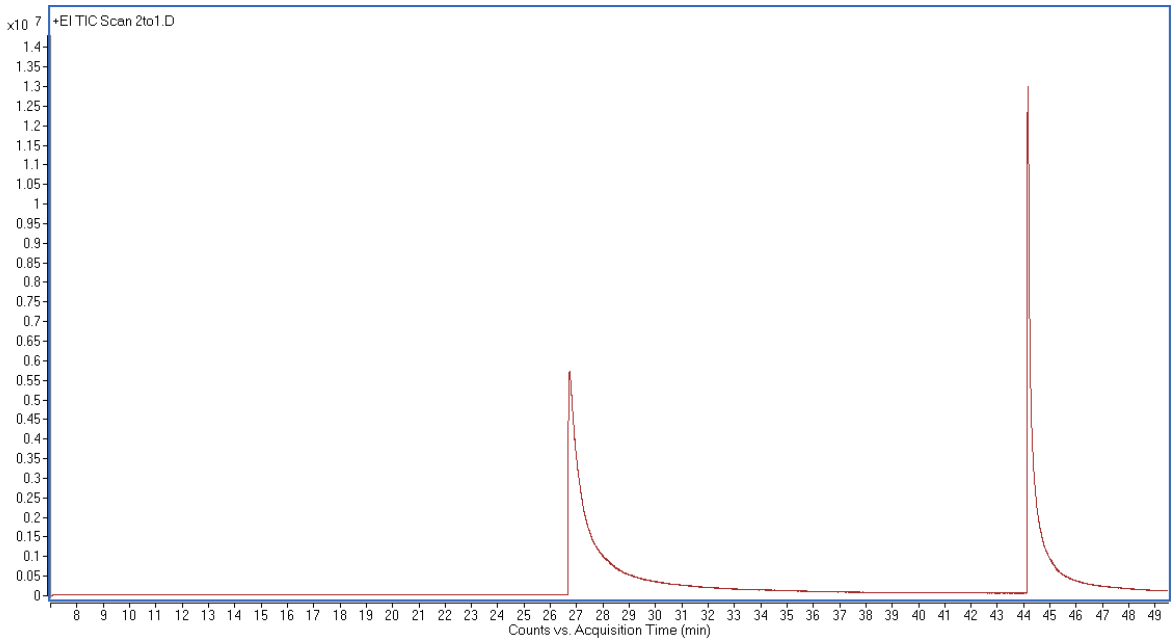

GC Traces Pertaining to Time Course

GC trace of General Procedure A for **10** after 72 H (on initial photoreactor)

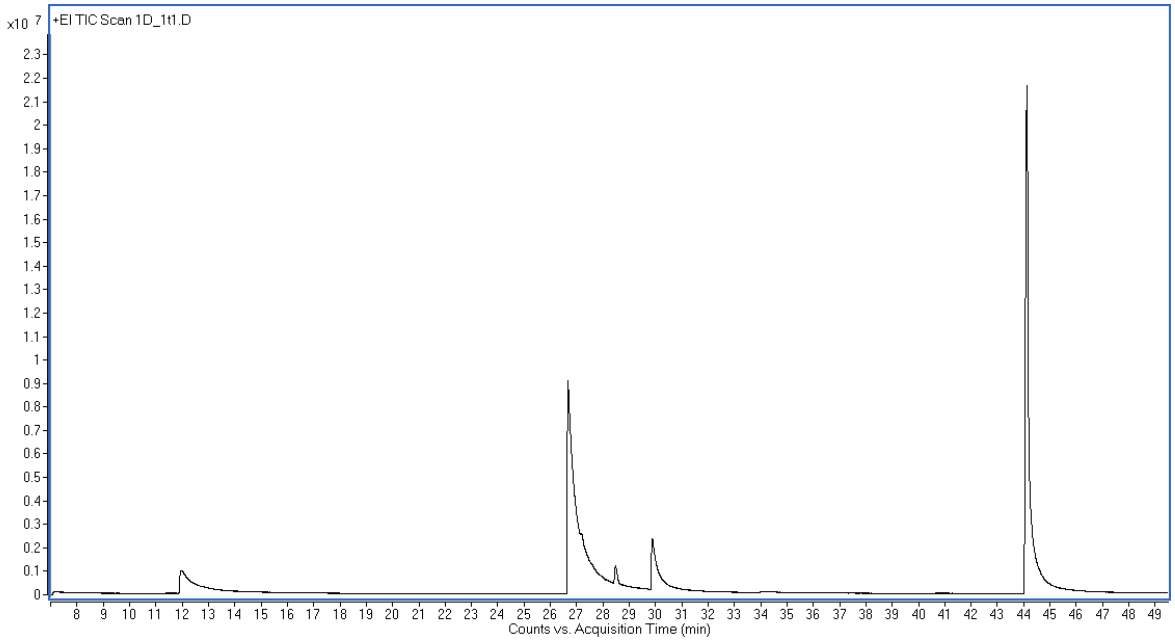

GC trace of General Procedure A for **10** after 48 H (on initial photoreactor)

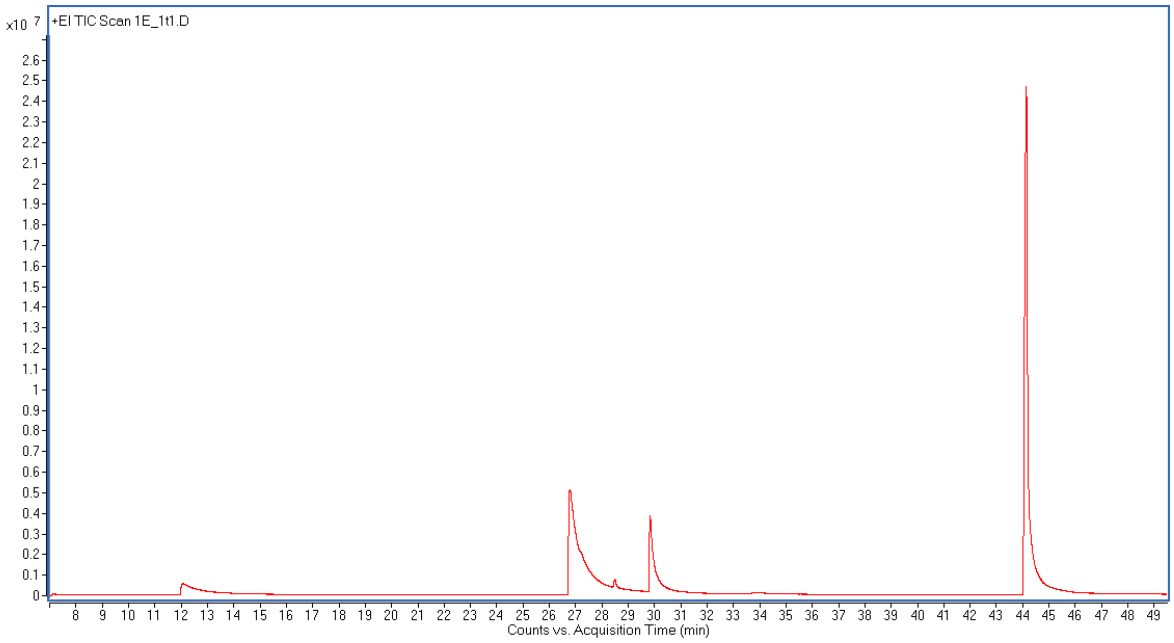

GC trace of General Procedure A for **10** after 24 H (on initial photoreactor)

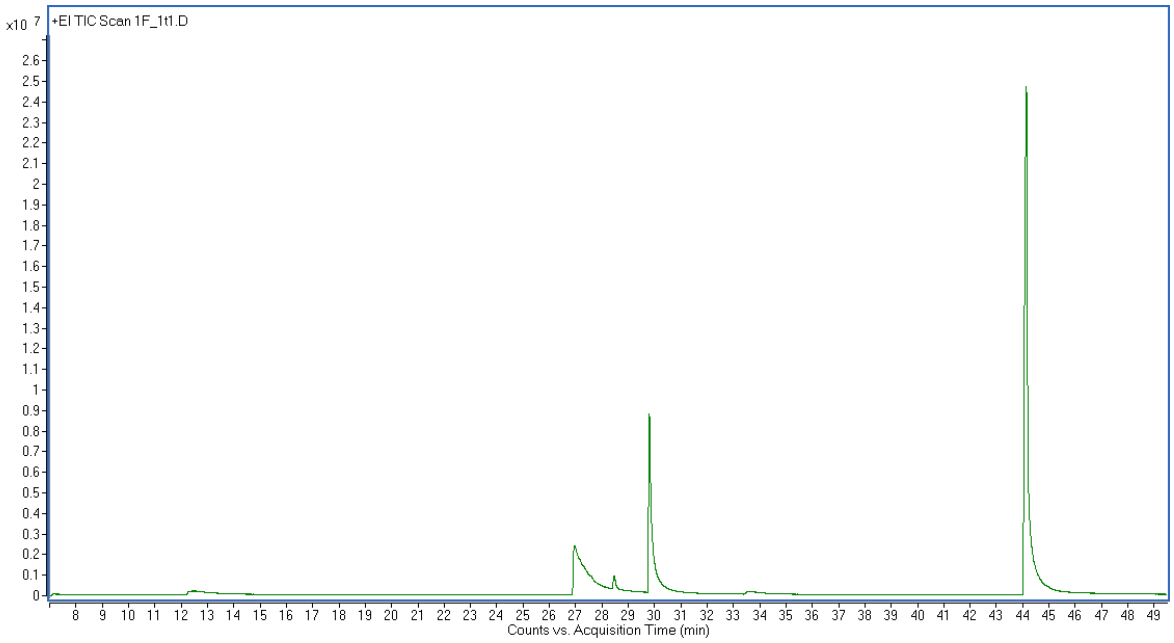

GC trace of General Procedure A for **10** after 7 H (on initial photoreactor)

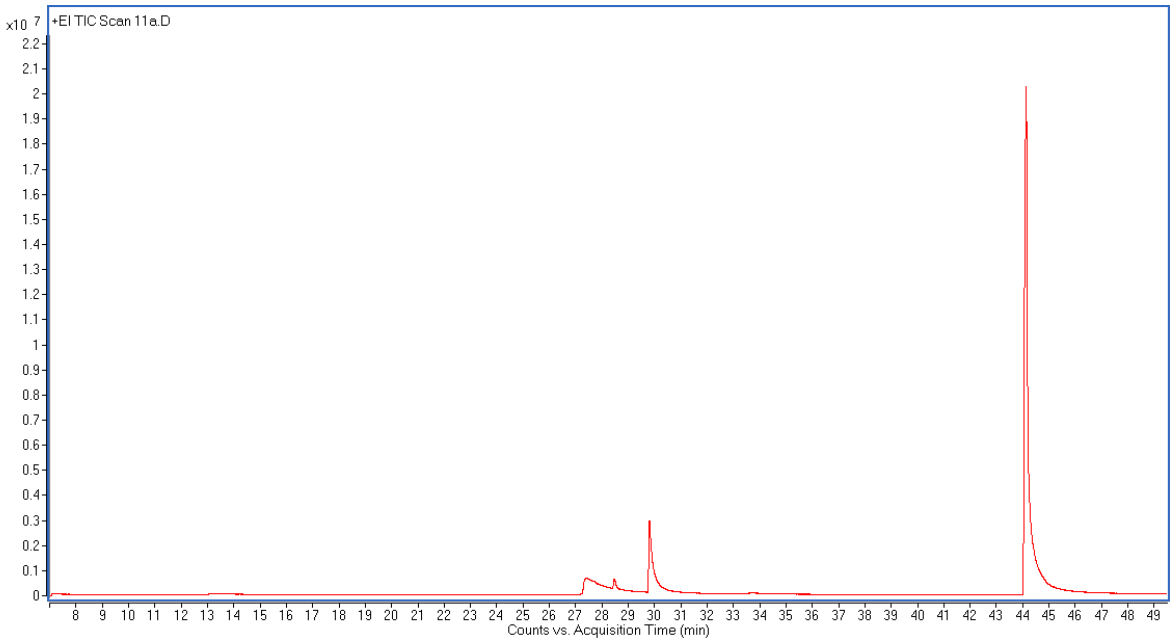

GC trace of General Procedure A for **10** after 1 H (on initial photoreactor)

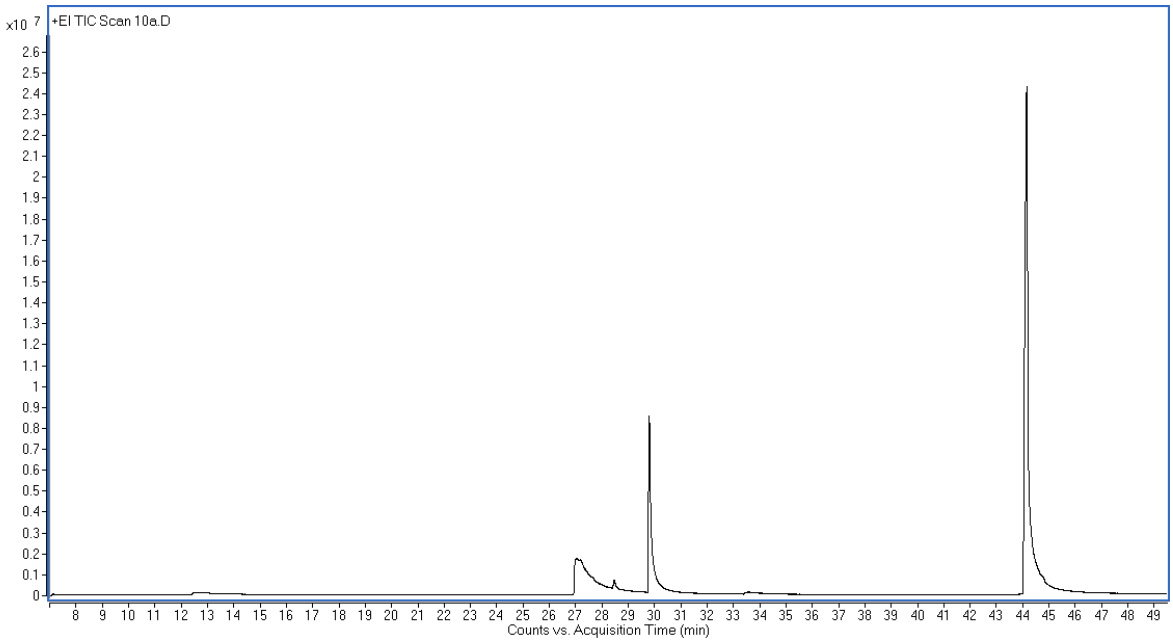

GC trace of General Procedure A for **10** after 7 H (on second generation photoreactor)

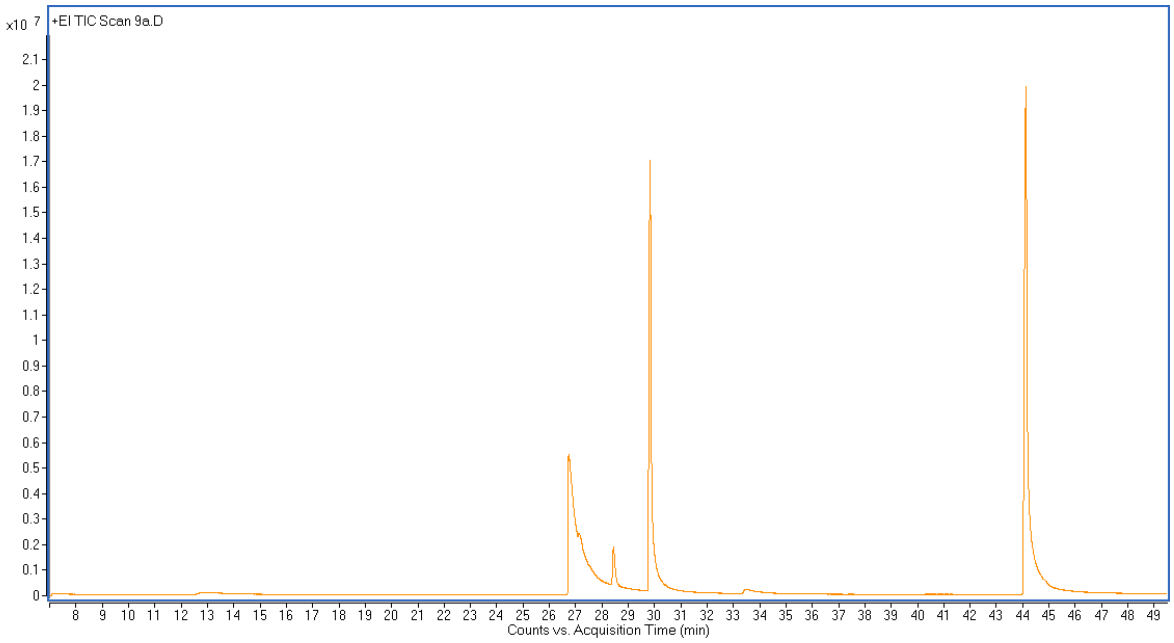

GC trace of General Procedure A for **10** after 1 H (on second generation photoreactor)

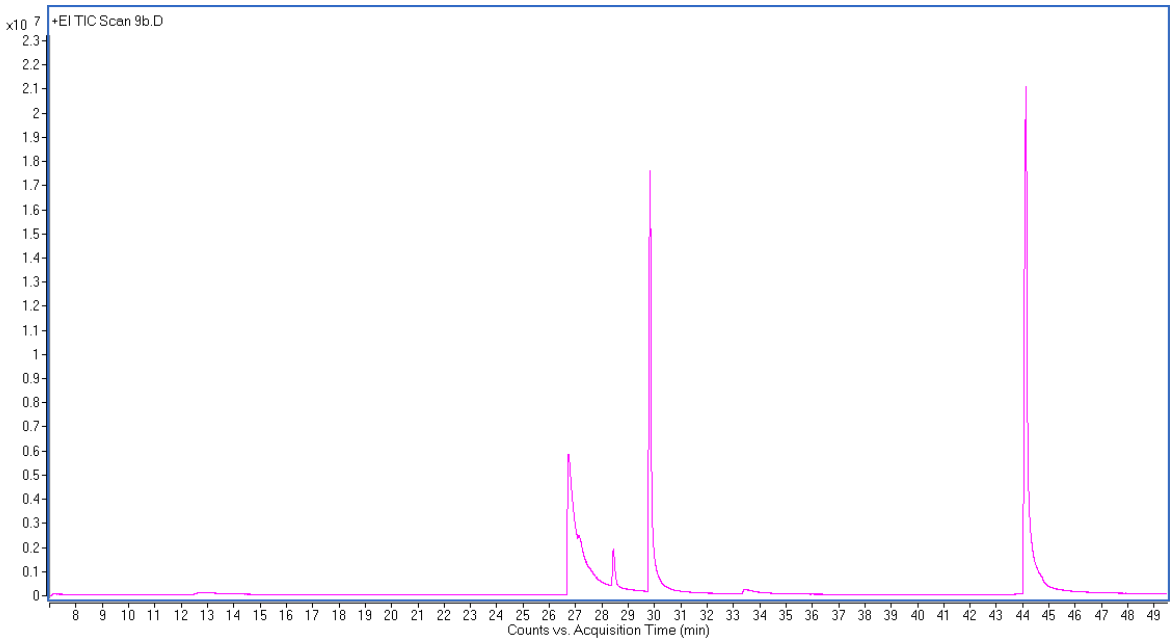

GC trace of General Procedure A for **10** after 7 H (on second generation photoreactor - without cooling)

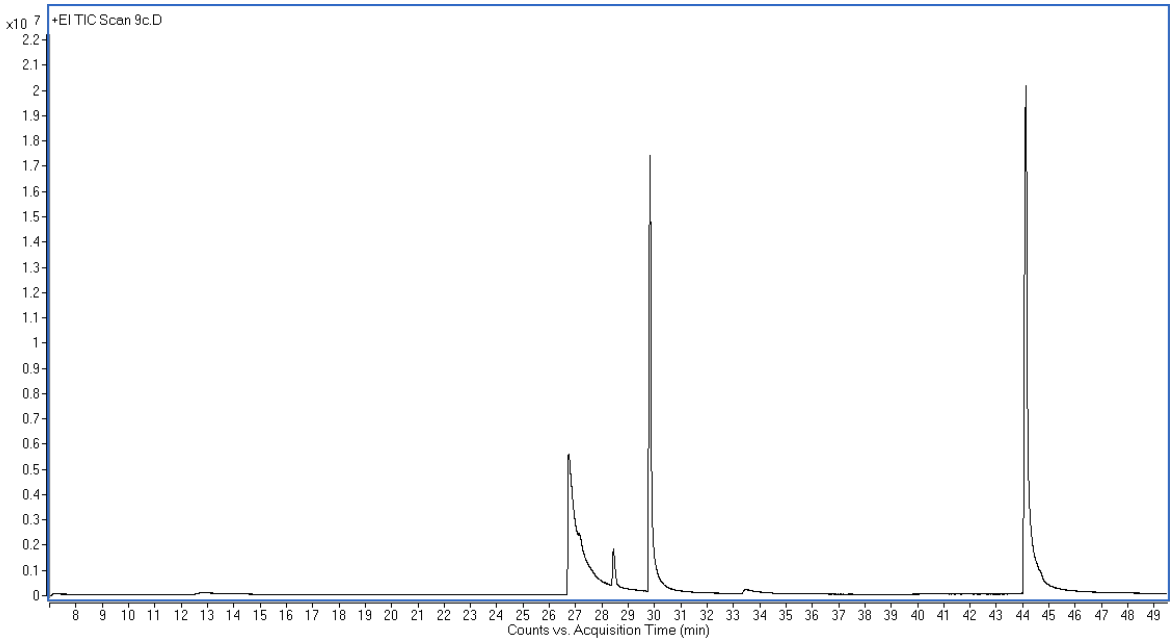

GC Traces Pertaining to the Effect of Additives

GC trace of General Procedure A for **10** with TFA

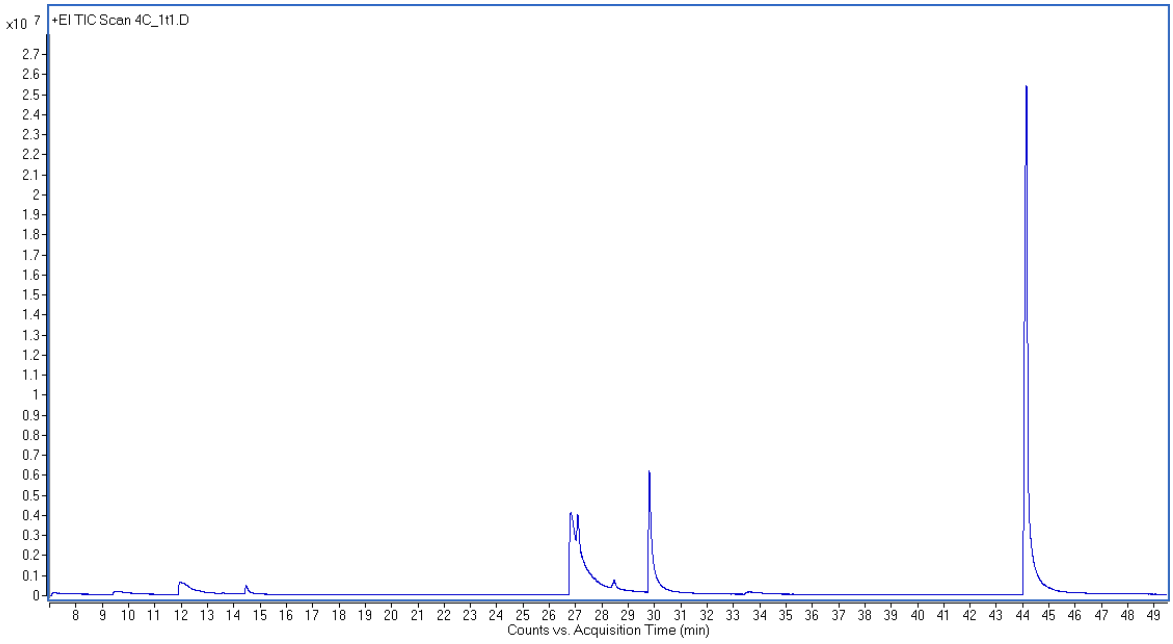

GC trace of General Procedure A for **10** with Acetic acid

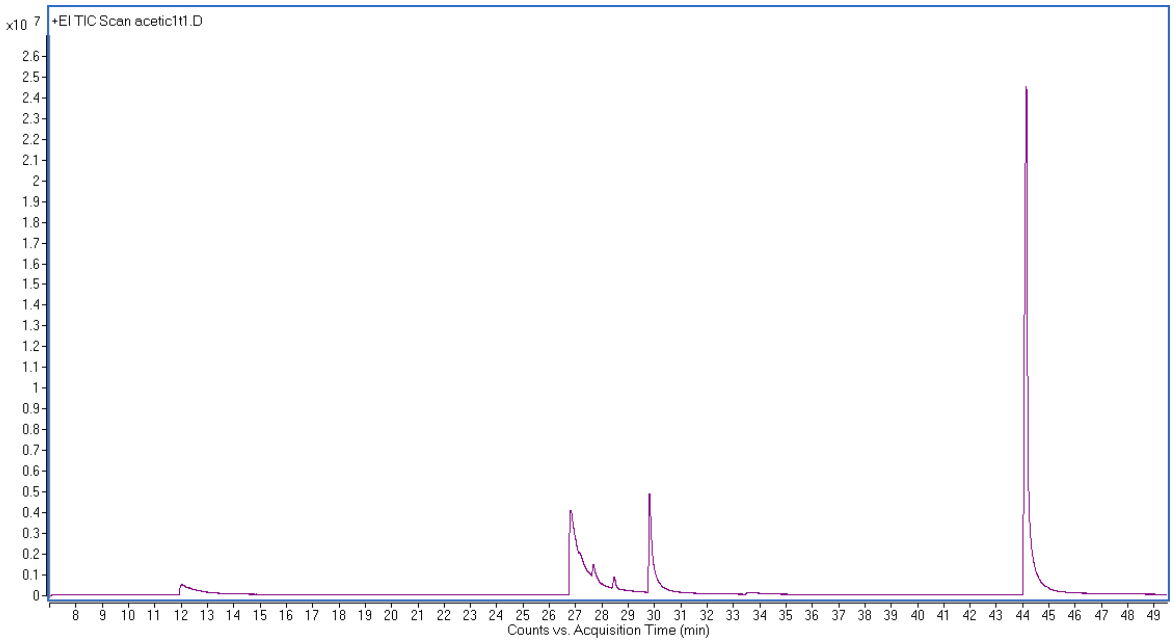

GC trace of General Procedure A for **10** with Phosphoric acid

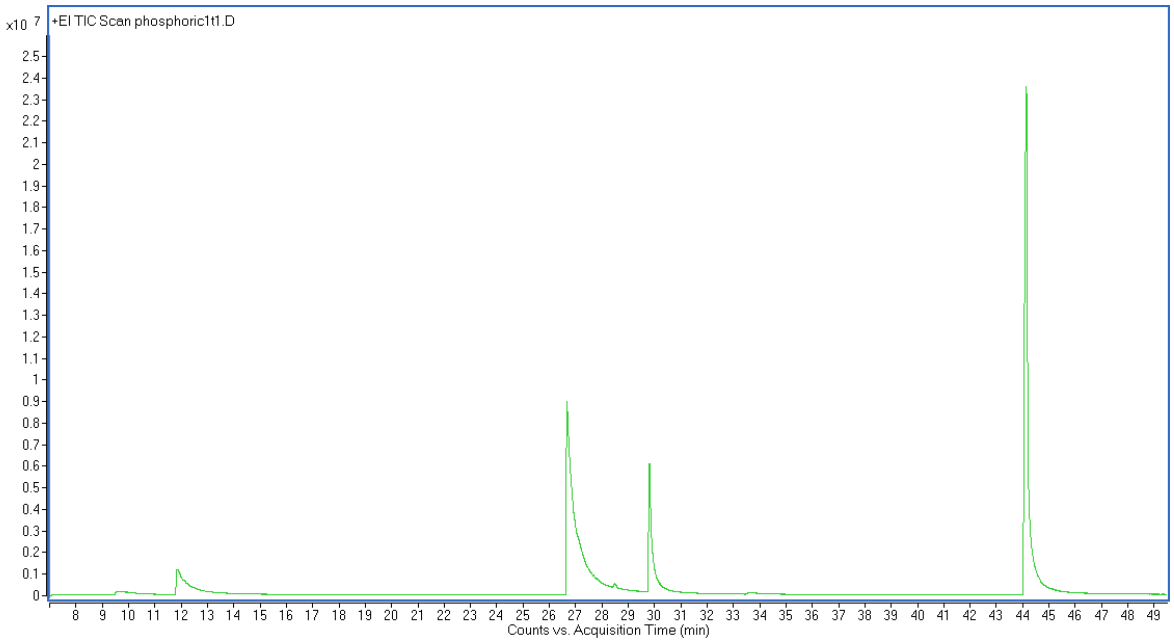

GC trace of General Procedure A for **10** with Hydrochloric acid

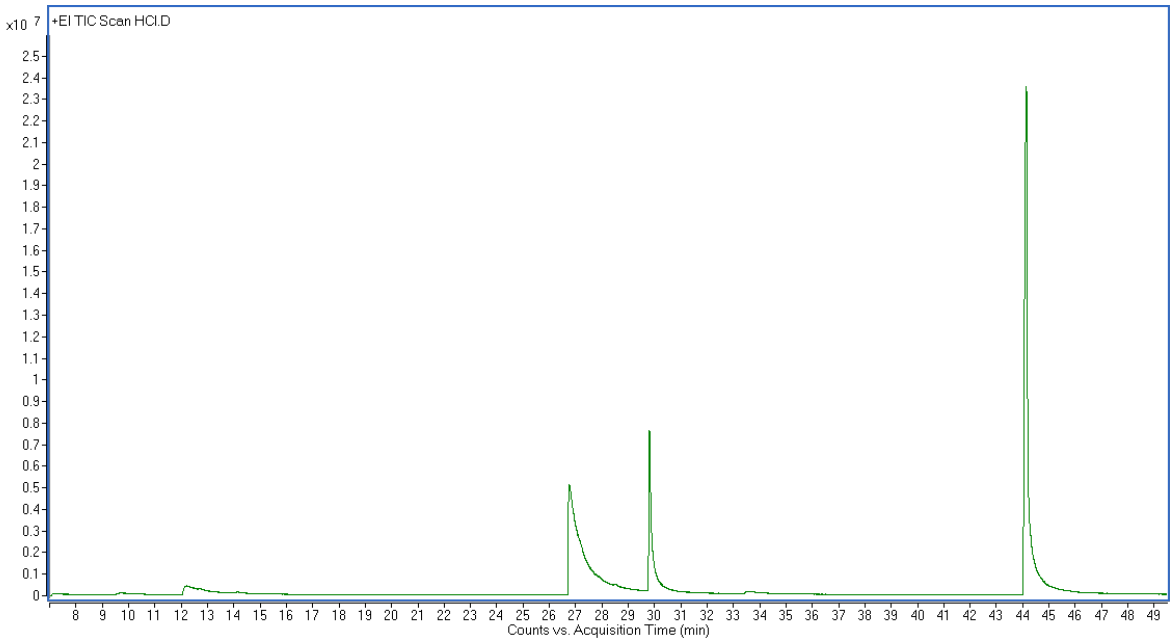

GC trace of General Procedure A for **10** with Sulfuric acid

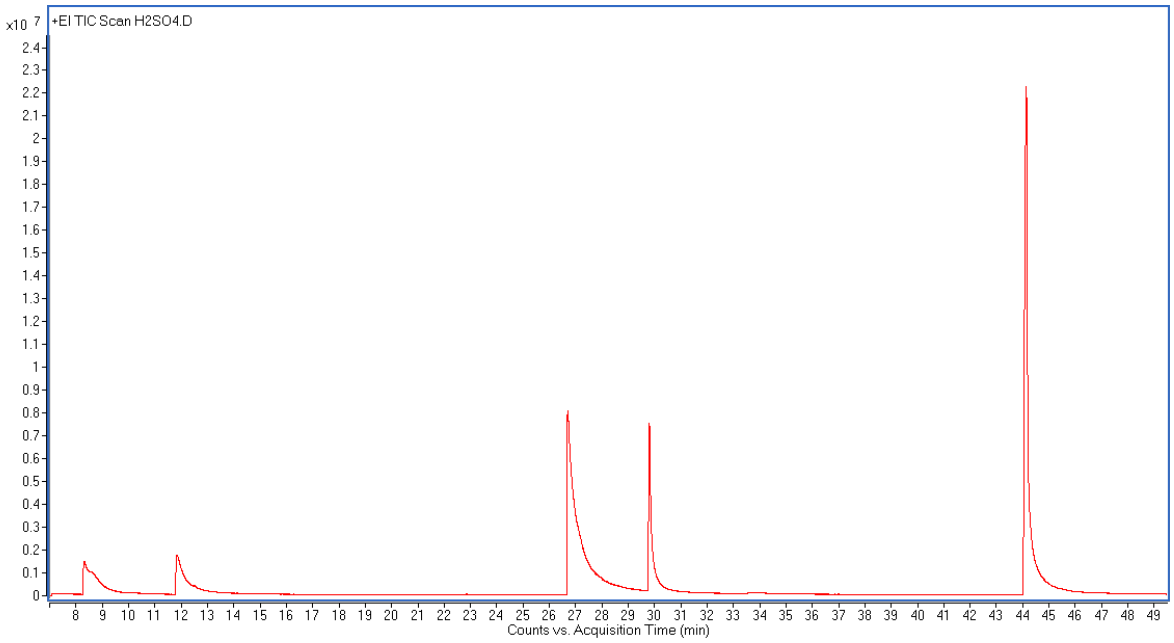

GC trace of General Procedure A for **10** with Sulfuric acid and No TBN

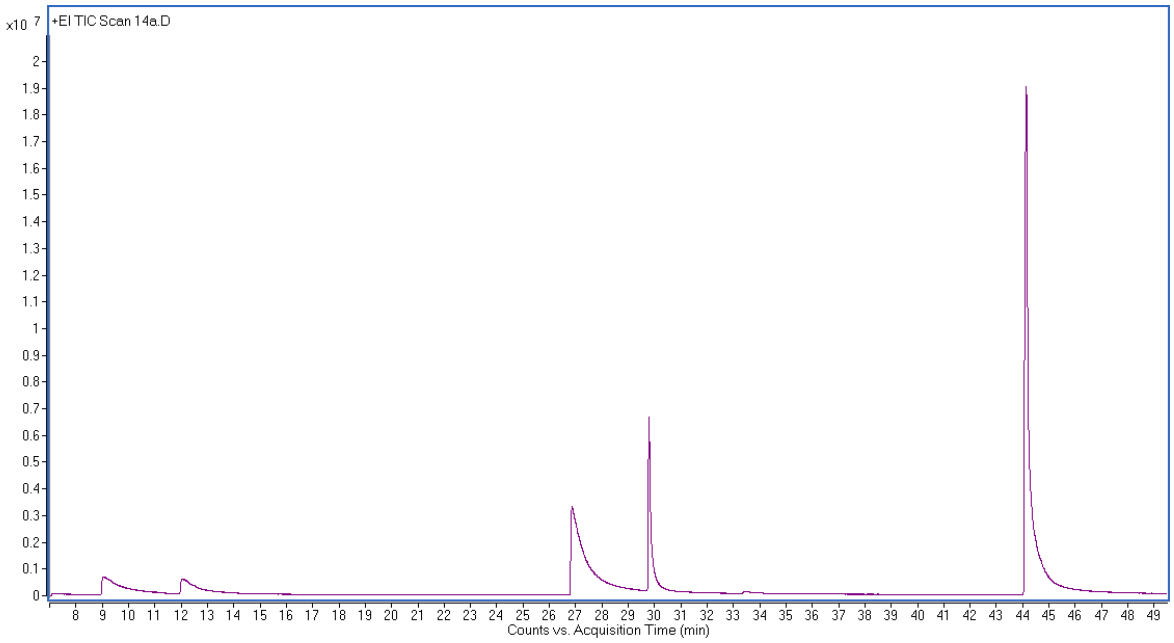

GC Traces Pertaining to the Effect of Catalyst Loading

GC trace of General Procedure A for **10** with 70 mol% DDQ

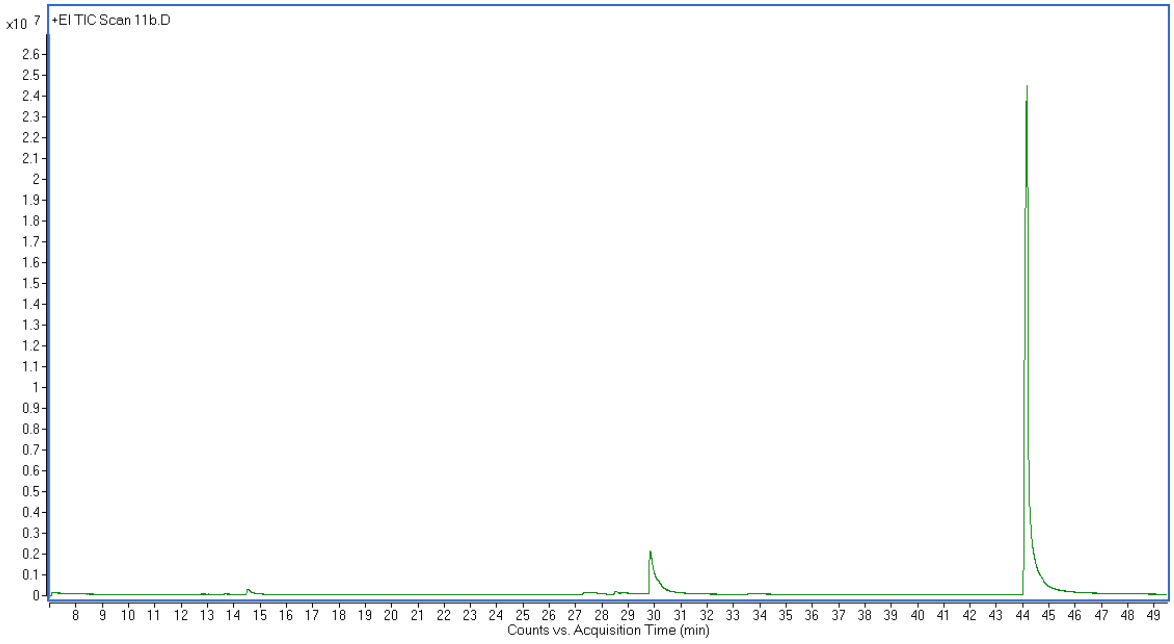

GC trace of General Procedure A for **10** with 50 mol% DDQ

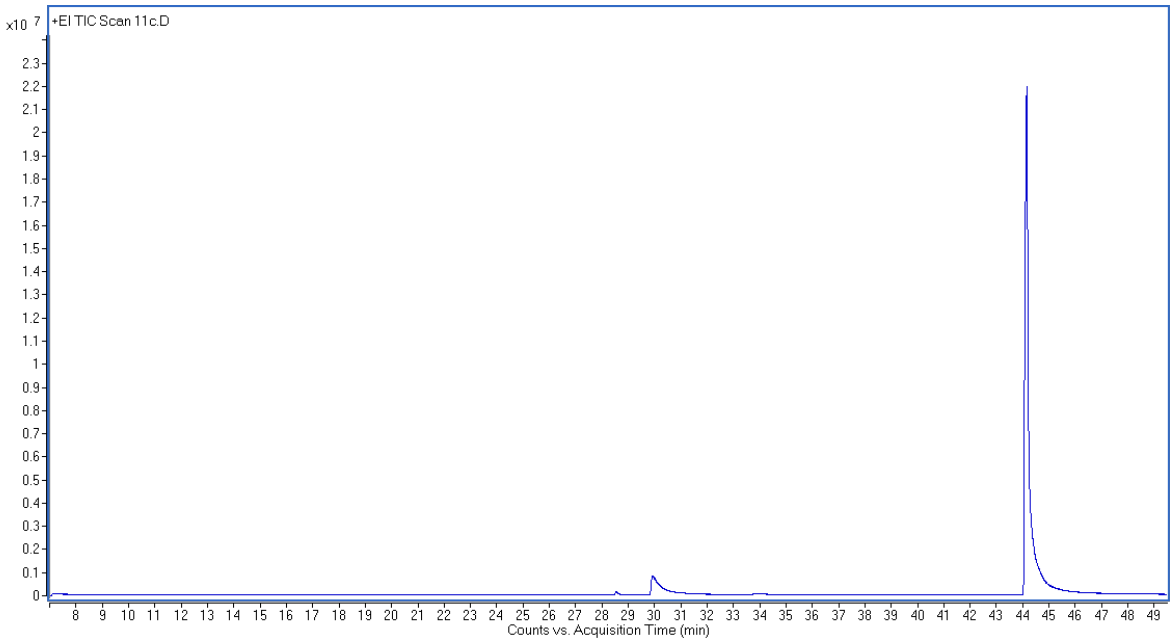

GC Traces Pertaining to Denitration Controls

GC trace of speciation test for **10c** with standard conditions

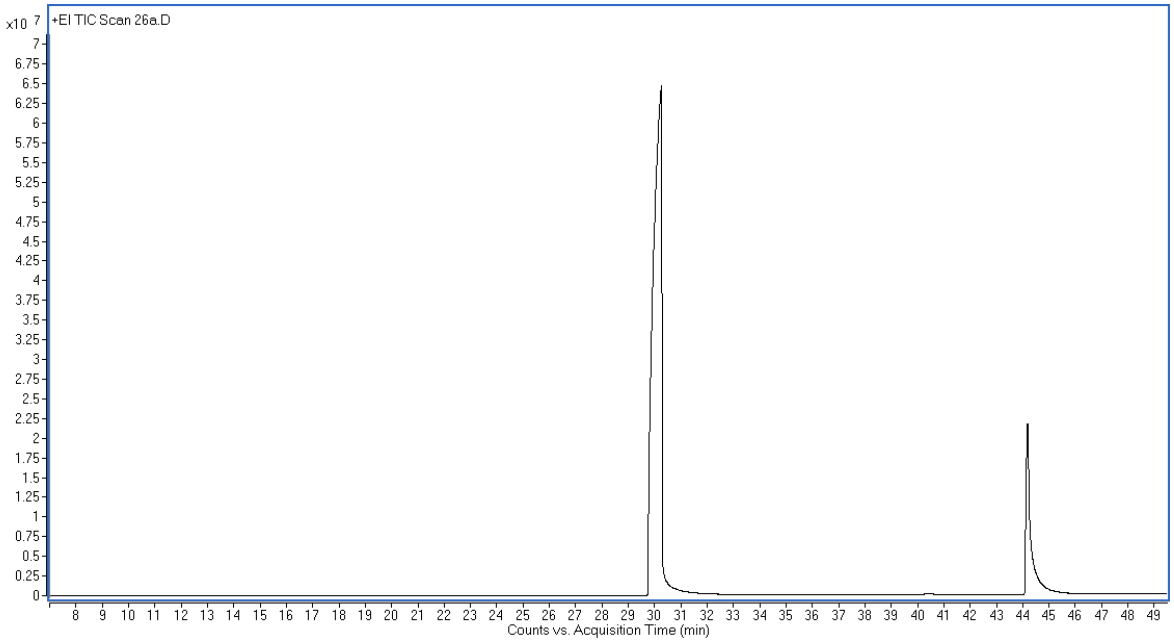

GC trace of speciation test for **10c** without light

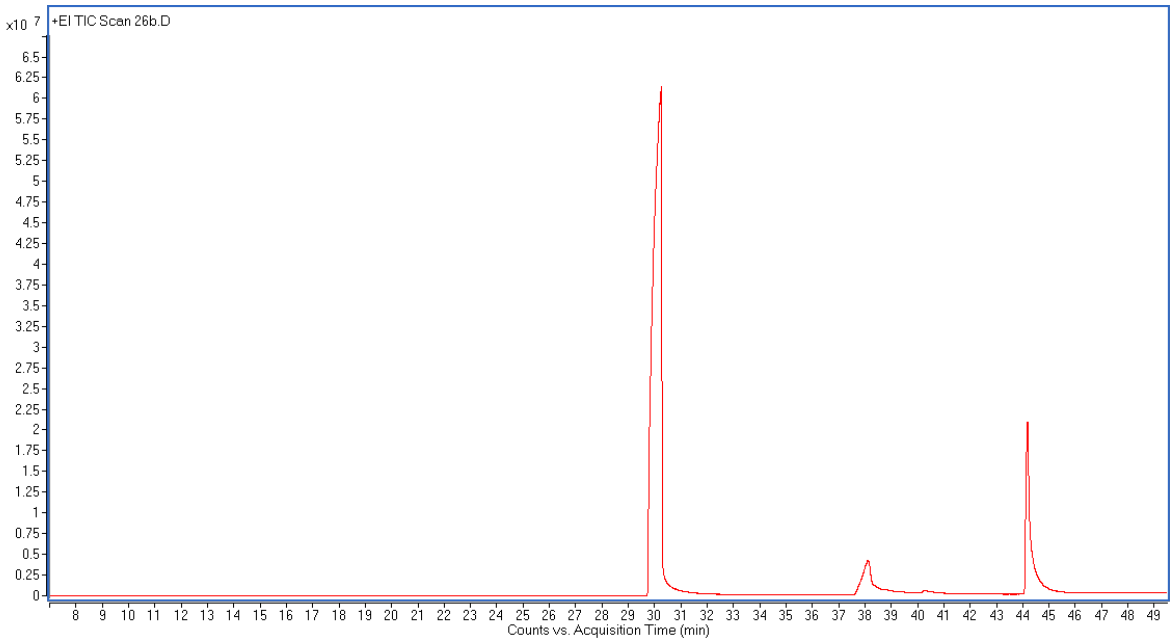

GC trace of speciation test for **10c** without TBN

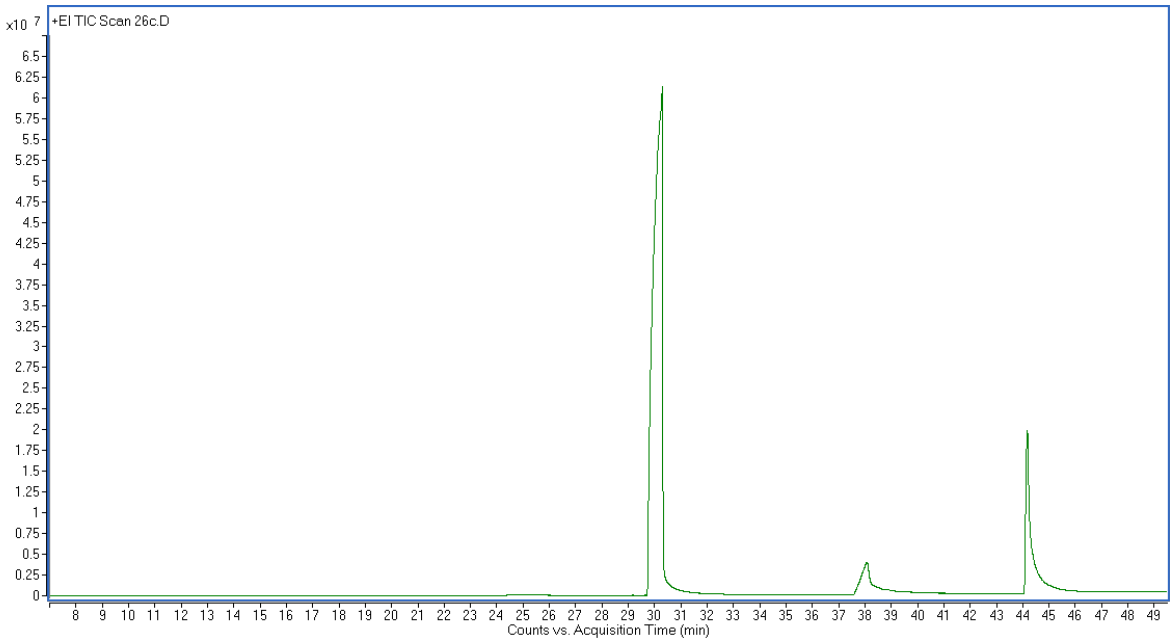

GC trace of speciation test for **10c** without light or TBN

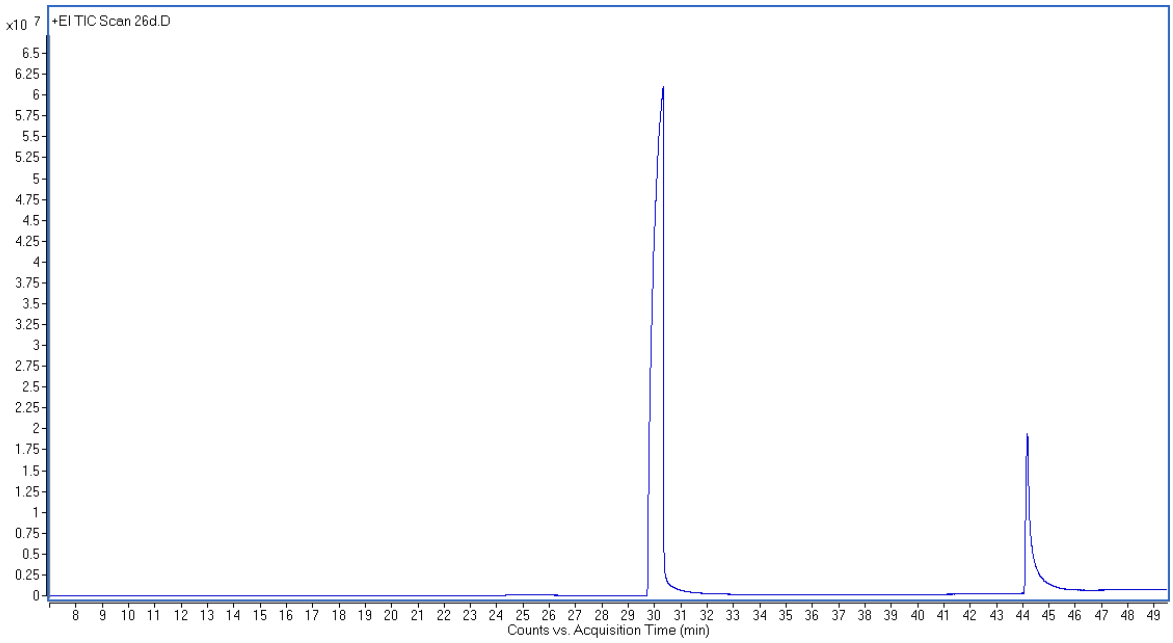

Time Course Study of S_NAr Chemistry

A time course study for the conversion of 2,4-dichlorofluorobenzene (**100**) to 2,4-dichloroanisole (**100a**), under our S_NAr conditions (see below).

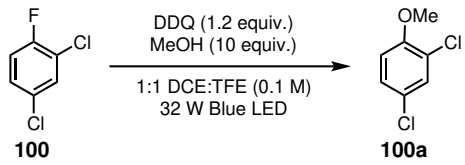

Standard condtions for time course.

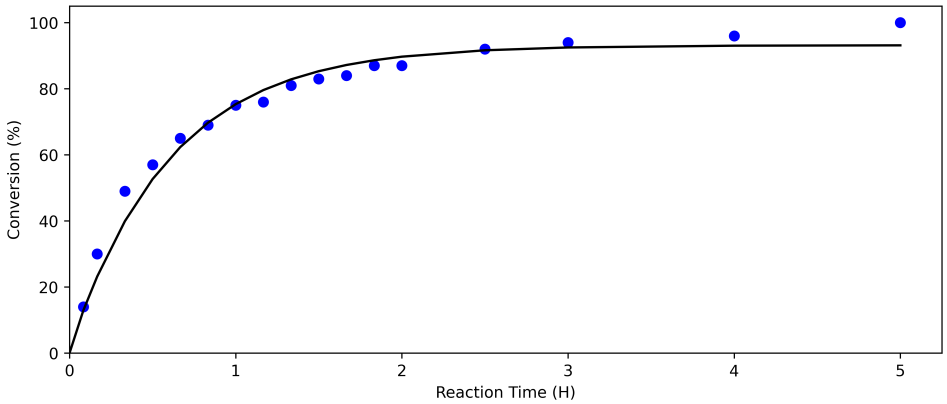

Time course results after 5 H for S_NAr chemistry, including nonlinear regression.

GC trace of S_NAr reaction after 5 min

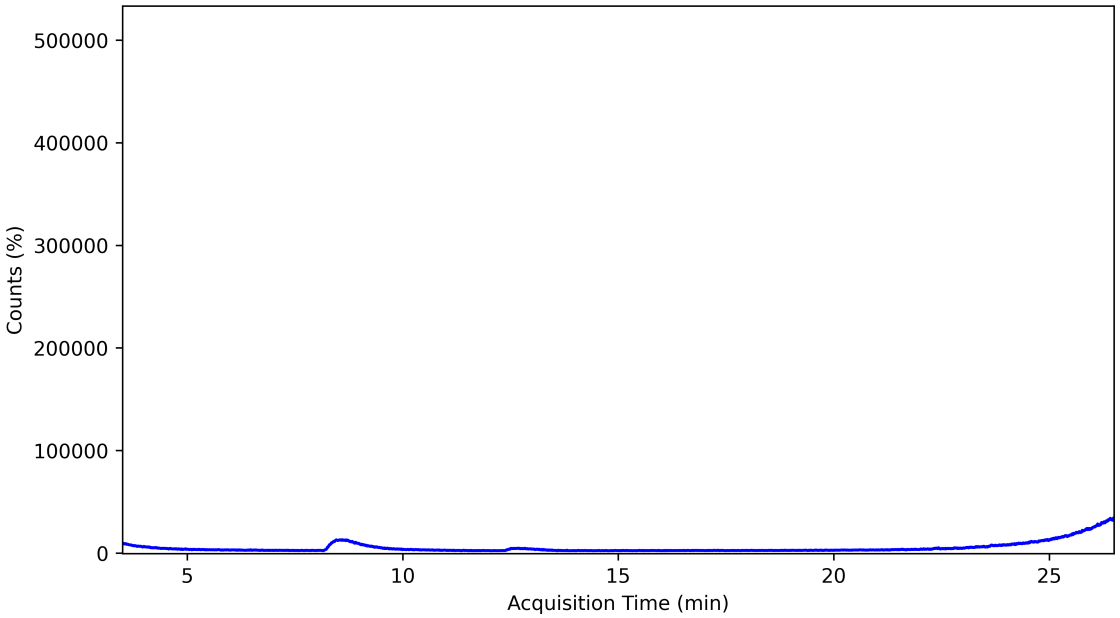

GC trace of S_NAr reaction after 10 min

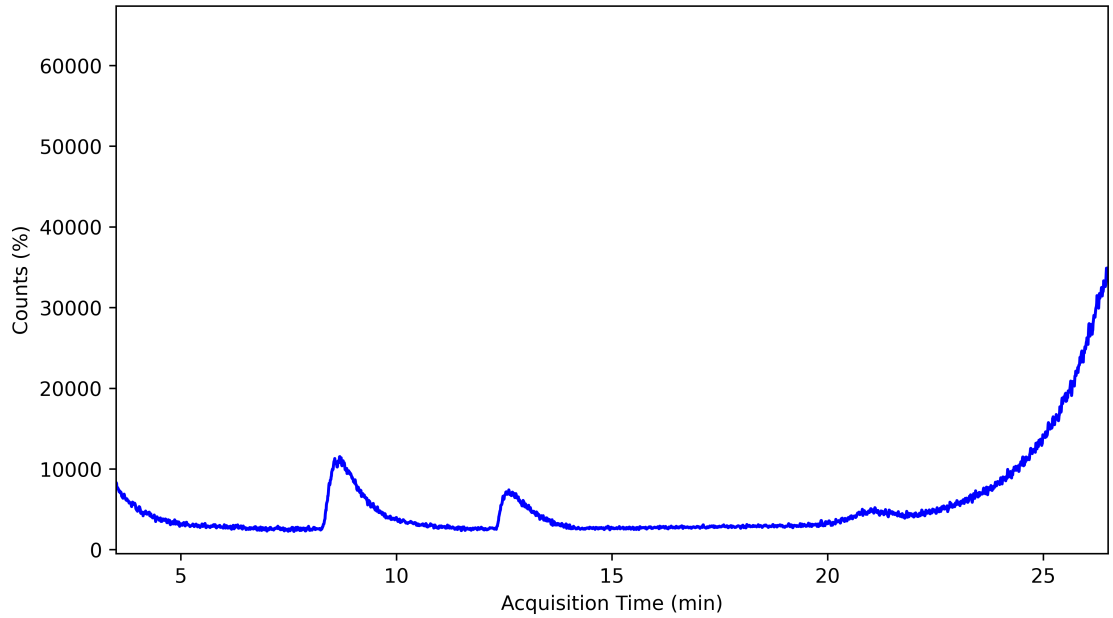

GC trace of S_NAr reaction after 20 min

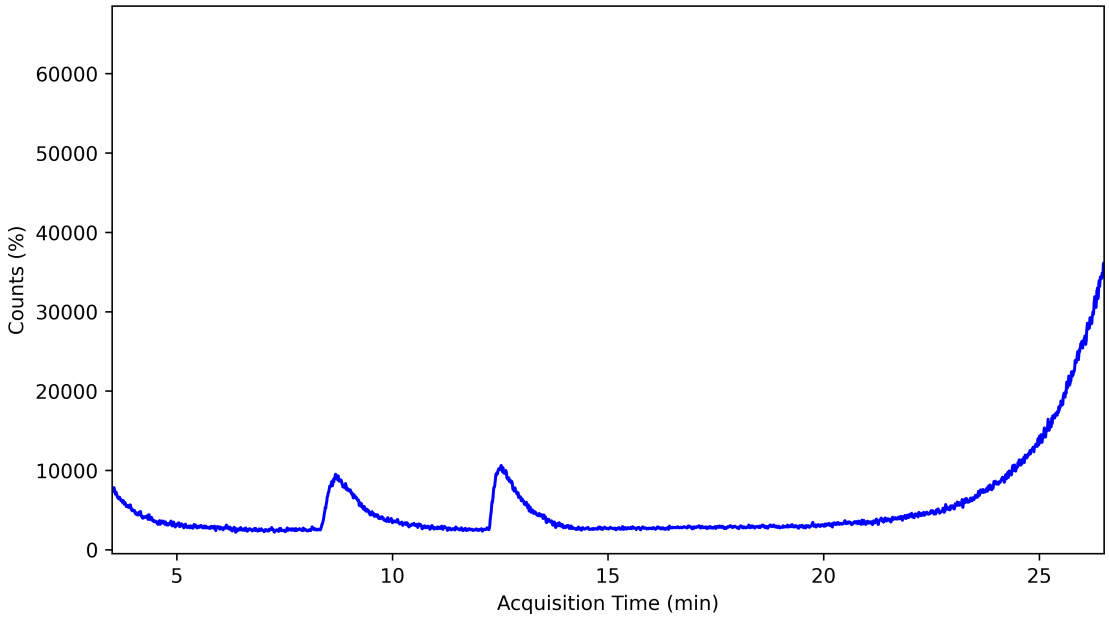

GC trace of S_NAr reaction after 30 min

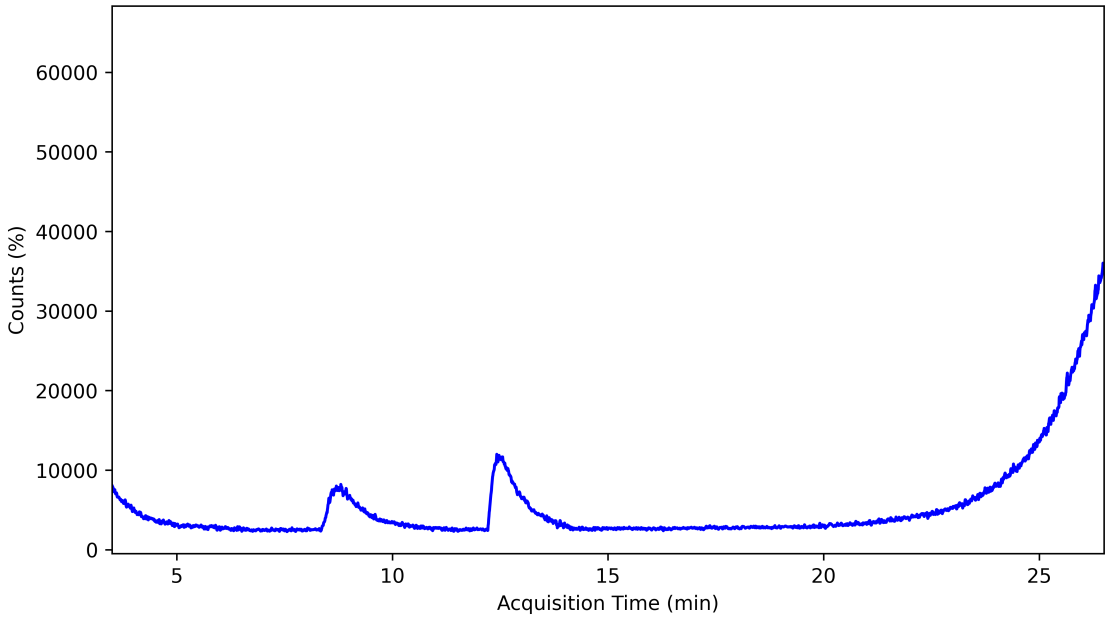

GC trace of S_NAr reaction after 40 min

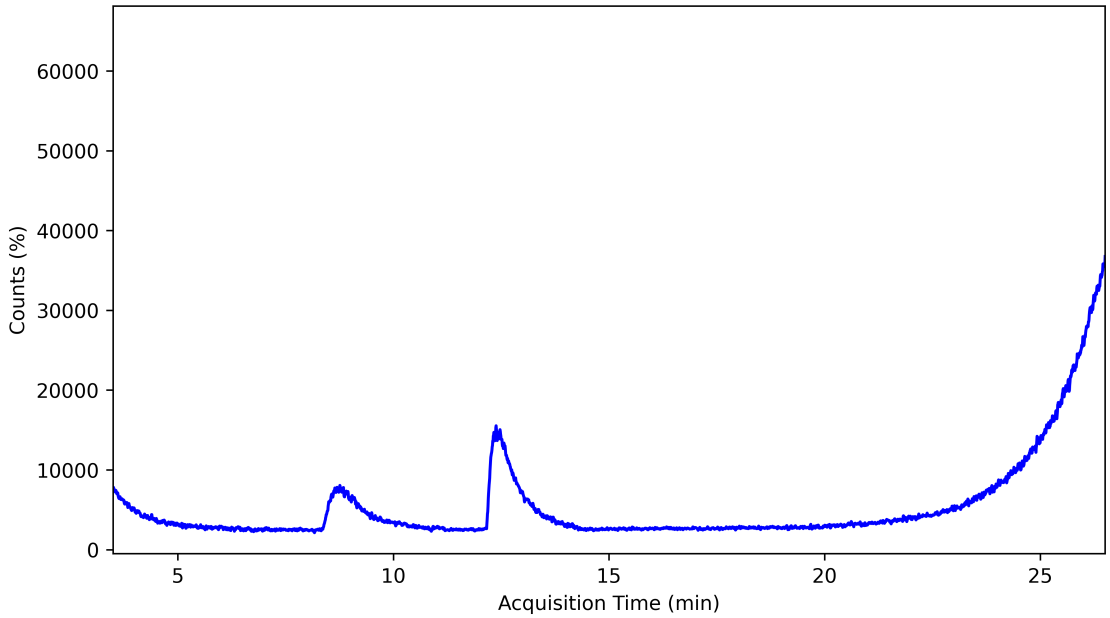

GC trace of S_NAr reaction after 50 min

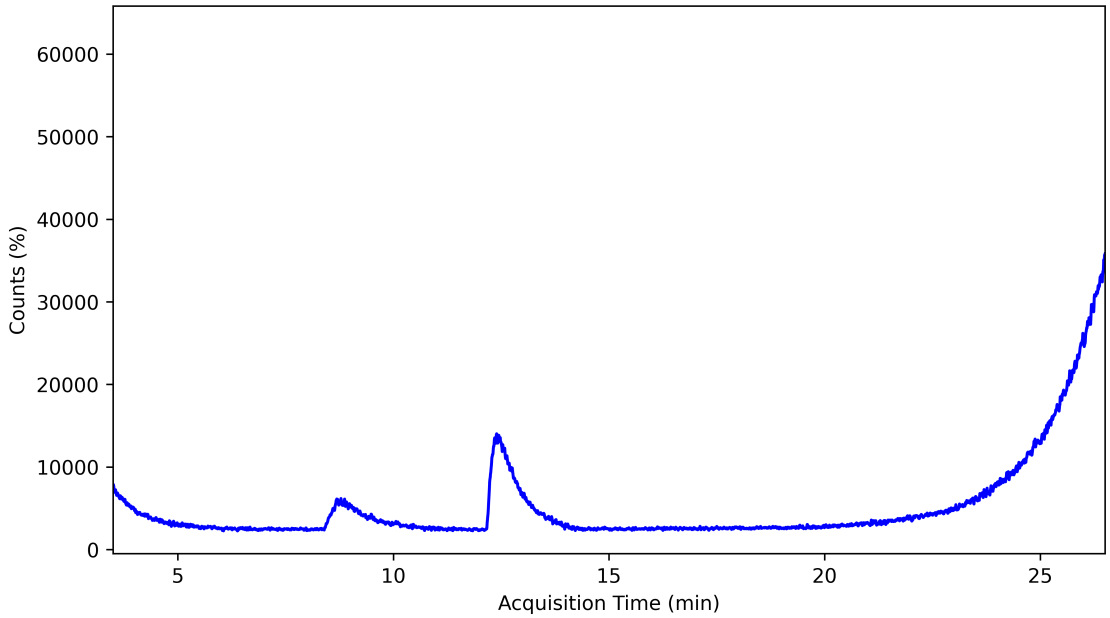

GC trace of S_NAr reaction after 1 H

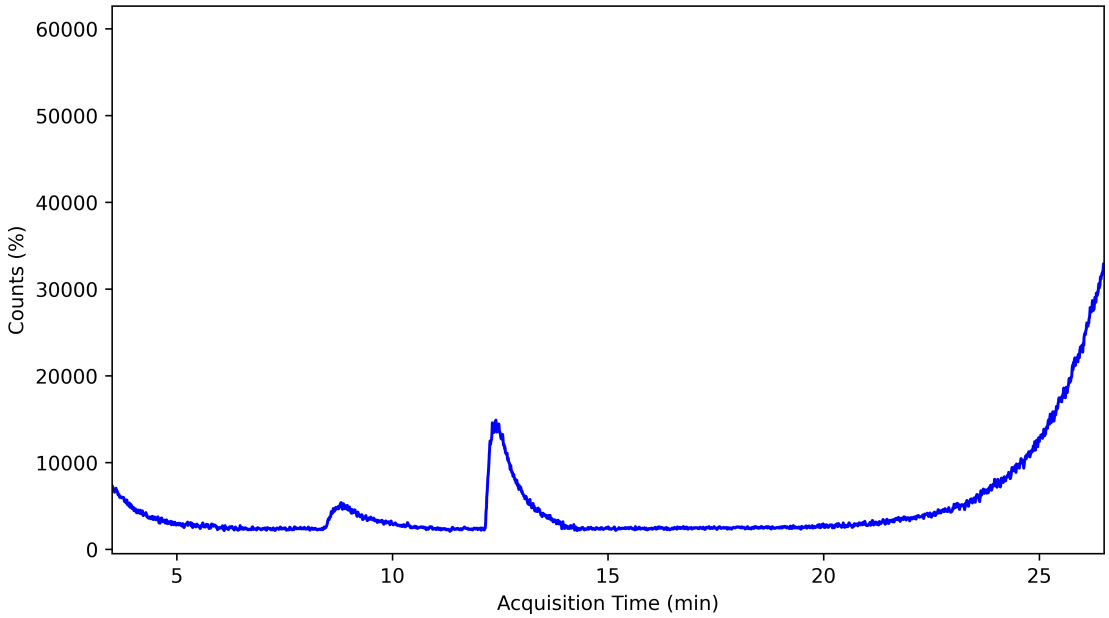

GC trace of S_NAr reaction after 1 H 10 min

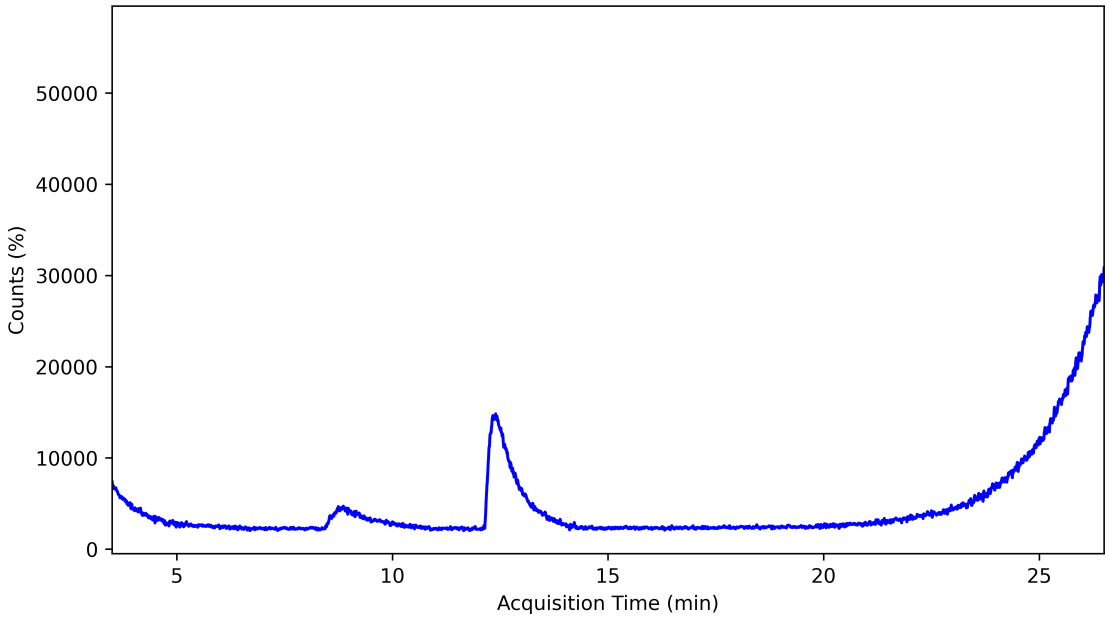

GC trace of S_NAr reaction after 1 H 20 min

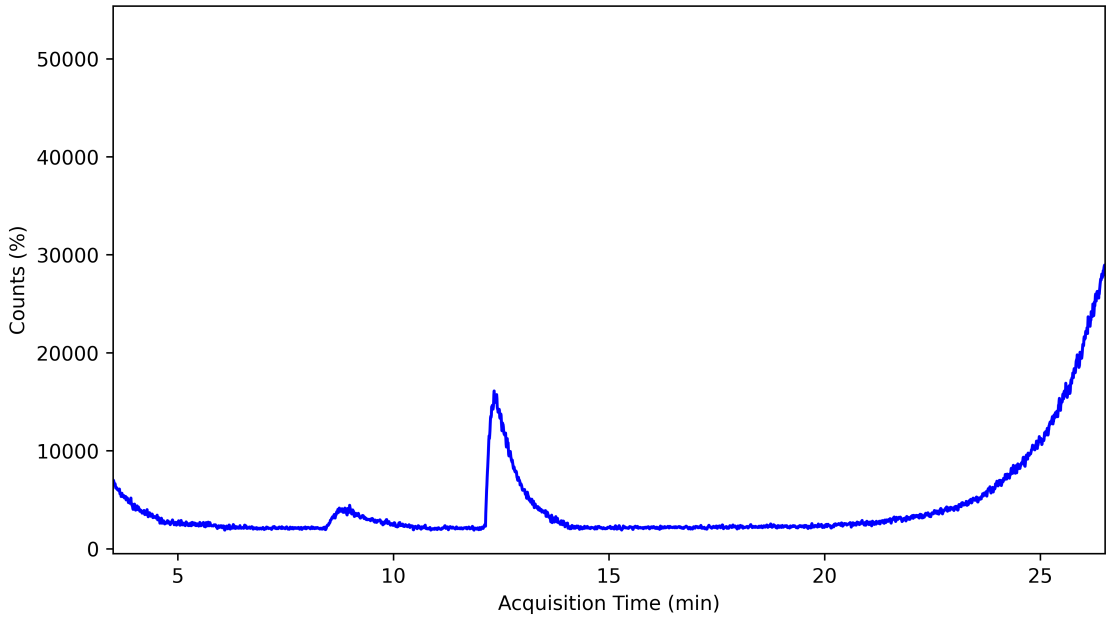

GC trace of S_NAr reaction after 1 H 30 min

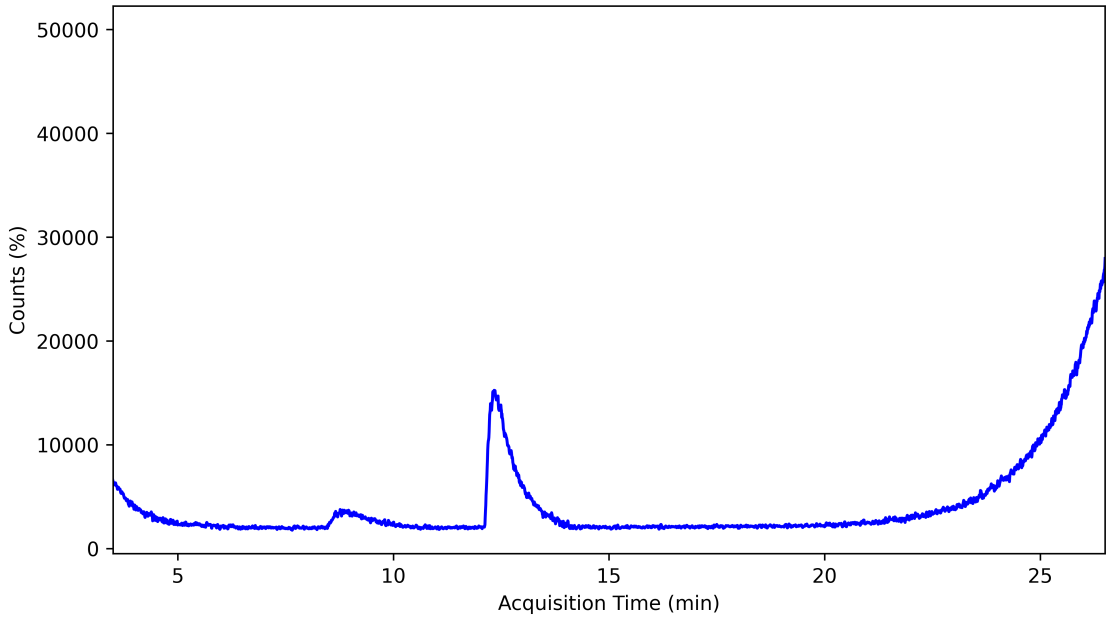

GC trace of S_NAr reaction after 1 H 40 min

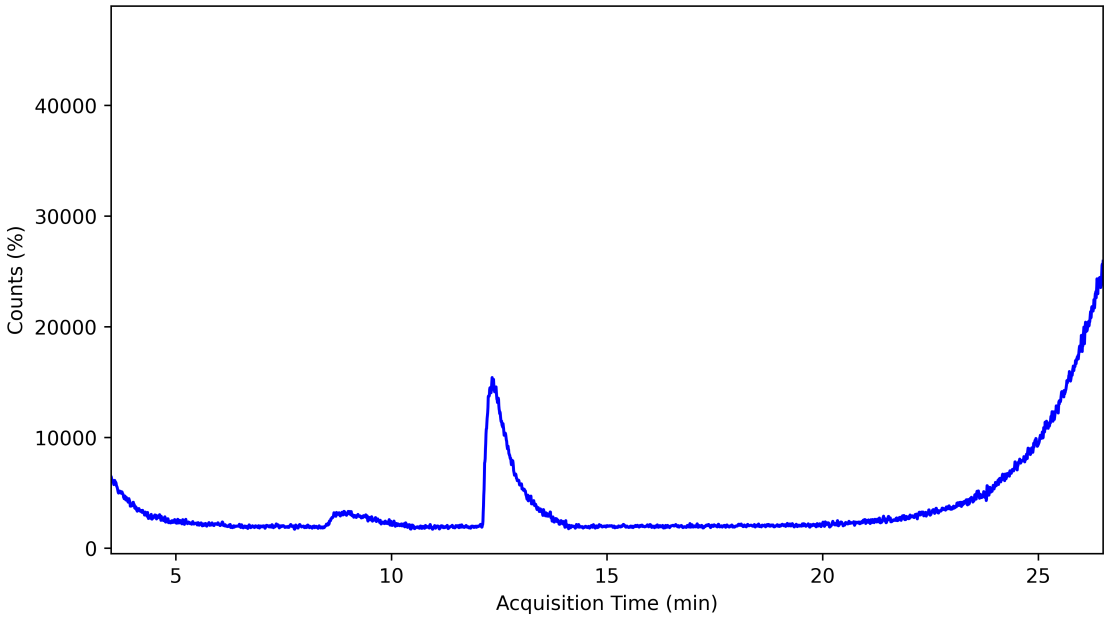

GC trace of S_NAr reaction after 1 H 50 min

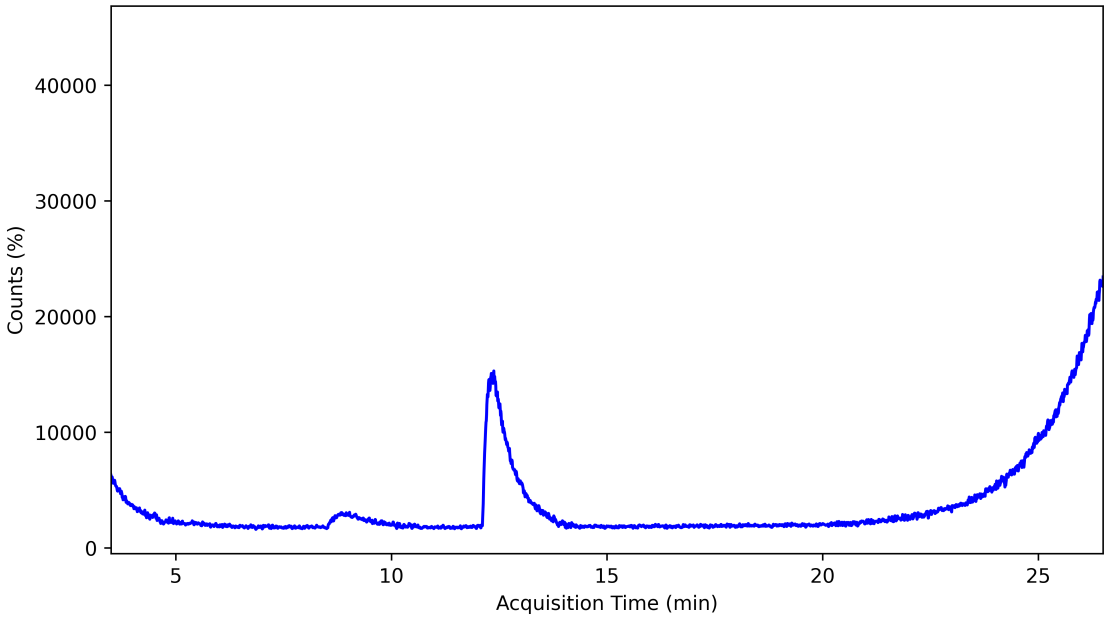

GC trace of S_NAr reaction after 2 H

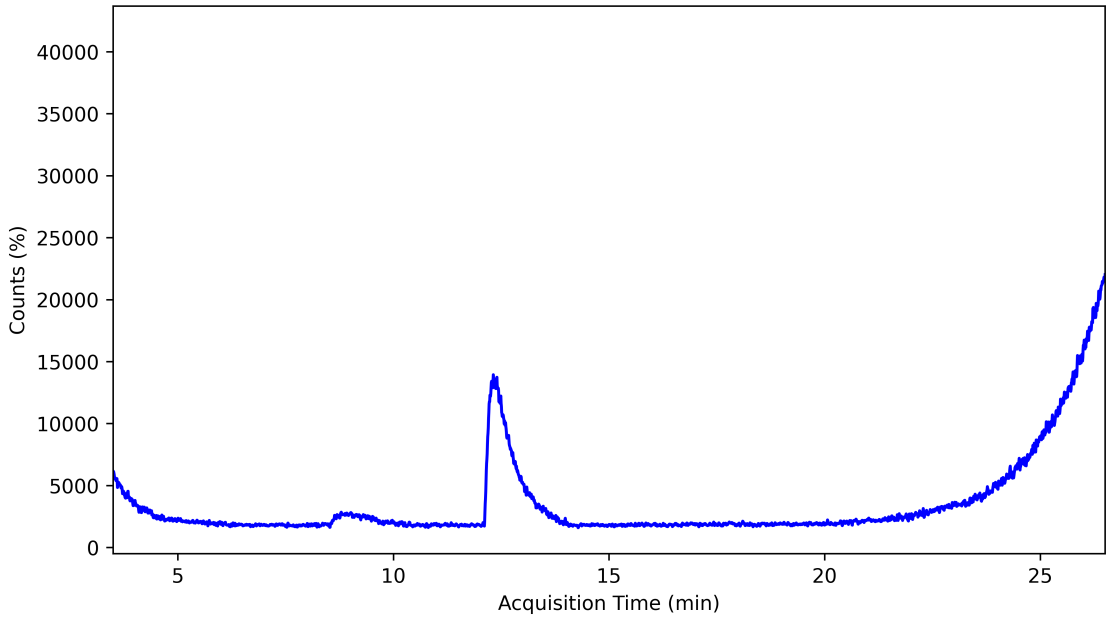

GC trace of S_NAr reaction after 2 H 30 min

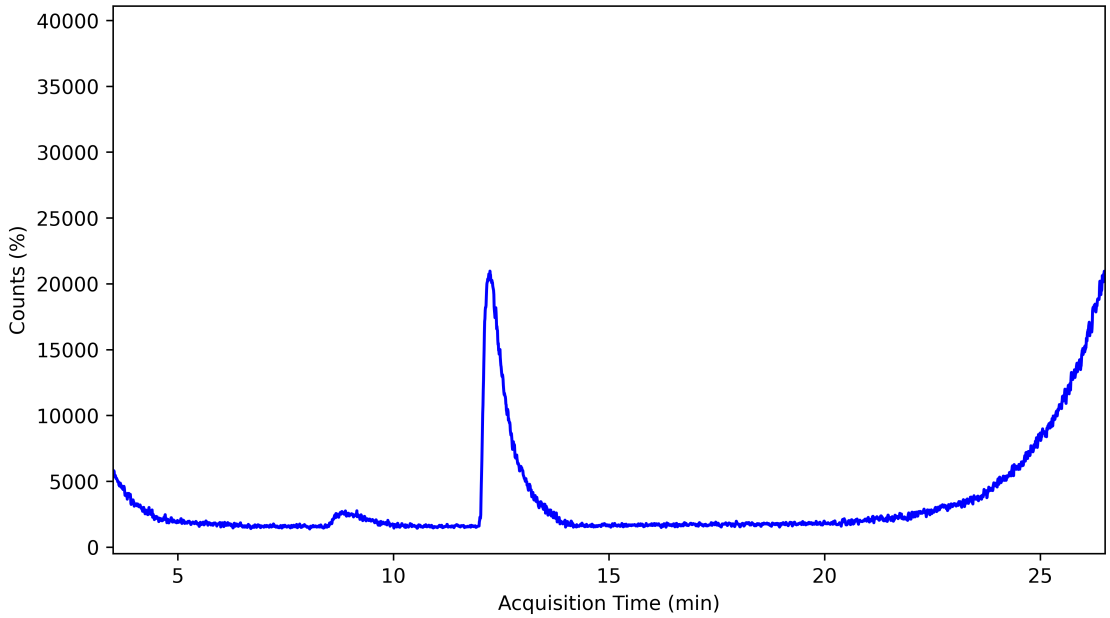

GC trace of S_NAr reaction after 3 H

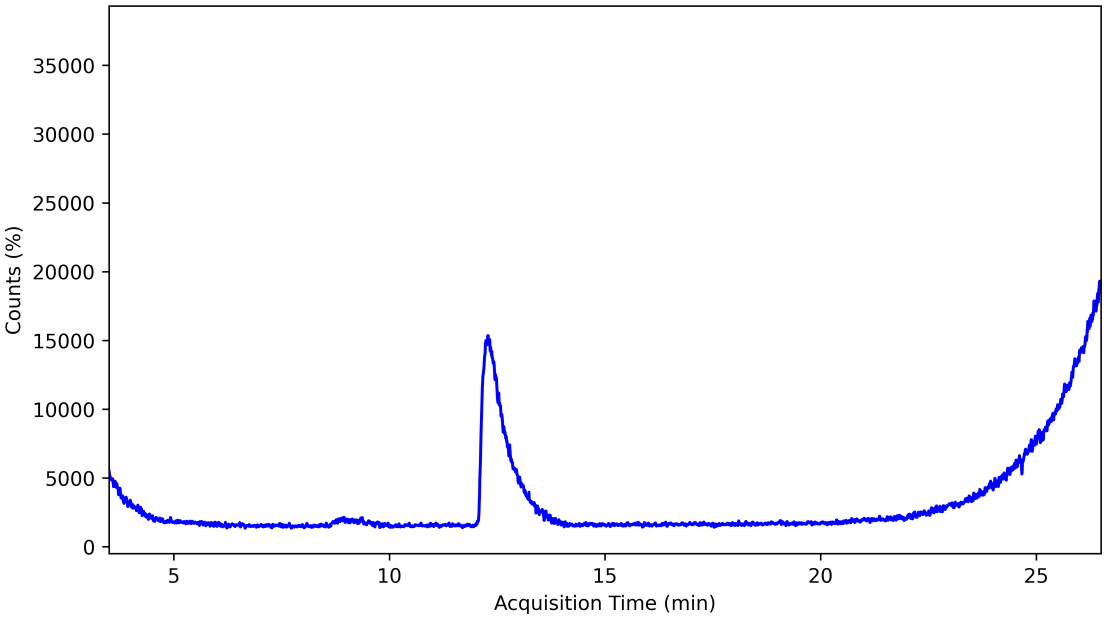

GC trace of S_NAr reaction after 4 H

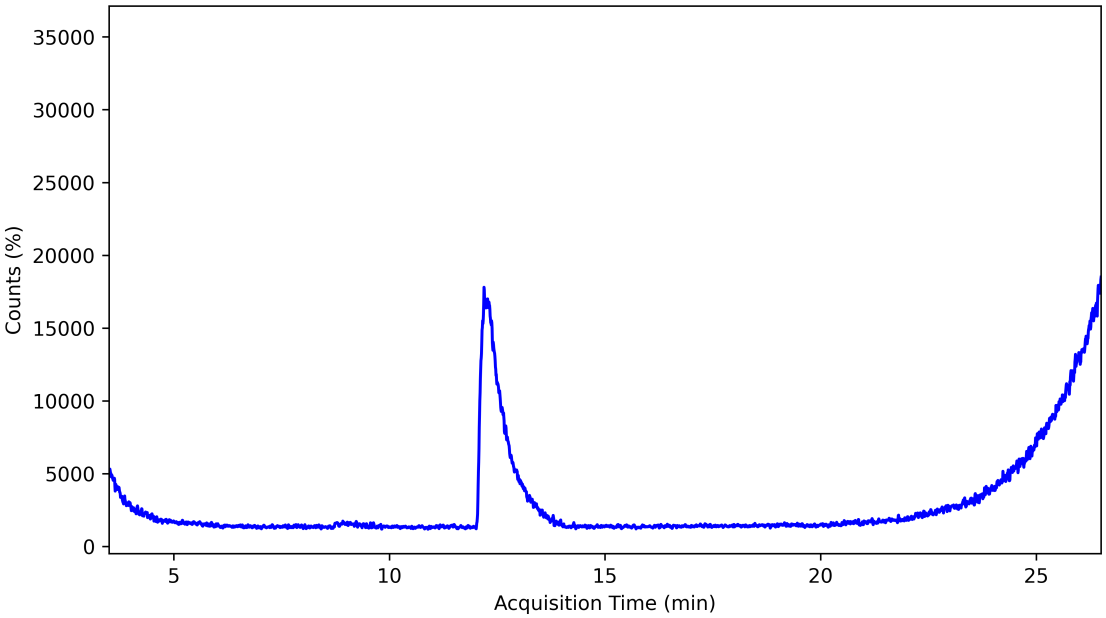

GC trace of S_NAr reaction after 5 H

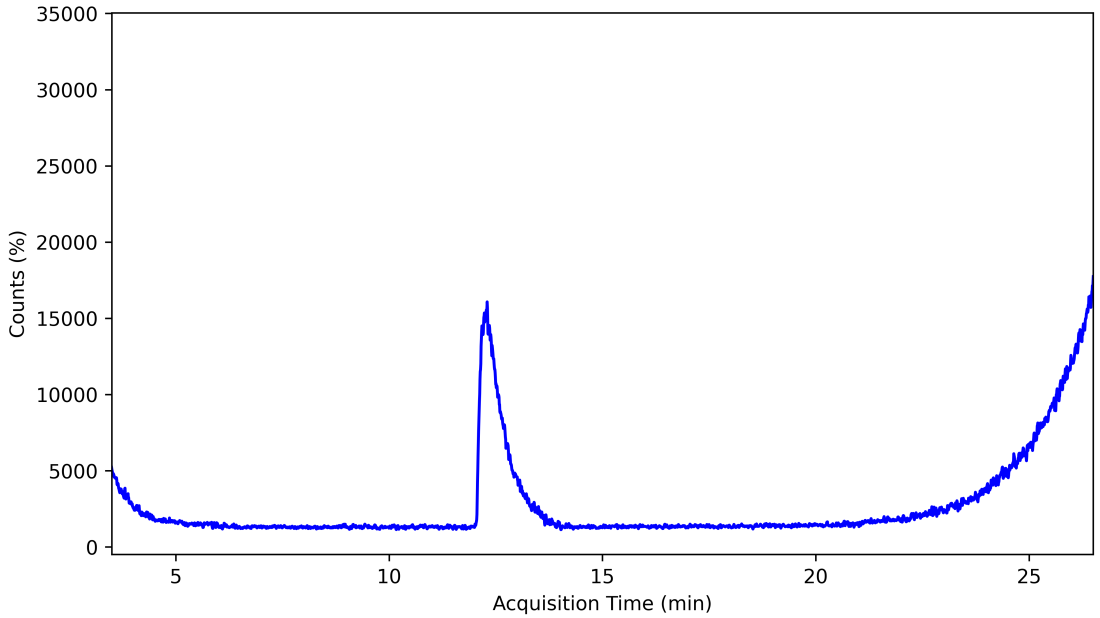

Resubjection of S_NAr product to reaction

A resubjection of the 2,4-dichloroanisole (**100a**) S_NAr product to the reaction condtions, with an ethanol nucleophile (see below).



S_NAr resubjection experiment.

GC trace of S_NAr resubjection experiment.

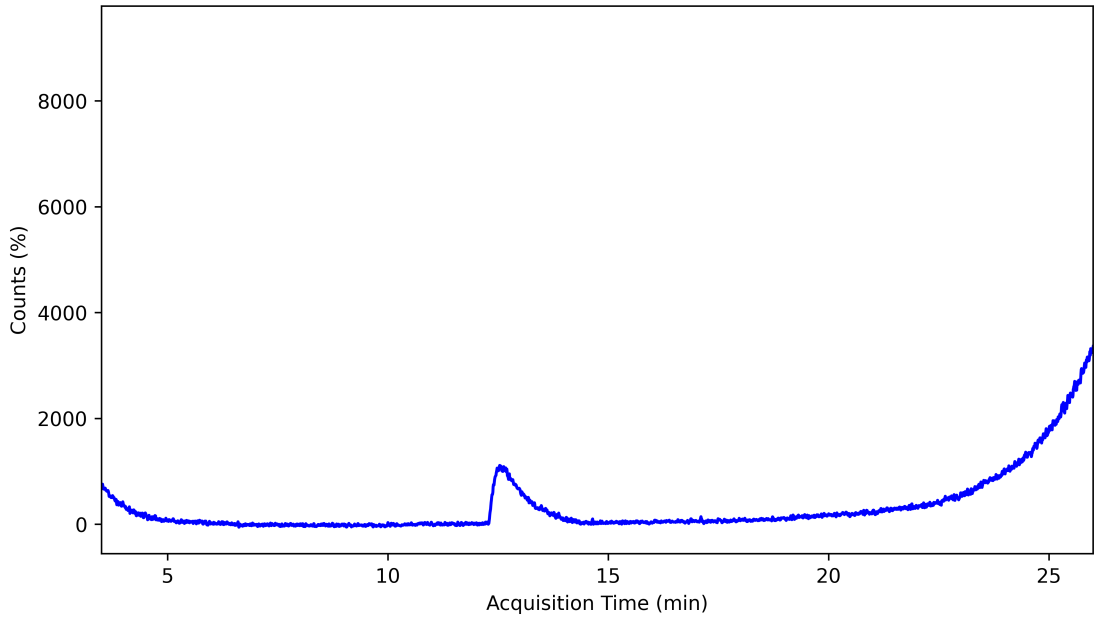



S_NAr resubjection experiment.

GC trace of S_NAr resubjection experiment.

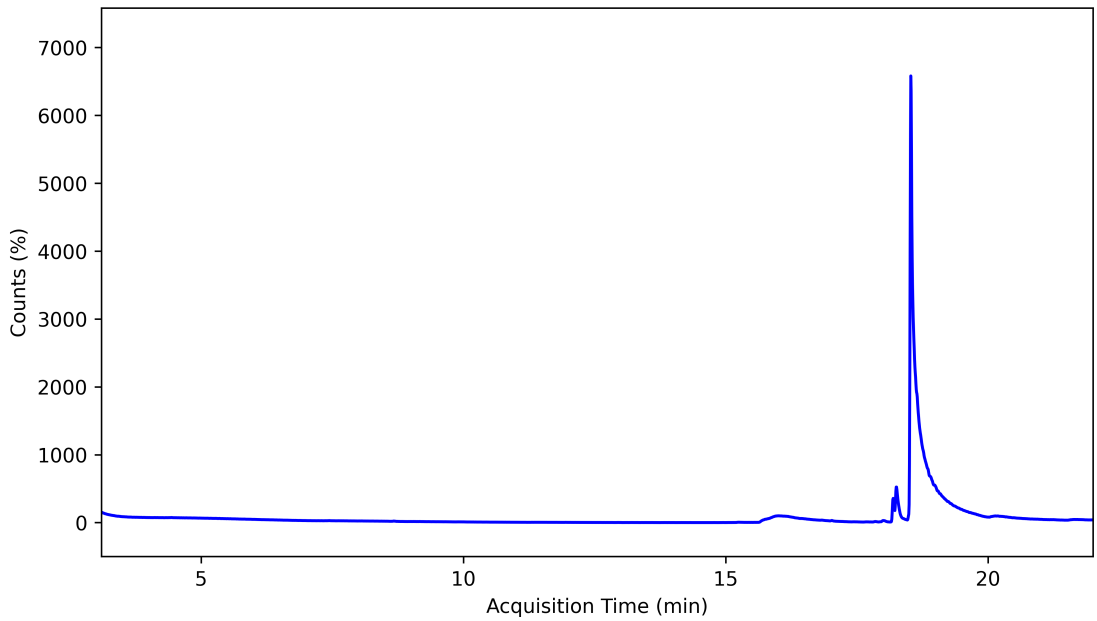

GC Traces Pertaining to the Arene Scope for the S_NAr Methodology

GC trace of the crude S_NAr reaction of **100** with MeOH

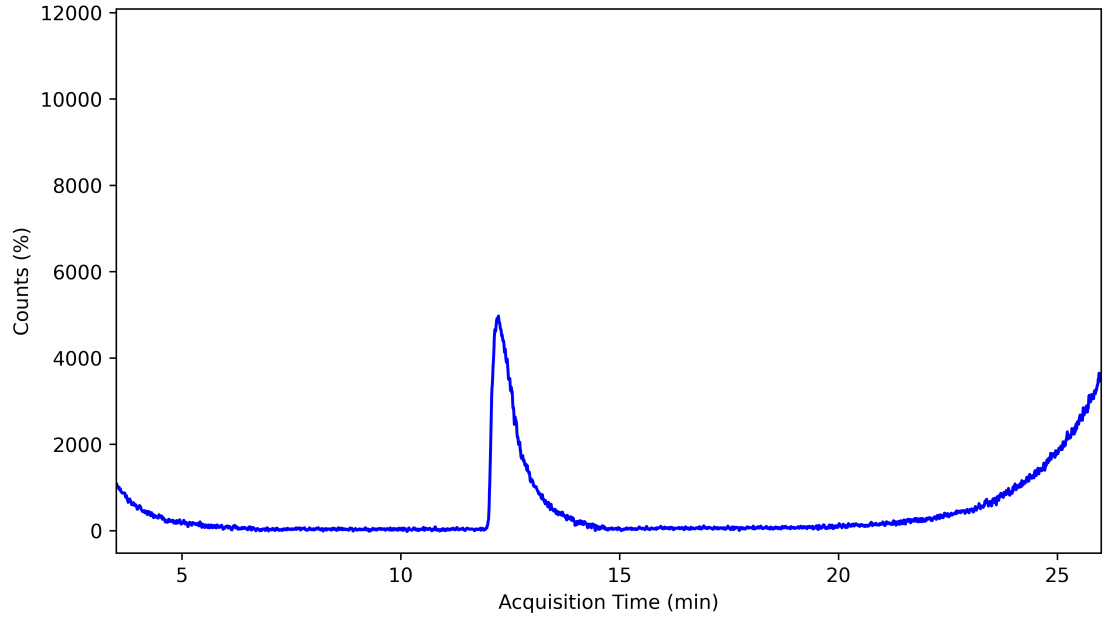

GC trace of the crude S_NAr reaction of **102** with MeOH

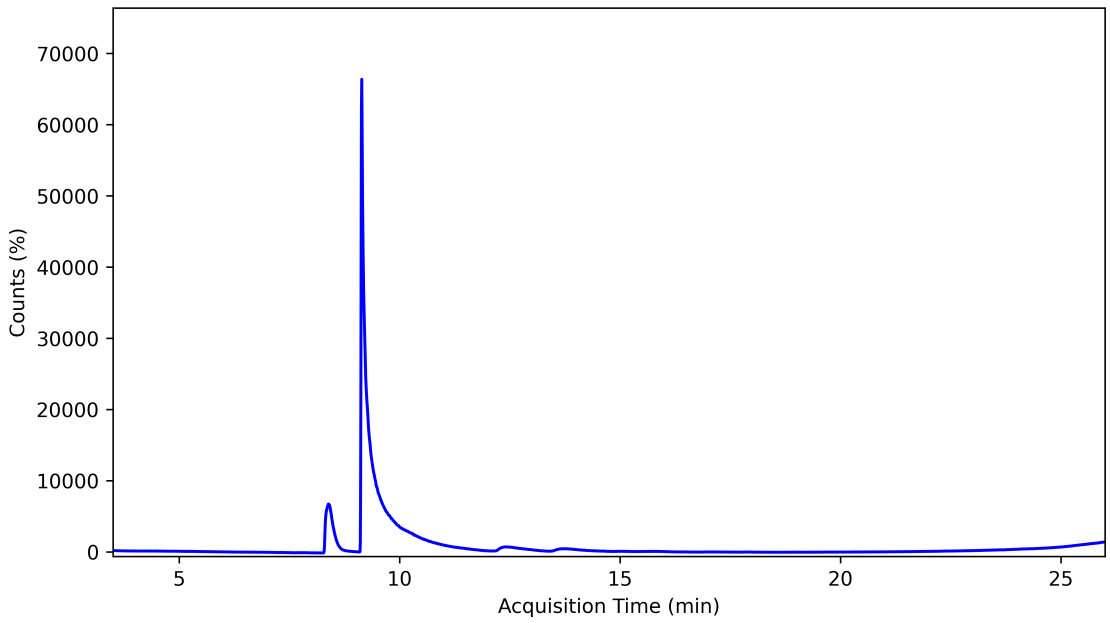

GC trace of the crude S_NAr reaction of **103** with MeOH

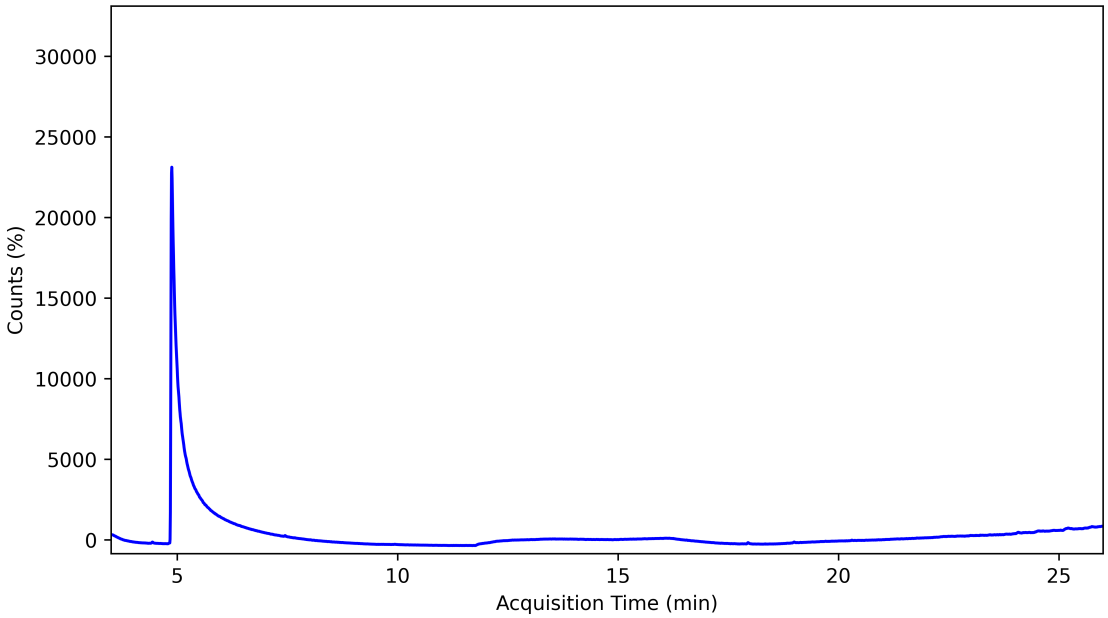

GC trace of the crude S_NAr reaction of **104** with MeOH

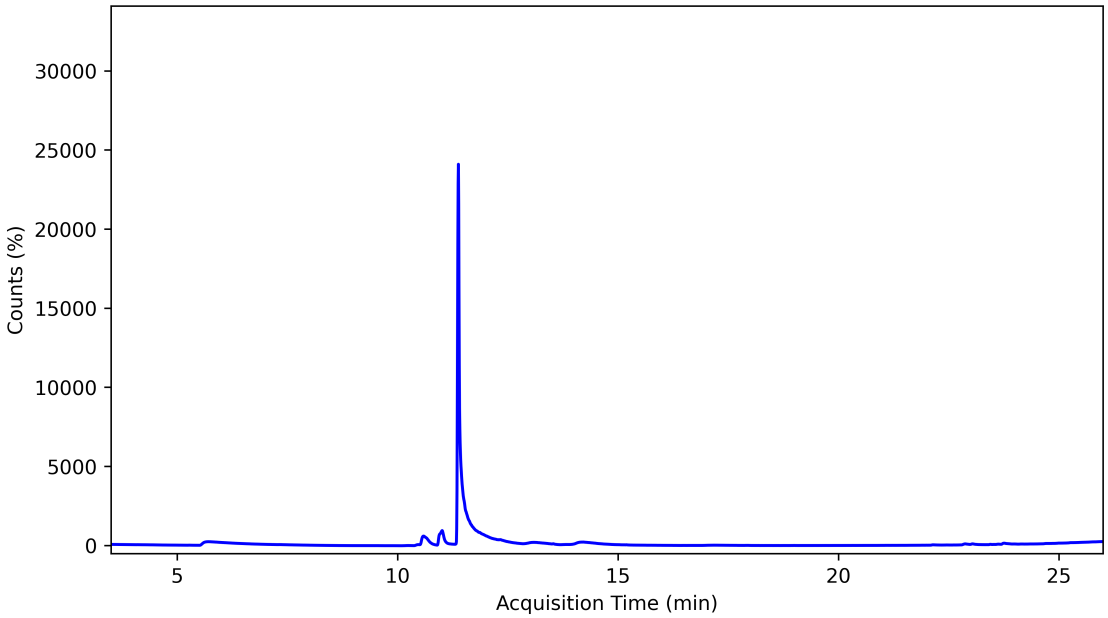

GC trace of the crude S_NAr reaction of **105** with MeOH

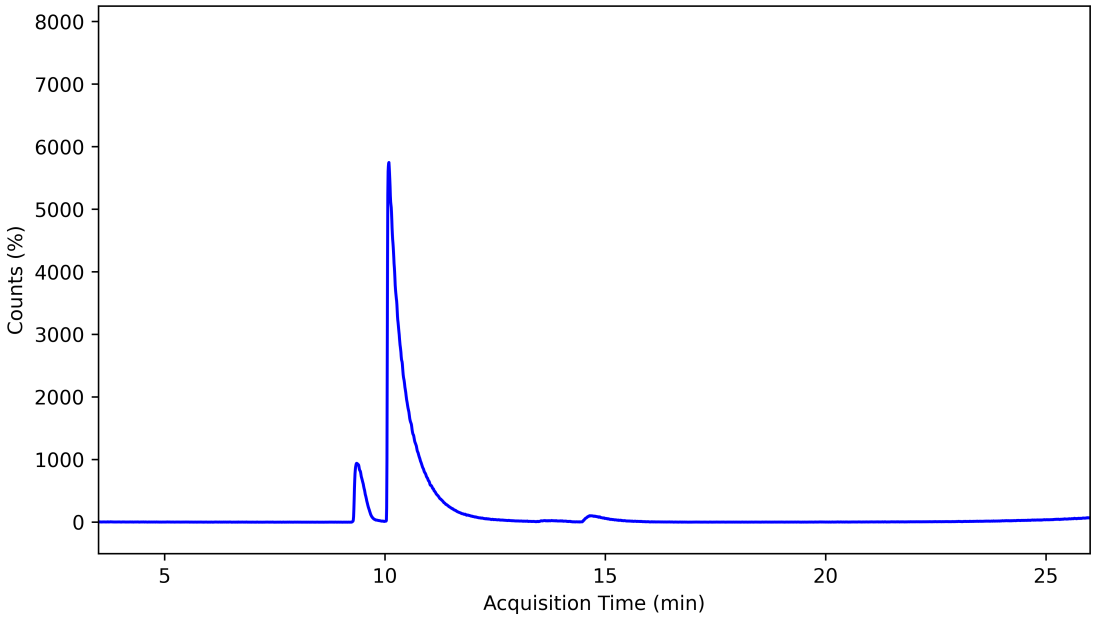

GC trace of the crude S_NAr reaction of **106** with MeOH

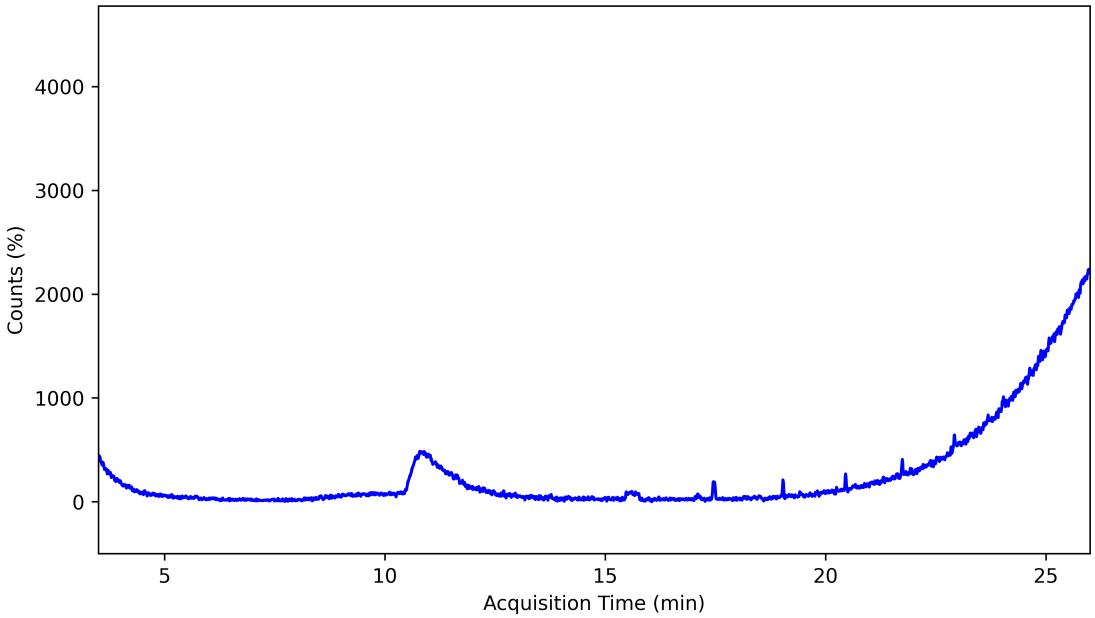

GC trace of the crude S_NAr reaction of **107**/**108** with MeOH

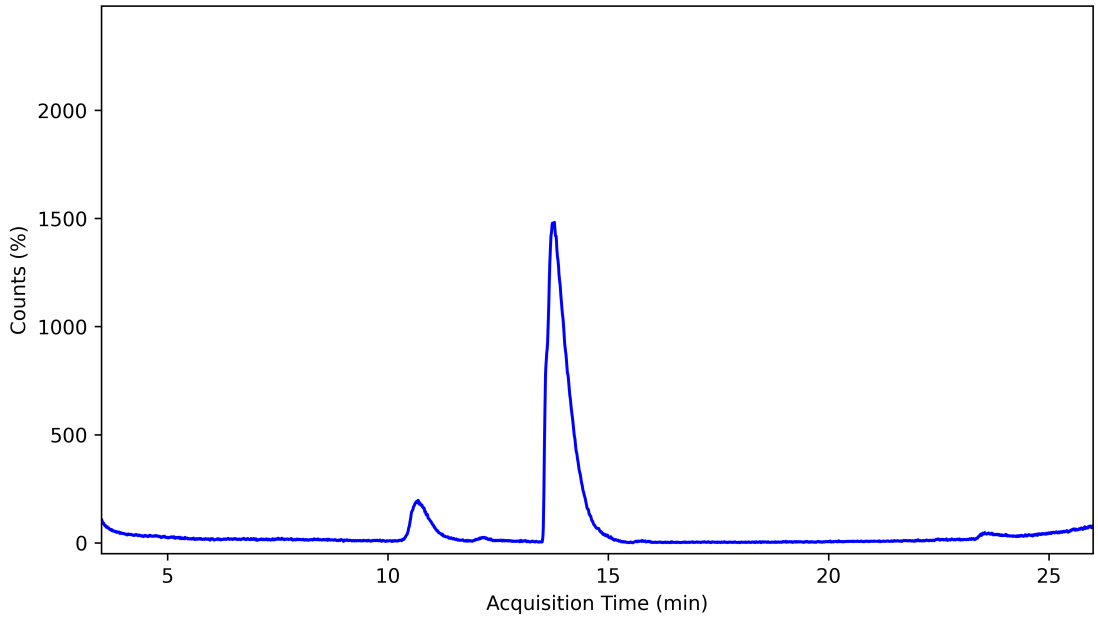

GC trace of the crude S_NAr reaction of **109** with MeOH

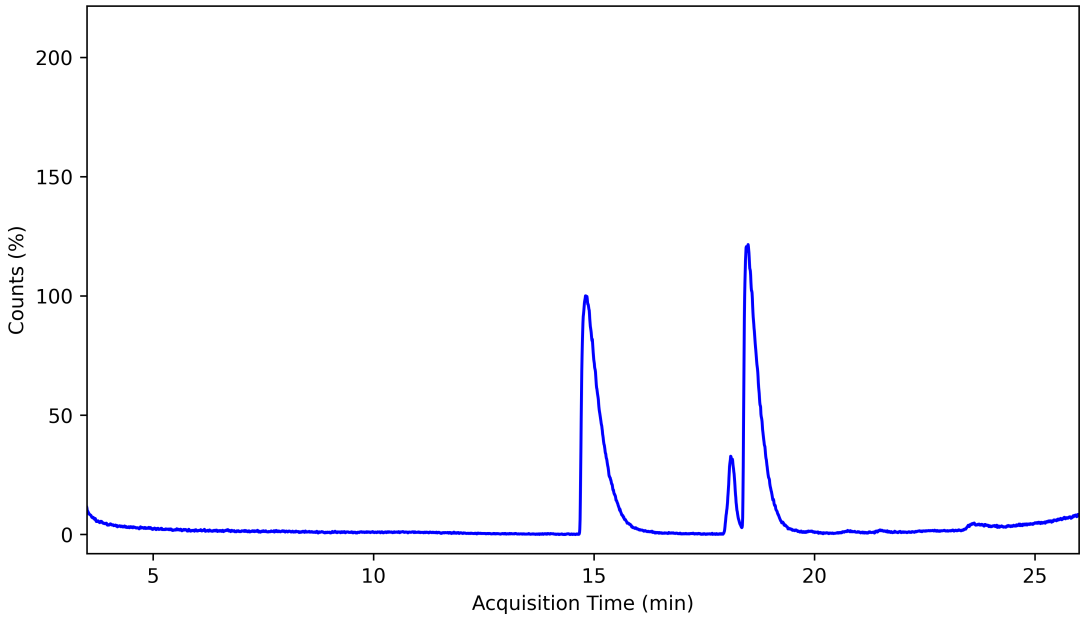

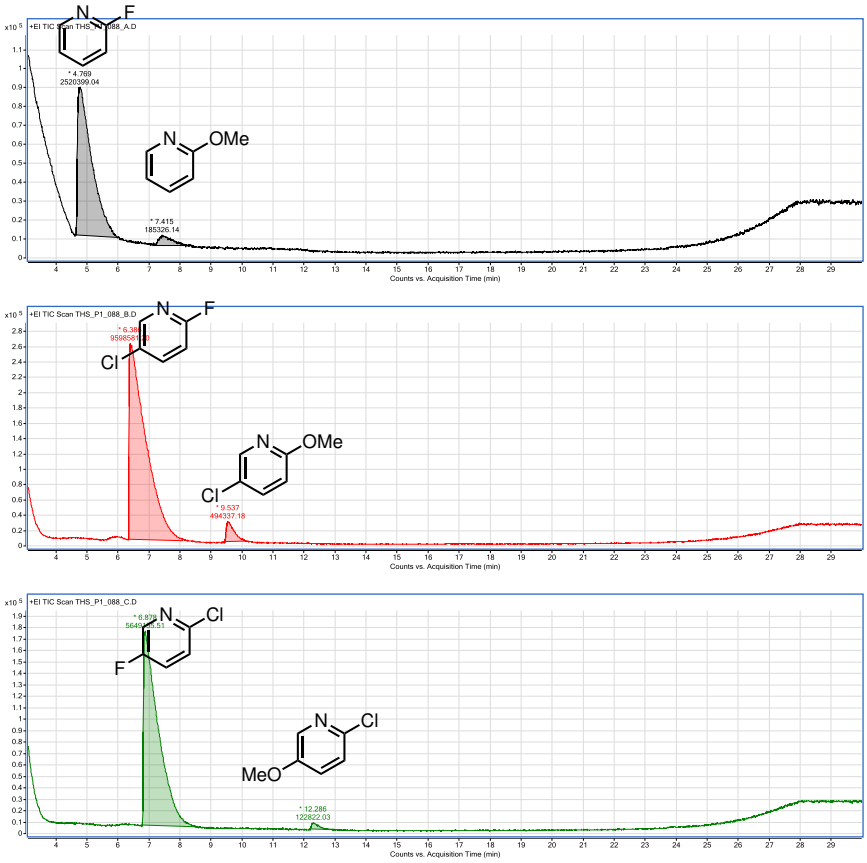

GC traces (from GCMS analysis) of crude reaction mixtures of the fluoropyridines as shown under the standard S_NAr conditions with 32 W blue light irradiation.

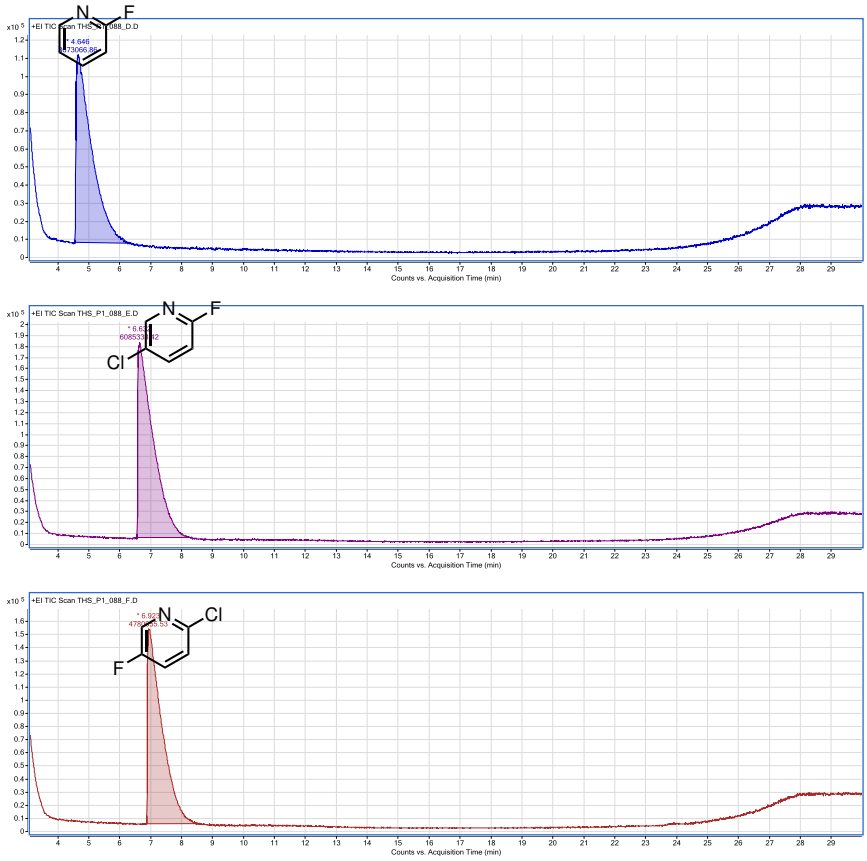

GC traces (from GCMS analysis) of crude reaction mixtures of the fluoropyridines as shown under the standard S_NAr conditions but in darkness.

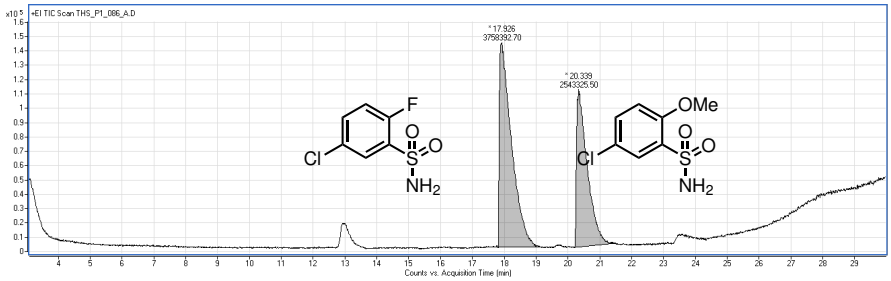

*GC traces (from GCMS analysis) of crude reaction mixtures of the reaction of 5-chloro-2-fluorobenzenesulfonamide **110** under the standard S_NAr conditions.*

GC trace of the crude S_NAr reaction of **132** with MeOH

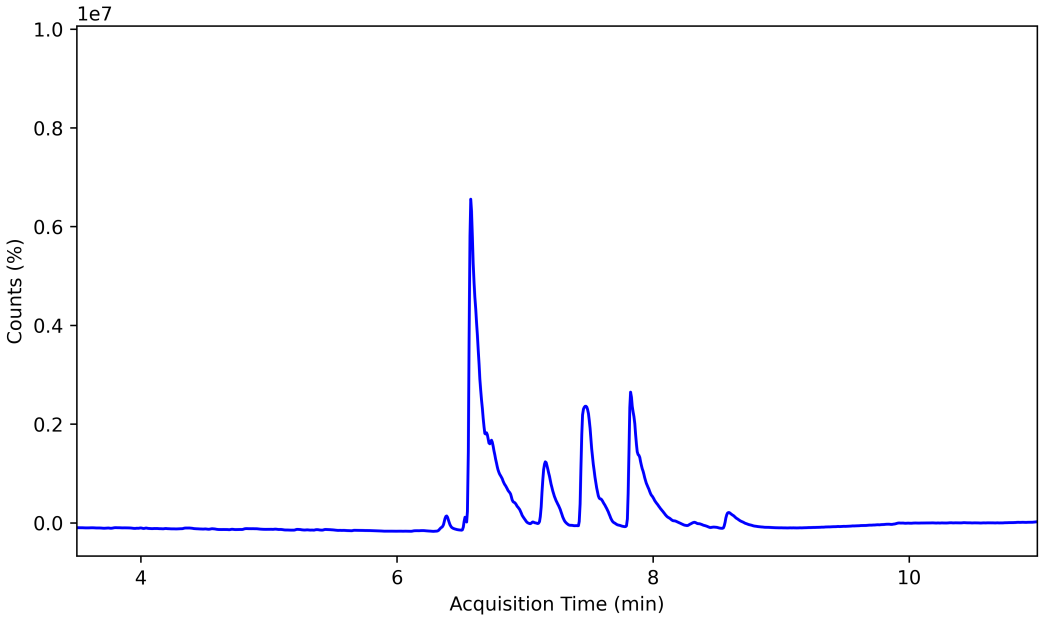

GC trace of the crude S_NAr reaction of **133** with MeOH

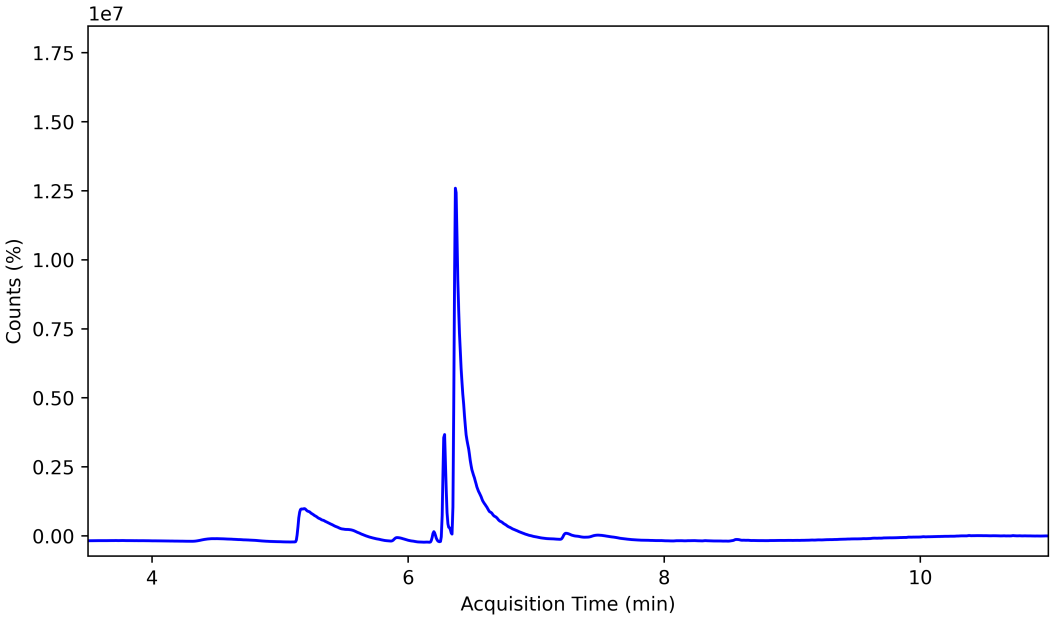

GC trace of the crude S_NAr reaction of **134** with MeOH

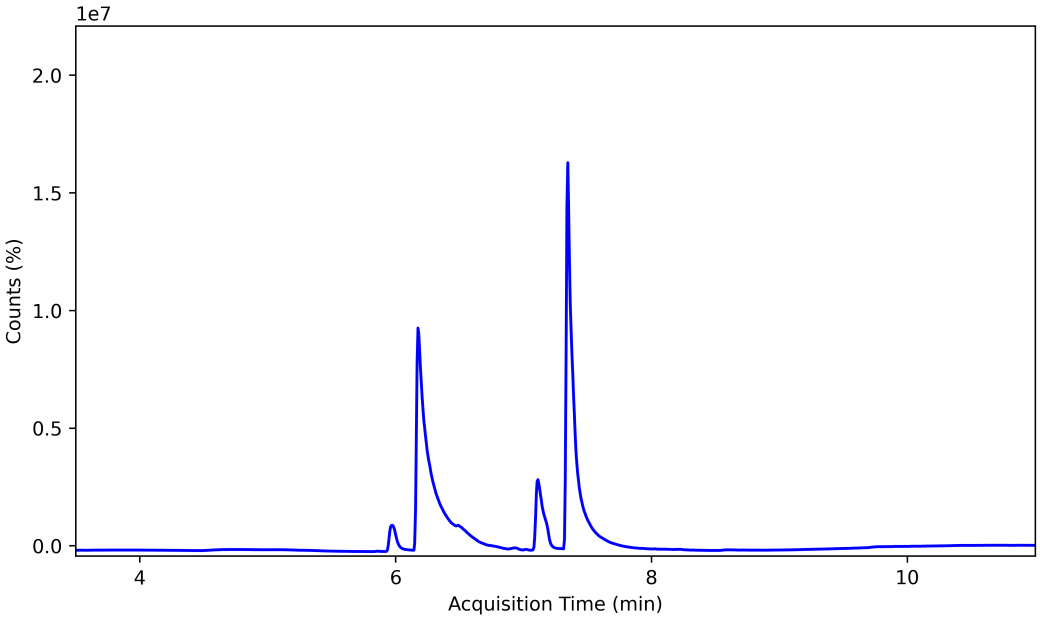

GC trace of the crude S_NAr reaction of **139** with MeOH

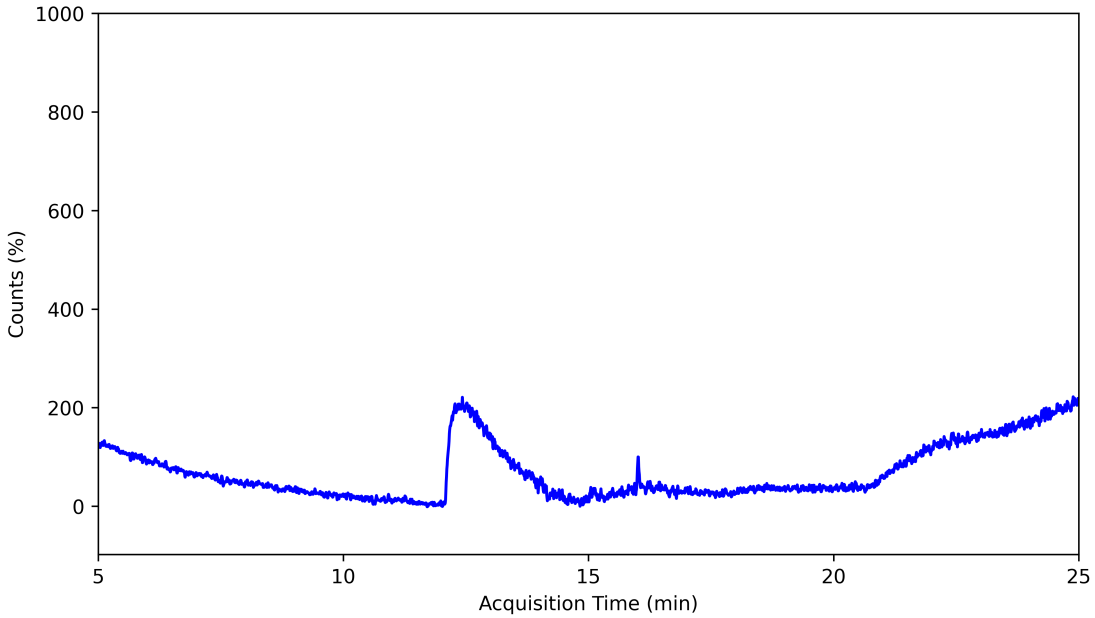

GC Traces Pertaining to the Nucleophile Scope for the S_NAr Methodology

GC trace of the crude S_NAr reaction of **100** with iPrOH

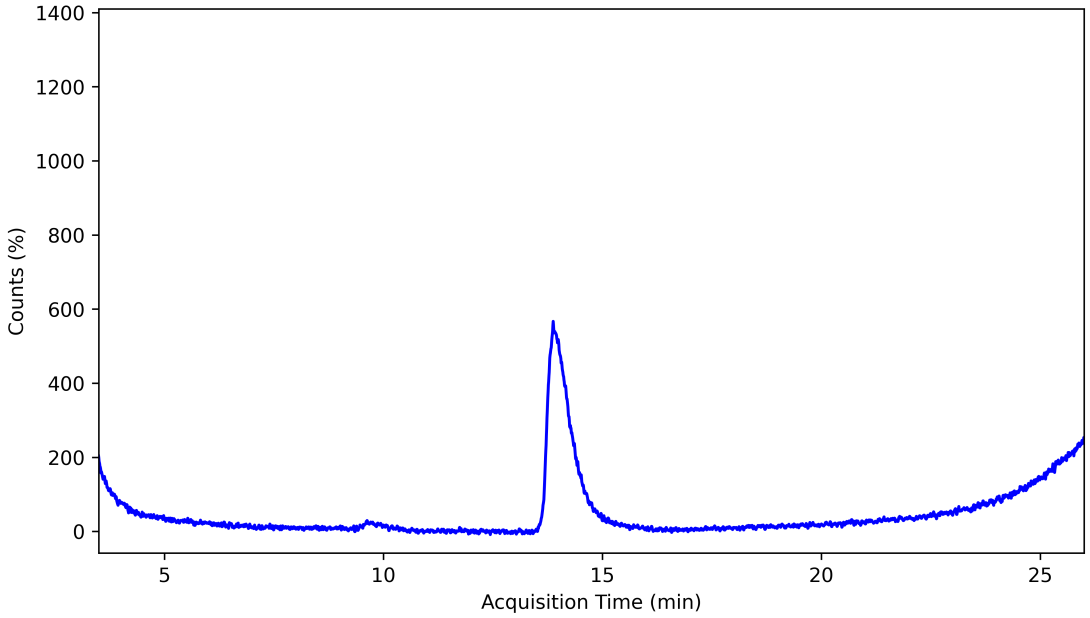

GC trace of the crude S_NAr reaction of **100** with *t*BuOH (yielding a TFE adduct)

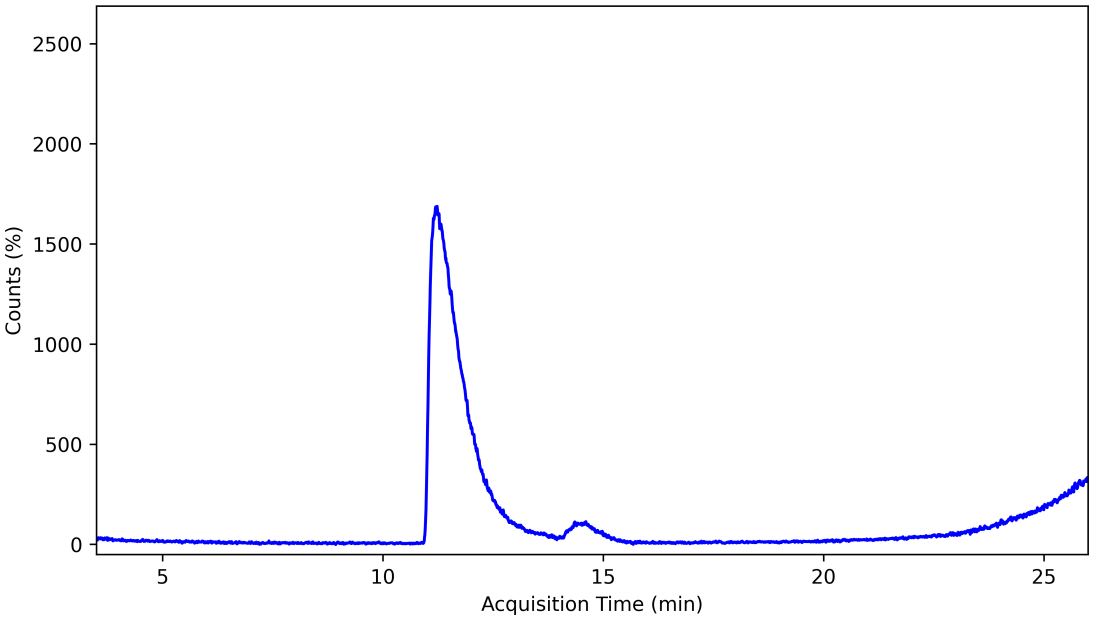

GC trace of the crude S_NAr reaction of **100** with (-)-menthol

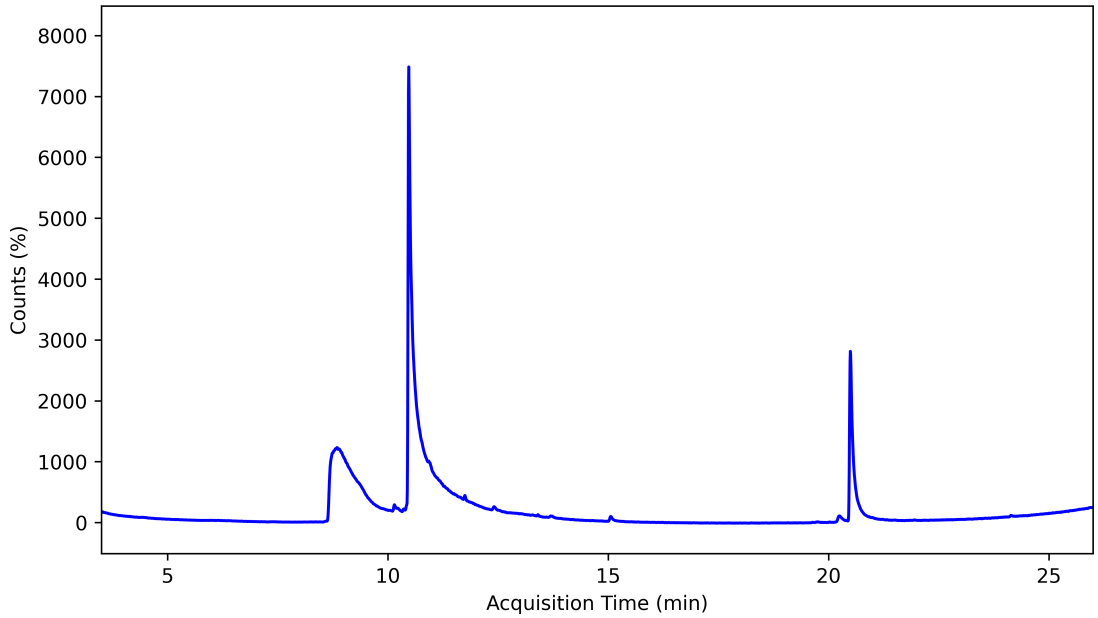

GC trace of the crude S_NAr reaction of **100** with CyOH

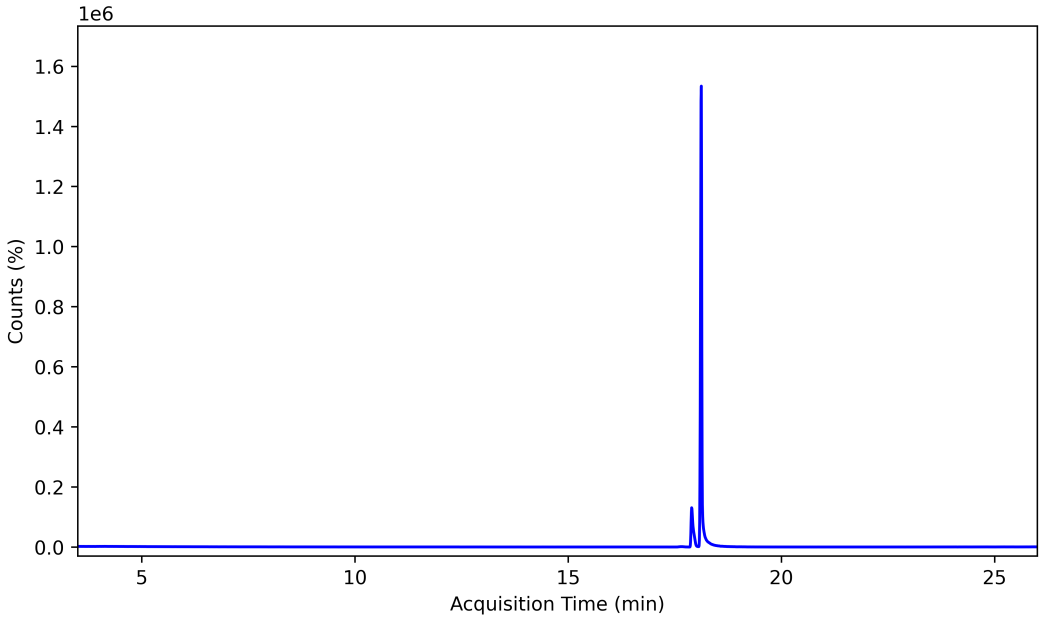

GC trace of the crude S_NAr reaction of **100** with cyclopropylmethanol

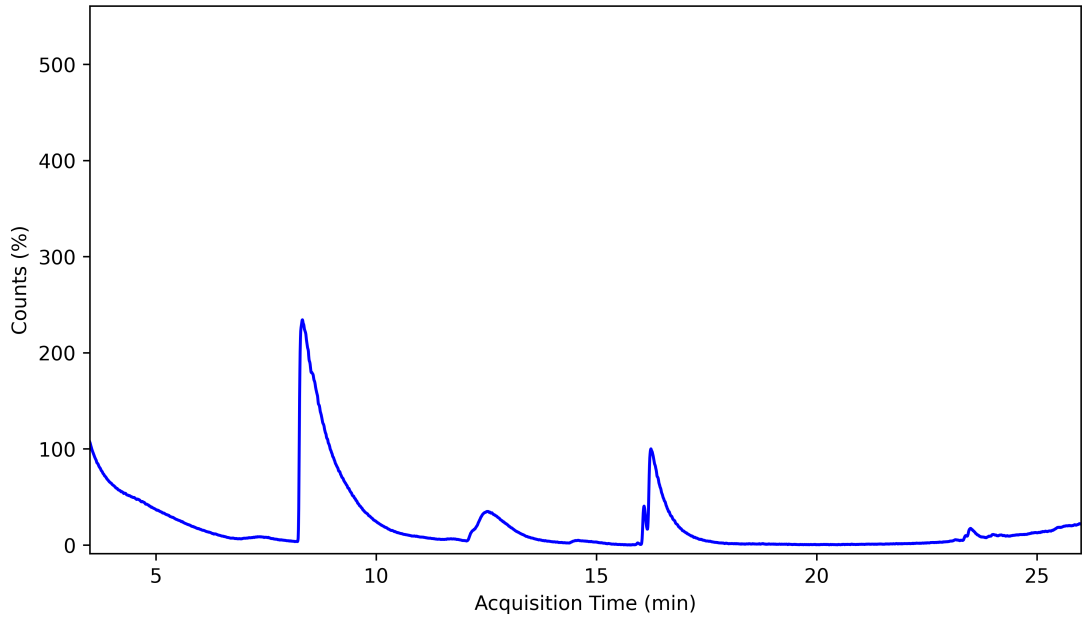

GC trace of the crude S_NAr reaction of **100** with (R)−$BrCHCH_2OH$

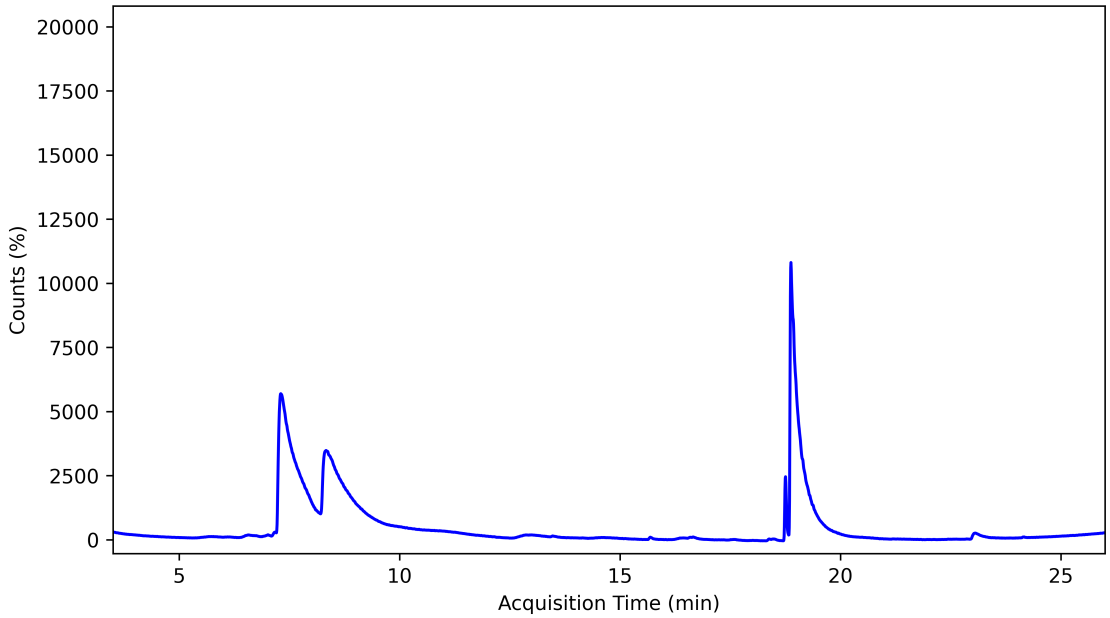

GC trace of the crude S_NAr reaction of **100** with (R)-1,3-butanediol)

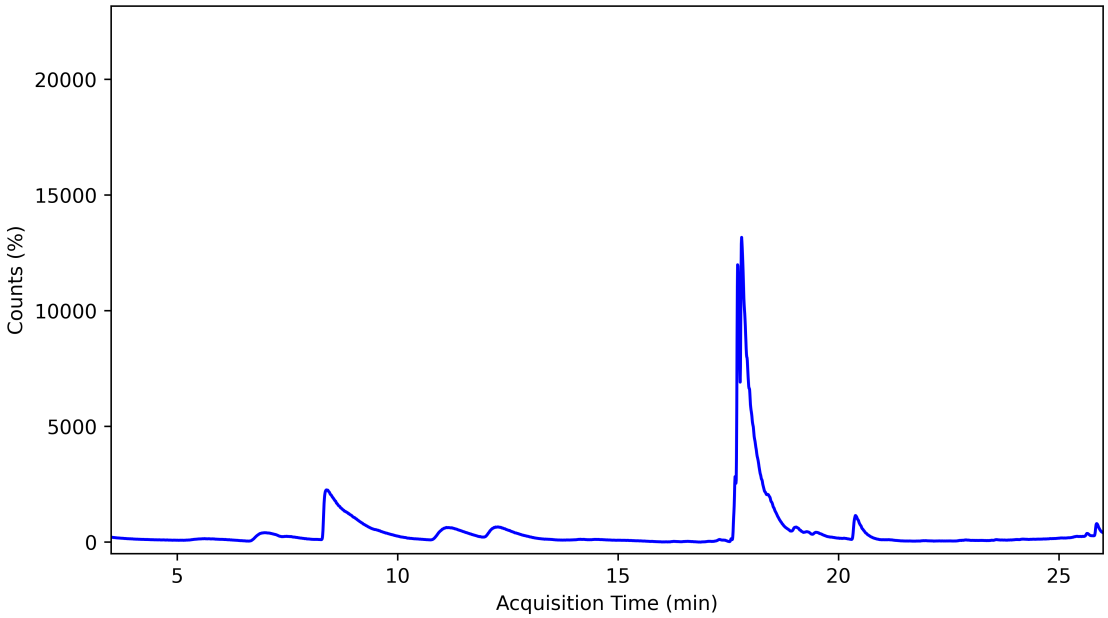

GC trace of the crude S_NAr reaction of **103** with pyrazole (**174**)

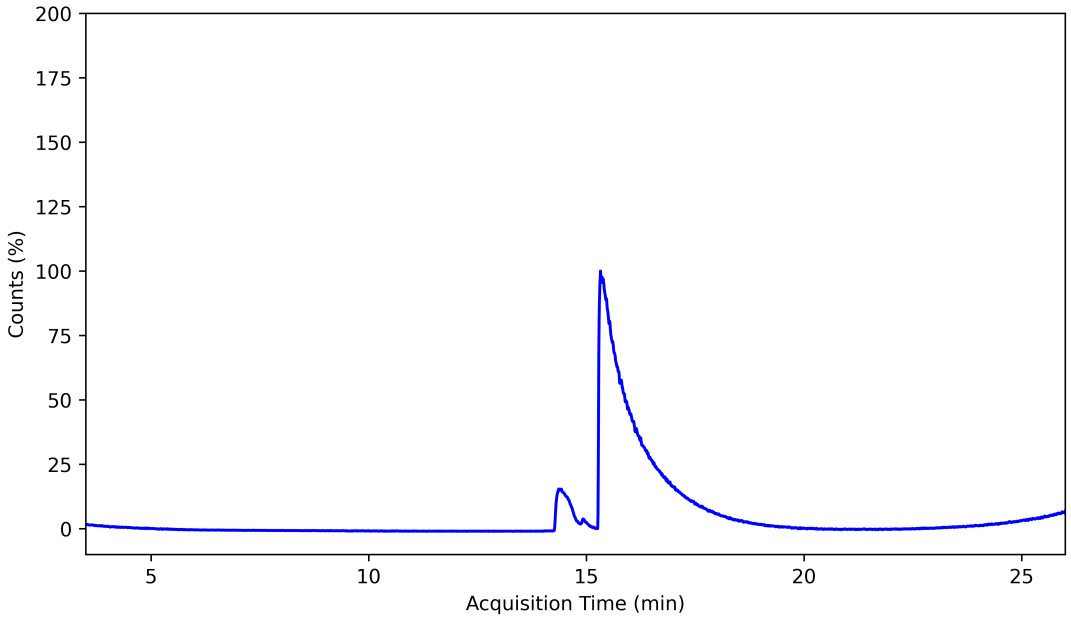

GC trace of the crude S_NAr reaction of **103** with chloropyrazole (**175**)

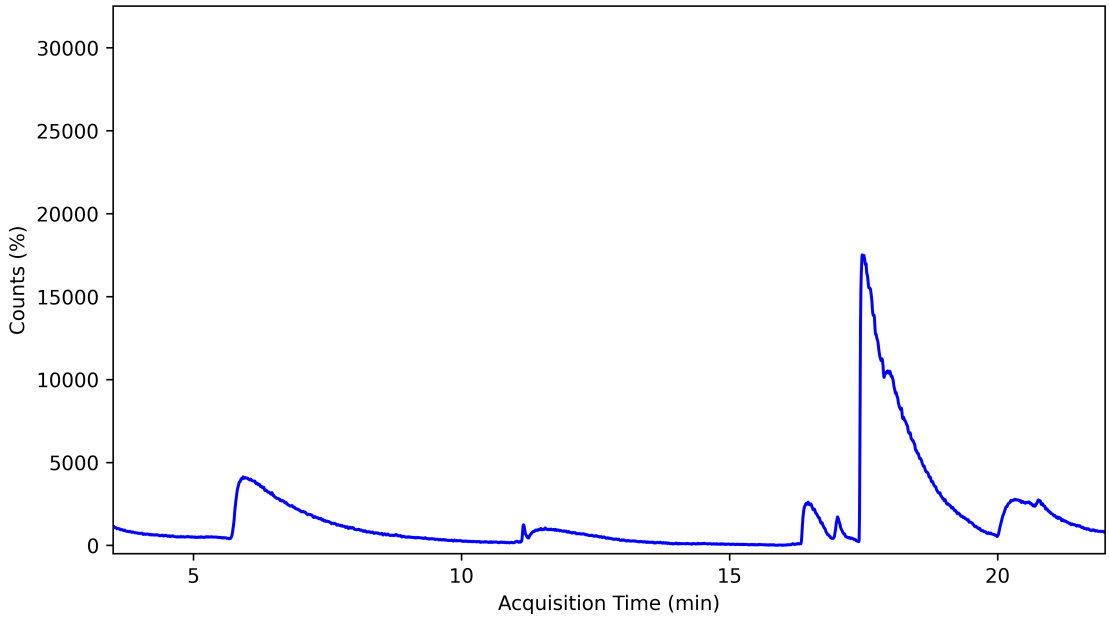

GC trace of the crude S_NAr reaction of **103** with pyrazole boronic ester (**176**)

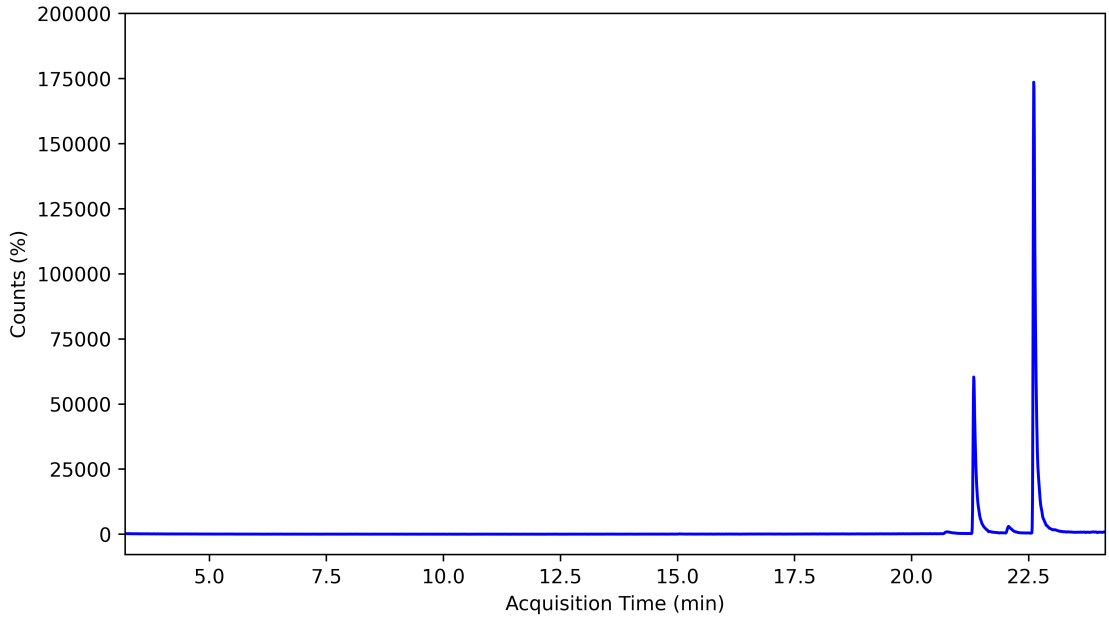

GC trace of the crude S_NAr reaction of **103** with trifluoromethylpyrazole (**177**)

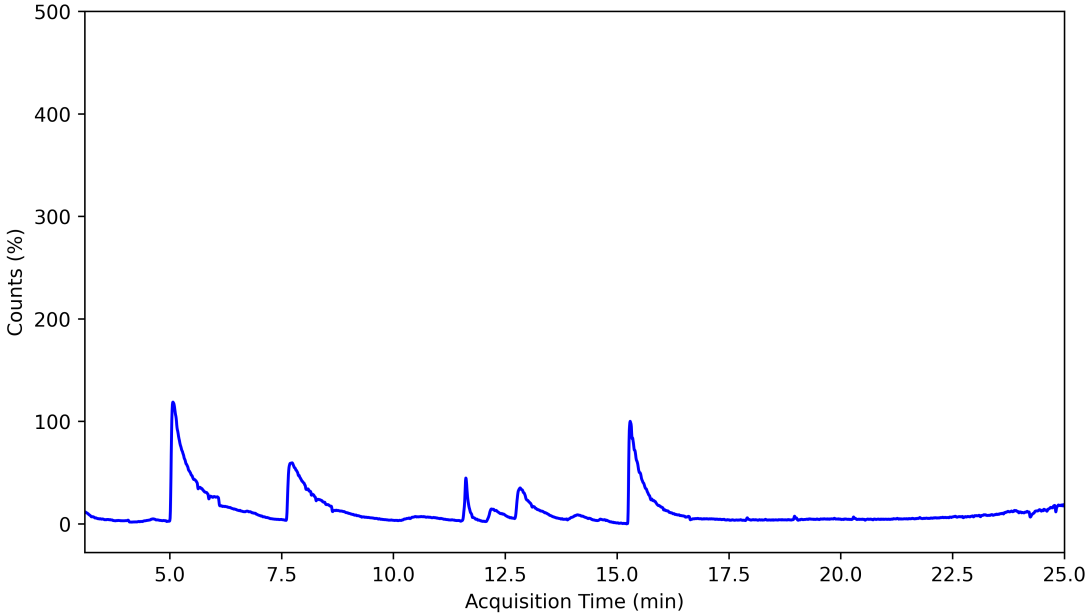

GC trace of the crude S_NAr reaction of **103** with pyrazole ester (**178**)

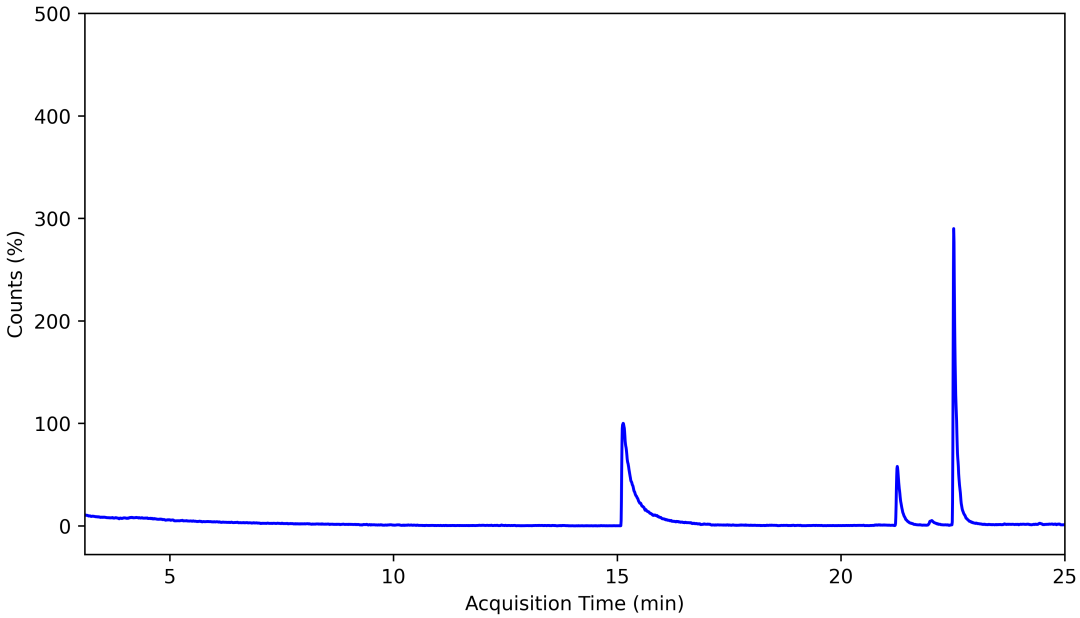

References

[1] E. R. Lankester, in *Library of the world's best literature ancient and modern*, ed. C. D. Warner, R. S. Peale & J. A. Hill, New York, Vol 2 edn., 1896, ch. Charles Robert Darwin, pp. 4835–4393.

[2] C. K. Prier, D. A. Rankic and D. W. C. MacMillan, *Chem. Rev.*, 2013, **113**, 5322–5363.

[3] J. Twilton, C. C. Le, P. Zhang, M. H. Shaw, R. W. Evans and D. W. C. MacMillan, *Nat. Rev. Chem.*, 2017, **1**, 52.

[4] N. A. Romero and D. A. Nicewicz, *Chem. Rev.*, 2016, **116**, 10075–10166.

[5] M. Melchionna and P. Fornasiero, *ACS Catal.*, 2020, **10**, 5493–5501.

[6] B. M. Hockin, C. Li, N. Robertson and E. Zysman-Colman, *Catal. Sci. Technol.*, 2019, **9**, 889–915.

[7] R. Costa e Silva, L. Oliveira da Silva, A. de Andrade Bartolomeu, T. J. Brocksom and K. T. de Oliveira, *Beilstein J. Org. Chem.*, 2020, **16**, 917–955.

[8] C. Tanielian, *Coord. Chem. Rev.*, 1998, **178-180**, 1165–1181.

[9] M. D. Tzirakis, I. N. Lykakis and M. Orfanopoulos, *Chem. Soc. Rev.*, 2009, **38**, 2609–2621.

[10] D. Ravelli, M. Fagnoni, T. Fukuyama, T. Nishikawa and I. Ryu, *ACS Catal.*, 2018, **8**, 701–713.

[11] S. G. E. Amos, M. Garreau, L. Buzzetti and J. Waser, *Beilstein J. Org. Chem.*, 2020, **16**, 1163–1187.

[12] H. Kotani, K. Ohkubo and S. Fukuzumi, *J. Am. Chem. Soc.*, 2004, **126**, 15999–16006.

[13] K. Ohkubo, K. Suga and S. Fukuzumi, *Chem. Commun.*, 2006, 2018–2020.

[14] K. Suga, K. Ohkubo and S. Fukuzumi, *J. Phys. Chem. A*, 2006, **110**, 3860–3867.

[15] K. Ohkubo, K. Mizushima, R. Iwata, K. Souma, N. Suzuki and S. Fukuzumi, *Chem. Commun.*, 2010, **46**, 601–603.

[16] K. Ohkubo, A. Fujimoto and S. Fukuzumi, *Chem. Commun.*, 2011, **47**, 8515–8517.

[17] D. S. Hamilton and D. A. Nicewicz, *J. Am. Chem. Soc.*, 2012, **134**, 18577–18580.

[18] T. M. Nguyen and D. A. Nicewicz, *J. Am. Chem. Soc.*, 2013, **135**, 9588–9591.

[19] A. J. Perkowski and D. A. Nicewicz, *J. Am. Chem. Soc.*, 2013, **135**, 10334–10337.

[20] T. M. Nguyen, N. Manohar and D. A. Nicewicz, *Angew. Chemie Int. Ed.*, 2014, **53**, 6198–6201.

[21] N. J. Gesmundo, J.-M. M. Grandjean and D. A. Nicewicz, *Org. Lett.*, 2015, **17**, 1316–1319.

[22] A. Joshi-Pangu, F. Lévesque, H. G. Roth, S. F. Oliver, L.-C. Campeau, D. Nicewicz and D. A. DiRocco, *J. Org. Chem.*, 2016, **81**, 7244–7249.

[23] N. E. S. Tay and D. A. Nicewicz, *J. Am. Chem. Soc.*, 2017, **139**, 16100–16104.

[24] J. B. McManus, N. P. R. Onuska and D. A. Nicewicz, *J. Am. Chem. Soc.*, 2018, **140**, 9056–9060.

[25] I. A. MacKenzie, L. Wang, N. P. R. Onuska, O. F. Williams, K. Begam, A. M. Moran, B. D. Dunietz and D. A. Nicewicz, *Nature*, 2020, **580**, 76–80.

[26] N. Holmberg-Douglas, N. P. R. Onuska and D. A. Nicewicz, *Angew. Chemie Int. Ed.*, 2020, **59**, 7425–7429.

[27] J. B. McManus, J. D. Griffin, A. R. White and D. A. Nicewicz, *J. Am. Chem. Soc.*, 2020, **142**, 10325–10330.

[28] N. E. S. Tay, W. Chen, A. Levens, V. A. Pistritto, Z. Huang, Z. Wu, Z. Li and D. A. Nicewicz, *Nat. Catal.*, 2020, **3**, 734–742.

[29] C. Fischer, C. Kerzig, B. Zilate, O. S. Wenger and C. Sparr, *ACS Catal.*, 2020, **10**, 210–215.

[30] E. Speckmeier, T. G. Fischer and K. Zeitler, *J. Am. Chem. Soc.*, 2018, **140**, 15353–15365.

[31] C. Bottecchia, R. Martín, I. Abdiaj, E. Crovini, J. Alcazar, J. Orduna, M. J. Blesa, J. R. Carrillo, P. Prieto and T. Noël, *Adv. Synth. Catal.*, 2019, **361**, 945–950.

[32] L. Dell'Amico, A. Vega-Penaloza, J. Mateos, X. Companyo and M. Escudero-Casao, *Angew. Chemie Int. Ed.*, 2020, Accepted Author Manuscript. doi:10.1002/anie.202006416.

[33] D. A. Nicewicz and D. W. C. MacMillan, *Science*, 2008, **322**, 77–80.

[34] M. Neumann, S. Füldner, B. König and K. Zeitler, *Angew. Chemie Int. Ed.*, 2011, **50**, 951–954.

[35] D. Mangion, J. Kendall and D. R. Arnold, *Org. Lett.*, 2001, **3**, 45–48.

[36] Z. Liang, S. Xu, W. Tian and R. Zhang, *Beilstein J. Org. Chem.*, 2015, **11**, 425–430.

[37] N. J. Gesmundo and D. A. Nicewicz, *Beilstein J. Org. Chem.*, 2014, **10**, 1272–1281.

[38] L. Lu, Y. Li and X. Jiang, *Green Chem.*, 2020, **22**, 5989–5994.

[39] M. H. Aukland, M. Šiaučiulis, A. West, G. J. P. Perry and D. J. Procter, *Nat. Catal.*, 2020, **3**, 163–169.

[40] M. Wang and J. Waser, *Angew. Chemie Int. Ed.*, 2020, **59**, 16420–16424.

[41] K. Ohkubo, A. Fujimoto and S. Fukuzumi, *J. Am. Chem. Soc.*, 2013, **135**, 5368–5371.

[42] S. Das, P. Natarajan and B. König, *Chem. Eur. J.*, 2017, **23**, 18161–18165.

[43] G. Pandey and R. Sochanchingwung, *J. Chem. Soc., Chem. Commun.*, 1994, 1945–1946.

[44] M. Nakamura, the late Reizo Dohno and T. Majima, *Chem. Commun.*, 1997, 1291–1292.

[45] G. Pandey, M. Karthikeyan and A. Murugan, *J. Org. Chem.*, 1998, **63**, 2867–2872.

[46] M. Nakamura, R. Dohno and T. Majima, *J. Org. Chem.*, 1998, **63**, 6258–6265.

[47] G. Pandey and R. Laha, *Angew. Chemie Int. Ed.*, 2015, **54**, 14875–14879.

[48] J. B. Birks, *Photochem. Photobiol.*, 1976, **24**, 287–289.

[49] S. Gazi and R. Ananthakrishnan, *Appl. Catal. B Environ.*, 2011, **105**, 317–325.

[50] Q. Liu, Y.-N. Li, H.-H. Zhang, B. Chen, C.-H. Tung and L.-Z. Wu, *Chem. - A Eur. J.*, 2012, **18**, 620–627.

[51] M. Neumann and K. Zeitler, *Chem. - A Eur. J.*, 2013, **19**, 6950–6955.

[52] T. Keshari, V. K. Yadav, V. P. Srivastava and L. D. S. Yadav, *Green Chem.*, 2014, **16**, 3986.

[53] A. U. Meyer, S. Jäger, D. Prasad Hari and B. König, *Adv. Synth. Catal.*, 2015, **357**, 2050–2054.

[54] J. Davies, S. G. Booth, S. Essafi, R. A. W. Dryfe and D. Leonori, *Angew. Chemie Int. Ed.*, 2015, **54**, 14017–14021.

[55] M. Riener and D. A. Nicewicz, *Chem. Sci.*, 2013, **4**, 2625–2629.

[56] D. Bello, R. Ramon and R. Lavilla, *Curr. Org. Chem.*, 2010, **14**, 332–356.

[57] T. Shen, Z.-G. Zhao, Q. Yu and H.-J. Xu, *J. Photochem. Photobiol., A*, 1989, **47**, 203–212.

[58] K. Vogel, C. Reichardt and K. Dimroth, *Org. Synth.*, 1969, **49**, 121.

[59] T. Peglow, S. Blechert and E. Steckhan, *Chem. Commun.*, 1999, 433–434.

[60] F. Wilkinson and A. A. Abdel-Shafi, *J. Phys. Chem. A*, 1997, **101**, 5509–5516.

[61] F. Wilkinson and A. A. Abdel-Shafi, *J. Phys. Chem. A*, 1999, **103**, 5425–5435.

[62] A. A. Abdel-Shafi and D. R. Worrall, *J. Photochem. Photobiol. A Chem.*, 2005, **172**, 170–179.

[63] R. Akaba, H. Sakuragi and K. Tokumaru, *J. Chem. Soc., Perkin Trans. 2*, 1991, 291–297.

[64] M. A. Miranda and H. Garcia, *Chem. Rev.*, 1994, **94**, 1063–1089.

[65] H. Kawata and S. Niizuma, *Bull. Chem. Soc. Jpn.*, 1989, **62**, 2279–2283.

[66] F. Strieth-Kalthoff, M. J. James, M. Teders, L. Pitzer and F. Glorius, *Chem. Soc. Rev.*, 2018, **47**, 7190–7202.

[67] T. Koike and M. Akita, *Inorg. Chem. Front.*, 2014, **1**, 562–576.

[68] D. M. Schultz, J. W. Sawicki and T. P. Yoon, *Beilstein J. Org. Chem.*, 2015, **11**, 61–65.

[69] M. Haga, E. S. Dodsworth, G. Eryavec, P. Seymour and A. B. P. Lever, *Inorg. Chem.*, 1985, **24**, 1901–1906.

[70] S. Fukuzumi, K. Ohkubo, Y. Tokuda and T. Suenobu, *J. Am. Chem. Soc.*, 2000, **122**, 4286–4294.

[71] S. Yamago, H. Miyazoe, K. Iida and J.-I. Yoshida, *Org. Lett.*, 2000, **2**, 3671–3673.

[72] J. B. Gerken and S. S. Stahl, *ACS Cent. Sci.*, 2015, **1**, 234–243.

[73] A. E. Wendlandt and S. S. Stahl, *Angew. Chemie Int. Ed.*, 2015, **54**, 14638–14658.

[74] P. B. Merkel, P. Luo, J. P. Dinnocenzo and S. Farid, *J. Org. Chem.*, 2009, **74**, 5163–5173.

[75] T. Osako, K. Ohkubo, M. Taki, Y. Tachi, S. Fukuzumi and S. Itoh, *J. Am. Chem. Soc.*, 2003, **125**, 11027–11033.

[76] X.-P. Chang, G. Cui, W.-H. Fang and W. Thiel, *ChemPhysChem*, 2015, **16**, 933–937.

[77] H. Tachikawa, *J. Phys. Chem. A*, 2018, **122**, 4121–4129.

[78] A. Błoch-Mechkour and T. Bally, *Phys. Chem. Chem. Phys.*, 2015, **17**, 10624–10629.

[79] A. A. Frost and B. Musulin, *J. Chem. Phys.*, 1953, **21**, 572–573.

[80] H. A. Jahn and E. Teller, *Proc. R. Soc. London. A*, 1937, **161**, 220–235.

[81] L. Eberson, M. P. Hartshorn, O. Persson and F. Radner, *Chem. Commun.*, 1996, 2105–2112.

[82] N. Shida, Y. Imada, S. Nagahara, Y. Okada and K. Chiba, *Commun. Chem.*, 2019, **2**, 24.

[83] I. Colomer, A. E. Chamberlain, M. B. Haughey and T. J. Donohoe, *Nat. Rev. Chem.*, 2017, **1**, 0088.

[84] A. Studer and D. P. Curran, *Nat. Chem.*, 2014, **6**, 765–773.

[85] S. Lin, M. A. Ischay, C. G. Fry and T. P. Yoon, *J. Am. Chem. Soc.*, 2011, **133**, 19350–19353.

[86] J. F. Bunnett and R. E. Zahler, *Chem. Rev.*, 1951, **49**, 273–412.

[87] F. Terrier, *Modern Nucleophilic Aromatic Substitution*, Wiley-VCH Verlag GmbH & Co. KGaA, Weinheim, Germany, 2013.

[88] H. Amii and K. Uneyama, *Chem. Rev.*, 2009, **109**, 2119–2183.

[89] Y.-R. Luo, *Comprehensive handbook of chemical bond energies*, CRC Press, 2007.

[90] P. A. Champagne, A. Saint-Martin, M. Drouin and J. F. Paquin, *Beilstein J. Org. Chem.*, 2013, **9**, 2451–2456.

[91] P. A. Champagne, J. Pomarole, M. È. Thérien, Y. Benhassine, S. Beaulieu, C. Y. Legault and J. F. Paquin, *Org. Lett.*, 2013, **15**, 2210–2213.

[92] P. A. Champagne, Y. Benhassine, J. Desroches and J. F. Paquin, *Angew. Chemie - Int. Ed.*, 2014, **53**, 13835–13839.

[93] P. A. Champagne, M. Drouin, C. Y. Legault, C. Audubert and J. F. Paquin, *J. Fluor. Chem.*, 2015, **171**, 113–119.

[94] R. Hemelaere, P. A. Champagne, J. Desroches and J. F. Paquin, *J. Fluor. Chem.*, 2016, **190**, 1–6.

[95] N. S. Keddie, P. A. Champagne, J. Desroches, J. F. Paquin and D. O'Hagan, *Beilstein J. Org. Chem.*, 2017, **14**, 106–113.

[96] D. G. Brown and J. Boström, *J. Med. Chem.*, 2016, **59**, 4443–4458.

[97] M. J. Rarick, R. Q. Brewster and F. B. Dains, *J. Am. Chem. Soc.*, 1933, **55**, 1289–1293.

[98] H. B. Gottlieb, *J. Am. Chem. Soc.*, 1936, **58**, 532–533.

[99] K. Walsh, H. F. Sneddon and C. J. Moody, *ChemSusChem*, 2013, **6**, 1455–1460.

[100] A. J. Blacker, G. Moran-Malagon, L. Powell, W. Reynolds, R. Stones and M. R. Chapman, *Org. Process Res. Dev.*, 2018, **22**, 1086–1091.

[101] A. Williams, *Chem. Soc. Rev.*, 1994, **23**, 93–100.

[102] A. H. M. Renfrew, J. A. Taylor, J. M. Whitmore and A. Williams, *J. Chem. Soc. Perkin Trans. 2*, 1993, 1703–1704.

[103] E. E. Kwan, Y. Zeng, H. A. Besser and E. N. Jacobsen, *Nat. Chem.*, 2018, **10**, 917–923.

[104] A. J. J. Lennox, *Angew. Chemie*, 2018, **130**, 14898–14900.

[105] S. Rohrbach, A. J. Smith, J. H. Pang, D. L. Poole, T. Tuttle, S. Chiba and J. A. Murphy, *Angew. Chemie Int. Ed.*, 2019, **58**, 16368–16388.

[106] H. J. Schneider, *Chem. Sci.*, 2012, **3**, 1381–1394.

[107] H. Huang and T. H. Lambert, *Angew. Chemie Int. Ed.*, 2020, **59**, 658–662.

[108] T. Sheridan, H. G. Yayla, Y. Lian, J. Genovino, N. Monck and J. W. Burton, *European J. Org. Chem.*, 2020, **2020**, 2766–2770.

[109] N. L. Reed, M. I. Herman, V. P. Miltchev and T. P. Yoon, *Org. Lett.*, 2018, **20**, 7345–7350.

[110] Y. Yu, P. Guo, J.-S. Zhong, Y. Yuan and K.-Y. Ye, *Org. Chem. Front.*, 2020, **7**, 131–135.

[111] M. Sender and D. Ziegenbalg, *Chemie Ing. Tech.*, 2017, **89**, 1159–1173.

[112] T. P. Yoon, M. A. Ischay and J. Du, *Nat. Chem.*, 2010, **2**, 527–532.

[113] S. Berto, E. Chiavazza, V. Ribotta, P. G. Daniele, C. Barolo, A. Giacomino, D. Vione and M. Malandrino, *Spectrochim. Acta Part A Mol. Biomol. Spectrosc.*, 2015, **149**, 75–82.

[114] L. E. Hofmann, L. Mach and M. R. Heinrich, *J. Org. Chem.*, 2018, **83**, 431–436.

[115] C. Huang, R. Liu, C. Zhang, Q. Cheng and H. Zhu, *J. Chem. Sci.*, 2017, **129**, 1587–1594.

[116] Y. Hong, T. Fang, M. Li, Z. Shen, X. Hu, W. Mo, B. Hu, N. Sun and L. Jin, *RSC Adv.*, 2016, **6**, 51908–51913.

[117] D. R. Buckle, *Encyclopedia of Reagents for Organic Synthesis*, John Wiley & Sons, Ltd, 2nd edn., 2005.

[118] F. Eckert, I. Leito, I. Kaljurand, A. Kütt, A. Klamt and M. Diedenhofen, *J. Comput. Chem.*, 2009, **30**, 799–810.

[119] C. Sambiagio and T. Noël, *Trends Chem.*, 2020, **2**, 92–106.

[120] D. Cambié, C. Bottecchia, N. J. W. Straathof, V. Hessel and T. Noël, *Chem. Rev.*, 2016, **116**, 10276–10341.

[121] B. D. A. Hook, W. Dohle, P. R. Hirst, M. Pickworth, M. B. Berry and K. I. Booker-Milburn, *J. Org. Chem.*, 2005, **70**, 7558–7564.

[122] J. H. Bannock, S. H. Krishnadasan, M. Heeney and J. C. de Mello, *Mater. Horizons*, 2014, **1**, 373.

[123] M. B. Plutschack, B. Pieber, K. Gilmore and P. H. Seeberger, *Chem. Rev.*, 2017, **117**, 11796–11893.

[124] C. R. Sagandira, M. Siyawamwaya and P. Watts, *Arab. J. Chem.*, 2020, **13**, 7886–7908.

[125] K. Sasaki, T. Kashimura, M. Ohura, Y. Ohsaki and N. Ohta, *J. Electrochem. Soc.*, 1990, **137**, 2437–2443.

[126] *https://www.kessil.com/science/main_PhotoReaction.php*, Visited: 12th December 2020.

[127] C. C. Le, M. K. Wismer, Z.-C. Shi, R. Zhang, D. V. Conway, G. Li, P. Vachal, I. W. Davies and D. W. C. MacMillan, *ACS Cent. Sci.*, 2017, **3**, 647–653.

[128] H. J. Eichler, B. Eppich, J. Fischer, R. Güther, G. G. Gurzadyan, A. Hermerschmidt, A. Laubereau, V. A. Lopota, O. Mehl, C. R. Vidal, H. Weber and B. Wende, *Laser Physics and Applications – Subvolume A: Laser Fundamentals*, Springer, 1st edn., 2005.

[129] K. C. Harper, E. G. Moschetta, S. V. Bordawekar and S. J. Wittenberger, *ACS Cent. Sci.*, 2019, **5**, 109–115.

[130] W. Chen, Z. Huang, N. E. S. Tay, B. Giglio, M. Wang, H. Wang, Z. Wu, D. A. Nicewicz and Z. Li, *Science*, 2019, **364**, 1170–1174.

[131] F. Glaser, C. Kerzig and O. S. Wenger, *Angew. Chemie Int. Ed.*, 2020, **59**, 10266–10284.

[132] N. Suzuki, T. Fujita, K. Y. Amsharov and J. Ichikawa, *Chem. Commun.*, 2016, **52**, 12948–12951.

[133] X. Fang, X. Pan, A. Rahmann, H.-P. Schuchmann and C. von Sonntag, *Chem. - A Eur. J.*, 1995, **1**, 423–429.

[134] J. Dean, *Lange's Handbook Of Chemistry*, McGraw-Hill New York, 15th edn., 1999.

[135] D. Lloyd, M. Bylsma, D. K. Bright, X. Chen and C. S. Bennett, *J. Org. Chem.*, 2017, **82**, 3926–3934.

[136] G. Chen, Q. Yin, J. Yin, X. Gu, X. Liu, Q. You, Y.-L. Chen, B. Xiong and J. Shen, *Org. Biomol. Chem.*, 2014, **12**, 9781–9785.

[137] X. Gu, L. Chen, X. Wang, X. Liu, Q. You, W. Xi, L. Gao, G. Chen, Y.-L. Chen, B. Xiong and J. Shen, *J. Org. Chem.*, 2014, **79**, 1100–1110.

[138] P. K. Chattaraj, U. Sarkar and D. R. Roy, *Chem. Rev.*, 2006, **106**, 2065–2091.

[139] H. Tandon, T. Chakraborty and V. Suhag, *J. Struct. Chem.*, 2019, **60**, 1725–1734.

[140] M. M. González, C. Cárdenas, J. I. Rodríguez, S. Liu, F. Heidar-Zadeh, R. A. Miranda-Quintana and P. W. Ayers, *Acta Phys. - Chim. Sin.*, 2018, **34**, 662–674.

[141] B. Galabov, D. Cheshmedzhieva, S. Ilieva and B. Hadjieva, *J. Phys. Chem. A*, 2004, **108**, 11457–11462.

[142] R. G. Parr, L. V. Szentpály and S. Liu, *J. Am. Chem. Soc.*, 1999, **121**, 1922–1924.

[143] W. S. Johnson, M. B. Gravestock and B. E. McCarry, *J. Am. Chem. Soc.*, 1971, **93**, 4332–4334.

[144] M. J. Frisch, G. W. Trucks, H. B. Schlegel, G. E. Scuseria, M. A. Robb, J. R. Cheeseman, G. Scalmani, V. Barone, G. A. Petersson, H. Nakatsuji, X. Li, M. Caricato, A. V. Marenich,

J. Bloino, B. G. Janesko, R. Gomperts, B. Mennucci, H. P. Hratchian, J. V. Ortiz, A. F. Izmaylov, J. L. Sonnenberg, D. Williams-Young, F. Ding, F. Lipparini, F. Egidi, J. Goings, B. Peng, A. Petrone, T. Henderson, D. Ranasinghe, V. G. Zakrzewski, J. Gao, N. Rega, G. Zheng, W. Liang, M. Hada, M. Ehara, K. Toyota, R. Fukuda, J. Hasegawa, M. Ishida, T. Nakajima, Y. Honda, O. Kitao, H. Nakai, T. Vreven, K. Throssell, J. A. Montgomery, Jr., J. E. Peralta, F. Ogliaro, M. J. Bearpark, J. J. Heyd, E. N. Brothers, K. N. Kudin, V. N. Staroverov, T. A. Keith, R. Kobayashi, J. Normand, K. Raghavachari, A. P. Rendell, J. C. Burant, S. S. Iyengar, J. Tomasi, M. Cossi, J. M. Millam, M. Klene, C. Adamo, R. Cammi, J. W. Ochterski, R. L. Martin, K. Morokuma, O. Farkas, J. B. Foresman and D. J. Fox, *Gaussian 16 Revision A.03*, 2016, Gaussian Inc. Wallingford CT.

[145] A. A. Isse and A. Gennaro, *J. Phys. Chem. B*, 2010, **114**, 7894–7899.

[146] M. A. Zolfigol, A. Khazaei, A. R. Moosavi-Zare, A. Zare, H. G. Kruger, Z. Asgari, V. Khakyzadeh and M. Kazem-Rostami, *J. Org. Chem.*, 2012, **77**, 3640–3645.

[147] S. Pasnoori, S. Muppidi, R. K. C. and K. G., *Int. J. Chem. Kinet.*, 2017, **49**, 209–218.

[148] Z.-T. Du, J. Lu, H.-R. Yu, Y. Xu and A.-P. Li, *J. Chem. Res.*, 2010, **34**, 222–227.

[149] W.-T. Wei, W.-M. Zhu, W. Liang, Y. Wu, H.-Y. Huang, Y.-L. Huang, J. Luo and H. Liang, *Synlett*, 2017, **28**, 2153–2156.

[150] M. Hosseini-Sarvari and M. Tavakolian, *J. Chem. Res.*, 2008, **2008**, 722–724.

[151] D.-Y. Wang, Z.-K. Yang, C. Wang, A. Zhang and M. Uchiyama, *Angew. Chem. Int. Ed.*, 2018, **57**, 3641–3645.

[152] H.-J. Lehmler and L. W. Robertson, *Chemosphere*, 2001, **45**, 1119–1127.

[153] G. Barker, S. Webster, D. G. Johnson, R. Curley, M. Andrews, P. C. Young, S. A. Macgregor and A.-L. Lee, *J. Org. Chem.*, 2015, **80**, 9807–9816.

[154] S. Ushijima and H. Togo, *Synlett*, 2010, **2010**, 1067–1070.

[155] A. Seggio, G. Priem, F. Chevallier and F. Mongin, *Synthesis*, 2009, **2009**, 3617–3632.

[156] V. Dichiarante, A. Salvaneschi, S. Protti, D. Dondi, M. Fagnoni and A. Albini, *J. Am. Chem. Soc.*, 2007, **129**, 15919–15926.

[157] Y.-W. Zheng, P. Ye, B. Chen, Q.-Y. Meng, K. Feng, W. Wang, L.-Z. Wu and C.-H. Tung, *Org. Lett.*, 2017, **19**, 2206–2209.

[158] R.-J. Tang, T. Milcent and B. Crousse, *J. Org. Chem.*, 2018, **83**, 930–938.

[159] M. J. Climent and M. A. Miranda, *J. Agric. Food Chem.*, 1997, **45**, 1916–1919.

[160] S. K. Chakraborty, A. Chowdhury, A. Bhattacharyya, S. Ghosh, S. Pan, R. Waters and N. Adityachaudhury, *J. Agric. Food Chem.*, 1995, **43**, 2964–2969.

[161] X. Tan, Z. Liu, H. Shen, P. Zhang, Z. Zhang and C. Li, *J. Am. Chem. Soc.*, 2017, **139**, 12430–12433.

[162] R. Mao, J. Balon and X. Hu, *Angew. Chemie Int. Ed.*, 2018, **57**, 13624–13628.

[163] H.-J. Cristau, P. P. Cellier, J.-F. Spindler and M. Taillefer, *Eur. J. Org. Chem.*, 2004, **2004**, 695–709.

[164] Y.-Q. Ouyang, Z.-H. Yang, Z.-H. Chen and S.-Y. Zhao, *Synth. Commun.*, 2017, **47**, 771–778.

[165] Q. Zhang, L.-G. Meng, K. Wang and L. Wang, *Org. Lett.*, 2015, **17**, 872–875.